NOTTINGHAM TRENT UNIVERSITY

TRANSGLUTAMINASE 2 IN CALCIUM HOMEOSTASIS AND NEURODEGENERATION

Elisa Tonoli

A thesis submitted in partial fulfilment of the requirement of Nottingham Trent University for the degree of Doctor of Philosophy

August 2019

Copyright Statement

To my family,

especially the new little

miracle who is about to come

Abstract

Transglutaminase 2 (TG2) is a calcium-dependent protein crosslinking enzyme activated in misfolding diseases and it is implicated in multiple disorders linked to calcium dysregulation, including neurodegeneration. *In vitro*, TG2 has been involved in the generation of toxic amyloid-β (Aβ) oligomers by post-translational modification (PTM), and literature data suggest that TG2 is activated in disease, e.g. the early stages of Alzheimer's disease (AD). TG2 is also involved in cell-matrix dynamics and has been suggested to be a cargo of extracellular vesicles (EVs) in cancer and tissue fibrosis. EVs have been implicated in the spreading of pathogenic proteins in neurodegenerative diseases (e.g. Aβ and tau) and represent a new field of research in dementia. The aims of this study are to: i. investigate the role of extracellular TG2 in neuron-glia cross-talk in the context of neurodegeneration; ii. explore substrates of TG2 PTM in a cell model simulating AD; iii. evaluate TG2 as a potential marker of dementia. To this purpose, both primary cells (embryonic rat brain cells) and biological samples from dementia patients were analysed. We found that when raised at levels compatible with inflammatory states, extracellular TG2 consistently increased basal calcium concentration ($[Ca^{2+}]_i$) in hippocampal neurons, affecting calcium homeostasis, which is at the basis of neuronal functions. This effect was mediated by TG2-driven membrane depolarisation, which may be caused by the interaction of TG2 with plasma membrane ionic channels [i.e. Voltage Operated Calcium Channels (VOCCs) and Na^+/Ca^{2+} exchanger (NCX)]. We confirmed previous evidence showing that astrocytes are a rich source of extracellular TG2 in brain and showed for the first time that TG2 is released as a cargo of astrocytic EVs. Simulation of AD pathology in primary hippocampal neurons stimulated with $Aβ_{1-42}$ led to the identification of 11 TG2 substrates (TG2 transamidome) using a global quantitative proteomic approach (SWATH™-MS/MS proteomics). These included proteins involved in ion transport [Plasma Membrane Ca^{2+} Transporting ATPase 2 (AT2B2) and Transmembrane Channel-like Protein 5 (TMC)], which could be involved in TG2-mediated alteration of calcium homeostasis in pathology. We also found that a number of neurotrophic proteins involved in neuronal growth and apoptosis were significantly decreased upon TG2 inhibition, suggesting that TG2 might play a dual role in neuronal survival during neurodegeneration. Finally, analysis of plasma from 45 dementia patients and healthy controls by an optimised ELISA assay revealed no significant changes in TG2 between the study groups. Our preliminary data suggest that quantitation of TG2 should be performed in plasma-derived EVs for a more accurate and sensitive evaluation.

Acknowledgements

I would like to express my gratitude to Dr Elisabetta Verderio Edwards, my Director of Studies, for being a driving force in this project as the supervisor who guided my work, but also a constant support and for creating a nice environment that made me feel welcomed and appreciated for my efforts. Thanks also to my other supervisors, Prof Ellen Billet, Dr Jody Winter and especially Dr Claudia Verderio for your guidance and suggestions.

This work was accomplished thanks to the support of many people, first of all my Italian collaborators: Dr Ghidoni's group at the IRCCS Fatebenefratelli Institute in Brescia, Dr Verderio's group at the CNR Institute of Neuroscience in Milan and Prof. Mazzanti's group at the University of Milan. Special thanks to Dr Ilaria Prada and Ivan Verduci for their experimental contribution, together with Giulia and Martina who greatly assisted me during my stay in Milan. I would also like to acknowledge Dr David Boocock and Claire Coveney, who helped me with the proteomic work.

And I should not forget my colleagues and friends, especially Grace and MaryP. You have made my everyday work so much easier just by being there with me, sharing the ups and downs that characterise the life of the average PhD student. I don't think I would have reached the end of these 4 years with a smile without you! Grace, I especially admire and look up to you, who went through this with two kids at home waiting for you… no idea how you did it, you are a super mum!! A special thanks also to Nick, who was always supportive!

My biggest thanks go to my parents, who have always supported me and given me the strength to be the person I am today. My lifestyle and work ethics come from what you have taught me, the basic principles I live by and shape my daily choices on are the result of your teachings and love… I wouldn't be here if it were not for you!

Then come my sisters… well, they still think I am an alien ("ET phone home" to be precise) and that I cannot possibly be their sister, that I am too smart to be! That is the inside joke of three women who have grown up together and learned to appreciate and love each other, with our own quirks, strengths and weaknesses. I might have some academic degrees more than you, but that for sure doesn't make you any less amazing or me any better… just smarty maybe!!

Special thanks also to my closest friends, who are now busy with their own families and kids, but still find the time to meet with me every time I go back home. Giuly, Iaia, Lola e Jo, you have always believed in me, since the time we were the four musketeers (way back in the far, very far past!!). I love how you still make me part of your lives and that of your

children… I think I have gone to more weddings and celebrated births in these past 3 years than in the previous 29 all together!!! I would like to thank Chicca, for always listening to me and confiding in me… your friendship is very important to me and I am happy we have become such close friends in these past years.

And finally, I thank God, who has graced me with the strength to overcome all difficulties and allowed me to meet many wonderful people in this long journey. I am grateful for all the people I could help and inspire, for those who hurt me and made me better, for those you have put in front of me to challenge my views and principles, for those I have lost way too early and always will carry with me. All is for your glory and I pray to be a person worthy of your immense love.

List of publications

1. Savoca MP, **Tonoli E**, Atobatele AG, Verderio EAM. Biocatalysis by Transglutaminases: A Review of Biotechnological Applications. Micromachines (Basel). 2018 Oct 31;9(11). Review.
2. Furini G, Schroeder N, Huang L, Boocock D, Scarpellini A, Coveney C, **Tonoli E**, Ramaswamy R, Ball G, Verderio C, Johnson TS, Verderio EAM. Proteomic profiling reveals the transglutaminase-2 externalization pathway in kidneys post-UUO. J Am Soc Nephrol. 2018 Mar;29(3):880-905.

Manuscript

Elisa Tonoli, Ivan Verduci, Ilaria Prada, Michele Mazzanti, Claudia Verderio, Elisabetta AM Verderio. "Involvement of TG2 in the modulation of calcium homeostasis in rat primary embryonic hippocampal neurons".

Conference communications and awards

1. **Elisa Tonoli**, Ilaria Prada, Claudia Verderio, Elisabetta AM Verderio. Type-2 transglutaminase affects calcium homeostasis in neurons and is released in association with astrocytes-derived exosomes. International Society of Extracellular Vesicles (ISEV) Annual Meeting 2019, 24-28 April 2019, Kyoto, Japan. Late Breaking Oral with Poster Presentation. Travel grant from NTU (500£) and Particle Metrix (500£).
2. **Elisa Tonoli**, Ilaria Prada, Ivan Verduci, Michele Mazzanti, Claudia Verderio, Elisabetta AM Verderio. TG2 in the brain: modulation of calcium homeostasis in hippocampal neurons. Life Sciences 2019: Post-Translational Modifications and Cell Signalling, 17-18 March 2019, Nottingham, UK. Oral communication.
3. **Elisa Tonoli**, Ilaria Prada, Ivan Verduci, Michele Mazzanti, Claudia Verderio, Elisabetta AM Verderio. Involvement of TG2 in the modulation of calcium homeostasis in rat primary embryonic hippocampal neurons**.** 1st Gordon Research seminar (GRS)/ 4th Gordon Research Conference (GRC): Transglutaminases in Human Disease Processes, 16–22 June 2018, Les Diablerets, Switzerland. Oral presentation. Travel grant from Biochemical Society (500£) and GRS (300$).

4. **Elisa Tonoli**, Ilaria Prada, David Boocock, Claudia Verderio, Elisabetta AM Verderio. The transglutaminase-2 “transamidome” in Aβ-exposed primary rat hippocampal neurons. 17th Young Scientists’ Forum (YSF), 7-10 September 2017. FEBS Congress 2017, 10–14 September 2017, Jerusalem, Israel. Oral presentation. Travel grant from YSF and FEBS.
5. **Elisa Tonoli**, Ilaria Prada, Claudia Verderio, Elisabetta AM Verderio. Involvement of TG2 in calcium homeostasis in rat primary hippocampal neurons. TGase Debrecen University Symposium: Transglutaminases in Medicine. Debrecen, Hungary, 3-6 August 2017. Travel grant from TGase Symposium.
6. **Elisa Tonoli**, Ilaria Prada, David Boocock, Clare Coveney, Claudia Verderio, Elisabetta AM Verderio. Molecular markers for Alzheimer’s disease: Transglutaminase 2 – amyloid β interplay in primary rat hippocampal neurons. School of Science & Technology Annual Research (STAR) Conference. Nottingham Trent University, Nottingham, United Kingdom, 10-11 May 2017. Oral presentation.
7. **Elisa Tonoli**, Ilaria Prada, Claudia Verderio, Elisabetta AM Verderio. Characterisation of TG2 in primary rat hippocampal neurons. Gordon Research Conference: Transglutaminases in Human Disease Processes. Girona, Spain, 10-15 July 2016.
8. “InEurope short stay grant” award (December 2015) for funding the collaboration with the CNR Institute of Neuroscience (Milan, Italy) (£2000).

Table of Contents

List of Abbreviations

$[Ca^{2+}]_i$	Intracellular Calcium concentration
2-ME	β-Mercaptoethanol
5-HT	Serotonin
Abs	Absorbance
AC	Adenylate cyclase
Ach	Acetylcholine
ACM	Astroglial conditioned media
AD	Alzheimer's Disease
AICD	Amyloid Intracellular Domain
AIDA	Advanced Image Data Analyzer
ALS	Amyotrophic Lateral Sclerosis
AMPARs	α-amino-3-hydroxy-5-methyl-4-isoxazole-propionic acid receptors
APH1	Anterior pharynx-defective
APOE	Apolipoprotein E
APP	Amyloid precursor protein
APS	Ammonium Persulfate
APV	2-amino-5-phosphonovaleric acid
AT2B2	Plasma membrane Ca^{2+} transporting ATPase 2
ATP	Adenosine Triphosphate
AUC	Area Under the Curve
Aβ	Amyloid β peptide
BACE1	β-secretase
BBB	Blood Brain Barrier
BCA	Bicinchoninic acid
BSA	Bovine Serum Albumin
BTC	Biotin-cadaverine
bvFTD	behavioural variant Frontotemporal dementia
Ca^{2+}	Calcium
$CaCl_2$	Calcium Chloride
CaM	Calmodulin
cDNA	Complementary DNA
Cl^-	Chloride ion
CN	Calcineurin
CNQX	6-Cyano-7-Nitroquinoxaline
CNS	Central Nervous System
CSF	Cerebrospinal fluid
CTR	Control
$CuSO_4$	Copper Sulphate
DA	Dopamine
DAPI	4',6-diamidino-2-phenylindole
DDA/IDA	Data Dependent acquisition / Information Dependent Acquisition
DG	Dentate gyrus
DIA	Data Independent acquisition
DIV	Days In Vitro
DLK	Dual leucine zipper-bearing kinase

DMSO	Dimethylsulfoxide
DNA	Deoxyribonucleic acid
dNTPS	Deoxynucleotide Triphosphates
DSS	Disuccinimidyl Suberate
DTT	1,4-Dithiothreitol
ECL	Enhanced Chemiluminescence
ECM	Extracellular matrix
EDTA	Ethylenediaminetetraacetic acid
EGFP	Green Fluorescent Protein
EGGL	ε-(γ-glutamyl)-lysine (dipeptide/crosslink)
EGTA	Ethylene Glycol-bis(β-aminoethyl ether)-N,N,N’,N’-tetraacetic acid
ELISA	Enzyme-Linked Immunosorbent Assay
EMEM	Eagle's Minimum Essential Medium
ENOB	β-enolase
EOAD	Early onset AD
EPSCs	Excitatory Postsynaptic Currents
EPSP	Excitatory Postsynaptic Potential
ER	Endoplasmic Reticulum
EVs	Extracellular Vesicles
FAAH1	Fatty-acid amide hydrolase 1
fAD	Familial AD
FBS	Fetal Bovine Serum
FC	Fold Change
fFTD	Familial FTD
FITC	Fluorescein isothiocyanate
FITC-Cad	FITC-cadaverine
FLOT-2	Flotillin-2
FN	Fibronectin
FN_{FL}	Full-length FN
FTD	Frontotemporal dementia
FTLD	Frontotemporal Lobar Degeneration
FUS	Fused in sarcoma
FXIII	Factor XIII
FXIIIa	Factor XIII activated
GABA	γ-aminobutyric acid
GAPDH	Glyceraldehyde 3-phosphate dehydrogenase
GDP	Guanosine Diphosphate
GFA	Glial Filaments
GFAP	Glial Fibrillary Acidic Protein
GluRs	Glutamate receptors
gly	Glycine
GO	Gene Ontology
gplTG2	Guinea pig liver TG2
GRN	Progranulin
GSDB	Goat Serum Dilution Buffer

GTP	Guanosine Triphosphate
H_2SO_4	Sulphuric acid
HCl	Hydrochloric acid
HAPs	High Abundance Proteins
HD	Huntington's disease
Hepes	(4-(2-hydroxyethyl)-1-piperazineethanesulfonic acid
HPLC	High Performance Liquid Chromatography
HRP	Horseradish Peroxidase
HS Solution	High Salt Solution
HSP70	70-kDa Heat Shock Protein
HSPG	Heparan sulphate proteoglycans
Htt	Huntingtin
IF	Immunofluorescence
IgG	Immunoglobulin G
IGG2A	Ig γ-2A chain C region
iGluRs	Ionotropic Glutamate receptors
IL-6	Interleukin-6
IP	Immunoprecipitation
IPSP	Inhibitory Postsynaptic Potential
IRCCS	Istituto di Ricovero e Cura a Carattere Scientifico
JNK	c-Jun amino terminal kinase
K^+	Potassium ion
K1C40	Keratin type I cytoskeletal 40
KARs	Kainic acid receptors
KCl	Potassium Chloride
KO	Knock Out
KRH	Krebs–Ringer's HEPES solution
K-S test	Kolmogorov–Smirnov test
LB	Lysis Buffer
LC/MS	Liquid chromatography / Mass Spectrometry
LOAD	Late onset AD
$\log_2$(FC)	Logarithm base 2 of Fold change
LPS	Lipopolysaccharide
LS Solution	Low Salt Solution
LSS	Low speed supernatant
LTD	Long-Term Depression
LTP	Long-Term potentiation
L-VOCCs	L-Type Voltage Operated Calcium Channels
MAPs	Microtubule associated proteins
MAPT	Microtubule associated protein tau
MCI	Mild Cognitive Impairment
$MgCl_2$	Magnesium Chloride
mGluRs	Metabotropic Glutamate receptors
MMSE	Mini-Mental State Examination
MRI	Magnetic Resonance Imaging

MS	Mass Spectrometry
MS	Multiple Sclerosis
MVs	Microvesicles
MW	Molecular Weight
NA	Noradrenaline
Na^+	Sodium ion
Na_2CO_3	Sodium Carbonate
NaCl	Sodium Chloride
NaH_2PO_4	Sodium Dihydrogen sulphate
NaK tartrate	Potassium sodium tartrate
NaOH	Sodium Hydroxide
NCS-1	Neuronal Calcium sensor-1
NCSs	Neuronal Ca^{2+} sensors
NCX	Na^+/Ca^{2+} exchanger
NDs	Neurodegenerative Diseases
NF	Neuronal filament
NF-kB	Nuclear Factor kappa-light
NfL	Neurofilament light
NFT	Neurofibrillary tangle
NMDARs	N-methyl-D-aspartate receptors
NO	Nitric oxide
NPY	Neuropeptide Y
NR2B	N-methyl-D-aspartate (NMDA) receptor subtype 2B
NTA	Nanoparticle Tracking Analysis
NTU	Nottingham Trent University
OGD	Oxygen and glucose deprivation
P2XRs	Purinergic ionotropic P2X receptors
PAGE	Polyacrylamide Gel Electrophoresis
PANTHER	Protein ANalysis Through Evolutionary Relationships
PBS	Phosphate Buffered Saline
PCR	Polymerase Chain Reaction
PCYOX	Prenylcysteine oxidase
PD	Parkinson’s disease
Pen/Strep	Penicillin-Streptomycin
PEN2	Presenilin enhancer
PET	Positron Emission Tomography
PFA	Paraformaldehyde
PGC-1α	Peroxisome proliferator-activated receptor-γ coactivator-1α
PKA	Protein Kinase A
PKC	Protein Kinase C
PL	Plasma
PLL	Poly-L-Lysine
PMCA	Plasma Membrane Ca^{2+} ATPase
PNFA	Progressive non-fluent aphasia
PP1	Protein phosphatase 1

PPA	Primary progressive aphasia
PS1	Presenilin1
PS2	Presenilin2
PSD-95	Postsynaptic Density Protein-95
PSP	Progressive Supranuclear Palsy
p-Tau	Hyperphosphorylated tau
PTM	Post-translational Modification
PV	Parvalbumin
qPCR	Real Time PCR
RIPA	Radio Immunoprecipitation Assay
RNA	Ribonucleic acid
ROS	Reactive Oxygen Species
RPMI 1640	Roswell Park Memorial Institute 1640
RT	Room temperature
RT-PCR	Reverse-transcription Polymerase Chain Reaction
S1P	sphingosine-1-phosphate
sAD	sporadic Alzheimer's disease
SAM50	Sorting and assembly machinery component 50 homolog
SD	Semantic Dementia
SDS	Sodium Dodecyl Sulphate
SE	Standard Error
SERCA	Sarco-endoplasmic reticular Ca^{2+}-ATPase
sFTD	sporadic FTD
SHANK2	SH3 And Multiple Ankyrin Repeat Domains 2
shRNA	Short hairpin RNA
SN1	Supernatant 1
SN2	Supernatant 2
SNAREs	Soluble NSF Attachment protein REceptors
SN_f	Filtered supernatant
SOCE	Store Operated Calcium Entry
SP	Substance P
SPs	Senile plaques
SQSTM1	Sequestosome 1
STD	Standard
SWATH-MS	Sequential Window Acquisition of All Theoretical Mass Spectra
SYN	Synaptosomes
SynI	Synapsin I
SYT-1	Synaptotagmin-1
TAE	Tris-acetate-EDTA
TBS	Tris Buffered Saline
TBST	Tris Buffered Saline - Tween 20
TCA	Trichloroacetic acid
TCP	Tissue Culture Plastic
TDP-43	Transactivator regulatory DNA binding protein
TEMED	Tetramethylethylenediamine
TFA	Trifluoroacetic acid

TG1	Transglutaminase 1
TG3	Transglutaminase 3
TG4	Transglutaminase 4
TG5	Transglutaminase 5
TG6	Transglutaminase 6
TG7	Transglutaminase 7
TGF-β	Transforming Growth Factor- β
TGM2, TG2, tTG	Transglutaminase 2 /Type-2 transglutaminase
TGs	Transglutaminases
TLR4	Toll Like Receptor 4
TMB	3,3’,5,5’-Tetramethylbenzidine
TMC5	Transmembrane channel-like protein 5
TNF-α	Tumour Necrosis Factor alpha
TOF-MS	Time Of Flight Mass Spectrometry
TREM2	Triggering Receptor Expressed on Myeloid Cells 2
TRIS	Tris(Hydroxymethyl) Aminomethane
TRY1	Anionic trypsin-1
TSG 101	Tumor Susceptibility Gene 101
TTX	Tetrodotoxin
UBQLN2	Ubiquilin 2
UPS	Ubiquitin Proteasome System
VaD	Vascular Dementia
VGAT	Vesicular GABA Transporter
VGLUT1	Vesicular Glutamate Transporter 1
VOCCs	Voltage Operated Calcium Channels
WB	Western Blotting
YKT6	Synaptobrevin homolog
β-TUB	β-tubulin

CHAPTER 1:

General Introduction

1.1 Cells of the Central Nervous System

The Central Nervous System (CNS) comprises the spinal cord and brain structures. The brain is the most complex organ of the human body, with functions that are based on the passage of electrochemical signals between its constituent cells. The main cell types that form the brain are neurons and glial cells, which together are organised in the gray matter (the outer layer mainly made of neuronal cell bodies and glia), and the white matter (internal area made of oligodendrocytes and nerve fibers) (Watson et al., 2010). This section will focus on these cell types and their main characteristics.

1.1.1 Hippocampal neurons

The hippocampus (or hippocampus proper) is located under the cerebral cortex in the temporal lobe and together with dentate gyrus (DG) and subiculum is part of the hippocampal formation (Witter and Amaral, 2004; Watson et al., 2010) (**Fig. 1.1**).

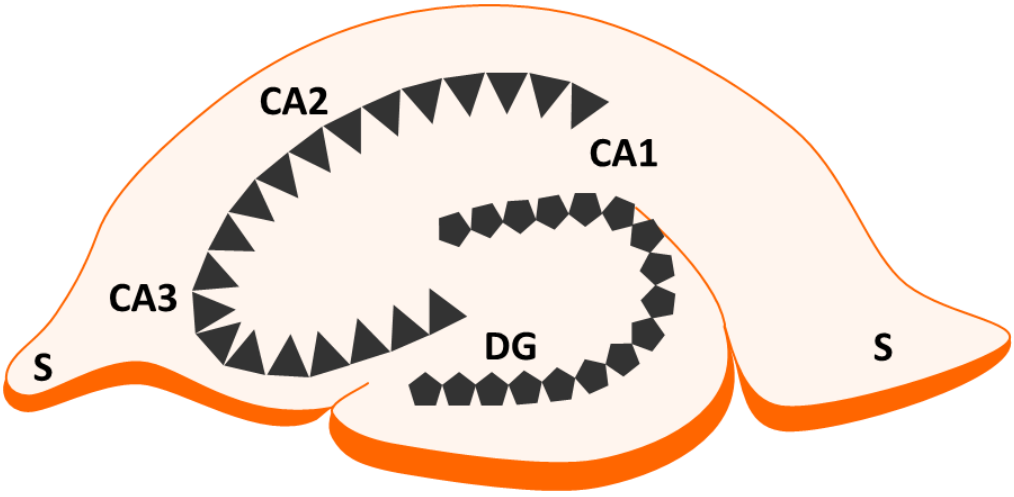

Figure 1.1. Schematic representation of the mammalian hippocampus. *The hippocampus (or hippocampus proper) is divided in 3 fields: CA1, CA2 and CA3. It resides above the dentate gyrus (DG) and together with the subiculum (S), they constitute the hippocampal formation. This image was generated with the scientific illustration toolkit Motifolio (https://www.motifolio.com/).*

The most abundant neuronal cell type of the hippocampus are pyramidal neurons, which present a common basic morphology but differ in length and organisation according their localisation (Kandel et al., 2012). Pyramidal cells are multipolar neurons characterised by a conical cell body, a basal axon and dendritic tree and an apical dendritic tree, both very rich in dendritic spines (**Fig. 1.2A**). Other neuronal cells localised in the stratum pyramidale are basket neurons, which are a heterogeneous population characterised by dendritic trees less rich in spines compared to pyramidal cells (Witter and Amaral, 2004) (**Fig. 1.2B**). Basket neurons, together with other cell types present in the hippocampus like bistratified neurons and O-LM cells, are defined interneurons and form thick local circuits in constant communication. Neurons communicate through synaptic transmission and can either excite or inhibit their target cell.

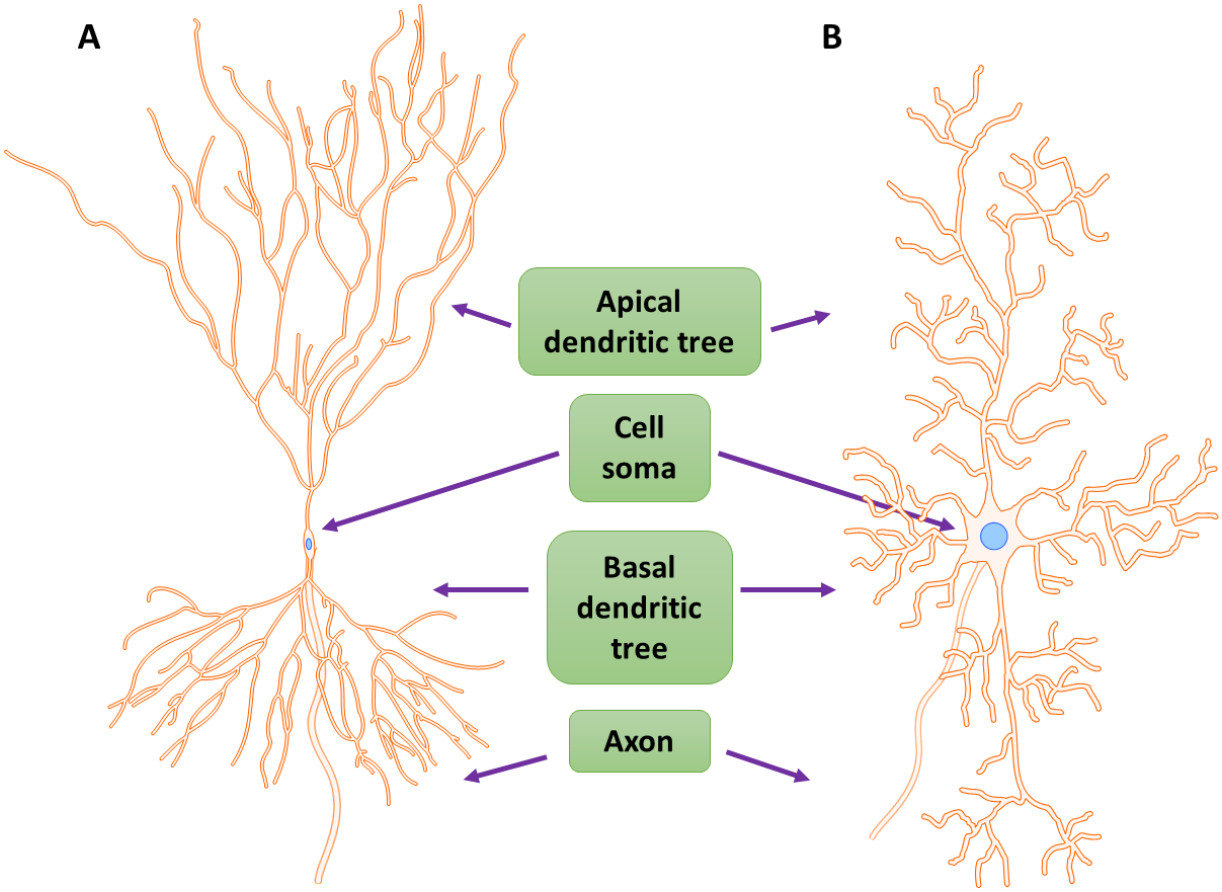

Figure 1.2. Schematic representation of hippocampal neurons. *Multipolar neurons are characterised by a cell body (soma) from which the axon and apical/basal dendritic arborisations extend.* ***A)*** *Pyramidal neuron (CA3 field).* ***B)*** *Basket neuron. This image was generated with Motifolio (https://www.motifolio.com/).*

1.1.2 Glial cells

Glia are non-neuronal cells which play a fundamental support role in the CNS and, unlike neurons, they cannot propagate action potentials. Their name comes from the Greek word 'γλία', which means “stick, glue”, which is indicative or their supportive function. Glial cells can be classified as micro- and macroglia according to their structure and functions, i.e. microglia are immunocompetent cells with phagocytic activity (Kettenmann et al., 2013), while macroglia consist of oligodendrocytes (responsible for axon myelination), ependymal cells (which produce the cerebrospinal fluid) and astrocytes, the most abundant category in the CNS and characterised by a star shape. The focus of this section will be on astrocytes, the main kind of glial cells which were utilised in the course of this project.

1.1.2.1 Astrocytes

Astrocytes, also referred to as astroglia, are the most abundant cell type in the CNS and they are estimated to be about 1.5 to 5-fold more than neurons (Nedergaard et al., 2003; Hamby and Sofroniew, 2010). Their main function is to act as multifunctional housekeepers, providing a structural scaffold for neuronal growth, supporting neurotransmitters metabolism, maintenance of the blood-brain barrier (BBB), synaptogenesis and balance of extracellular ionic and pH conditions (Verkhratsky and Nedergaard, 2018). They can be classified in two main categories with distinct functions and morphology: protoplasmic and fibrous astrocytes (Oberheim et al., 2006; Barres et al., 2008). Protoplasmic astrocytes are present in the gray matter, where they wrap around synapses and blood vessels, promoting neuronal functions. Fibrous astrocytes are located in the white matter and are less branched, presenting a more elongated shape extending alongside myelinated fibers, for which they provide metabolic support (Oberheim et al., 2006; Barres et al., 2008). Two additional categories of astrocytes have been described in human brain: interlaminar and polarised (Oberheim et al., 2006). Atrocytes can be either quiescent or in a reactive state following brain injury, which has been shown to promote myelination (Nash et al., 2011). Reactive astroglia present enhanced production of extracellular matrix (ECM) proteins and immune system molecules, which together with prominent morphological changes lead to the formation of the glial scar, one of the most severe responses to CNS insults (Kindy et al., 1992; Zamanian et al., 2012).

Especially in the hippocampus, each astrocyte can support thousands of synapses, and about 50% of synaptic sites are in proximity of an astrocyte (Ventura and Harris, 1999).

Astrocytes, together with the pre- and post-synaptic membranes, form structures called "tripartite synapses" characterised by bi-directional communication among all parts (Perea et al., 2009) (**Fig. 1.3**). In physiological conditions, one of their most important functions at synapses is the regulation of GABA and glutamate concentrations (Coco et al., 1997, Oliet et al., 2001). Indeed, glutamate needs to be rapidly removed from the extracellular space to avoid neurotoxicity and astrocytes are able to uptake it through the GLT-1 and GLAST1 transporters (Rothstein et al., 1996). Glutamate is then converted into glutamine by astrocytic glutamine synthetase (Hallermayer et al., 1981), released and used by neurons to synthesise new glutamate (Verkhratsky and Nedergaard, 2018). Another means of communication between astrocytes and neurons is the release of gliotransmitters, that is neurotransmitters originating from astrocytes. These include ATP, glutamate and GABA (Verkhratsky and Nedergaard, 2018). Interestingly, astrocytes are characterised by both spontaneous and neurotransmitters-driven calcium oscillations, which participate to the modulation of gliotransmitters release (Nett et al., 2002; Fiacco and McCarthy, 2006).

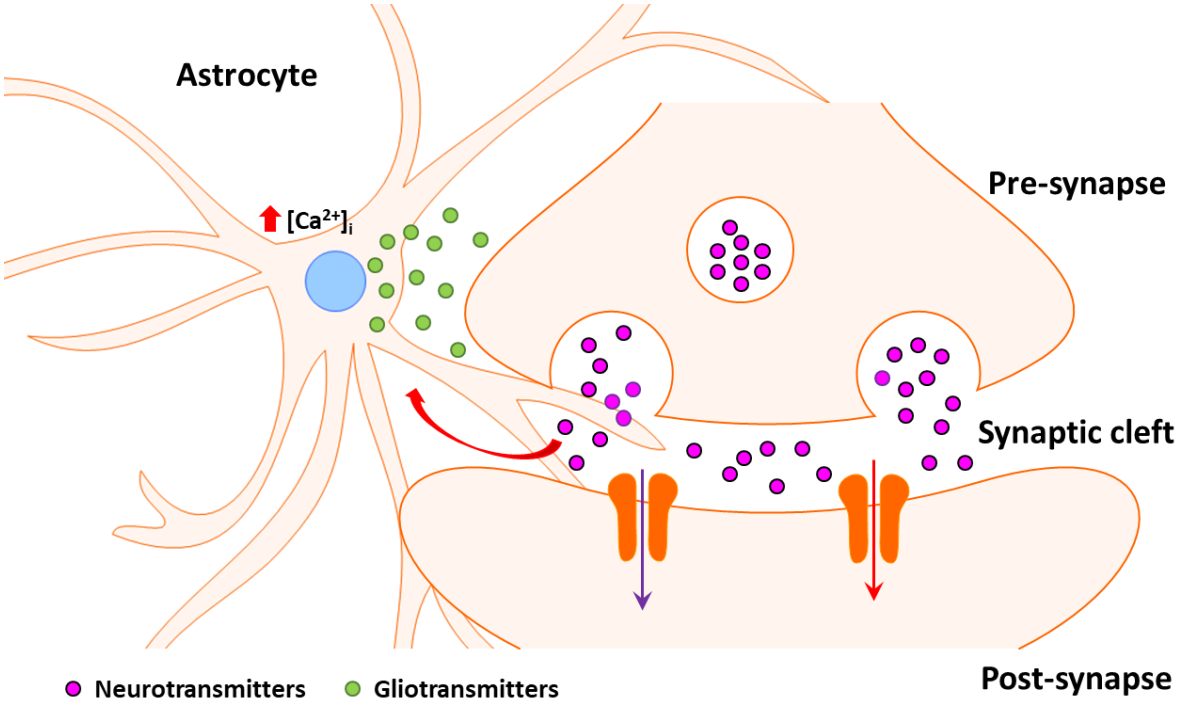

Figure 1.3. Schematic representation of a tripartite synapse *(based on Perea et al., 2009). This image was generated with Motifolio (https://www.motifolio.com/).*

1.2 Calcium homeostasis in neurons

Calcium is a critical player in most cellular functions, as it is the main second signalling messenger which mediates a variety of activities in all eukaryotic cells. The modulation of Ca^{2+} homeostasis is particularly fundamental in neurons, which synaptic activities are based on calcium fluctuations, including synaptic plasticity. Moreover, dysregulation of calcium homeostasis has been associated with neurodegeneration, having profound deleterious effects on neuronal survival (Marambaud et al., 2009). Indeed, the regulation of neuronal Ca^{2+} concentration is an intricate process and the result of a "team effort" involving both membrane and intracellular channels, pumps, receptors, sensors and buffering system (Brini et al., 2014). This section will be focused on the main effectors that are involved in this complicated mechanism.

1.2.1 Voltage Operated Ca^{2+} Channels (VOCCs)

Voltage Operated Ca^{2+} Channels (VOCCs) are the main channels responsible for the release of neurotransmitters and are also involved in the modulation of synaptic plasticity (Catterall and Few, 2008; Catterall, 2011; Brini et al., 2014). They can be classified according to the physiological properties of the currents they mediate (L, N, P/Q, R, and T-type) or by their subunit composition (Ca_v1, Ca_v2 and Ca_v3). They are composed of 5 subunits in total (α1 and 2, β, γ, δ), where α1 is the pore subunit which determines their Ca_v nomenclature (Brini et al., 2014) (**Fig. 1.4**).

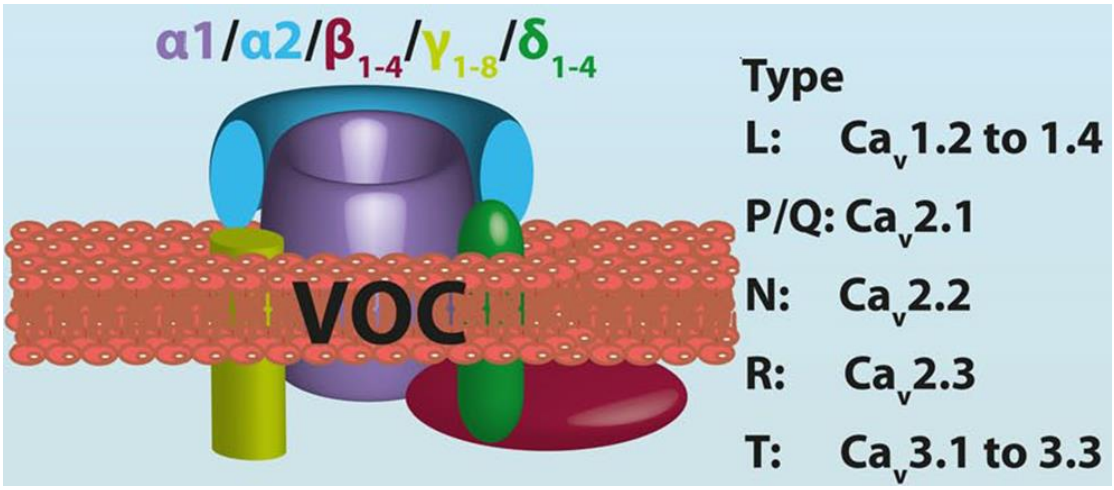

Figure 1.4. Schematic representation of VOCCs (Brini et al., 2014).

L-type VOCCs (L-VOCCs) are mainly expressed at dendrites and in the cell soma, hence they are thought to be responsible for mediating secretion and affect gene expression (Catterall, 2011; Brini et al., 2014). It is possible to identify 3 subtypes in brain ($Ca_v1.2$-1.4), which present different subcellular localisations and functions (Brini et al., 2014). The modulation of Long-Term potentiation (LTP) and Long-Term Depression (LTD) is one of their most prominent functions (Navakkode et al., 2018). L-VOCCs open in response to glutamate-driven cell depolarisation and promote local increase of calcium concentration, which in turn induces the release of Ca^{2+} from the intracellular stores (endoplasmic reticulum, ER). Increase in $[Ca^{2+}]_i$ leads to the activation of a series of proteins, including protein kinase C (PKC) and adenylate cyclase (AC), which downstream effect is the enhancement of AMPAR function and LTP. At the same time, modest and slow increases of Ca^{2+} follow LTD induction, with consequent activation of phosphatases like protein phosphatase 1 (PP1) and calcineurin (CN) (Navakkode et al., 2018). Dysregulation of L-VOCCs has been reported in various neurodegenerative diseases and also as a common process that accompanies aging. In fact, it has been shown that age-related neurodegeneration mostly affects the CA1 field of the hippocampus, which neurons present the highest expression of L-VOCCs (Wang and Mattson, 2014).

N-, R- and P/Q-type VOCCs (Ca_v2) are mainly present at pre-synaptic terminals and are responsible for inducing exocytosis of neurotransmitters-containing synaptic vesicles. Their function is implemented by direct interaction and activation of SNAP-Receptor proteins (SNARE complex), composed of syntaxin, synaptosomal nerve-associated protein 25 (SNAP-25) and synaptobrevin (VAMP) (Sudhof 2004). Additionally, they are regulated by interaction with G-protein pathways (Catterall, 2011). These VOCCs are also expressed along dendrites where they promote calcium transients (Catterall, 2011; Brini et al., 2014). T-type VOCCs (Ca_v3) are less widespread and are characterised by rapid voltage-dependent inactivation, hence they are particularly efficient at maintaining the repetitive firing of action potential typical of cardiac myocytes and thalamic neurons (Catterall, 2011; Brini et al., 2014). They are involved in the generation of rhythmic bursts of action potentials in thalamic circuits that are associated with sleep states (Lee et al., 2004; Catterall, 2011).

1.2.2 Receptor Operated Ca^{2+} Channels (ROCCs)

Receptor Operated Ca^{2+} Channels (ROCCs) are channels that mediate the passage of calcium upon binding to a specific ligand, e.g. neurotransmitters. This is the case of glutamate receptors (GluRs) and purinergic receptors (Brini et al., 2014).

GluRs are classified in 2 major groups: ionotropic (iGluRs) and metabotropic (mGluRs) (Kandel et al., 2012). Ionotropic glutamate receptors serve as ion channels and directly mediate the influx of positively charged ions in response to glutamate binding, always eliciting a depolarisation. These are the N-methyl-D-aspartate receptors (NMDARs), α-amino-3-hydroxy-5-methyl-4-isoxazole-propionic acid receptors (AMPARs) and Kainic acid receptors (KARs) (Kandel et al., 2012) (**Fig. 1.5A**).

NMDARs are permeable to Ca^{2+}, Na^{+} and K^{+}, however, to allow the passage of ions the binding to glutamate is not sufficient; they also need the presence of extracellular glycine as cofactor and membrane depolarisation to remove a Mg^{2+} ion plugging the channel (Kandel et al., 2012). These receptors are selectively blocked by the drug 2-amino-5-phosphonovaleric acid (AVP). Interestingly, also a type of non-neuronal cells called astrocytes or astroglia have been shown to express NMDARs (Fellin et al., 2004). Excessive activation of NMDAR by glutamate has been associated to neurotoxicity, which is thought to be caused by abnormal increase of cytoplasmic calcium levels (Budd and Nicholls, 1996).

AMPA receptors are prevalently permeable to Na^{+} and K^{+} and, to a lesser extent, also Ca^{2+}, which passage is regulated by the GluR-B subunit (Burnashev et al., 1992). One of the most used antagonists of AMPAR is 6-cyano-7-nitroquinoxaline-2,3-dione (CNQX), which can selectively block also kainic acid receptors (Kandel et al., 2012).

KARs are very similar to AMPAR, in the sense that they present common structural features, conduct the same cations and are inhibited by the same drugs. However, they have been shown to have distinct functions and they are not as concentrated at the excitatory post-synaptic terminals as NMDAR and AMPAR (Contractor et al., 2011). Indeed, KARs are expressed at the pre-synaptic membrane and play an important role in the modulation of neuronal excitability and synaptic transmission (Contractor et al., 2011).

The glutamate metabotropic receptors are G-coupled receptors that trigger an intracellular cascade and modulate channels through second messengers (effectors), such as inositol 1,4,5-trisphosphate (IP3) or adenylyl cyclase. As such they can mediate either EPSP or IPSP depending on the ionic currents that they regulate (**Fig. 1.5B**). mGluRs can be selectively

activated by ACPD (trans-(1S,3R)-1-amino-1, 3-cyclopentanedicarboxylic acid) (Kandel et al., 2012).

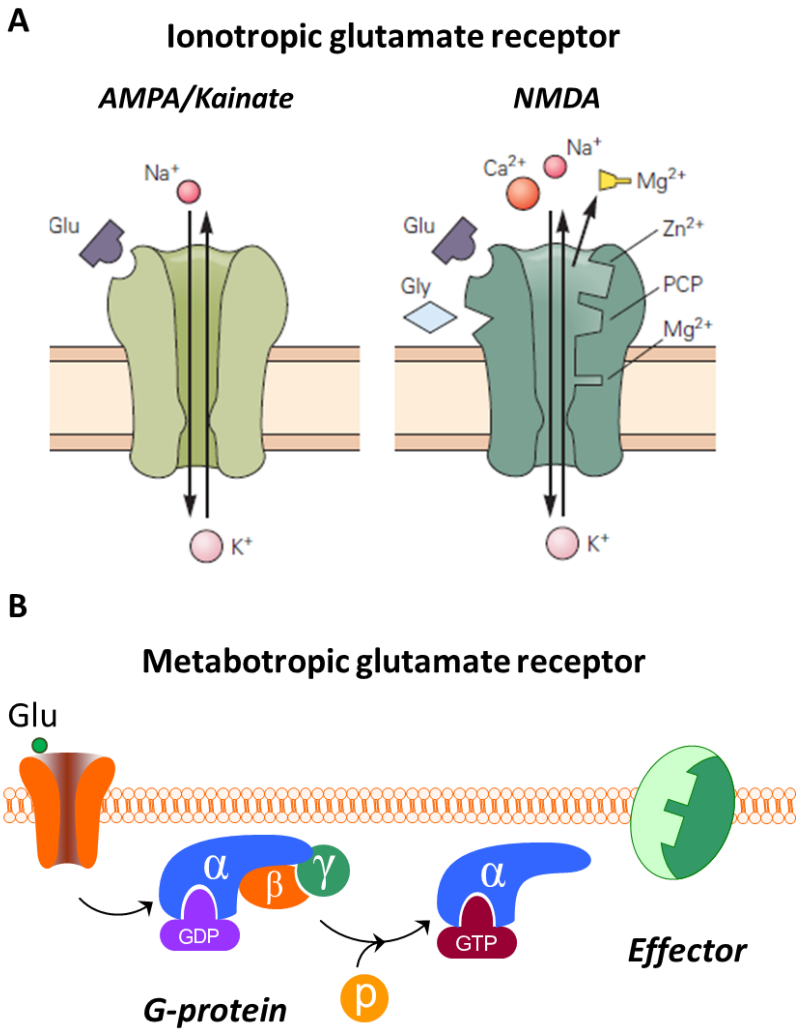

Figure 1.5. Schematic representation of glutamate receptors. A) *Ionotropic glutamate receptors mediate the entrance of positively charged ions in response to ligand-binding. They are the AMPA, kainic acid and NMDA receptors.* ***B)*** *Metabotropic glutamate receptors. This image was modified from Kandel et al., 2012, using the scientific illustration toolkit Motifolio (https://www.motifolio.com/).*

The purinergic ionotropic P2X receptors (P2XRs) bind extracellular ATP released by glial cells or damaged neurons and induce a calcium influx, which have been shown to modulate various processes, including synaptic plasticity (Pankratov et al., 2009).

1.2.3 Store operated Ca^{2+} channels (SOCCs)

Store operated Ca^{2+} channels (SOCCs) are responsible for the influx of calcium in response to ER calcium depletion, in a process called Store Operated Calcium Entry (SOCE). SOCCs are constituted by ORAI protein subunits and interact with Stromal interaction molecule proteins (STIM), which are calcium sensors located in the ER membrane (Brini et al., 2014; Venkiteswaran and Hasan, 2009). When Ca^{2+} is released from the ER, STIM interacts with ORAI to induce calcium influx from the extracellular milieu and together with the sarco-endoplasmic reticular Ca^{2+}-ATPase pump (SERCA) promotes reconstitution of ER Ca^{2+} stores (Venkiteswaran and Hasan, 2009).

1.2.4 Plasma Membrane Ca^{2+} ATPase (PMCA) and Na^{+}/Ca^{2+} exchanger (NCX)

The Plasma Membrane Ca^{2+} ATPase (PMCA) and the Na^{+}/Ca^{2+} exchanger (NCX) are the main mediators of calcium extrusion and are thus responsible for maintaining cytosolic Ca^{2+} at physiological concentrations (Brini and Carafoli, 2011). The PMCA pump is characterised by high affinity but low capacity for Ca^{2+} and is ubiquitously expressed in most cell types. It is a P-type pump able to self-phosphorylate an aspartic residue (D) located within the enzyme and form an intermediate phospho-enzyme with hydrolysed ATP (Brini et al., 2014). PMCA is regulated by a variety of molecules (e.g. ATP and PKC) and interacts with cytoplasmic proteins such as calmodulin, which is able to activate the pump upon binding (Brini and Carafoli, 2011). Defects in PMCA have been associated with a variety of pathologies especially linked to oxidative stress such as brain ischemia and diabetes, or other conditions linked to alteration of neuronal calcium signalling (Brini et al., 2014).

NCX is a low affinity but high capacity calcium channel, which mediates the influx of three Na^{+} ions in exchange for the efflux of one Ca^{2+}, working against the calcium gradient (Blaustein and Lederer, 1999). Three main isoforms have been characterised (NCX1, 2 and 3) and they are all co-expressed in neurons. Interestingly, NCX channels have been shown to work in reverse mode and allow Ca^{2+} entry (and Na^{+} exit) when $[Ca^{2+}]_i$ increases in the low µM range, which is usually the case in neurons during the calcium spikes the accompany synaptic transmission (Blaustein and Lederer, 1999). NCX is hence regulated by both Ca^{2+} and Na^{+} concentrations, but also by other molecules, including ATP, PKC and redox agents (Brini and Carafoli, 2011).

These two proteins work in conjunction, as PMCA is able to mediate calcium efflux even following low increases of calcium, whereas NCX activates only upon large Ca^{2+} variations and is responsible for transporting higher amounts of Ca^{2+} ions.

1.2.5 Ca^{2+} binding proteins

The activation of calcium transport across the plasma membrane and cell organelles is often prompted by cytoplasmic sensors which detect alterations in cytoplasmic calcium levels and in response activate specific signals for either clearance or influx of Ca^{2+} to reconstitute physiological concentrations (Brini et al., 2014). One of the most well characterised sensors is calmodulin (CaM), which is involved in the modulation of PMCA and also VOCCs (James et al., 1998; Lee et al., 1999; Chin and Means, 2000; Catteral and Few, 2008). Upon binding to Ca^{2+}, CaM undergoes prominent conformational changes and re-localisation, binding to other secondary effectors such as Ca/CaM-dependent kinases, AC and phosphatase calcineurin (Chin and Means, 2000; Brini et al., 2014). Other proteins, such as parvalbumin (PV), function as Ca^{2+} transporters or buffers which activate in response to Ca^{2+} rise and modulate its rapid sequestration (Schwaller et al., 2003; Brini et al., 2014). Finally, a family of Ca^{2+} binding proteins particularly expressed in the CNS is that of the Neuronal Ca^{2+} sensors (NCSs), among which NCS-1 is the most described, being involved in the regulation of synaptic plasticity and release of neurotransmitters (McFerran et al., 1998-1999; Tsujimoto et al., 2002; Sippy et al., 2003).

1.3 Neurodegeneration

Neurodegenerative diseases (NDs) are a group of heterogeneous conditions that affect the CNS and are characterised by the progressive deterioration of brain activity and functionality. The pathophysiology and progression of these diseases is extremely complex, especially because they are rarely caused by single factors and indeed they are classified as multifactorial pathologies, where the convergence of several elements, both genetic and environmental, contributes to the disease insurgence and progression (Sheikh et al., 2013; Kovacs, 2016). Although the different diseases present specific characteristics, they share some common features, such as the chronic activation of the immune system leading to prominent neuroinflammation, bioenergetic defects deriving from oxidative stress and mitochondrial dysfunction, and the accumulation of abnormally modified and misfolded proteins, which is the reason why most NDs are also defined as proteinopathies (Sheikh et al., 2013; Kovacs 2016). Here are briefly introduced the most relevant NDs of this PhD project.

1.3.1 Mild cognitive Impairment

Mild cognitive impairment (MCI) is a condition characterised by minor decrease in memory, which on one hand is beyond the expected decline that comes with aging, but on the other hand is not severe enough to be defined as dementia (DeCarli, 2003). While most cognitive functions do not significantly differ from those of healthy controls (CTR), memory deficit is the discriminating factor which allows the distinction between MCI, CTR and subjects affected by mild AD (Petersen et al., 1999). Notably, longitudinal studies have shown that MCI patients are characterised by a more rapid cognitive decline compared to CTR, and a slower rate of decline compared to AD subjects, revealing that they could be considered as a possible phase of transition between normal aging and dementia (prodromal AD) (Petersen et al., 1999; DeCarli, 2003). However, although most MCI patients progress into AD pathology (up to 80% in 6 years from diagnosis), not all of them do and might stabilise as MCI without developing dementia (Petersen et al., 2001).

There is a keen interest in the characterisation and stratification of MCI patients, especially to predict which ones are more likely to convert to AD. This is mainly because any disease modifying drug would be more effective at the early stages of disease as opposed to the treatment of the advanced stages, when it would be too late to positively affect a more

severe and widespread neurodegenerative state (Garcia-Allonza et al., 2009; Das et al., 2001; Blennow et al., 2010).

1.3.2 Alzheimer's Disease

1.3.2.1 General characteristics and aetiopathogenesis

AD is the most common form of dementia in the elderly population and to date, no effective treatment to cure the disease has been developed. According to a report published by the UK Alzheimer's Society in 2014, about 850,000 people were affected with dementia in the UK at the time, and more than 44 million worldwide (Prince et al., 2014). This chronic disease is characterised by a progressive deterioration of cognitive functions, which results in impaired language skills, memory loss and a general deficit in basic skills that affect the person's ability to perform standard daily tasks (Kovacs, 2016). The pathology initiates with neuronal degeneration and synapses loss in the hippocampus, which then spreads to other parts of the brain, leading to cerebral atrophy (Terry et al., 1991). AD is generally classified in two categories: familial AD (fAD) and sporadic AD (sAD). fAD is driven by genetic mutations and is typically characterised by an early onset (before 65 years). Only about 5% of AD cases are of genetic origin, and up to now more than 450 causative mutations have been identified in 3 genes: amyloid precursor protein (*APP*), Presenilin-1 (*PS1*) and Presenilin2 (*PS2*) (https://www.alzforum.org/mutations; April 2018 update). On the other hand, sAD is caused by multiple risk factors, of which Apolipoprotein E (*APOE*) ε4 allele is the most established. Sporadic forms are characterised by a late onset and account for the large majority of all AD cases (Betram and Tanzi, 2005; Blennow et al., 2015). The main hallmark of AD, either familial or sporadic, is the accumulation of two misfolded proteins, namely hyperphosphorylated tau (p-Tau) forming intracellular neurofibrillary tangles (NFT) (Kosik et al., 1986) and Amyloid β (Aβ), which aggregates extracellularly and forms amyloid plaques (Glenner and Wong, 1984). Decades of research on the aetiopathogenesis of AD gave rise to different theories trying to elucidate the mechanisms underlying the insurgence of the disease. One of the most accepted theories is the amyloid cascade hypothesis (Hardy and Selkoe, 2002; Blennow et al., 2015), which postulates that the alteration of Aβ production is the driving factor of AD progression (**Fig. 1.6**). Aβ peptide is formed by cleavage of APP in the N-terminus domain by the β-site APP-cleaving enzyme 1 (BACE1 or β-secretase). This leads to the generation of a soluble N-

terminal fragment (sAPPβ) and a membrane embedded C-terminal fragment (β-CTF or C99). β-CTF is then target of further cleavage by a multi-subunit complex comprising PS1, PS2, Nicastrin, presenilin enhancer (PEN2) and anterior pharynx-defective (APH1), collectively referred to as γ-secretase. This step generates the amyloid Intracellular Domain (AICD) and a series of Aβ peptides of different lengths according to γ-secretase processing, which are released in the extracellular milieu (Blennow et al., 2015). The most studied peptides are $Aβ_{1-40}$, which is the most abundant among the released fragments, and $Aβ_{1-42}$, less present but more prone to aggregation and therefore the main constituent of amyloid plaques (Wang et al., 1996). Overall, the amyloidogenic pathway leads to the formation of a heterogeneous population of Aβ peptides and under pathological conditions, abnormal amounts of Aβ are released, leading to their accumulation and aggregation in amyloid plaques, which differ in composition among patients (Di Fede et al., 2018). Cerebrospinal fluid (CSF) and plasma levels of Aβ ($Aβ_{1-42}/Aβ_{1-40}$ ratio specifically), together with total/p-Tau and Neurofilament Light (NfL) correlate with AD and are used nowadays by clinicians to help with patients' diagnosis (Nakamura et al., 2018; Zetterberg et al., 2019).

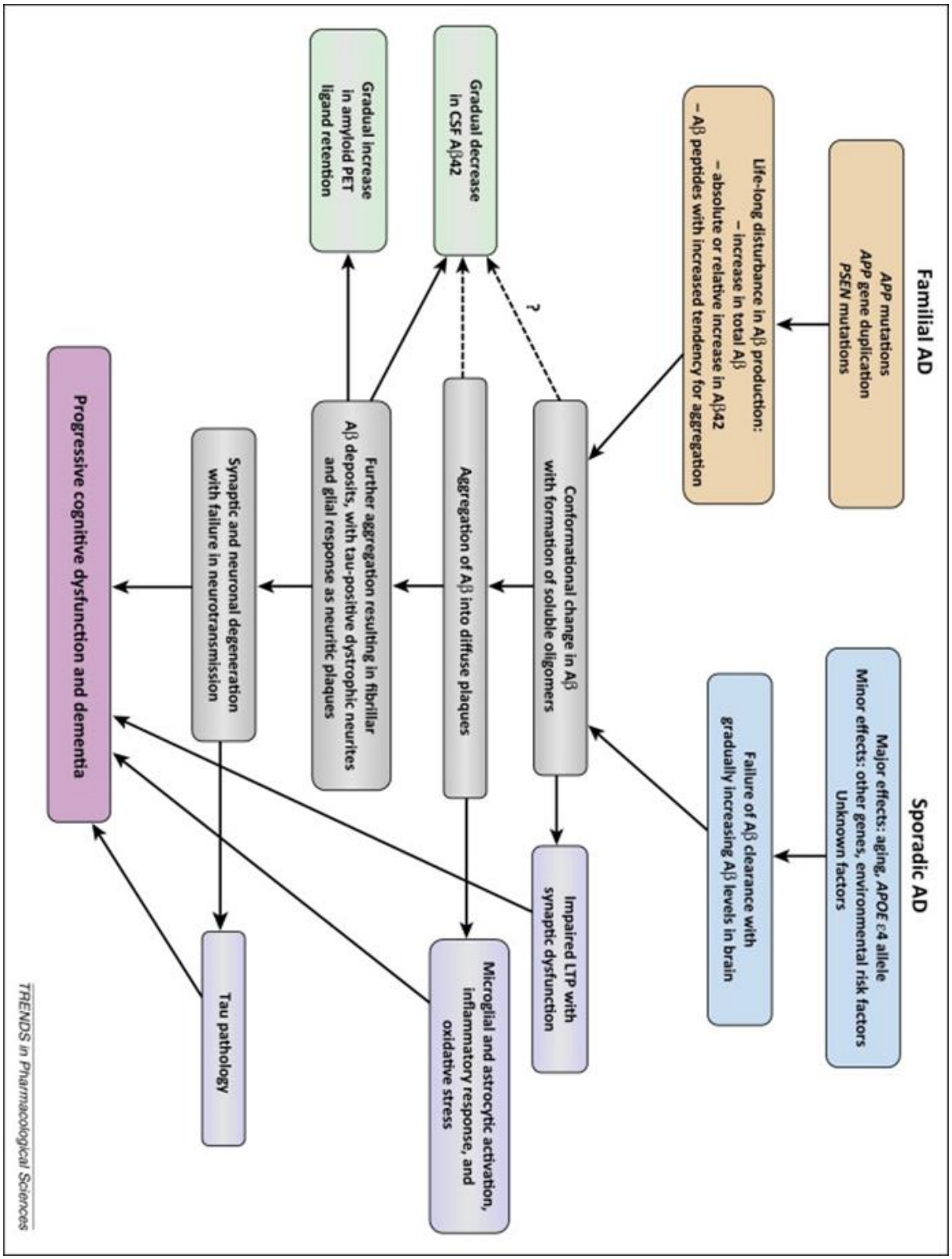

Figure 1.6. The Amyloid cascade hypothesis *(Blennow et al., 2015).*

Although the role of Aβ in AD progression is well documented and there are many evidences of its neurotoxic effect on neuronal functionality (Wang et al., 1996; Lacor et al., 2007), the topic is still widely debated, especially after the discovery that the oligomeric forms of Aβ are more neurotoxic compared to the fibrillary forms (Walsh et al., 2002; Wang et al., 2002; Campioni et al., 2010). Moreover, no correlation has been found between the amount of plaques and the severity of cognitive impairment, as plaques appear several years before clinical symptoms become evident (Dickson et al., 1995; Perrin et al., 2009; Benilova et al., 2012). In this scenario, amyloid plaques could have a beneficial effect by reducing the amount of free oligomers, at least in the initial stages of the pathology, before the activation of an inflammatory response which ultimately would lead to neurotoxicity.

An alternative to the amyloid cascade hypothesis is the "calcium hypothesis", which postulates that the major trigger of neurodegeneration is the dysregulation of Ca^{2+} homeostasis in the brain (Green and LaFerla, 2008; Berridge, 2010). Increased levels of Ca^{2+} have been observed in neurons of AD mouse models, and various groups have theorised that this effect could be mediated by Aβ through formation of new ionic pores, or by interaction with calcium channels like ROCCs and VOCCs, or the promotion of ER stress and consequent leakage of calcium from the intracellular stores (Kawahara and Kuroda, 2000; Mattson et al., 1992; Price et al., 1998; Tu et al., 2006). The two theories are closely related and equally controversial, as the details of the mechanisms underlying the neurodegeneration process have not been completely elucidated.

1.3.2.2 Diagnosis

AD diagnosis in the memory clinics is based on the National Institute of Neurological Disorders and Stroke–Alzheimer Disease and Related Disorders (NINCDS–ADRDA) criteria (McKhann et al., 1984; Dubois et al., 2007). These consist in a multidisciplinary approach which relies on cognitive assessments together with well-established biomarkers (Blennow et al., 2010). The main criteria are as follow:

- Presence of a memory impairment lasting for at least 6 months, verified by objective tests, such as the widely used Mini-Mental State Examination (MMSE) (Folstein et al., 1975)
- Measurement of medial temporal lobe atrophy (in the hippocampus, entorhinal cortex or amygdala) by Magnetic resonance imaging (MRI) (Frisoni et al., 2009).
- Positive CSF biomarkers (low $A\beta_{1-42}$, high total/p-tau), generally assayed by ELISA

- Positron Emission Tomography (PET) measuring either an increased binding of Aβ ligands (e.g. ^{11}C-labeled Pittsburgh compound B, C-PiB) or a reduced glucose metabolism in bilateral temporal parietal regions
- Presence AD-causing mutation (fAD)

Although these criteria are commonly accepted, research has been focused on the identification of less invasive biomarkers, such as blood-derived biomarkers (Zetterberg and Burnham, 2019). Among these, plasma levels of NfL, as well as circulating microRNAs and extracellular vesicles (EVs) have been characterised.

1.3.3 Frontotemporal Lobar Degeneration

1.3.3.1 General characteristics and aetiopathogenesis

Frontotemporal lobar degeneration (FTLD) is a term comprising a heterogeneous group of neurodegenerative disorders, which differ at the genetic, molecular and clinical level and develop a clinical condition defined as Frontotemporal dementia (FTD). FTD is the second most represented dementia after AD that affects subjects younger than 65 years of age (Ratnavalli et al., 2002). The pathology is characterized by focal atrophy of the frontal and temporal lobes of the cerebral cortex, leading to the progressive decline of functions associated with these areas (Ratnavalli et al., 2002; Ikeda et al., 2004; Seelaar et al., 2011). Specifically, the disease can be classified in two subcategories according to the brain regions that are mostly affected by atrophy and the predominant clinical symptoms: behavioural variant (bvFTD) and primary progressive aphasia (PPA). bvFTD, where the frontal lobe is mainly affected, is characterised by changes in behaviour and personality, while PPA, distinguished by the impairment of language and comprehension skills, presents greater atrophy in the temporal lobes. PPA can be further divided in progressive non-fluent aphasia (PNFA) and semantic dementia (SD) according to the specific atrophied lobar region and language impairment (Neary et al., 1998; Gorno-Tempini et al., 2011; Rascovsky et al., 2011). Another classification of FTD is based on neuropathological features, specifically on the composition of the aggregates that characterise protein deposition. Indeed, similarly to other proteinopathies, also FTD is associated with the aggregation of abnormally modified proteins and specifically four different kind of inclusions have been described: Tau, transactivator regulatory DNA binding protein (TDP-43), Fused in sarcoma (FUS) and ubiquitin proteasome system (UPS)-positive inclusions, which refer to unknown

ubiquitinaded proteins. In the case of no detectable inclusions, the terminology FTLD-ni have been used (Mackenzie et al., 2010).

Up to 50% of FTD cases have been associated with a family history of disease, suggestive of a strong genetic background (Rademakers and Rovelet-Lecrux, 2009) and to date three main causative genes have been identified for familial FTD (fFTD): *MAPT,* progranulin (*GRN*) and chromosome 9 open reading frame 72 *(C9orf72*). Additionally, genes variants associated with an increased risk of developing FTD have been identified, including TDP-43 (*TARDP*), Ubiquilin 2 (*UBQLN2*), triggering receptor expressed on myeloid cells 2 *(TREM2*), *FUS* and Sequestosome 1 (*SQSTM1*) (Goldman et al., 2007; Rademakers et al., 2012; Rubino et al., 2012; Borroni et al., 2014). However, the majority of cases is still sporadic (sFTD), without a clear genetic cause (Rademakers and Rovelet-Lecrux, 2009).

1.3.3.2 Diagnosis

The diagnosis of FTD is particularly challenging because of the wide heterogeneity of the diseases which, although characterised by some specific features, often present overlapping phenotypes (Mackenzie and Neumann, 2016). Diagnosis is generally performed by a multidisciplinary team according to international guidelines (Neary et al., 1998; Gorno-Tempini et al., 2011; Rascovsky et al., 2011) relying on neuropsychological tests, imaging studies and circulating biomarkers. In general, the identification of clear blood or CSF biomarkers specific for FTD subtype has not been achieved (Carecchio et al., 2011; Oeckl et al., 2016). Notably, for FTD patients carrying specific mutations in *GRN*, which account for the majority of fFTD, CSF and plasma levels of progranulin (PGRN) were able to predict the disease with a specificity and sensitivity of 100% (Ghidoni et al., 2008).

1.4 Transglutaminases: a multi-faceted family of enzymes

1.4.1 Transglutaminases family: background information

Transglutaminases (TGs) (EC 2.3.2.13) are a family of Ca^{2+}-dependent enzymes that catalyse the post-translational modification (PTM) of target proteins through the transamidation of available glutamine residues (Greenberg et al., 1991). This reaction mainly results in the formation of inter- and intramolecular Nε(γ-glutamyl)-lysine (EGGL) isopeptide bonds or crosslinks, which are covalent, stable and resistant to proteolysis (Folk and Finlayson, 1977). Specifically, a cysteine residue (Cys) located in the enzyme catalytic core binds the γ-carboxamide group of a peptide-bound glutamine residue (Gln) (acyl donor) through the nucleophilic active thiolate group (SH). This generates a thioester intermediate formed by TG and the acyl donor substrate, with release of ammonia. The first reaction is followed by TGs-mediated transfer of the acyl intermediate to an acyl acceptor, such as the ε-amino group of a peptide-bound lysine residue (Lys), which results in the restoration of the TGs thiol group and the formation of a EGGL isopeptide bond or crosslink (**Fig. 1.7A**). TGs catalytic activity may also mediate the incorporation of primary amines (monoamines and polyamines) into the γ-carboxamide group of peptide-bound Gln (**Fig. 1.7B,C**) (Folk et al., 1969; Greenberg et al., 1991, Lorand and Graham, 2003). These reactions lead to changes in protein conformation and induce the formation of rigid and insoluble supramolecular structures (Aeschliman, 1994, Folk and Finlayson, 1977). TGs catalytic activity is a finely regulated process that involves multiple factors, i.e. calcium, redox conditions and purine nucleotide binding (Demeny et al., 2015).

The TGs family consists of nine members, eight of which are catalytically active in humans: TG1 (cheratinocyte TG), TG2 (tissue or type-2 TG), TG3 (epidermal TG), TG4 (prostatic TG), TG5 (or TGX), TG6 (or TGY), TG7 (or TGZ), coagulation Factor XIIIa subunit (plasma TG) and the inactive band 4.2 protein (Grenard et al., 2001, Sárvári et al., 2002). TGs activity has been implicated in several phenomena of cell biology, including cell proliferation, differentiation and death, extracellular matrix assembly, and also complex physiological processes like blood coagulation, sperm immunosuppression and keratinocyte barrier function (summarised in **Table 1.1**) (Aeschliman, 1994, Chen and Mehta, 1999, Martin et al., 2013, Nemes and Steinert, 1999, Sárvári et al., 2002).

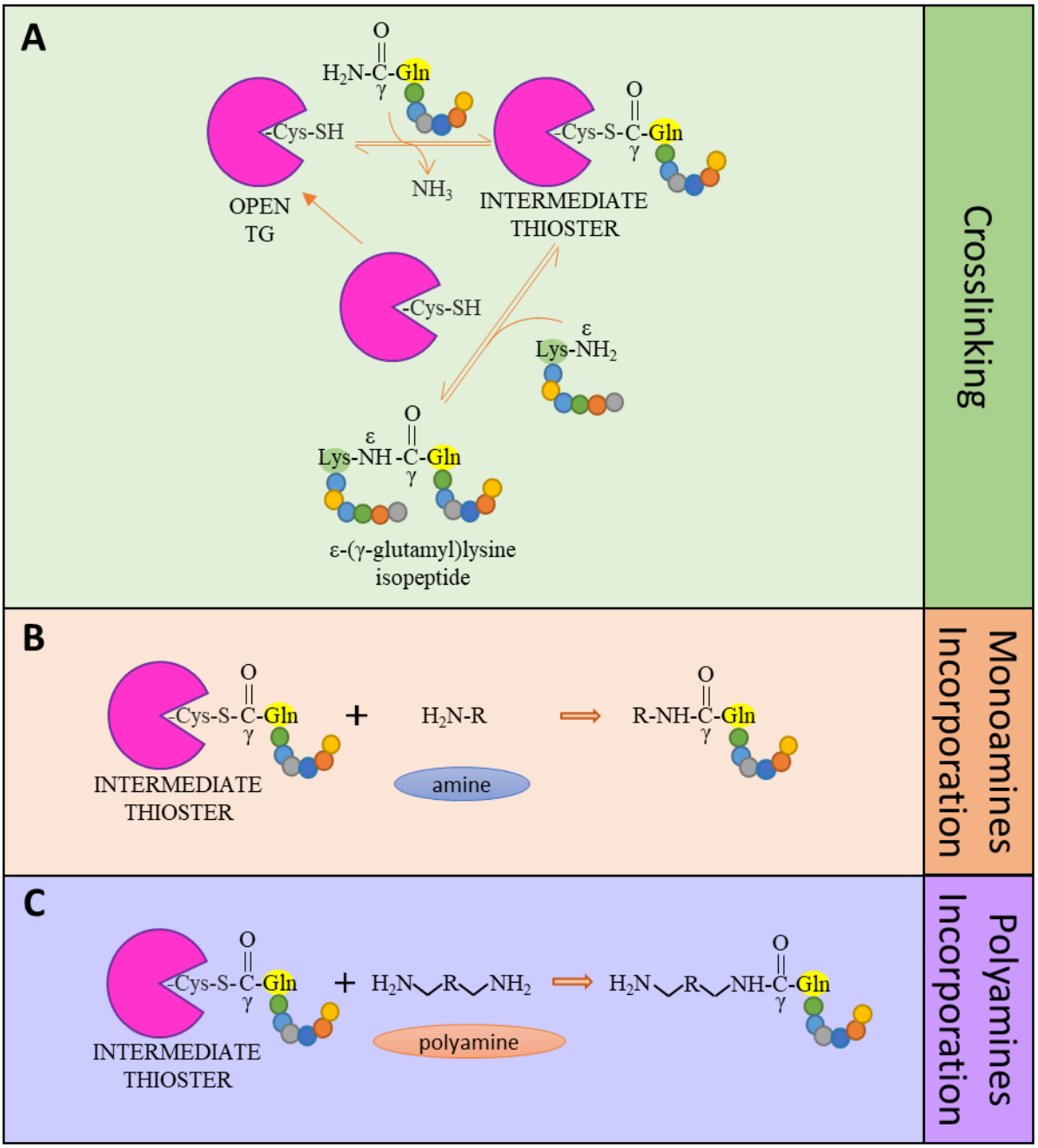

Figure 1.7. Transamidation reactions catalysed by transglutaminases. A) *Transamidation leading to the formation of a crosslink.* ***B)*** *Transamidation leading to incorporation of a monoamine and* ***C)*** *polyamine into a peptide-bound glutamine residue. This image was modified from Savoca et al., 2018.*

Table 1.1. General features of TGs *(Mehta and Eckert, 2005; Furutani and Kojima, 2015; Lorand and Iismaa, 2019)*

Protein	***Main functions***	***Localisation (organ)***	***Disease***
TG1	Formation of the cornified envelop (keratinocytes)	PM, cytosol (brain, epidermis)	Lamellar Ichthyosis (TG1 deficiency)
TG2	ECM stabilisation, cell adhesion, apoptosis and autophagy regulation, cell survival signalling	PM, cytosol, ER, nucleus, autophagosome, endosome, mitochondria, ECM (ubiquitous)	Celiac disease (TG2 autoantigen), tissue fibrosis (TG2 overexpression-hyperactivity)
TG3	Formation of the cornified envelop (keratinocytes)	PM (epidermis, hair follicles, brain)	Uncombable hair syndrome (TG3 deficiency), dermatitis herpetiformis and celiac disease (TG3 autoantigen)
TG4	Plug formation in rodents	ECM, seminal vesicle fluid (prostate gland)	Reduced fertility (TG4 deficiency), Autoimmune polyglandular syndrome type 1 (TG4 autoantigen), prostate cancer progression
TG5	Formation of the cornified envelop (keratinocytes)	PM, cytosol (skeletal muscle, epidermis)	Acral peeling skin syndrome (TG5 deficiency)
TG6	Neurogenesis	Unknown (brain and epidermis)	Gluten ataxia and gluten axonal neuropathy (TG6 autoantigen), Spinocerebellar ataxia-35 (TG6 mutation)
TG7	Unknown	Unknown (Testis and lung)	Unknown
FXIIIa	Blood clotting, bone matrix stabilisation, would healing	ECM, PM, cytosol (blood)	Bleeding disorders (FXIII deficiency and autoantigen)
Band 4.2	Structural role in erythrocytes cytoskeleton	PM, cytosol (erythrocytes)	Hereditary spherocytosis type 5 (band 4.2 deficiency)

PM: Plasma membrane; ER: Endoplasmic reticulum; ECM: Extracellular matrix.

1.4.1.1 Transglutaminase 1 (TG1)

TG1 is involved in the differentiation and cornified envelope formation of keratinocytes and it is mainly expressed in the granular layer of the epidermis and upper digestive tract. TG1-mediated crosslinking of envelope proteins is in fact responsible for the keratinization process (Steinert and Marekov, 1995). TG1 is localised in the cytoplasm but also at the plasma membrane, and it is released as 10, 33, 66 kDa fragments (Kim et al., 1995). Mutations of the TG1 gene (*TGM1*) resulting in TG1 decrease cause Lamellar Ichthyosis, an

autosomal recessive skin disorder characterised by the aberrant cornification of the epidermis (Candi et al., 1998; Huber et al., 1995; Cserhalmi-Friedman et al., 2001).

1.4.1.2 Transglutaminase 3 (TG3)

TG3 is mainly expressed in the epidermis, brain and hair follicles, where it plays a central role in hair fiber morphogenesis by catalysing the crosslinking of keratin intermediate filaments and trichohyalin, which hardens the inner root sheath of hair follicles (Hitomi et al., 2003; Hitomi et al., 1999; Hitomi et al., 2001). In the late stages of keratinocytes differentiation, TG3 participates to the formation of the cornified envelope (John et al., 2012). Mutations in this gene (*TGM3*) are associated with a reduction in skin barrier function and impairment in hair development (Bognar et al., 2014; John et al., 2012).

1.4.1.3 Transglutaminase 4 (TG4)

TG4 is mainly found in the prostate gland, seminal plasma, prostatic fluids and prostate cancer cells (Grenard et al., 2001; Williams-Ashman et al., 1977). Decreased expression of TG4 is associated with prostate cancer, and the presence of variants generated by alternative splicing have been described in prostate cancer tissues (Cho et al., 2010). TG4 is involved in epithelial–mesenchymal transition (EMT) in prostate cancer cells and has been shown to interact with ECM proteins (Jiang and Ablin, 2011; Cho et al., 2010).

1.4.1.4 Transglutaminase 5 (TG5)

TG5 is mostly present in skeletal muscle cells, foreskin keratinocytes and the lining of epithelial barrier (Cassidy et al., 2005). Mutations in TG5 (*TGM5*) lead to skin peeling syndrome. Similarly to TG1 and TG3, TG5 participate to the crosslinking of envelope proteins in the epidermis (Candi et al., 2002; Candi et al., 2001).

1.4.1.5 Transglutaminase 6 (TG6)

Although TG6 localisation was initially thought to be mainly found in skin, testis and lung, more recently its presence and activity have been prevalently associated with the CNS, where it is involved in neurogenesis (Thomas et al., 2013; Schulze-Krebs et al., 2016). Mutations in the TG6 gene (*TGM6*) are associated with a rare autosomal-dominant form of familial ataxia, i.e. Spinocerebellar ataxia type 35 (SCA35) (Tripathy et al., 2017). Moreover, autoantibodies to TG6 has been identified in patients affected by gluten ataxia

(Hadjivassiliou et al., 2008; Hadjivassiliou et al., 2013). This is suggestive of a vital role for TG6 in cortical and cerebellar neurons (Thomas *et al.*, 2013).

1.4.1.6 Transglutaminase 7 (TG7)

TG7 is the less known member of the TGs family. It is ubiquitously expressed, with a predominance to testis and lung (Mehta and Eckert, 2005). Elevated mRNA levels of TG7, together with TG2 and TG3, have been associated with poor prognosis in breast cancer patients (Jiang et al., 2003).

1.4.1.7 Factor XIII (FXIII)

Factor XIII, also called plasma TG, is a component of the blood coagulation cascade (Lorand et al., 1993; Lorand and Graham, 2003). It is mainly present in platelets, macrophages and blood, but has also been reported in other compartments, such as brain (astrocytes), placenta, eyes, heart and osteoblasts (Eckert et al., 2014). FXIII is a heterotetramer consisting of two A and two B subunits (A2B2), where the A dimer contains the catalytic core, while the B dimer functions as a carrier for A. The enzyme is activated by thrombin-mediated cleavage, which removes the N-terminal activation peptides and leads to the dissociation of the A and B dimers, and consequent activation of A (FXIIIa) (Muszbek et al., 2011). Fibrin, which is a substrate of FXIIIa transamidation in the clotting system, as well as a target of other TGs, has been reported to be involved in FXIIIa activation process (Hethershaw et al., 2018). Inherited FXIII deficiency is an autosomal recessive disorder characterised by reduced FXIIIa, which leads to defective wound healing and excessive bleeding (Anwar et al., 1995).

1.4.1.8 Erythrocyte membrane protein band 4.2 (Band 4.2)

Band 4.2 is the only member of the TGs family without a catalytic activity. This is because the Cys catalytic residue which is conserved in the other TGs and is responsible for the catalytic activity (as shown in **Fig. 1.7**), in Band 4.2 is substituted by an alanine residue (Ala) (Sung et al., 1990). Band 4.2 is mainly expressed in erythrocytes, fetal liver, bone marrow and spleen and primarily localises at the plasma membrane, where it is involved in the maintenance of the membrane integrity and regulation of cell stability (Mehta and Eckert, 2005). In red blood cells, Band 4.2 has been shown to bind to the N-terminal domain of

band 3 (B3, also known as red-cells anion exchanger) and also interact with ankyrin (Bennett and Stenbuck 1980; Korsgren and Cohen, 1986).

1.4.1.9 Transglutaminase 2 (TG2)

Transglutaminase 2, also called tissue or type-2 transglutaminase, is the most extensively studied member of the TGs family. With a molecular weight (MW) of approximately 78 kDa, this enzyme is ubiquitously expressed and it is mainly defined by its Ca^{2+}-dependent transamidating activity (Mycek et al., 1959). Moreover, TG2 is known for its ability to catalyse the hydrolysis of target glutamine residues (deamidation) (Mycek et al., 1960), e.g. gluten peptides, which has been linked to the development of the gluten-induced enteropathy called celiac disease (CD) (Dieterich et al., 1997; Molberg et al., 1998). Other targets of TG2 hydrolysis are guanosine triphosphate (GTP) and adenosine triphosphate (ATP) (GTPase and ATPase activity). Less characterised functions of TG2 are disulphide isomerase activity and protein kinase activity (Savoca et al., 2018).

At the transcriptional level, TG2 gene (*TGM2*) is modulated by multiple regulatory factors which directly interact with its promotor, such as interleukin-6 (IL6), retinoic acid response, transforming growth factor β1 response element (TGF-β1) and two AP2-like response elements (Eckert et al., 2014). Furthermore, a number of additional factors have been reported to affect TG2 levels, including tumour necrosis factor (TNF), chemokines, cytokines, epidermal growth factor (EGF) and nuclear factor kappa-light-chain-enhancer of activated B cells (NF-κB) (Eckert et al., 2014; Nurminskaya and Belkin, 2012).

1.4.1.9.1 TG2 isoforms

Four different isoforms of TG2, generated by alternative splicing, have been identified to date: TGM2_V1 (canonical full length), TGM2_V2 (short), TGM2_V3 (very short) and TGM2_V4 (a and b, deleted forms) (Phatak, et al. 2013). TGM2_V2 and TGM2_V3 derive from an intron retention which results in an altered and truncated C-terminus. Specifically, TGM2_V2 is a 548 amino acids long protein with MW of ~62 kDa, whereas TGM2_V3 is a 349 amino acids long protein with a predicted MW of ~38 kDa (Fraij, et al. 1992, Fraij and Gonzales 1996, Antonyak, et al. 2006). TGM2_V4 (a and b) derive by atypical splicing which results in a variation of the C-terminal without affecting the protein MW (Lai, et al. 2007). These alterative isoforms lose the GTP-binding domain located at the C-terminal, and for this reason they are predicted to constitutively active (Begg, et al. 2006). Even though they

have been detected in a variety of cells, either at the transcript or protein level (e.g. astrocytes, neurons, endothelial and vascular smooth muscle cells (Nurminskaya and Belkin, 2012), not much is known yet about their functions. Notably, some works have reported a possible role in cancer progression (Phatak, et al. 2013) and kidney fibrosis (Burhan, et al. 2016).

1.4.1.9.2 TG2 protein

TG2 secondary structure consists of four globular domains (**Fig. 1.8**) (Mehta et al., 2010). The N-terminal β-sandwich domain (aa 1-139), which contains the fibronectin (FN) binding site. The core domain (aa 140-460), which is responsible for TG2 transamidation activity, includes the catalytic triad, cysteine-histidine-aspartic acid [Cys(277)-His(335)-Asp(358)] and two tryptophan residues [Trp(241) and Trp(332)], which participate to the stabilisation of the intermediate thioester. The two C-terminal β-barrel domains (aa 461-586 and 587-687) are involved with ATP/GTP binding (Nurminskaya and Belkin, 2012).

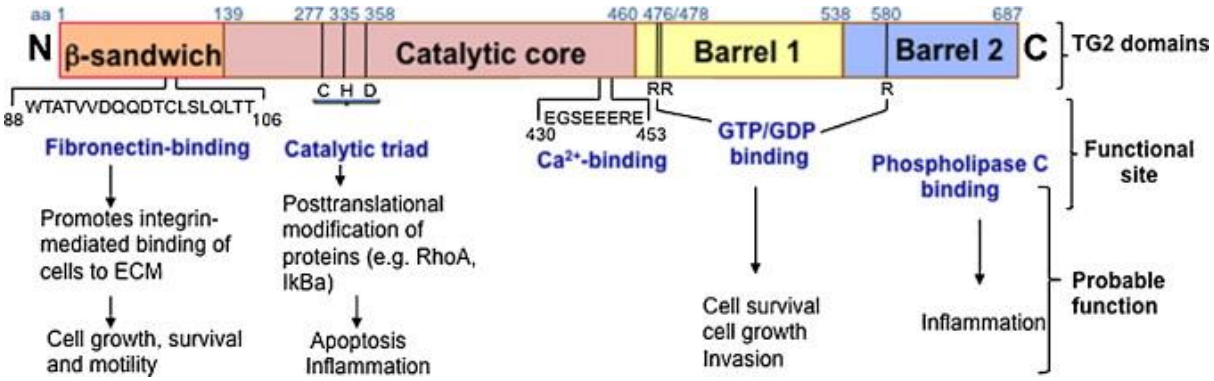

Figure 1.8. Structural representation of TG2 *(Mehta et al., 2010).*

1.4.1.9.3 Regulation of TG2 catalytic activity

TG2 activity is regulated by three main factors: Ca^{2+}, GTP binding and redox environment. Ca^{2+} promotes the allosteric activation of TG2 by binding to specific bindings sites, which acts in a cooperative manner and promote an open conformation of the enzyme (Bergamini et al., 1988; Casadio et al., 1999; Kiraly et al., 2009). Equally important for the modulation of TG2 activity is the binding to GTP, which has an inhibitory effect and promotes a closed conformation (Achyuthan et al., 1987; Bergamini et al., 1987). Intracellularly, where under

physiological conditions Ca^{2+} concentration is low (100-200 nM) and GTP concentration is high (100-150 µM), TG2 is mostly inhibited. Extracellularly, where calcium levels are in the mM range, GTP binding is inhibited and TG2 can be activated (Achyuthan et al., 1987; Bergamini et al., 1987; Casadio et al., 1999). However, if the Cys thiol group in TG2 catalytic core is oxidised, TG2 is catalytically inactive even at high Ca^{2+} concentrations (Stamnaes et al., 2010). It is now believed that TG2 continuously shifts between three distinct conformations: closed and GTP-bound (inactive), open and Ca^{2+}-bound but oxidised (inactive) and open, Ca^{2+}-bound and reduced (active) (Jin et al., 2011) (**Fig. 1.9**).

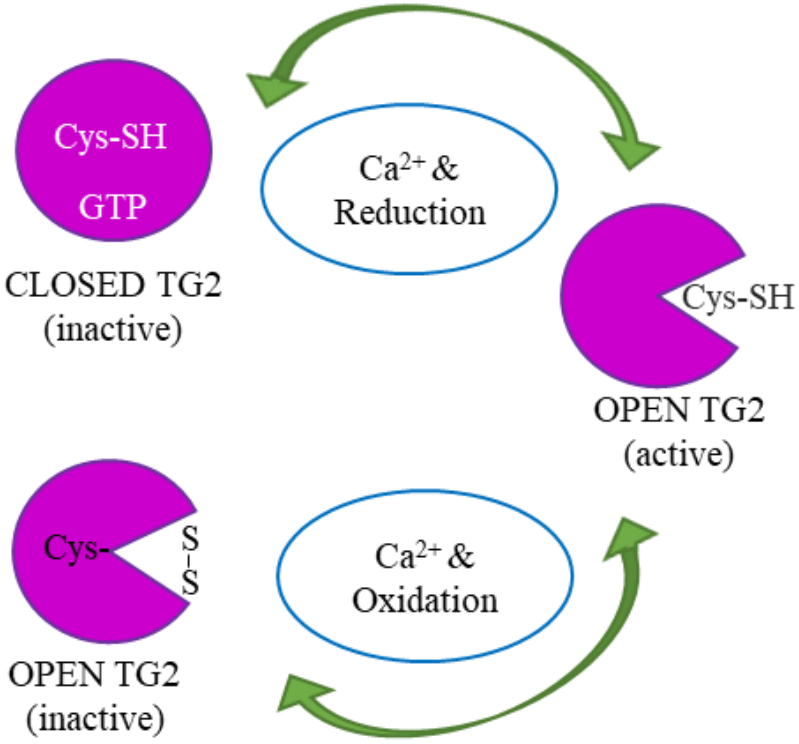

Figure 1.9. Effect of calcium, GTP and redox conditions on TG2 conformation and activity. *This image was modified from Savoca et al., 2018.*

1.4.1.9.4 TG2 localisation

Cytoplasm: TG2 has been identified in the cytoplasm of numerous cell lines, where it is believed to be mostly inactive due to low Ca^{2+} and high GTP levels (Nurminskaya and Belkin, 2012). However, under pathological conditions such as oxidative stress, Ca^{2+} dysregulation and excitotoxicity, TG2 could be activated and crosslink endogenous intracellular substrates (Nurminskaya and Belkin, 2012; Walther et al., 2011). Cytoplasmic TG2 has been shown to interact with small GTPases, such as RhoA and Rac, modulating their activity by serotonylation (Walther et al., 2003; Walther et al., 2011) and also in an activity-

independent manner (Kim et al., 2010). Notably, overexpression of TG2 GTP-binding defective forms in fibroblasts was shown to promote apoptosis independently from TG2 activity (Datta et al., 2007), thus revealing that TG2 could have multiple additional functions independently from its activation state.

Mitochondria: TG2 expression has been detected in mitochondria especially in response to apoptotic signals (Piacentini et al., 2002). The analysis of neuroblastoma cells has revealed that almost 50% of the total cellular TG2 was located in mitochondria (Rodolfo et al., 2004; Piacentini et al., 2002), specifically interacting with both outer and inner membrane (Park et al., 2010). Notably, TG2 has been shown to be involved in BAX translocation to mitochondria and indirectly modulate the release of cytochrome c, thus inducing the apoptotic pathway (Yoo et al., 2012; Rodolfo et al., 2004). Moreover, mitochondrial substrates of TG2 transamidation have been identified *in situ* under apoptotic stimuli (Park et al., 2010; Sarang et al., 2009). In physiological conditions, TG2 was shown to contribute to the correct assembly of respiratory complexes at the mitochondrial level *in vivo,* by its disulphide isomerase activity, and lack of TG2 in TG2 KO mice caused energy impairment (Mastroberardino et al., 2006; Malorni et al., 2009).

Nuclear TG2: Nuclear TG2 accounts for about ~5-7% of total intracellular TG2 (Nurminskaya and Belkin, 2012). Translocation of TG2 to nucleus is usually driven by a variety of stress stimuli, including $[Ca^{2+}]_i$ increase, retinoic acid, VEGF and hypoxia (Dardik and Inbal, 2006; Balajthy et al., 2006; Filiano et al., 2008). The mechanism regulating this localisation change is not yet clear, although the interaction with a nuclear transporter (Importin-α3) has been proposed (Peng et al., 1999). One of the most commonly known effects of nuclear TG2 is the regulation of transcription factor SP1. TG2-mediated crosslinking of SP1 was shown to inhibit SP1 and consequently affect the expression of c-Met, which resulted in the activation of caspase-mediated apoptosis (Tatsukawa et al., 2009; Tatsukawa and Kojima, 2010). Another possible effect of nuclear TG2 is the PTM of histone proteins. Indeed, several histones (e.g. H2A, H2B, H3 and H4) have been described as substrates of TG2 transamidation both *in vitro* and *in vivo*, suggesting a possible role in apoptosis-induced condensation of chromatin (Ballestar et al., 2001; Ballestar et al., 1996).

Extracellular TG2: Extracellular TG2 has been mostly associated with the PTM of ECM proteins, such as FN, osteonectin, osteopontin, laminin, vitronectin, fibrinogen and

collagen (Savoca et al., 2018). The most prominent effect of TG2-mediated crosslinking is a general stabilisation and stiffening of the ECM structure (Folk and Finlayson, 1977; Johnson et al., 1999; Chau et al., 2005; Jones et al., 2006), which however can degenerate to excessive levels in conditions like tissue fibrosis. Indeed, several disorders have been described where the increase of extracellular TG2 was involved in aberrant ECM transamidation and fibrosis progression, such as in kidney (Johnson et al., 1999; Johnson et al., 1997; Johnson et al., 2003; Burhan et al, 2016), lung (Griffin et al., 1979; Richards et al., 1991; Oh et al., 2011; Olsen et al., 2011), liver (Mirza et al., 1997; Grenard et al., 2001; Tatsukawa et al., 2017) and heart (Small et al., 1997; Shinde et al., 2017; Wang et al, 2018). Among all TG2 substrates, FN is one of the most well characterised, and it is known to also directly interact with TG2 thanks to a FN binding site present in TG2 N-terminal domain (Jeong et al., 1995; Hang et al., 2005). Via this interaction, TG2 has been shown to form adhesive complexes and promote cell adhesion by acting as a bridge between FN and syndecan-4, a cell surface heparan sulfate proteoglycan (HSPG) (Verderio et al., 2003; Telci et al., 2008). Furthermore, by functioning as an integrin co-receptor, TG2 was shown to support integrin-dependent cell adhesion, thus revealing an important function as a structural adhesive protein in the ECM (Lortat-Jacob et al., 2012; Wang et al., 2012; Teesalu et al., 2012).

1.4.2 TGs role in the CNS: physiological functions in the brain

TGs activity was first detected in the giant cholinergic neurons of *Aplysia californica* (Ambron and Kremzner, 1982), then in other neuronal cells such as rat cerebellar granule neurons (Perry et al., 1995) and rat cultured astrocytes (Monsonego et al., 1997) and generally in various areas of mammalian CNS and peripheral nerves, human brain included (Hand et al., 1993, Kim et al., 1999).

A substantial amount of evidence suggests that TGs may have a role in numerous and diverse processes in neurons. TG2 was and still is the most well characterized TGs in the nervous system; in 1986, Maccioni and Seeds reported a prominent role for TG2 in microtubule assembly, showing its involvement in neurite outgrowth during morphological differentiation of neuroblastoma cells (Maccioni and Seeds, 1986), which was confirmed in primary samples, consolidating the hypothesis that TG2 may be involved in brain development (Bailey and Johnson, 2004). Different studies also propose a possible involvement of TG2 in processes that are crucial for dendrite and axon formation, such as

the stabilization of focal adhesions (Perry et al., 1995) and cytoskeletal stabilization (Maccioni and Seeds, 1986). Furthermore, TG2 ability to crosslink proteins involved in cytoskeletal motility and shape, such as neurofilaments, actin and vimentin, suggest its potential effect on cell functions and survival (Clement et al., 1998, Nemes et al., 1997, Selkoe et al., 1982). As confirmation of this hypothesis, TG2 is activated in apoptotic cells (Fesus, 1993, Melino and Piacentini, 1998) and its overactivation in neurons leads to impaired mitochondrial respiration and oxidative stress and may be thus instrumental for the induction and/or execution of apoptosis (Piacentini et al., 2002, Piacentini et al., 2005). Moreover, the co-immunoprecipitation of histone 2B with tissue-TG in apoptotic SK-N-BE neuroblastoma cells, together with the evidence that some core histones react with TG2, infers that TG2 may be involved in chromatin condensation during apoptotic cell death (Ballestar et al., 1996, Piredda et al., 1999).

Kim and colleagues did not limit their analysis to TG2 and demonstrated the presence of multiple functional TGs in human brain tissues, with TG2 as the most abundant enzyme, followed by TG1 and lesser amounts of TG3 (Kim et al., 1999). Interestingly, they gave evidence of differential expression of these TGs enzymes in different regions of the brain, giving rise to a more complex view of TGs action in the brain (Kim et al., 1999).

Wilhelmus and colleagues have published many papers about TGs role in the brain, especially their possible involvement in neurodegeneration, as shown in their most recent review (Wilhelmus et al., 2014). They demonstrated that TG1 is localised in the cytoplasm of grey matter's neurons, in astrocytes and microglial cells of the neocortex's white matter, while TG2 was observed in both cytoplasm and nucleus of neurons in the neocortex, in white matter's astrocytes, in capillaries and other parenchymal vessels (Wilhelmus et al., 2009).

1.4.3 TGs involvement in neurodegeneration

The first studies implicating a possible role of TGs in neurodegeneration date back to 1982, when Selkoe and colleagues demonstrated that both neuronal (NF) and glial filaments (GFA) isolated from normal and AD brains were substrates of TGs crosslinking activity (Selkoe et al., 1982). Several experimental data have been published since then, suggesting the involvement of TGs in the deposition of protein aggregates in NDs; however, they do not indicate whether aberrant TG activity is directly responsible for the disease's

progression (Iannaccone et al., 2012, Martin et al., 2013) (**Fig. 1.10**). The strongest supporting evidence for this hypothesis comes from studies on AD, PD and HD.

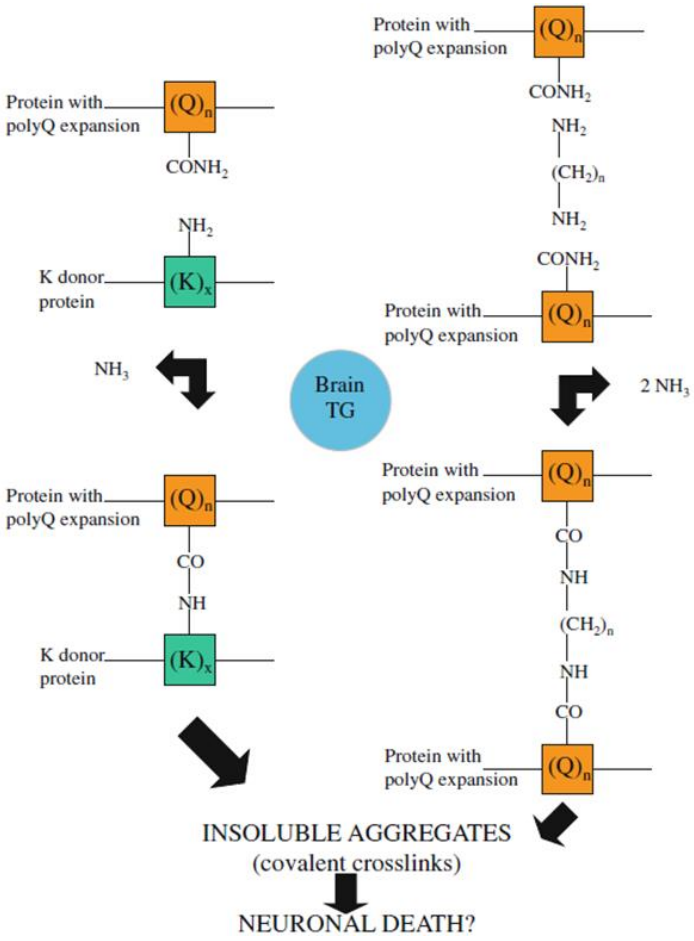

Figure 1.10: Possible mechanisms responsible for protein aggregate formation catalysed by TGs *(Martin et al., 2013).*

1.4.3.1 TGs in AD

AD is characterized by the formation and deposition of stable insoluble protein complexes, in particular amyloid-β and tau protein, which lead to microglia activation, neuroinflammation and neurodegeneration. The catalytic activity of TGs clearly represents one of the possible factors that come into play during the disease pathological progression. The demonstration that TG2 is implicated in Aβ oligomers generation/modulation in vitro is only one part of the substantial evidence that support this hypothesis (Benilova et al., 2012, Hartley et al., 2008). Starting from Selkoe work in 1982 (Selkoe et al., 1982) and going forward with later reports, many papers have been published on this topic, all demonstrating that TGs RNA expression, activity and protein levels are significantly

elevated in AD patients compared to controls, e.g. in the prefrontal cortex (Citron et al., 2001, Johnson et al., 1997, Kim et al., 1999) and CSF (Bonelli et al., 2002, Nemes et al., 2001) (**Table 1.2**). TG2 was found to be co-localised with tau in neurofibrillary tangles (NFTs) (Citron et al., 2001) and with Aβ in amyloid plaques (Zhang et al., 1998b) as shown in **Fig. 1.11A-B**. Interestingly, Wilhelmus and colleagues demonstrated that also TG1 is expressed in both NFTs and senile plaques (SPs), while TG2 can be additionally found in cerebral amyloid angiopathy (CAA) (de Jager et al., 2015, Wilhelmus et al., 2009). Notably, Citron and colleagues also detected the presence of TG2 short isoform transcript (i.e. TG2_V2) in AD brains, whereas this was absent in healthy normal controls (Citron et al., 2001; Citron et al., 2002).

As mentioned previously, a relevant pathophysiological mechanism of AD is the inflammatory response mediated by microglial cells and astrocytes and their subsequent proliferation (Sárvári et al., 2002). Oxidative damage inflicted to cells by activated microglia causes elevation of intracellular calcium, resulting in the activation of TGs and cell death signalling (Basso and Ratan, 2013, Caccamo et al., 2012). Moreover, TG2 expression is upregulated by inflammatory cytokines such as TNFα, IL-6 and TGFβ, which are also dramatically upregulated in AD (Ikura et al., 1994, McGeer and McGeer, 1998).

Table 1.2. Detection of TG2 protein and activity in CSF reported in the literature.

Cerebrospinal Fluid (CSF)			
Variable quantified	**Method**	**Disease**	**References**
TG2 protein levels	ELISA	AD, VaD, PD	Bonelli et al., 2002 Vermes et al., 2004
EGGL (Nε(γ-glutamyl)- lysine isodipeptide) levels	- Internal standard tracer - Precolumn phenylisothiocyanate derivatization - HPLC separation	AD, VaD	Nemes et al., 2001
γ-Glutamylamines levels	- Reversed phase HPLC - Electrochemical detection (EC)	HD	Jeitner et al., 2001 Jeitner et al., 2008
Enzymatic activity	Incorporation of ^{3}H-putrescine into dimethyl casein (radioactivity)	ASL	Fujita et al, 1998

Abbreviations: Alzheimer's Disease, AD; Vascular dementia, VaD; Parkinson Disease, PD; Huntington's Disease, HD; Amyotrophic Lateral Sclerosis, ALS.

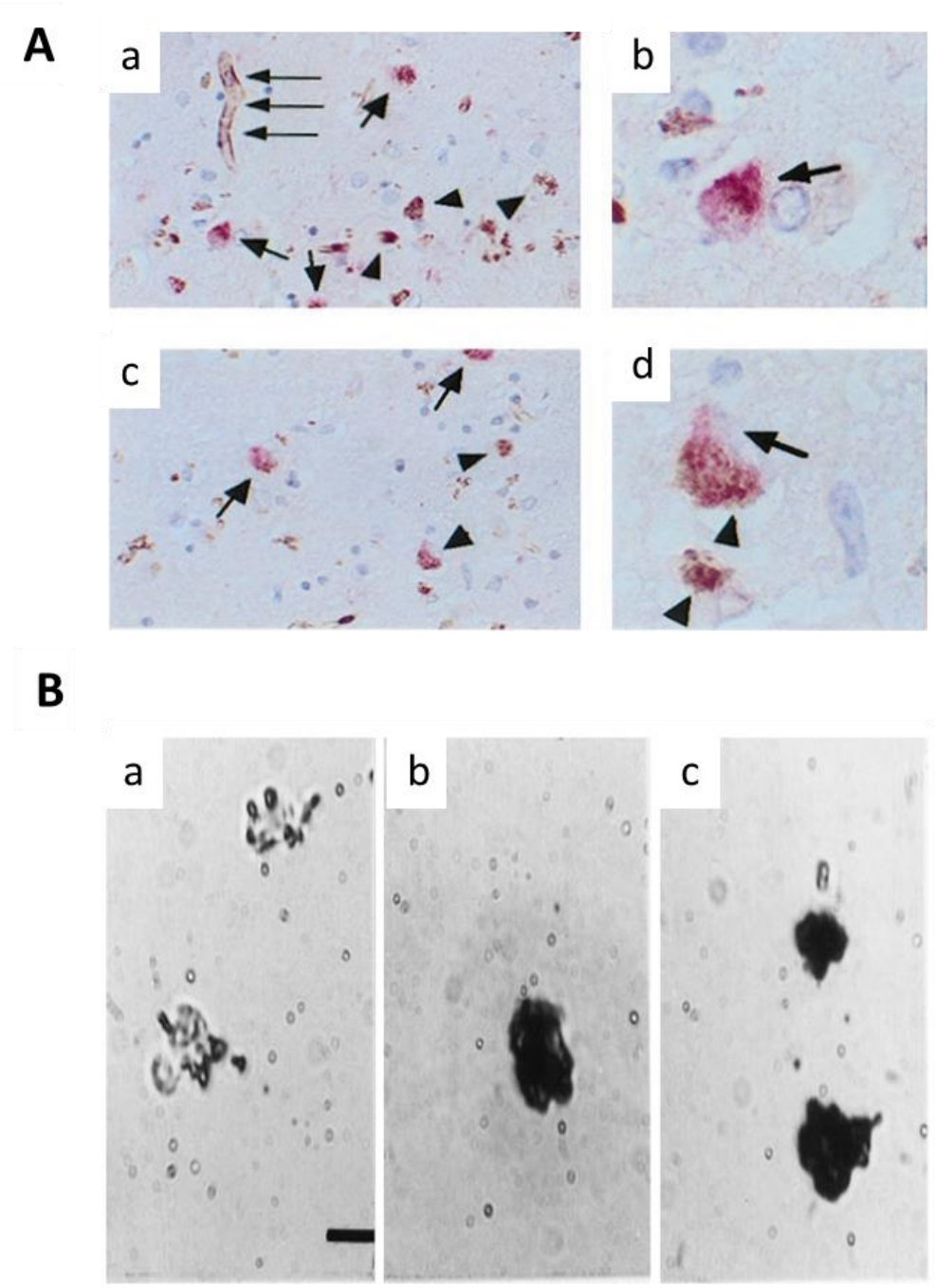

Figure 1.11*: Visualisation of TG2 in AD Neurofibrillary tangles (NTF) and amyloid plaques by immunohistochemistry.* ***A)*** *Co-localisation of TG2 and tau in the NTFs of AD patients. Panels a) and b) show sections of the frontal cortex, while c) and d) show sections of the hippocampus, both isolated from a patient at an advanced stage of AD (modified from Citron et al., 2001).* ***B)*** *Immunohistochemical staining of TG2 in amyloid plaques isolated from the brain of an AD patient. Plaques were treated with a) normal goat serum; b) TG2 antibody or c) Aß antibody (modified from Zhang et al., 1998).*

Overall, these data demonstrate above all that TGs can be considered a good molecular marker for AD and that inhibitors of their crosslinking activity may represent a new therapeutic approach for AD. It is in fact known that TGs, especially TG2, is activated in AD early stages and that its inhibition reduces the formation of protein aggregates in vitro (Wilhelmus et al., 2009, Wilhelmus et al., 2014). Moreover it has recently been demonstrated that isoform non-selective inhibitors have a neuroprotective effect in rat cortical neurons subjected to oxidative stress (Basso et al., 2012). Hence, the inhibition of TGs activity could potentially stop the TGs-contribution to disease progression and formation of Aβ and tau toxic oligomers.

Among all this strong evidence, Wolf and colleagues are the only contrary voice; in one of their reports they stated that TG2 is not a molecular marker of AD, because neither TG2 concentration nor transamidation activity were significantly increased in AD brain homogenates (Wolf et al., 2013). Furthermore, they didn't observe any co-localisation of TG2 in neocortex sections with tau or Aβ deposits (Wolf et al., 2013). The discrepancy between their results and what is reported in the vast majority of published data is probably due to a main limitation in the brain tissue fixation method utilised by Wolf et al., which was not ideal for TG2 detection, as is clearly stated by Wilhelmus in a letter to editor published in the same journal (Wilhelmus and Drukarch, 2014). Taking all of this into account, it is fair to state that TGs may be considered a promising biochemical marker of AD.

1.4.3.2 TGs in PD

Parkinson's Disease (PD) is characterized by accumulation of α-synuclein and other proteins into insoluble cytoplasmic inclusions called Lewy bodies, which leads to the degeneration of melanised, catecholaminergic neurons of the substantia nigra compacta (Watson et al., 2010). Various papers report that α-synuclein is a known target of TGs transamidating activity *in vitro* and *in vivo* (Andringa et al., 2004, Grosso et al., 2014, Junn et al., 2003) and that TG2 protein levels are increased in PD CSF (Vermes et al., 2004) (**Table 1.2**). Moreover, in the substantia nigra of PD brain, TG2 mRNA, protein levels and activity are significantly elevated (Andringa et al., 2004, Citron et al., 2002). In addition, TG2 co-immunoprecipitates with α-synuclein and they co-localise in Lewy bodies (Citron et al., 2002, Junn et al., 2003). The increased levels of TGs-induced crosslinking observed in Parkinson's disease brains implies a possible involvement of tissue TG in aggregation of α-synuclein into Lewy bodies.

Hence, targeting TGs activity might prevent the development of Lewy bodies and Lewy neurites, and thus the development of PD (Tarazi et al., 2014, Wilhelmus et al., 2008).

1.4.3.3 TGs in HD

Huntington's Disease (HD) is neuropathologically characterized by extensive neuronal loss in the striatum and cerebral cortex, caused by polyglutamine expansion within the huntingtin protein as a result from the elongation of a specific trinucleotide repeat in the coding region of the gene, *HTT*. Mutated huntingtin is cleaved into smaller, toxic fragments that bind together and accumulate in neurons, leading to their eventual death. Huntingtin is another target of TGs; they were in fact found to be co-localised in intranuclear inclusion (Zainelli et al., 2003, Zainelli et al., 2005). TG2 activity is increased in HD brain (Lesort et al., 1999) and both protein and activity are elevated in HD CSF respect to controls (Jeitner et al., 2001, Jeitner et al., 2008) (**Table 1.2**). In a mouse model of HD (BACHD mice), TG6 inhibition was shown to increase the levels of insoluble huntingtin aggregates while decreasing the more toxic soluble forms, suggesting a possible neuroprotective role (Dedeoglu et al., 2002, Karpuj et al., 2002, Mastroberardino et al., 2002).

1.4.3.4 TGs in other NDs

Even if the majority of data about TGs involvement in neurodegeneration is mainly referred to AD, PD and HD, some reports have been published about other form of dementia, albeit in a limited amount, e.g. for Progressive Supranuclear Palsy (PSP) and Amyotrophic Lateral Sclerosis (ALS).

PSP is the second most common form of parkinsonian movement disorder after Parkinson disease and is characterized neuronal loss, gliosis, tau immunoreactive astrocytes, and neurofibrillary tangle (NFT) formation. Elevated levels of TG1 and TG2 protein (especially the short isoform), crosslinking activity and mRNA has been observed in PSP brain, while TG3 was not detectable (Zemaitaitis et al., 2000, Zemaitaitis et al., 2003).

The main pathological feature of ALS is the selective degenerative loss of motor neurons in the ventral horn, and scarring of lateral fasciculi of the spinal cord. Data about TGs possible role in ALS progression is scarce; Fujita et al. showed that TGs activity values in patients' serum are higher at the initial stage of the disease, whereas they became extremely low at the late stage of ALS (Fujita et al., 1998). Their data suggest that a leakage of TGs from the spinal cord into the CSF and then to the blood-stream tissue may happen during the

progression of ALS, and that TGs activity results depleted at the terminal stages of the disease when most of the spinal motor neuronal perikaryon have been destroyed (Fujita et al., 1998). Moreover, recent data show that in a mouse model of ALS, TG2 is involved in the aberrant assembly of misfolded superoxide dismutase (SOD1) proteins, hence contributing to neuroinflammation and disease progression (Oono et al., 2014). Interestingly, another study states that in some cases, the neurologic presentation of a gluten-related disorder mimicking ALS might occur in some patients that are seropositive to T6 (Gadoth et al., 2015). The concept that antibodies against TG6 may serve as an additional to identify patients with gluten sensitivity who may also be at risk for developing a neurological disease, gives rise to a completely new perspective to be considered for TGs involvement in neurodegeneration (Hadjivassiliou et al., 2008).

1.5 Extracellular Vesicles

Extracellular vesicles (EVs) are a newly emerged mechanism of intercellular communication, which has been identified in most organisms, from prokaryotes to plants and higher eukaryotes (Yanez-Mo et al., 2015; Gyorgy et al., 2011; Cocucci and Meldolesi, 2015; Raposo and Stoorvogel, 2013). EVs consist of a phospholipid bilayer membrane which includes a variety of bioactive molecules, such as nucleic acids, lipids and proteins (**Fig. 1.12**) (Raposo and Stoorvogel, 2013; Thery et al., 2018). These include membrane proteins like tetraspanins (CD63, CD81, CD82, CD53 and CD37) and protein associated with lipid rafts (membrane lipid microdomains rich in cholesterol, sphingomyelin and ceramide), such as flotillin and glycosylphosphatidylinositol-anchored proteins. Conversely, proteins derived from intracellular compartments (e.g. mitochondria, ER and nucleus) should be absent (Raposo and Stoorvogel, 2013).

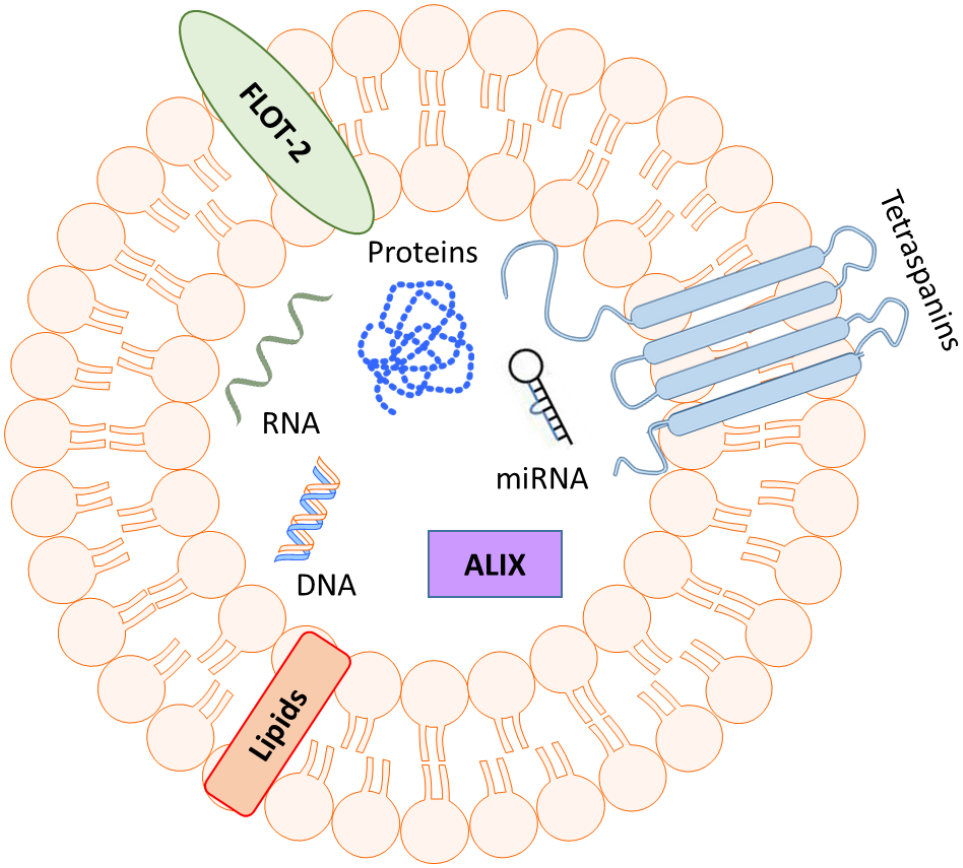

***Figure 1.12**: Schematic representation of an EV, carrying a variety of molecules: nucleic acids (DNA, RNA and miRNA), lipids, luminal proteins (ESCRT complex proteins such as Alix and TSG101; enzymes) and transmembrane proteins (tetraspanins, MHC class I, HSPG like syndecans, Flotillin). This image was generated with Motifolio (https://www.motifolio.com/).*

EVs cargo molecules are carried from donor to recipient cells, which may be in proximity or distant from the source. Indeed, EVs lipid structure is able to protect their contents from degradation, allowing the delivery of intact molecules to distant targets (Yanez-Mo et al., 2015; Cocucci and Meldolesi, 2015). EVs have been detected in the conditioned media of many cultured cells, including neurons and glial cells (Fauré et al., 2006; Bianco et al., 2005) as well as *in vivo,* in a variety of body fluids, including CSF, blood, saliva, urines, bile, amniotic fluid, seminal fluid and breast milk (Verderio et al., 2012; Raposo and Stoorvogel, 2013; Yanez-Mo et al, 2015). Given their heterogeneous content and ability to travel throughout the body, it is not surprising that EVs would be able to affect biological functions both at the physiological and pathological level (Yanez-Mo et al., 2015).

1.5.1 Biogenesis

EVs can be divided in two categories according to their cellular origin: microvesicles (MVs) and exosomes. MVs derive from direct shedding of the plasma membrane and present a broad size range, with diameters that range from 100 nm up to 1 µm (Cocucci and Meldolesi, 2011; Mause and Weber, 2010; Raposo and Stoorvogel, 2013). Exosomes derive from the endosomal pathway, and specifically generate within the multivesicular bodies (MBVs), which then fuse with the plasma membrane, thus releasing the exosomes in the extracellular space. They are smaller than MVs, ranging from 40 to 150 nm in diameter (Mause and Weber, 2010; Raposo and Stoorvogel, 2013; Andaloussi et al., 2013).

Exosomes biogenesis is regulated by a variety of proteins, among which the endosomal sorting complex responsible for transport (ESCRT) complex plays a central role (Raposo and Stoorvogel, 2013; Andaloussi et al., 2013) (**Fig. 1.14**). Specifically, they are formed by the inward budding of the MVB membrane, where the interaction with the ESCRT complex and other associated protein, e.g. programmed cell death 6 interacting protein (PDCD6IP or ALIX) and tumour susceptibility gene 101 protein (TSG101) regulates their cargo loading (Andaloussi et al., 2013). In some cell types, other molecules are also involved in this process independently from ESCRT proteins, such as ceramide, neutral sphingomyelinase and small GTPases like RAB27a and RAB27a (Trajkovic et al., 2008; Ostrowski et al., 2010). Additionally, the soluble N-ethylmaleimide-sensitive factor attachment protein receptor (SNARE) protein Synaptobrevin homolog (YKT6) was also shown to participate in exosomes release, mediating the loading of Wnt signalling proteins (Gross et al., 2012) (**Fig. 1.13A**).

On the other hand, the release of MVs is mediated by outward budding and fission of the plasma membrane, which has been shown to be facilitated by regulatory proteins like ADP-ribosylation factor 6 (ARF6), as well as by lipid rafts (Muralidharan-Chiari et al. 2009; Cocucci and Meldolesi, 2015) (**Fig. 1.13B**).

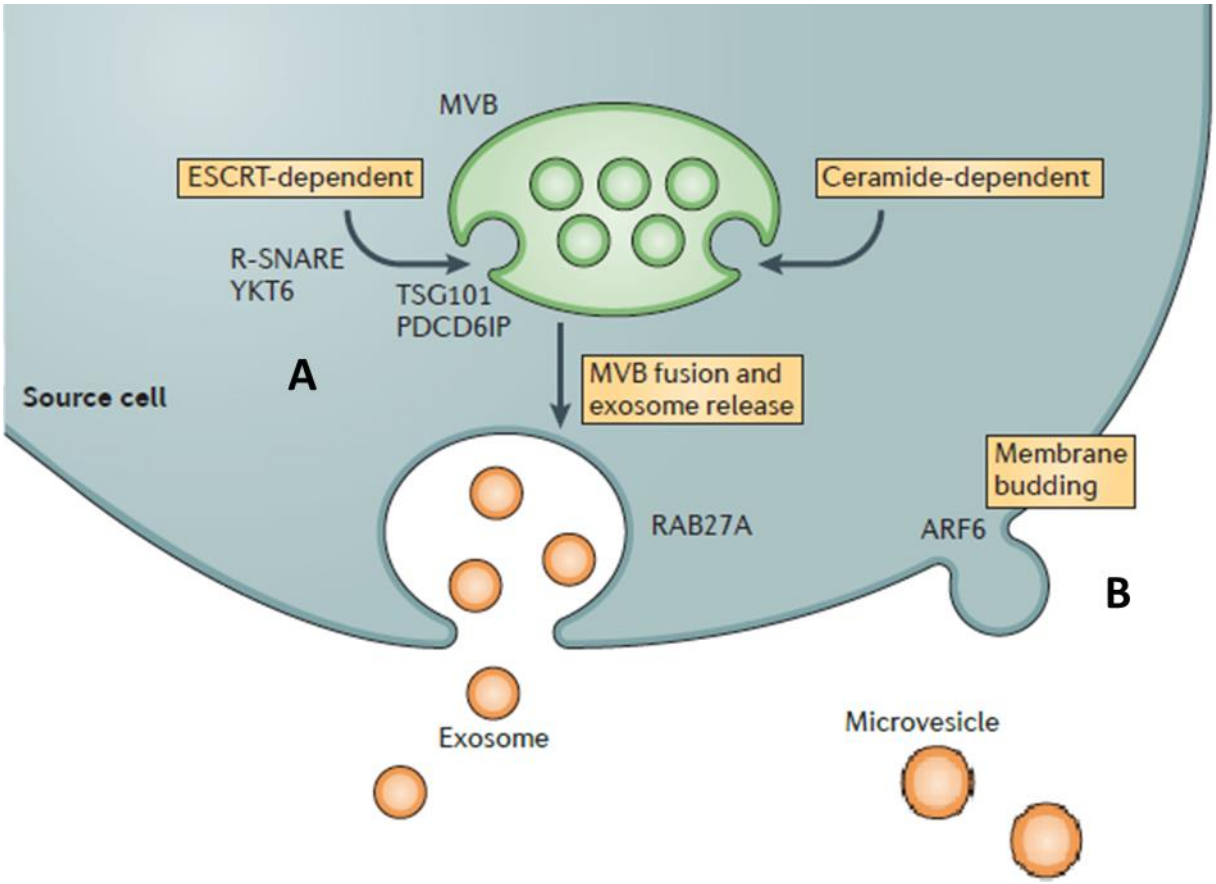

Figure 1.13: Biogenesis of EVs and their interactions with target cells *(modified from Andaloussi et al., 2013).*

The budding and release of EVs requires the remodelling of the cytoskeleton, involving a series of elements such as actin, microtubules, myosins and kinesins (Raposo and Stoorvogel, 2013). This process is triggered by multiple factors, among which is the increase of $[Ca^{2+}]_i$, as has been shown in mast cells (Raposo et al., 1997) and human erythroleukemia cell line (Savina et al., 2005). Literature data report that in some cell types (i.e. microglia, macrophages and dendritic cells) MVs release can be induced by ATP-dependent activation of the P2X7 purine receptor (Bianco et al., 2005; Cocucci and Meldolesi, 2015), although the specific mechanism has not been completely elucidated (Raposo and Stoorvogel, 2013). Similarly, even though some of the molecules involved in EVs cargo loading have been

identified, the specific mechanisms regulating the sorting process have not yet been wholly defined (Raposo and Stoorvogel, 2013; Cocucci and Meldolesi, 2015).

1.5.2 Biological functions

A number of reports have described a role of EVs as mediators of various biological processes, including inflammation, neuromodulation, angiogenesis, coagulation and tumour progression, where EVs content and consequent effects are dependent on the state and nature of the parental cells (Antonucci et al, 2012; Nakano et al, 2015; Rajendran et al, 2014; Smith et al, 2015). Moreover, EVs have been proposed as molecular markers for multiple diseases, including inflammation (Colombo et al., 2012; Verderio et al., 2012), neurodegeneration (Goetzl et al., 2015-2019), renal fibrosis (Merchant et al., 2017) and cancer (D'Souza-Schorey and Clancy, 2012), and also as possible therapeutic agents or drug delivery systems (Ratajczak et al., 2006; Thery et al, 2009; Verderio et al, 2012). Although united by some common characteristics, MVs and exosomes are believed to exert distinct functions (Cocucci and Meldolesi, 2015; Keerthikumar et al., 2015).

EVs can deliver their bioactive contents by releasing soluble molecules in the extracellular space or by direct contact with the recipient cells (Montecalvo et al., 2012). This would likely involve the interaction with adhesion molecules (e.g. integrins, ICAM-1, MHC class II), which are expressed of the EVs surface (Andaloussi et al., 2013). After binding, EVs can fuse with the cell membrane and transfer their cargo molecules into the recipient cell or alternatively be internalised by clathrin-dependent endocytosis, phagocytosis or micropinocytosis (Cocucci and Meldolesi, 2015).

Within the CNS, different cell types have been shown to release EVs, including neurons, oligodendrocytes, astrocytes and microglial cells (Bianco et al., 2005; Fauré et al, 2006; Doeuvre et al, 2009). EVs have been reported to participate to basic processes such as myelin formation, neurite outgrowth and neuronal survival (Raposo and Stoorvogel, 2013) and to have a central role in both intra-neuron and glia-neuron communication (Chivet et al., 2012; Luarte et al., 2017). For example, the mRNA of *Arc*, a gene involved in the modulation of synaptic plasticity, has been recently shown to be released by neuronal EVs and be transferred to recipient neurons (Pastuzyn et al., 2018). MVs derived from microglial cells have been shown to affect neurotransmission *in vivo* by increasing EPSPs currents, when injected in a rat visual cortex (Antonucci et al, 2012). Moreover, they were shown to

mediate the transfer of pro-inflammatory miRNAs from activated microglia to neurons, thus mediating the spreading of inflammatory stimuli and loss of excitatory synapses (Prada et al., 2018).

Furthermore, various proteins involved in the pathogenesis of NDs have been detected in EVs, such as Aβ (Rajendran et al., 2006; Ghidoni et al., 2011), α-synuclein (Emmanouilidou et al., 2010), tau/p-tau (Saman et al., 2012; Wang et al., 2017) and prion protein (Fevrier et al., 2004). Microglial MVs were shown to mediate the formation and spreading of soluble Aβ oligomers starting from less toxic fibrillar Aβ forms and to be increased the CSF of patients affected by AD (Joshi et al, 2014). On the other hand, neuroblastoma cells-derived exosomes were shown to have a neuroprotective effect *in vivo* by sequestrating toxic Aβ assemblies and thus decreasing the amount of free amyloid neurotoxic species (An et al., 2013).

These findings highlight a central role for EVs in both normal and diseased states, revealing a new perspective in cell-to-cell communication in the CNS.

1.5.3 Nomenclature

Although EVs are commonly referred to as microvesicles (or ectosomes) and exosomes, a recent publication from the International Society of Extracellular Vesicles (ISEV) highlights that to date there are not clear markers which can distinguish between the two populations, as both dimension and markers quite often partially overlap (Thery et al., 2018). Moreover, the technical limitations of EVs isolation techniques do not allow the separation of completely pure EVs preparations, hence defining isolated EVs as either MVs or exosomes would be incorrect. Therefore, the guideline from the EVs research community is to refer to isolated vesicles as “large” or “small” EVs depending on their size/density (Thery et al., 2018). In this thesis, the MISEV 2018 guidelines were taken into account, hence vesicles were defined as either “large EVs” or “small EVs” accordingly.

1.6 General aims

The aims of this study are to:

i. investigate the role of extracellular TG2 in neuron-glia cross-talk in the context of neurodegeneration, particularly in relation to EVs;
ii. explore the substrates of TG2 post-translational modification in neurons incubated with $A\beta_{1-42}$ peptide, a cell model simulating AD pathology;
iii. evaluate TG2 as a potential marker of dementia in biological samples (plasma and primary fibroblasts) from healthy subjects and dementia patients.

CHAPTER 2:

Materials and Methods

2.1 Materials

2.1.1 Cell culture

2.1.1.1 Reagents

Table 2.1. List of cell culture reagents

Cell culture reagents	Product code	Company
Neurobasal medium	21103049	Fisher Scientific
B27 supplement	17504044	Fisher Scientific
EMEM (with glutamine)	BE-12-125	Lonza
RPM1 1640 (with glutamine)	BE-12-115	Lonza
Fetal Bovine Serum (FBS)	S1900-500	Biosera
Penicillin-Streptomycin (10,000units/ml penicillin and 10mg/ml streptomycin)	DE17-602E	Lonza
Trypsin solution (2.5% (v/w) trypsin - 10X)	59427C	Sigma
L-Glutamine solution (200mM - 100X)	G7513	Sigma
EDTA solution 0.5M pH 8.0	3690	Sigma
G418 Sulphate (potency=800 µg/ml)	345810	Merck
MEM Non-essential amino acid solution (100X)	13-114E	Lonza
Bovine Serum Albumin (BSA)	A8022	Sigma
Fibronectin	F2006	Sigma

2.1.1.2 Plastic wares

Sterile tissue culture plastic (TCP) wares were supplied by either Sarstedt or Nest.

Glass coverslips (24 mm Ø) were supplied by ThermoScientific Nunc.

2.1.2 Laboratory reagents

2.1.2.1 Antibodies

Table 2.2. List of Primary and secondary antibodies used in this study.

Primary antibody	Company	Dilutions
Monoclonal mouse anti TG2 (CUB7402)	Thermofisher Scientific	1:1000 (WB & ELISA) 1:200 (IF)
Monoclonal mouse anti TG2 (IA12)	Sheffield University	1:1000 (WB) 1:400 (IF)
Polyclonal rabbit anti TG2 (ab421)	Abcam	1:1000 (WB)
Monoclonal mouse anti fluorescein	Roche	2.5 µg/µl (IP)
Polyclonal rabbit anti β-tubulin	Abcam	1:10000 (WB)
Whole serum rabbit anti actin	Sigma	1:500 (WB)
Monoclonal mouse anti flotillin-2	BD Transduction lab	1:5000 (WB)
Monoclonal mouse anti TSG-101	Abcam	1:1000 (WB)
Polyclonal rabbit anti Alix	Covalab	1:1000 (WB)
Monoclonal rabbit anti SV2B	Synaptic systems	1:1000 (WB)
Monoclonal mouse anti Syt-1	Synaptic systems	1:1000 (WB)
Monoclonal mouse anti PSD-95	Neuromab	1:5000 (WB)
Polyclonal rabbit anti NR2B	Alomone	1:1000 (WB)
Monoclonal rabbit anti VGAT	Synaptic systems	1:1000 (WB)
Monoclonal rabbit anti VGLUT1	Synaptic systems	1:5000 (WB)
Monoclonal guinea pig anti VGLUT1	Synaptic systems	1:500 (IF)
Monoclonal rabbit anti SHANK2	Neuromab	1:500 (IF)
Monoclonal rabbit anti GFAP	Dako	1:500 (IF)
Polyclonal rabbit anti GFAP	GeneTex	1:10000 (WB)
Polyclonal rabbit anti FN (F3648)	Sigma	1:500 (WB) 1:200 (IF)
Monoclonal rabbit anti EGFP	LifeSpan BioSciences	1:250 (IF)
Monoclonal mouse anti EGGL	Covalab	1:500 (WB)
Secondary antibody	**Company**	**Dilution**
Polyclonal Goat anti mouse IgG Horseradish Peroxidase (HRP)-conjugated	Dako	1:2500 (WB)
Polyclonal Goat anti rabbit IgG HRP-conjugated	Dako	1:2500 (WB)
Sheep anti mouse IgG Alexa-488-conjugated	Invitrogen	1:200 (IF)
Sheep anti rabbit IgG Alexa-555-conjugated	Invitrogen	1:250 (IF)
Sheep anti guinea pig IgG Alexa-633-conjugated	Invitrogen	1:250 (IF)

2.1.2.2 Chemicals and enzymes

2.1.2.2.1 Enzymes

Guinea pig liver Transglutaminase 2 (gplTG2) was from Sigma-Aldrich (T5398, 80% purity) or Zedira (T006, 85% purity). 1 mg/ml stock solution in dH_2O was aliquoted and stored at -20°C. Unit of an enzyme activity is 1.5 U/mg. Inactive human TG2, carrying the Cys(277)Ser

mutation in the catalytic core, was from Zedira (T018, 95% purity). Apyrase was from Sigma (500 U/ml) and used at 30 U/ml.

2.1.2.2.2 Chemicals

Table 2.3. List of chemicals and reagents used in this study.

Chemicals	Company	Catalogue no
1,4-Dithiothreitol (DTT)	Melford	MB1015
3,3,5,5-tetramethylbenzidine (TMB)	Sigma	T9281
Agarose (powder)	Web Scientific	AGR100
Amaxa Nucleofector™	Lonza	VCA1003
Ammonium persulphate	Sigma	A0502
Ampicillin	Sigma-Aldrich	A9518
APV	Tocris	0106/1
Apyrase	Sigma	A6535
Aβ 1-42	Anaspec	ANA20276
Bicuculline	Tocris	0130/50
Biotin Cadaverine	Sigma	A5348
BOCDON	Zedira	B003
Bovine Serum Albumin (BSA)	Sigma	A4503
Bradford reagent	Sigma	B6916
Bromophenol blue	Sigma	B5525
Cadmium	Sigma	202908
Calcium chloride	Sigma	C3881
CNQX	Tocris	0190/10
Dimethly sulfoxide(DMSO)	Sigma	D2438
DNA ladder (100bp)	Promega	G2101
dNTPs mix	Promega	U1511
Ethanol (Nuclease-free)	Sigma	D7023
Ethidium Bromide	Sigma	1510
Ethylenediaminetetraacetic acid (EDTA)	Sigma	EDS
ExtrAvidin®–Peroxidase	Sigma	E2886
EZ-Chemiluminescence HRP-Detection Kit	Geneflow	K1-0170
Fibronectin from human plasma	Sigma	F1056
First strand buffer, 5X	Invitrogen	18064-014
Fluorescein isothiocyanate (FITC) Cadaverine	Invitrogen	A10466
Glacial Acetic Acid	Fisher	A360OB17
Glycerol	Sigma	G5516
Glycine	Melford	G0709
Hydrogen peroxide H_2O_2	Sigma	H1009
iQ™ SYBR® Green Supermix	Biorad	170-8880
Isopropanol	Fisher	P749017
LB Broth Lennox	Fisher Scientific	BP1427
Loading Dye (Blue/Orange)		

Chemicals	Company	Catalogue no
Methanol	Fisher	M40017
N,N,N,N'-Tetramethylethylenediamine (TEMED)	Sigma	T9281
Nickel	Sigma	339350
Nifedipine	Sigma	N7634
Nitrocellulose membrane	Biorad	1620115
Phosphatase Inhibitor Cocktail 2	Sigma	P5726
Phosphate-Citrate Buffer with Urea Hydrogen Peroxide	Sigma	P4560
Ponceau S	Sigma	P3504
Potassium Chloride (KCl)	Sigma	P9541
Potassium dihydrogen phosphate	Sigma	P5504
Prestained Prism Ultra Protein Ladder (10-245kDa)	Abcam	ab116028
Protease inhibitor cocktail	Sigma	P8340
Protogel - 30% Acrylamide/ Bisacrylamidesolution (37.5:1 ratio)	Geneflow	A2-0072
QIAGEN Plasmid Midi Kit	Qiagen	12143
Random primers	Promega	C1181
Sodium Chloride (NaCl)	Sigma	S7653
Sodium Deoxycholate	Sigma	D6750
Sodium Dodecyl Sulphate (SDS)	Melford	B2008
Sodium Hydroxide (NaOH)	Fisher	10010650
Sodium Phosphate Dibasic Heptahydrate (Na2HPO4)	Melford	S2317
Sulphuric acid (H_2SO_4)	Fisher	59160PB
SuperScript® (II) Reverse Transcriptase	Invitrogen	18064-014
Tetrodotoxin (TTX)	Tocris	1078/1
Triton-X100	Sigma	X100
Trizma Base / TRIS (Tris (hydroxymethyl) aminomethane)	Melford	B2005
Tween® -20	Sigma	P1379
VECTASHIELD® Mounting Medium	Vectorlab	H-1000
VECTASHIELD® Mounting Medium with DAPI	Vectorlab	H-1200
YM-244769	Tocris	4544/10
ZDON	Zedira	Z006
β-Mercaptoethanol or 2-ME	Sigma	M3148

2.1.3 Laboratory equipment

Table 2.4. List of laboratory equipment.

Instrument	Company
ALC 4227 R Centrifuge (ALC 5690 rotor)	ALC
Amaxa Nucleofector™ Device	Lonza
Avanti J-301 high performance centrifuge	Beckman Coulter
Axopatch 200 B amplifier	Axon Instrument
Brown-Flaming P-97 puller	Sutter Instrument
CCD Imago-QE camera	TILL Photonics
Corbett Rotor-Gene™ 6000	Qiagen
Eppendorf refrigerated centrifuge 5417R	Eppendorf
GeneGenius system with UV transilluminator	Syngene
GyroStir 280H Magnetic Hotplate Stirrer	Sciquip
Harrier 18/80 Centrifuge	Sanyo
iMark microplate reader	Biorad
Heating Block QBT4	Heating block
Inverted microscopr	Axiovert 100, Zeiss
LAS4000 imaging system	GE Healthcare
Leica SP5 confocal microscope	Leica
Mini PROTEAN® Gel casting system	Bio-Rad
Mini PROTEAN® Tetra Cell	Bio-Rad
NanoDrop® 8000	Thermoscientific
New Brunswick™ Excella® E25R incubator shaker	Eppndorf
Polarstar Optima Luminometer	BMG Labtech
Powerpack	Bio-Rad
Soniprep 150 sonicator	MSE
Stuart shaking incubator	Geneflow
TC 3000X Thermocycler	Techne
Triple TOF 5600+	Sciex
Ultra Turrax T25 homoginiser	Merck
Water bath SUB14	Grant
Zetaview PMX 120	Particle Metrix

2.2 Methods

2.2.1 Cell cultures and culture growth conditions

2.2.1.1 Hippocampal neurons primary culture (standard)

Primary hippocampal neurons were obtained from the hippocampi of 18-days-old fetal Sprague Dawley Rats (Charles River Italia) as described by Banker and Cowan et al., 1977. Briefly, after animal sacrifice and brains extraction, cerebral hemispheres were dissected, the meninges were removed, and the isolated hippocampi were maintained at 4°C in sterile conditions. Hippocampi were then subjected to enzymatic digestion with 0.25% trypsin for 15 minutes at 37°C. After mechanical dissociation and counting, cells were plated on poly-L-lysine-treated (PLL, 1mg/ml, Sigma Aldrich) glass coverslips (24 mm Ø) at 38,000-40,000 cells/cm^2 density and maintained in Neurobasal Medium (Invitrogen) supplemented with 2% B27 (Invitrogen), L-Glutamine 0.5 mM (Gibco), glutamate 12 µM (SigmaAldrich), Penicillin/Streptomycin 1% (Gibco) at 37°C in a humidified incubator with 5% CO_2. Culture medium was partially replaced (50%) with glutamate-free medium at 3 days-in-vitro (3 DIV). These preparations have been used for immunofluorescence and TG activity *in situ* assays (Chapter 3), all calcium imaging and electrophysiology experiments (chapter 4) and mass spectrometry (chapter 5).

2.2.1.2 Astrocytes and microglia primary culture (standard)

Primary mixed glial cultures, containing both astrocytes and microglia, were obtained from embryonic rats (18-days-old embryos) as described by Calegari et al., 1999. Cortices underwent a double enzymatic digestion with 0.25% trypsin and DNAse 1.25% (10 mg/ml) for 15 minutes at 37°C. In order to remove not dissociated tissue, the supernatant obtained after digestion was filtered through an 80 µm nytex membrane (Millipore) and then centrifuged at 800 rpm for 10 minutes. The supernatant was discarded, and the pelleted cells were resuspended, counted and plated on PLL-treated (10 µg/ml, Sigma-Aldrich) T75 flasks at 1x10^6 cells/flask density, grown in MEM (Invitrogen Life Technologies) supplemented with 20% FBS (Fetal Bovine Serum, Gibco), Glucose 5.5 g/L (Sigma-Aldrich), Penicillin/Streptomycin 1% (Gibco) and maintained at 37°C and 5% CO_2.

Purified microglial cultures were harvested by shaking for 30 minutes 10-14-days-old glial cultures and re-plated onto poly-D,L-ornithine-coated (Sigma-Aldrich) 60mm or 100mm tissue culture dishes (at a final concentration of 50 µg/ml) and maintained in the same

medium. After shaking glial cells at 200-210 rpm, the medium was collected and centrifuged at 300xg for 10 minutes. The pellet was resuspended and used within 2 days. After orbital shaking, the 10-14-days-old glial cultures contained a pure astrocyte monolayer.

These preparations have been used for astrocytes characterisation (Chapter 3) and calcium imaging experiments with astrocytic EVs (Chapter 4).

2.2.1.3 Hippocampal neurons and astrocytes primary culture – BrainBits protocol

Embryonic rat tissues purchased from BrainBits were processed according to their recommended protocol, with some modifications. Specifically, hippocampi (E18 Rat Hippocampus kit) and cortices (E18 Rat cortex kit) shipped in Hibernate EB media (HEB) were transferred in a cell dissociation solution containing 2mg/ml papain in HE media without calcium. Tissues were gently mixed, placed in a 30^{o}C water bath for 10 minutes and then returned to the vial containing HEB media for mechanical dispersion using a glass pasteur pipette. After letting undispersed pieces settle for 1 min, the supernatant containing dispersed cells was transferred to a sterile tube and centrifuged at 200 x g for 1 min at room temperature. The supernatant was discarded and pelleted cells were resuspended in either Neurobasal or EMEM complete media as described in sections 2.2.1.1 and 2.2.1.2. Cells were diluted 1:2 with trypan blue, counted using a TC20™ Automated Cell Counter (BioRad), plated on PLL coated surfaces and maintained at 37^{o}C in a humidified incubator with 5% CO_2. At 3 DIV, 50% of the hippocampal neurons medium was changed with fresh complete Neurobasal medium without glutamate.

These preparations have been used for cell surface activity assays and EVs isolation from astrocytes (Chapter 3).

2.2.1.4 Primary human fibroblasts and plasma

2.2.1.4.1 Ethical approval

Biological samples were collected after obtaining informed consensus from all subjects, according to IRCCS-Fatebenefratelli ethical committee. Ethical approval for the shipment and analysis of human samples for this project was obtained on 10 November 2015 from the IRCCS-Fatebenefratelli ethical committee and on 15 March 2016 from the College of Science and Technology Ethical committee (human) at Nottingham Trent University.

Shipment of frozen primary fibroblasts and plasma was carried out in dry ice and samples were stored in a -80°C freezer until use.

2.2.1.4.2 Power calculations

Supported by literature data on CSF and brain tissues of patients with AD and other neurodegenerative diseases (PD, HD, progressive supranuclear palsy) (Citron et al., 2001; Kim et al., 1999), we determined that TG2 concentration, activity and expression levels are increased of about 2-3-fold (200-300%) in pathological conditions compared to healthy subjects. Specifically, TG activity and mRNA were shown to be 1.5-8-fold higher in AD brain samples compared to normal (Citron et al., 2001) and isopeptide concentration was 4.7-fold higher in CSF of AD patients compared to healthy subjects (Nemes et al., 2001). Therefore, we calculated the sample size necessary to perform a statistically significant measure using a 2-fold variation with respect to the control condition. Specifically, the calculation was made by considering that the mean average value and standard deviation (SD) of TG2 activity in a control group were equal to about 22±11 µU/mg (the reference values are referred to serum samples and were deduced from Ahn et al., 2015), and defining as significant a variation (increase) equal to 200%, together with the precautionary hypothesis that the SD of the experimental group would be equal to that of the control group (i.e. with a SD / average coefficient of variation = 0.5). A two-tailed test for independent samples (with alpha 0.05 and power 80%) was applied, which indicated that a minimum sample size of 10 subjects would be necessary to observe a significant variation. Therefore, a sample size of 10 and 15 subjects per group, for fibroblasts and plasma respectively, was considered sufficient to measure a statistically significant variation for the selected variables.

2.2.1.4.3 Primary fibroblasts culture

Skin fibroblasts primary cultures were selected from the tissue repository of the IRCCS-Fatebenefratelli, National Centre for Alzheimer's and Mental Diseases (Brescia, Italy). Cells were established from skin biopsies as previously described (Govoni et al., 1993), grown on TCP and maintained in EMEM supplemented with 10% FBS, 2 mM L-Glutamine, 1% Penicillin/Streptomycin and 1% MEM Non-essential amino acid solution.

2.2.1.4.4 Plasma samples

Blood samples were collected according to standard procedures in tubes containing 3.2% sodium citrate anticoagulant. Tubes were centrifuged 5 minutes at 1000xg within 30 minutes from collection and plasma was removed (upper phase), supplemented with serine-proteases (4-(2-aminoethyl)benzenesulfonyl fluoride hydrochloride, AEBSF) and split in 250 µl to be stored at -80^{o}C.

2.2.1.5 Cell passaging and counting

Confluent cell monolayers were first washed once with sterile PBS pH 7.4 (137mM NaCl, 2.7 mM KCl, 10 mM Na_2HPO_4 and 1.8mM KH_2PO_4, pH 7.4) and incubated for 5 minutes at 37°C with a trypsin-EDTA solution [0.25% (w/v) trypsin, 2 mM EDTA in PBS, pH 7.4]. Cells were then detached by gentle tapping and at least two volumes of complete medium were added to inactivate trypsin. Cell suspensions were centrifuged at 300xg for 5 minutes and pelleted cells were re-suspended in complete medium (volume variable according to the pellet size) and plated in new flasks containing fresh culture medium at the desired dilution. When a specific number of cells was necessary for performing an experiment, cell suspensions were counted either manually with an Improved Neubauer Chamber haemocytometer of 0.1 mm thickness (HAE2112, Scientific Laboratory Supplies) or with a TC20™ Automated Cell Counter (BioRad). For manual counting, 10µl of cell suspension were loaded into the chamber and cells were counted under the microscope at 10x magnification. The values from at least three 4x4 quadrants were averaged and the number of cells per ml was calculated by multiplying the average value by 10^4. For primary neurons, cell suspension was diluted 1:2 in trypan blue before loading in the automated cell counter.

2.2.1.6 Mycoplasma detection and treatment

Detection of mycoplasma was performed for primary human fibroblasts one week after the first plating and then routinely every 2-3 months. Each newly thawed cell aliquot was kept in an apposite incubator and only moved together with other primary human cells lines after testing negative for mycoplasma contamination. One ml of conditioned media was taken from cells at least 48 hours after the last media change and centrifuged briefly at 200xg to pellet cells and debris in suspension. Supernatants were transferred in fresh tubes and centrifuged at 20,000xg 10 minutes. Pellets were then resuspended in 25 µl of sample buffer from the EZ-PCR Mycoplasma Test Kit (Biological Industries), boiled for 3 minutes at

97°C in a heating block and either stored at -20°C or analysed immediately by PCR following manufacturer's instructions. Briefly, 2.5 µl of test sample were mixed with 5 µl of reaction buffer and 17.5 µl of dH_2O, placed in a conventional thermocycler (Techne, TC3000X) with the following program:

Initial Denaturation 94°C 30 secs

Denaturation 94°C 30 secs	35 cycles
Annealing 60°C 120 secs	
Extension 72°C 60 secs	
Denaturation 94°C 30 secs	last cycle
Annealing 60°C 120 secs	
Final extension 72°C 5 min.	

A positive and negative control were always included. Amplified products were then analysed by agarose gel electrophoresis: samples were loaded in a 2% (w/v in TAE) agarose gel containing 1X SYBR Safe (Invitrogen) and run at constant voltage (120V) for 20 minutes. Gels were then placed in a UV transilluminator (Syngene) to visualised amplified bands. Samples positive to mycoplasma contamination presented a 270bp band. Contaminated cells were treated with BIOMYC-1 and 2 antibiotic solutions (Biological Industries) for 3 cycles following instructions. Cells were monitored once every week during treatment with the EZ-PCR Mycoplasma Test Kit, and treatment was stopped after the cells tested negative for contamination.

2.2.2 Immunofluorescence staining (IF)

2.2.2.1 IF of primary neurons and astrocytes

Primary neurons and astrocytes plated on PLL-treated glass coverslips were fixed in 4% paraformaldehyde - 4 % sucrose (w/v) for 10 and 20 minutes respectively, washed 3 times with PBS, followed by 3 washes with a low salts solution (LS: 150 mM NaCl, 10 mM NaH_2PO_4, 10 mM Na_2HPO_4) and high salts solution (HS: 500 mM NaCl, 20 mM NaH_2PO_4, 20 mM Na_2HPO_4), 5 minutes each. Coverslips were then blocked 20 minutes with Goat Serum Dilution Buffer (GSDB: 3% goat serum, 0.9 M NaCl, 40 mM NaH_2PO_4, 40 mM Na_2HPO_4) containing Triton-X100 (0.6% v/v) for permeabilisation, or without Triton-X100 for non-permeabilised cell staining. Primary antibodies were diluted in GSDB and incubated 1 h at room temperature or overnight (15 hours) at 4°C. After 3 washes with HS solution, secondary antibodies were diluted in GSDB and incubated 1 hour at room temperature.

Coverslips were then washed 3 times with HS solution, 3 times with LS solution, of which one containing either DAPI or Hoechst for nuclear staining and mounted on microscope slides using mounting medium (DAKO). Cells were visualised by laser scanning Leica SP5 confocal microscope using 63X oil immersion objective. Successive serial optical sections (0.5 µm) were recorded over 5 µm planes and either the middle z-stack or maximum projection were selected for quantification. Fluorescence intensity and co-localisation were estimated using the Leica LAS AF Lite software or ImageJ software. For the study of TG2 localisation at neuronal synapses, TG2 and VGLUT1 (or SHANK2) double-positive puncta were revealed by generating a TG2/VGLUT1 (or TG2/SHANK2) double-positive image. A fixed threshold was then set in the double-positive image and the number of TG2-positive puncta was measured and normalized to total number of VGLUT1 puncta or SHANK2 puncta to obtain the fraction of TG2 positive presynaptic or postsynaptic sites (Pravettoni et al., 2000).

2.2.2.2 IF of primary fibroblasts

Primary fibroblasts were plated in 8-well chamber slide (0.05 x 10^6 cells/well), washed with PBS pH 7.4 and fixed in 3% paraformaldehyde (w/v in PBS) for 8 minutes at room temperature. Cells were then washed 3 times with PBS, followed by permeabilisation with Triton-X100 (0.1% v/v in PBS) for 15 minutes and blocking in 3% BSA (w/v in PBS) 30 minutes at 37°C. Primary antibodies were diluted in blocking buffer and incubated overnight (15 hours) at 4°C. After 3 washes with PBS, secondary antibodies were diluted in blocking buffer and incubated 1 hour at room temperature. Cells were finally washed 3 times with PBS and mounted using Vectashield mounting medium containing DAPI for nuclear staining (Scarpellini et al., 2009). Cells were visualised by laser scanning Leica SP5 confocal microscope using 63X oil immersion objective as described above.

2.2.3 Western blotting

2.2.3.1 Sample preparation

Neurons plated on two PLL-coated glass coverslips for each condition were lysed in hot lysis buffer (1% w/v SDS, 2 mM EDTA, 10 mM Tris-HCl pH 7.4, proteases inhibitors 1X), diluted in 5x-Laemmli buffer in reducing conditions, incubated in a boiling water bath for 5 minutes and stored at -80°C. No quantification of the lysate was performed in this case before loading on acrylamide gels.

Primary fibroblasts (80-90% confluent) and astrocytes were washed with PBS pH 7.4 and harvested by cell scraping or trypsinisation. Cell pellet was collected by centrifugation at 300xg for 5 min and re-suspended in 100-500 µl of RIPA buffer (25 mM Tris-HCl pH 7.2, 150 mM NaCl, 1 mM EDTA, 0.5% Na-deoxycholate, 1% NP-40/IGEPAL, 0.1% SDS, proteases inhibitors 1X). Cells were incubated 15 minutes at 4°C and sonicated on ice (3 repetitions for 5 seconds, 1 minute hold in between) using a probe sonicator. Lysates were incubated for 20 minutes on ice, then centrifuged at 1000xg for 5 minutes at 4°C to remove un-lysed material. The pellet was discarded and supernatants (cell total lysates) were immediately quantified and then diluted in 6X Laemmli buffer (250mM Tris-HCl pH 6.8, 40% (v/v) glycerol, 8% (v/v) Sodium Dodecyl Sulphate (SDS), 20% (w/v) β-mercaptoethanol, 0.008% (w/v) bromophenol blue), boiled 10 minutes at 97°C in a heating block and either stored at -80°C or loaded on gel.

2.2.3.2 Protein quantification

2.2.3.2.1 Preparation of bovine serum albumin (BSA) standard curve

A standard curve of known protein concentrations was prepared by serial dilution of bovine serum albumin (BSA) to 1, 0.75, 0.5, 0.25, 0.125 and 0 mg/ml (blank) in respective sample buffer.

2.2.3.2.2 Bicinchoninic acid (BCA) protein quantification assay

BCA quantification assay was performed using a commercially available BCA quantification assay reagent kit (Sigma). BCA working solution was prepared immediately before use by combining Reagent A [1% (w/v) BCA, 2% (w/v) Na_2CO_3, 0.16% (w/v) NaK tartrate, 0.4% (w/v) NaOH, 0.95% (w/v) $NaHCO_3$] and Reagent B [4% (w/v) $CuSO_4$] in 50:1 proportion. 25 µl of samples (in triplicates) or BSA standards (0-1 mg/ml) (in duplicates) were incubated with 200 µl of BCA working solution in a 96-well plate. The plate was incubated 30 minutes at 37°C in the dark and the absorbance was measured at 595 nm using a plate reader (spectrophotometer). The unknown sample concentration was obtained by plotting the absorbance values on the BSA standard curve of known protein concentration.

2.2.3.2.3 Bradford protein quantification assay

Bradford quantification assay was performed using the commercially available Bradford reagent (Sigma). 5 µl of samples (in triplicates) or BSA standards (0-1 mg/ml) (in duplicates)

were incubated with 250 µl of Bradford reagent in a 96-well plate. The plate was incubated 20 min at room temperature in the dark and the absorbance is measured at 595 nm using a 96-well plate reader (spectrophotometer). The unknown sample concentration was obtained bas explained above.

2.2.3.3 SDS - polyacrylamide gel electrophoresis (SDS-PAGE)

SDS- PAGE gels 1.5mm thick were prepared manually using the Mini PROTEAN® gel casting system (Bio-Rad, UK). A 10-12% gel solution (prepared as described in **Table 2.5**) was poured into Mini PROTEAN III glass plates closely stacked together, with the addition of 1 ml of 100% (v/v) isopropanol on top, then allowed to polymerise. Isopropanol was discarded and the gel's top rinsed with dH_2O. Then 4% (w/v) acrylamide/bis-acrylamide stacking gel was prepared as described in **Table 2.6** and added unto the polymerised resolving gel, with the addition of a 10-well comb. The gel was left 15-20 minutes to polymerise and then moved in an electrophoresis chamber.

Table 2.5. Composition of SDS-PAGE resolving gel with different percentage of acrylamide (2 gels).

	Volume (ml)	
Stock solution	**10%**	**12%**
30% Protogel (30% acylamide/bisacrylamide solution - 37.5.1 ratio)	6.7 ml	8.0 ml
4X Protogel resolving buffer (1.5mM Tris-HCl, 0.4% SDS, pH 8.8)	5.0 ml	5.0 ml
Distilled water	8.3 ml	6.8 ml
10% (w/v) ammonium persulphate (APS)	200 µl	200 µl
N,N,N',N'-Tetramethylethylenediamine (TEMED)	30 µl	30 µl

Table 2.6.Composition of SDS-PAGE stacking gel (2 gels)

	Volume (ml)
Stock solution	**5%**
30% Protogel (30% acylamide/bisacrylamide solution at ratio of 37.5.1)	1.5 ml
4X Protogel stacking buffer (1.5mM Tris-HCl, 0.4% SDS, pH 8.8)	2.3 ml
Distilled water	5.1 ml
10% (w/v) Ammonium persulphate (APS)	90 µl
N,N,N',N'-Tetramethylethylenediamine (TEMED) (Sigma)	13 µl

Samples, prepared as described in section 2.2.3.1, and 2.5ul of pre-stained protein ladder (prism ultra-protein ladder - Abcam) with known molecular weights (MW) were loaded into the gel placed in the appropriate buffer tank filled with electrophoresis buffer (25mM Tris-HCl, 192mM glycine, 0.1% (w/v) SDS). Protein separation via electrophoresis was performed by applying constant voltage of 110 V until the samples reached below the stacking gel, then of 150 V until the dye front reached the bottom of the gel. Gels were removed from the chamber and either prepared for transfer or stained with InstantBlue (Blue Coomassie stain) for 1 hour at RT and decolouration with water.

2.2.3.4 Transfer

Following separation of protein by SDS-PAGE, proteins were transferred from gel to a nitrocellulose membrane (0.45um pore size, GE Healthcare, UK) using the Mini Trans-Blot® western blotting system (Bio-Rad). A sandwich was assembled starting from the negative electrode side as follows: fibre pad, 2 Whatman® cellulose chromatography paper squares, polyacrylamide gel, nitrocellulose membrane, 2 filter papers and final fibre pad touching the positive electrode side. All parts were soaked in Transfer buffer before assembling (48mM Tris, 39mM Glycine, 0.0375% (w/v) SDS, 20% (v/v) Methanol). The sandwich, closed in the appropriate chamber, was then immersed into a tank filled with cold transfer buffer, together with an ice pack, and run at constant current (180 mA) for 70 minutes.

2.2.3.5 Ponceau red staining

In order to visualise proteins on the nitrocellulose membranes, a red Ponceau S staining was used (0.1% w/v Ponceau S, 5% v/v glacial acetic acid). Membranes were immersed in the ponceau red solution for 5-10 minutes, washed with water to remove excess staining

and photographed for record. The protein staining was completely removed before blocking by washes with TBS-T (25mM Tris-HCl, 150mM NaCl, 2mM KCl, 0.1% (v/v) Tween-20).

2.2.3.6 Blocking and Immunoprobing

The membranes were then blocked to prevent non-specific binding of the antibodies in following steps. Blocking was performed by 1 hour shaking at room temperature with blocking buffer (5% (w/v) fat-free milk powder dissolved in TBS-T). Membranes were then incubated with appropriate primary antibody diluted in blocking buffer (as described in Table 2.2), and kept at 4°C shaking for 15 hours. On the next day, primary antibody was removed, followed by 3 washes with TBS-T (about 10 minutes each) and corresponding secondary antibody HRP-conjugated diluted in blocking buffer (as described in Table 2.2) was added, shaking at room temperature for 2 hours. The membranes were washed again with TBS-T as before and viewed using enhanced chemiluminescence.

2.2.3.7 Enhanced Chemiluminescence (ECL)

Detection of immunoreactive band was performed by using the ECL detection systems: EZ-ECL substrate (Geneflow) or SuperSignal West Femto Maximum Sensitivity Substrate (Thermo Scientific). Both systems require for reagent A and B to be mixed in equal volumes, left in the dark for 5 minutes and then applied on the membranes (facing upwards) for at least 1 minute, already placed on a tray in the LAS4000 imaging system. Images were acquired using the LAS software, with a range of exposure time from 10 seconds to a maximum of 16 minutes (increment feature).

2.2.3.8 Stripping and re-probing

In order to re-probe and investigate the expression levels of different proteins on the same membrane, nitrocellulose membranes were stripped with 0.5 M NaOH shaking for 8 minutes at room temperature and rinsed with TBS-T three times (5 minutes each). For re-probing, membranes were processed as described in section 2.2.3.6 starting from the blocking step.

2.2.3.9 Densitometry analysis

The quantification of the immuno-reactive bands intensities was carried out with the AIDA 2-D Densitometry (Advanced Image Data Analyzer) software, version 3.44. The formula used to calculate the intensity of bands against loading control was as follows:

$$\text{Normalised protein expression} = \frac{\text{Intensity/Area-bkg [a.u. / mm}^2\text{] of } \textit{protein of interest}}{\text{Intensity/Area-bkg [a.u. / mm}^2\text{] of } \textit{loading control}}$$

With bkg = background.

Normalised protein expressions were then further normalised to one control in each blot, to allow the comparison of blots performed at different times.

2.2.3.10 Dot blot

The dot blot technique was used to analyse EGGL crosslinks, as the dimension of protein aggregates was not conducive of using electrophoresis separation. Samples, either EGGL crosslinks generated *in vitro* or plasma diluted as indicated in relative figure legends, were spotted directly on a nitrocellulose membrane (5 µl per spot), allowed to dry at RT for few minutes and then processed as per classic western blotting (as described from section 2.2.3.4).

2.2.4 Crude synaptosomes preparation

Two adult mouse cortexes (kindly provided by Nottingham Trent University animal unit) were homogenised in 10 mL of cold SHE buffer (4 mM HEPES pH 7.3, 320 mM sucrose, 1 mM EGTA, protease inhibitors), using a glass-Teflon homogenizer on ice. Brain homogenates were then centrifuged at 1,000xg for 10 minutes at 4°C to obtain the Low speed supernatant (LSS). The pellet was discarded, while a part of LSS was saved for analysis (about 500 µl), while the rest was transferred to a new tube and centrifuged at 12,500xg for 20 minutes at 4°C to obtain the crude synaptosomes (pellet). Pelleted synaptosomes were washed once in SHE (10 mL/brain) and centrifuged again at 12,500xg for 20 minutes at 4°C. The final pellet (crude synaptosomal fraction) was resuspended in 1 ml SHE buffer, quantified by BCA and analysed by western blotting as described in section 2.2.3.

2.2.5 Transglutaminases activity assays

2.2.5.1 In situ TGs activity assay

In situ activity levels of TGs were visualised through incorporation of amine substrate fluorescein cadaverine (FITC-cad) as previously described (Verderio et al., 1998), with minor modifications. Briefly, cells plated on either coverslips (for primary rat neurons) or chamber slides (for primary human fibroblasts) were incubated with 0.4 mM FITC-cad in medium for 8 or 16 hours at 37°C in a humidified incubator with 5% CO_2. Additional treatments are stated for each specific experiment in the respective descriptions and figure legends. Coverslips were then gently washed 3 times with PBS pH 7.4, fixed in methanol 90% (v/v in PBS, for release of unbound FITC-cad) at -20°C for 10 minutes and then washed four times for 8 minutes in PBS. For neurons, DAPI was added during the second to last washing step, before mounting (DAKO mounting medium). For fibroblasts, microscope slides were mounted using VECTASHIELD® Mounting Medium with DAPI (Vectorlabs). Image acquisition and quantification of FITC signal were performed as described in section 2.2.2. This assay was also employed for the identification of TG2 crosslinking substrates by a quantitative proteomic approach (as described in section 2.2.14.1). For this set of experiments, hippocampal neurons were incubated for 8 hours at 37°C with FITC-Cad (0.4 mM) with or without Aβ peptide (4 μM) and TG2 inhibitor ZDON (100 μM) and lysed prior to processing for Mass Spectrometry analysis.

2.2.5.2 Cell-surface TGs activity assay

TGs activity levels on the extracellular surface were assayed in live cells by measuring the incorporation of the TGs amine substrate biotinylated cadaverine (BTC) into fibronectin (FN), as described in Jones et al., 1997. Briefly, cell monolayers were either trypsinised or detached using 5 mM EDTA in PBS pH 7.4, collected by centrifugation at 300xg for 10 minutes and counted. Cells were then plated in 96-well plates (about $0.02x10^6$ cells/well) pre-coated with human plasma FN in serum-free medium (which contains an activating concentration of Ca^{2+}, i.e. 1.8 mM), in the presence of 0.1 mM BTC. Cells were left to adhere 2 hours at 37°C, then washed with PBS pH 7.4, and incubated with 0.1% sodium deoxycholate (v/v in PBS) to induce cell lysis. The BTC incorporated into the deoxycholate-insoluble FN matrix was revealed by incubation with ExtrAvidin peroxidase (1 hour at 37°C), followed by addition of 3,3',5,5'-tetramethylbenzidine (TMB) and stopped by 2.5 N H_2SO_4 after 6-10 minutes development. Spectrophotometric absorbances were measured at 450

nm. For the detection of TG2 specific activity, cells were incubated in presence of TG2 inhibitor ZDON (100 µM). In the case of primary neurons, which cannot be trypsinised once adherent to PLL-coated surfaces, the assay was either carried out on the day of tissue dissociation (0 DIV) or cells were plated directly on FN and left to grow for a week before addition of BTC for 2 hours.

2.2.5.3 Total TGs activity assay

The total TGs activity in cell lysates was measured through incorporation of BTC into FN as previously described (Jones et al., 1997). Cells lysates were obtained as described in section 2.2.3.1, however sucrose lysis buffer (5 mM Tris-HCl pH 7.4, 0.25 M sucrose, 2 mM EDTA) was used instead of RIPA. About 60ug of total cell lysates or total volume of extracellular vesicles, were incubated 2 hours at 37°C with reaction buffer containing 50 mM Tris-HCl pH 7.4, 10 mM Dithiothreitol (DTT), 0.1 mM BTC and either 5 mM $CaCl_2$ or 5 mM EDTA. Samples were loaded in duplicates or triplicates, to a final volume of 100 µl. A standard curve with known quantities of gplTG2 (from 0 to 75 ng/well) in reaction buffer was also included. The reaction was stopped by addition of 10 mM EDTA in PBS, followed by 3 washes with 50 mM Tris-HCl pH 7.4. The plate was pre-incubated with 50 mM phosphate citrate buffer and the amount of BTC crosslinked by TGs activity was revealed as described in section 2.2.4.2 (addition of ExtrAvidin peroxidase, followed by TMB and H_2SO_4). Spectrophotometric absorbances were measured at 450 nm. TGs activity was calculated by removing the mean background values obtained for each sample in the presence of EDTA from the mean background value in the presence of calcium. Specific TG2 activity was expressed as µU/well or µU/µg of protein.

2.2.6 Total RNA isolation

Total RNA was isolated from frozen dry astrocytes and microglia pellets using the GenElute™ Mammalian total RNA miniprep kit (Sigma Aldrich, UK) according to manufacturer's instructions. Samples were eluted in 50 µl of kit elution buffer and immediately retrotranscribed. NanoDrop8000® (Thermo Scientific) was used to assess the purity and concentration of isolated RNA samples. An a260/a280 ratio between 1.8 and 2.1 was considered acceptable, indicating low protein contamination. Residual RNA samples were stored at -80^{o}C.

2.2.7 Retrotranscription (RT-PCR)

Two µg of total RNA were retrotranscribed using Superscript® II Reverse Transcriptase (Invitrogen, UK) (200U (100U/µg RNA) following manufacturer's instructions. Briefly, the reaction was prepared by mixing Oligo $(dT)_{15}$ or random primers (25 µg/ml), 1.25 mM dNTP's, 2 µg total RNA and nuclease free water to a final volume of 13 µl. The mixture was heated for 5 minutes at 65°C using a conventional thermocycler (Techne, TC3000X), briefly chilled on ice, then supplemented with First strand buffer and 10 mM DTT. If using Oligo $(dT)_{15}$ primers, the mixture was incubated at 42°C for 2 minutes, then supplemented with 200 units of Superscript® II Reverse Transcriptase and incubated at 42°C for 50 minutes, followed by inactivation by heating at 70°C for 15 minutes. If using random primers, the mixture was incubated at 25°C for 2 minutes, supplemented with 200 units of reverse transcriptase, then incubated for 10 minutes at 25°C, followed by 42°C for 50 minutes and 70°C for 15 minutes. Resulting cDNA (20 µl) was stored at -20°C.

2.2.8 Real-time PCR (qPCR)

Reaction mix was prepared as described in Table 2.7, and qPCR was carried out in a Corbett Rotor-Gene 6000 rotary analyser, each sample in duplicate, using the protocol described in table 2.8. GAPDH was utilized as the housekeeping gene. Primers are listed in table 2.9. Relative expression of each TG2 isoform was calculated according to Livak and Schmittgen, 2001.

Table 2.7. Composition of qPCR reaction

Components	Final concentration / Volume
Forward primer	400 nM
Reverse primer	400 nM
iTaq SYBR Green Supermix	1X
cDNA	1 µl
Nuclease free water	To final volume
Total	12.5 µl

Table 2.8. qPCR reaction protocol

Cycle	Cycle point
Hold	95°C, 5 min
Cycling (40 repeats)	95°C, 30 sec 60°C, 30 sec 72°C, 10 sec
Melt	Ramp from 60°C to 95°C 95°C, 90 sec 60°C, 5 sec 72°C, 5 sec

Table 2.10. Primers used in this study.

Primer name	Target	Sequence	Tm
5TG (FW)	TG2_V1/V4	5'-ACTTTGACGTGTTTGCCCAC-3'	64.9
3TG-L (RV)	TG2_V1	5'-CAATATCAGTCGGGAACAGGTC-3'	67.4
3TG-S (RV)	TG2_V4	5'-GCTGAGTCTGGGTGAAGACACAG-3'	67.4
TG2 (New) Rn F Sh (FW)	TG2_V2	5'-ATGGGTCTGTGCTCAAATCC-3'	63.9
TG2 (New) Rn R Sh (RV)	TG2_V2	5'-AAGAAAGAACATTTGGCCCTG-3'	64
TG2 Rn F Vs (FW)	TG2_V3	5'-GGAACTTTGGGCAGTTTGAG-3'	63.5
TG2 Rn R Vs (RV)	TG2_V3	5'-TTCAGGGTATGGAACTCATGG-3'	63.6
5' GDP (FW)	GAPDH	5'-GGCTGCCTTCTCTTGTGAC-3'	58
3' GDP (RV)	GAPDH	5'-GGCCGCCTGCTTCACCAC-3'	72

2.2.9 Extracellular Vesicles (EVs) isolation

EVs were isolated from biological fluids by serial centrifugations, using different protocols according to the sample type.

2.2.9.1 EVs isolation from primary astrocytes

EVs were isolated from conditioned medium (CM) of astrocytes by differential centrifugation as previously described (Prada et al., 2017; Furini et al., 2018) (**Fig. 2.1**). Specifically, 80% confluent monolayers were washed twice with PBS or Krebs–Ringer's HEPES solution (KRH) (125 mM NaCl, 5 mM KCl, 1.2 mM $MgSO_4$, 1.2 mM KH_2PO_4, 2 mM $CaCl_2$, 6 mM d-glucose, and 25 mM HEPES/NaOH pH 7.4) and incubated in serum-free media in the presence or absence of Lipopolysaccharide (LPS, 0.1 or 1 µg/ml), for 24 hours.

Conditioned media was then collected and supplemented with protease inhibitors, while cells were treated as described below for ECM preparation. Briefly, CM was first centrifuged 3 times at 300xg for 10 minutes each, in order to remove cells in suspension. This was followed by centrifugation at 1,200xg for 20 minutes to remove apoptotic bodies and then 30 minutes at 10,000xg to pellet large EVs. Finally, the supernatant was ultracentrifuged at 110,000xg to pellet small EVs. EVs were resuspended in particle-free PBS or lysed in either 40 µl of RIPA buffer (for WB analysis) or Sucrose LB (for TG activity assay). Residual proteins contained in the vesicle-free supernatants (EV-free) were precipitated using trichloroacetic acid (TCA) as follows: TCA was added to the medium (10% v/v), mixed and incubated one hour on ice. The mixture was then centrifuged for 5 minutes at 15,000xg at 4°C. The supernatant was discarded and pellet was washed once in cold acetone and collected by centrifuging for 5 min at 15,000xg. The obtained pellet was air-dried and resuspended in either PBS or lysis buffer.

ECM preparations were obtained as described in Verderio et al., 1999. Briefly, after removal of the CM, cells were washed once with PBS pH 7.4 and incubated 5 minutes with 1% sodium-deoxicholate (2 ml/flask). Lysed cells were removed and remaining ECM was scraped with Laemmli 2X diluted 1:2 in RIPA buffer (0.7 ml/flask), collected in a 1.5 ml vial and boiled. When large particulates were visible, the samples were briefly centrifuged at 1000xg prior to gel loading for WB analysis.

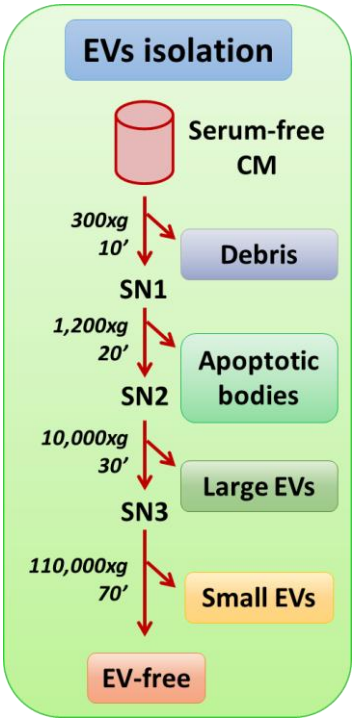

Figure 2.1. *Schematic representation of EVs isolation protocol from cell culture media*

2.2.9.2 EVs isolation from primary fibroblasts

Confluent monolayers were washed with PBS, trypsinised, counted and plated in equal number (about $0.5x10^6$ cells/flask) in T75 flasks. After 24 hours, when cells were about 60-80% confluent, fibroblasts were washed twice with PBS and incubated with serum-free media for 72 hours. Previous data showed that primary fibroblasts can be maintained in serum starvation up to 72 hours without affecting their proliferation and viability (Benussi et al., 2016). Conditioned media was collected, supplemented with protease inhibitors and serially centrifuged to separate EVs as described in section 2.1.5.1. (**Fig. 2.1**).

2.2.9.3 EVs isolation from plasma

EVs were isolated from 100 µl of plasma (pool of healthy subjects supplied by TebuBio or plasma from healthy and dementia patients) as described in Gagni et al., 2016 with minor modifications. Plasma was first diluted in 10.5 ml of particle-free PBS (1:100 dilution) and centrifuged at 29,500xg for 20 minutes at 4°C. The pellet was discarded and the supernatant (SN1) was filtered with a syringe filter (0.22 µm), then ultracentrifuged at 110,000xg for 120 minutes at 4°C. The obtained EVs pellet (P100') was either directly resuspended for analysis or washed once in PBS and ultracentrifuged again at 110,000xg for 120 minutes at 4°C to obtain the EVs pellet P100'' (**Fig. 2.2**).

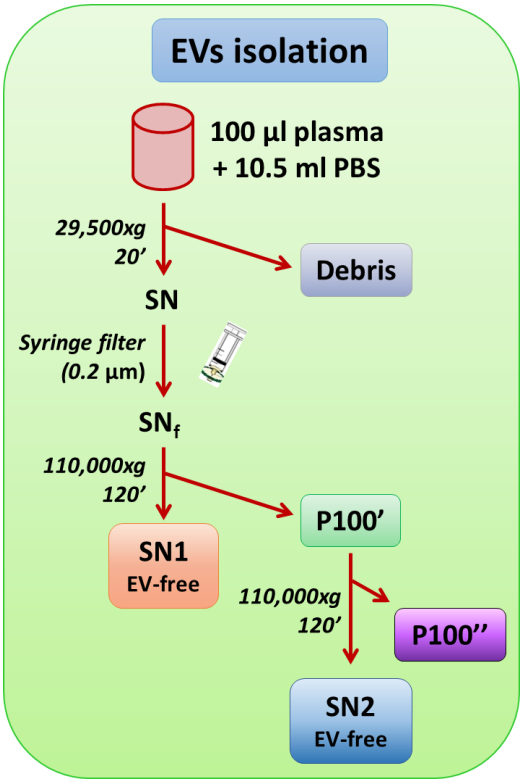

Figure 2.2. *Schematic representation of EVs isolation protocol from plasma.*

2.2.10 Nanoparticle tracking analysis

Nanoparticle tracking analysis (NTA) was performed using ZetaView PMX 120 (Particle Metrix, Meerbusch, Germany) and its corresponding software (ZetaView 8.04.02) to examine EVs size distribution and concentration. The instrument captures the Brownian motion of each particle in a video and calculates the hydrodynamic diameter of the particles based on the different diffusion movements that characterise large and small particles in suspension. Specifically, the Stokes-Einstein relationship determines that the particle diameter (d) can be calculated as a function of the diffusion coefficient (D) at a specific temperature (T) and viscosity (η) of the liquid (K_B Boltzmann's constant):

$$D = \frac{4k_B T}{3\pi\eta d}$$

Because the recording is in two dimensions, the Stokes-Einstein relationship is combined with the two dimensional mean square displacement, thus obtaining:

$$d = \frac{16k_B T}{3\pi\eta\overline{(x,y)^2}}$$

At the same time, the particles concentration is determined by counting all objects in the field of view and is automatically normalised to the measurement volume.

EVs samples, resuspended in particle-free PBS, were diluted to reach a number of 50-200 particles/frame and analysed with a flow cell sensitivity of 80% across two cycles of 11 positions/cycle.

2.2.11 Cytoplasmic calcium imaging

Intracellular calcium levels were assessed as previously described (Joshi et al., 2014). Briefly, neurons were incubated with 2 µM Fura-2/AM (Invitrogen, Life Technologies Ltd.) in neuronal conditioned medium for 40 min at 37°C. Fura-2/AM is a ratiometric calcium indicator that reaches absorption maxima at two different excitation wavelengths depending on its conjugation state. When bound to Ca^{2+} ions, Fura-2 is excited at 340 nm, while when unbound, it is excited at 380 nm. Fura-2-loaded neurons were then washed in KRH pH 7.4 supplemented with 1 µM TTX (except stated otherwise) and transferred to the recording chamber of an inverted microscope (Axiovert 100, Zeiss) equipped with a calcium imaging unit. In some experiments, sodium/potassium-free KRH was used instead, where both NaCl and KCl were isosmotically substituted for choline chloride. Polychrome V (TILL Photonics GmbH) was used as the light source with excitation at 340 and 380 nm wavelengths. Images were collected with a CCD Imago-QE camera (TILL Photonics GmbH)

and analysed with TILLvisION 4.5.66 software. Calcium concentration was expressed as F340/380 fluorescence ratio of selected regions of interest (ROI) corresponding to neuronal somata, calculated from sequences of images to obtain temporal analysis. Variations were calculated as difference between calcium concentration before (basal) and after treatments, or as Area Under the Curve (AUC) calculated by OriginLab 8 (AUC from T0 of stimulus up to 30 seconds after).

2.2.12 Patch clamp

Patch clamp experiments were performed in current clamp and voltage clamp configurations. The patch electrodes (BB150F-8P with filament, Science Products) with a diameter of 1.5 mm, were pulled from hard borosilicate glass on a Brown-Flaming P-97 puller (Sutter Instrument, Novato, CA) and fire-polished to a tip diameter of 1-1.5 µm and an electrical resistance of 4-6 MΩ. Neurons were voltage-clamped using an Axopatch 200 B amplifier (Axon Instrument) in the whole-cell configuration. Ionic currents were digitized at 5 kHz and filtered at 1 kHz. Clampex 9 was used as the interface acquisition program. The external solution was constituted of 140 mM NaCl, 5 mM TEA-Cl, 10 mM Hepes, 1 mM $MgCl_2$, 2 mM $CaCl_2$, 5 mM Glucose (314 mOsm). The internal solution was made of 127 mM Cs-Gluconate, 4 mM NaCl, 10 mM Hepes, 2 mM $MgCl_2$, 0.1 mM $CaCl_2$, 10 mM Glucose and 1 mM EGTA. 4 mM Mg-ATP and 0.3 mM Na-GTP were added fresh to the solution (295 mOsm). For current clamp experiments, the effect of TG2 on both neuron resting potential and currents was examined. Voltage clamp experiments were performed to observe the involvement of Voltage Operated Calcium Channels (VOCCs) in the phenomenon. Specifically, L-type VOCCs were isolated with a pre-pulse of 40 mV and a Δ10 mV step protocol from -30 to 0 mV.

2.2.13 Transient transfection of neurons

Neurons at 8 DIV were transfected with 1.5 µg of pEGFP-N1 vector (Clontech) or pEGFP-N1-TG2 vector (Furini et al., 2018) using 6 µl of Lipofectamine2000 (ThermoFisher Scientific). After 45 minutes incubation, transfected neurons were washed with Neurobasal and incubated in filtered conditioned neuronal medium for 48 hours before analysis.

2.2.14 Mass spectrometry (MS)

2.2.14.1 Sample preparation for MS analysis of FITC-immunoprecipitates (TG2 "Transamidome")

Neurons were obtained from the hippocampi of E18 fetal rats (13 embryos) as explained in section 2.1.1 (standard). Neurons at 9 DIV were incubated 8 hours at 37°C with FITC-Cad (0.4 mM) with or without Aβ peptide (4 µM) and ZDON (100 µM) and lysed in lysis buffer (25 mM Tris pH 7.4, 150 mM NaCl, 1 mM EDTA, 1% NP40, 5% glycerol, protease inhibitors). Nine coverslips were used for each condition and 3 coverslips were pooled together to obtain a single lysate (triplicates). The total cell lysates were centrifuged at 13,000xg at 4°C for 10 minutes and the supernatant stored at -80°C before processing. Protein concentrations were determined using the bicinchoninic acid (BCA) assay. In order to identify the protein substrates of TG2 crosslinking activity ("TG2 Transamidome"), immunoprecipitation of FITC-Cad associated proteins was performed with an anti-fluorescein monoclonal antibody (Roche) on total cell lysates, using the Pierce™ Crosslink Magnetic IP/Co-IP Kit (Thermo Scientific, UK) and following the manufacturer's instructions. Briefly, 20 µl of Pierce Protein A/G Magnetic Beads (1.6 µM) were incubated with 2.5 µg of anti-fluorescein antibody for 1 hour at room temperature in constant rotation. Antibody was then covalently bound to the beads by crosslinking with disuccinimidyl suberate (DSS, 16 µM) for 3 hours at room temperature in constant rotation. Equal amounts of neuronal lysates (14 µg) were then applied on the antibody-coated beads and incubated overnight (16 hours) at 4°C in constant rotation to allow antigen binding. Finally, proteins were not eluted in the provided elution buffer, but subjected to the trypsin digestion required for MS directly on the beads: magnetic beads – associated protein complexes were washed 3 times with 50 mM ammonium acetate and trypsin digested overnight (14 hours) at 37°C in a water bath using a final concentration of 0.02 mg/ml MS grade trypsin (Thermo Scientific, dissolved in 50 mM acetic acid) and 0.01% (w/v) ProteaseMAX™ Surfactant (Sigma) in 50 mM ammonium acetate. The next day, magnetic beads were removed using a magnetic stand, trypsin was inactivated by addition of 0.5% TFA and samples were vacuum concentrated to dryness and resuspended in 20 µl of 5% (v/v) acetonitrile/0.1% (v/v) formic acid for IDA shotgun and SWATH-MS analysis.

2.2.14.2 Samples preparation for MS analysis of total cell lysates (Proteome)

Proteins of total cell lysates (all remaining volume) were prepared as described above. First, proteins were precipitated using cold acetone (8 volumes of acetone, -80°C for 20 minutes, followed by centrifugation at 16,000×g for 10 min at 4°C and washing with cold acetone) then the pellets were solubilised in 50 mM tri-ethyl ammonium bicarbonate (TEAB) containing a final concentration of 0.02% (w/v) ProteaseMAX™ Surfactant. The protein concentrations were determined using the bicinchoninic acid (BCA) assay and used later for dry sample resuspension. Proteins were then subjected to reduction (5 mM DTT, 56°C for 20 minutes) and alkylation (15 mM iodoacetamide at room temperature in the dark for 15 minutes), then tryptically digested overnight at 37°C in a water bath using 0.02 mg/mL MS grade trypsin (ThermoScientific, dissolved in 50 mM acetic acid) and 0.01% (w/v) ProteaseMAX™ Surfactant. Trypsin was inactivated by addition of 0.5% TFA then samples vacuum concentrated to dryness and resuspended in appropriate volumes of 5% (v/v) acetonitrile/0.1% (v/v) formic acid to reach the same concentration for IDA shotgun and SWATH-MS analysis.

2.2.14.3 MS analysis: shotgun data dependent acquisition (DDA) and SWATH data independent acquisition (DIA)

Both total lysates and FITC-immunoprecipitates (FITC-IP) were analysed by reverse-phase high-performance liquid chromatography electrospray ionisation tandem mass spectrometry (RP-HPLC-ESI-MS/MS). A TripleTOF 5600+ mass spectrometer from SCIEX (Canada) was used, which is available at NTU proteomic facility (John van Geest Cancer Research Centre). MS runs were performed by Dr David Boocock and Dr Clare Coveney, while sample processing and data analysis were carried out by this thesis' author.

The mass spectrometer was used in two different modalities depending on the stage of the experiment: data dependent acquisition (DDA) was employed for spectral library construction, while SWATH data independent acquisition (DIA) was used for the acquisition of quantitative data (as described in Gillet et al., 2012).

Regarding the liquid chromatography, HPLC mobile phases were: A [0.1% (v/v) formic acid in LC/MS grade water] and B [LC/MS grade acetonitrile containing 0.1% (v/v) formic acid]. Samples were injected (trap/elute via 5 x 0.3µm YMC Triart C_{18} trap column) onto a YMC Triart-C_{18} column (15 cm, 3µm, 300 um i.d) at 5 µL/min using a microflow LC system (Eksigent ekspert nano LC 425) with an increasing linear gradient of B going from 3% to 30%

in 68 min; to 40% at 73 min then washing to 80% for 3 minutes before re-equilibration in a total time of 87 min (spectral library production by DDA), or 3% to 30% over 38 min; to 40% at 43 min followed by wash to 80% for 3 min and re-equilibrate for a total run time of 57 min (SWATH-DIA). Re-equilibration of the column were performed by loading 90% solvent B for 10 min followed by 5% solvent B for 10 min. Mass calibration (TOF-MS and Product ion) was performed by the MS every 4 samples using an injection of a standard of 40 fmol PepCal mix (Sciex, Canada) digest. Ionisation was via the Sciex DuoSpray™ source, using a 50 µm electrode at +5500 V.

2.2.14.3.1 Data/Information dependent acquisition (DDA/IDA)

First, a spectral library was produced in IDA mode on all samples singularly and a pool of all samples together, with the mass spectrometer set in high sensitivity mode. IDA MS files were searched using ProteinPilot 5 (SCIEX, Canada): the analysis was conducted by the software with an exhaustive identification strategy, searching the UniProt Swissprot database for rat species (January 2016 release), with addition of four TG2 isoforms (TG2_V1, TG2_V2, TG2_V3 and TG2_V4). The generated file was imported into PeakView 2.0 software (SCIEX, Canada) as an ion library and spiked in iRT retention time standards (Biognosys, Switzerland), after filtering for false discovery rate (FDR) of 1% and excluding shared peptides.

2.2.14.3.2 SWATH/Data independent acquisition (DIA), targeted data extraction and fold change analysis

SWATH DIA was then performed on all samples using 100 variable SWATH windows optimised for the samples. Unlike the DDA method in which during each cycle, an initial survey scan (TOF-MS) is performed followed by a MS/MS experiment on the highest precursors, in SWATH for each cycle the totality of the precursors are fragmented in discrete fixed or variable width *m/z* “windows” then measured (Gillet, et al. 2012). Each SWATH window was acquired with an accumulation time of 25 ms between 400-1250 *m/z* along with a single TOF-MS survey scan for 50 ms between 400-1250 *m/z*, for a cycle time of 2.6 seconds. Spectral alignment and targeted data extraction from the SWATH data were performed in PeakView 2.0 SWATH microapp (SCIEX, Canada) using the above mentioned reference spectral library generated by DDA. SWATH data was processed using an extraction window of 5 min and applying the following parameters: maximum 6

peptides/protein, maximum 6 transitions/peptide, exclude shared peptides, and XIC width set at 75 ppm.

Quantitation and fold change (FC) analysis between the different conditions were carried out using the OneOmics cloud processing software from SCIEX, employing weighted average of proteins spectral results among the different biological replica to calculate FC and relative significance. The outcome of the experiment is a list of protein identification names (IDs), with $\log_2$ of FC ($\log_2$FC) values, confidence level of FC [C(FC)] and p-values of FC, all calculated by the software. Fold change values (FC) were calculated manually as $2^{\log 2FC}$.

$$\log_2[FC_{A\ vs\ B}\ (X)] = \log_2 \frac{Mean\ Intensity\ of\ protein\ X\ in\ treatment\ A}{Mean\ Intensity\ of\ protein\ X\ in\ treatment\ B}$$

Under suggestion of Dr David Boocock and the SCIEX technical assistance for the software, the OneOmics confidence score was advised to be a better measure of the significance of the FC, over p-value. This is because the algorithms within OneOmics platform take into account the variance among all of the values for the peptides and the peptide fragments (transitions), to generate the confidence score, whereas, a p-value of FC calculated from the protein peak areas, does not. Fold changes with a confidence higher than the 0.80 (80%) were regarded as highly significant. Values with confidence between 0.80 (80%) and 0.5 (50%) were acceptable but less significant, and values with C(FC) lower than 0.5 should not be considered as significant. In the analyses performed in this thesis, data were regarded as significant if C(FC) was above 60% for the transamidome and 70% for the proteome.

2.2.14.3.3 Bioinformatic analysis

Once we obtained the proteome data, a functional analysis of the listed proteins was performed using PANTHER (Protein ANalysis Through Evolutionary Relationships) database (http://www.pantherdb.org), an open source bioinformatics resource (Mi et al., 2013). Proteins were classified according to PANTHER Gene Ontology (GO) terms for “Protein Class”, “Molecular Function”, “Biological Process” and “Cellular Component” (GO-Slim feature). Gene Ontology is in essence a project that aims to generate a common scientific vocabulary unifying the different properties and characteristics of genes in a standardised manner. Each term is matched to a specific and unique code, so that each gene would be

associated with a list of annotations that define its functions and characteristics, which in turn can be grouped in larger categories. The GO terms for the abovementioned ontologies were organised in tables, and in the case of molecular function were visualised in pie chart as percentage of representation of the specific GO annotation term (number of proteins belonging in that specific annotation term, or class) over the total number of class hits (for all the annotation terms individuated in the list of proteins).

2.2.15 TG2 enzyme-linked immune sorbent assay (ELISA) - Covalab

This assay is based on the double antibody sandwich technology for the detection of TG2 (human and guinea pig). Briefly, samples and TG2 standard curve were diluted in sample buffer (0-1 µg/ml), added to a 96-well plate pre-coated with a monoclonal antibody anti-TG2, and incubated at 37°C for 2 hours. After 3 washes with appropriate wash buffer, a second (different) monoclonal anti-TG2 detection antibody was added and incubated for 1 hour at 37°C, followed by washes and addition of HRP-conjugated secondary antibody. After 30 minutes at 37°C, the plate was washed and developed by addition of TMB substrate and H_2SO_4, then absorbance was detected by a spectrophotometer at 450 nm.

2.2.16 TG2 ELISA – optimised in the course of this project

This assay was optimised starting from an already published protocol developed by our research group (Verderio et al., 2003; Scarpellini et al., 2009). The principle is represented in **Fig. 2.3** (also Fig. 6.9). A 96-well plate was coated with 5 µg/ml FN in Tris-HCl 50 mM pH 7.4 (assay buffer), for which TG2 has high affinity, and incubated 15 hours at 4°C. After 2 washes with assay buffer, the plate was blocked with 3% BSA (w/v in assay buffer) for 1 hour at 37°C. A standard curve of gplTG2 from 0.0078 to 0.5 µg/ml was prepared in blocking buffer, with addition of 1.22 mM $CaCl_2$ and 2 mM EDTA. A blank with blocking buffer alone was included. The chelating agent EDTA was added to avoid possible interference in the TG2-FN binding due to active TG2 and crosslinking. After blocking, the plate was washed twice in assay buffer, then the samples were applied in duplicate (50 µl/well) and incubated 3 hours at 37°C. This was followed by 3 washes and addition of primary detection antibody against TG2 (CUB7402) diluted 1:1000 in blocking buffer, incubated 15 hours at 4°C. The plate was then washed 3 times with assay buffer supplemented with 0.05% Tween20 and incubated for 2 hours at room temperature with secondary antibody goat anti-mouse-HRP-conjugated (1:2000 dilution in blocking buffer). The plate was washed again 3 times (assay

buffer + 0.05% tween20) and incubated with a developing solution containing 7.5% TMB and 0.014% H_2O_2 in phosphate-citrate buffer 0.05 M, until a blue colour was detected (about 6-10 minutes incubation in the dark). Reaction was stopped by addition of H_2SO_4 and absorbance was read with a spectrophotometer at 450 nm.

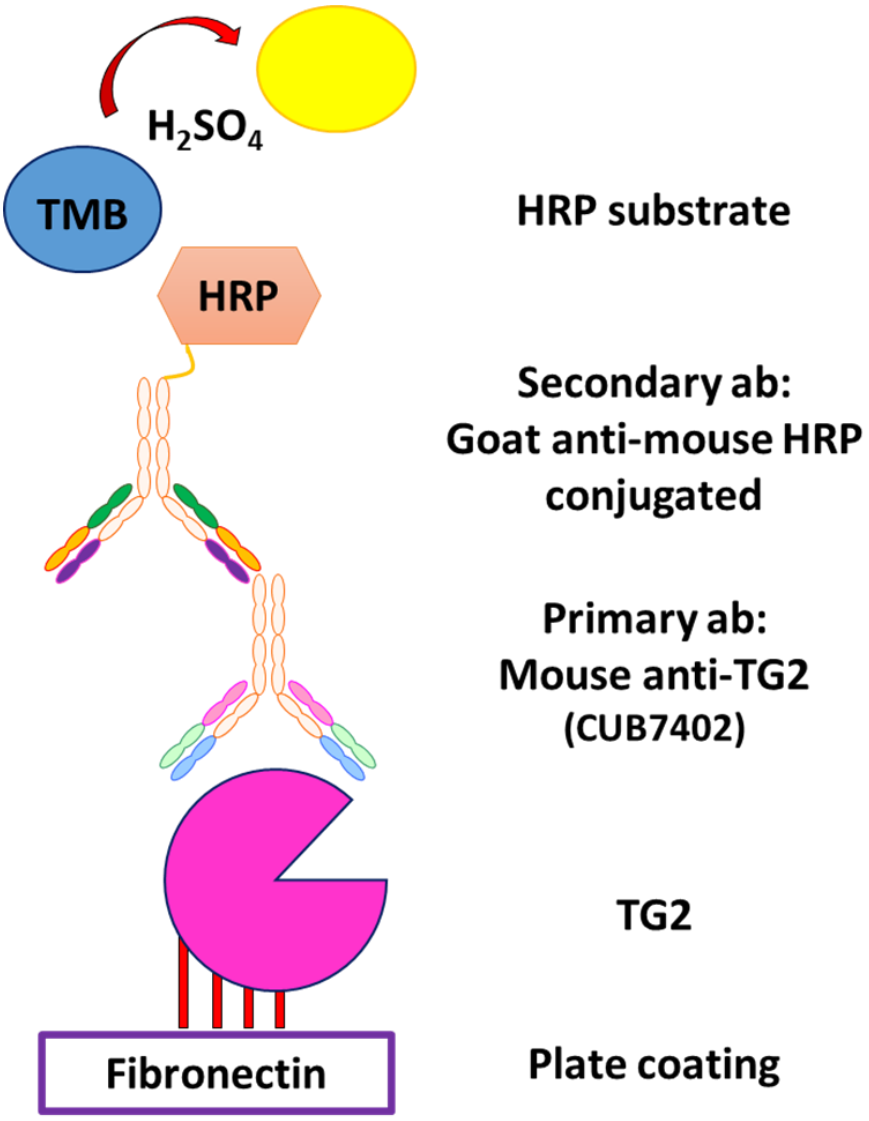

Figure 2.3. Principle of an ELISA-based assay for detection of TG2 in plasma.

2.2.17 Generation of crosslinking products (EGGL) *in vitro*

In order to have a positive control for the detection of crosslinking products in plasma, EGGL were generated *in vitro* by incubating 200 ng of gplTG2 with its substrate FN (either full length or the 30 kDa fragment, 500 ng) in activating conditions (Tris-HCl 50 mM pH 7.4, 5 mM $CaCl_2$ and 10 mM DTT). Different temperatures and time steps were tested, as indicated in the relative figure legends. Crosslinking products were either loaded in a 10% acrylamide gels in reducing conditions for SDS-page, or directly spotted on a nitrocellulose membrane for dot blot analysis, as described in section 2.2.3. Chelating agent EDTA (5 mM) was added to the mix prior to TG2 as negative control, to block TG2 catalytic activity and hence inhibit crosslinks generation.

2.2.18 Statistical analysis

Data are presented as mean ± S.E. for the indicated number of experiments. In order to test for normality of the distribution, all datasets were analysed with the Kolmogorov–Smirnov (K-S) test. Because all analysed data presented a normal distribution (K-S $p>0.05$), statistical analysis was performed using Student's t-test or one-way ANOVA and differences were considered to be significant by $p\leq0.05$.

CHAPTER 3:

Characterisation of TG2 in primary neuronal cells and astrocytes

3.1 Introduction

TG2 has been shown to be present in rat brain, as well as the in human CNS, specifically both in neurons and glial cells (Gilad and Varon, 1985; Campisi et al., 1992), mainly showing a cytoplasmic localisation (Kim et al. 1999; Maggio et al. 2001). Appelt and colleagues were the first to demonstrate the presence of TG2 specifically in hippocampal neurons by immunocytochemistry, however by using a non-specific antibody against FXIII, another member of the transglutaminase family (Appelt et al., 1996). To date, a detailed characterisation of TG2 localisation in hippocampal neurons has not been published yet.

Increased amounts of TG2 protein and activity in different brain regions or cells have been implicated in various neurodegenerative diseases, especially relating the enhanced crosslinking activity with the progressive accumulation of protein aggregates, a common hallmark of brain proteinopathies (Lorand, 1996; Johnson et al., 1997, Martin et al., 2011). However, a TG2 specific role in physiological conditions and disease progression is still unclear, and the available data support both a protective and a neurotoxic role. For example, early work on TG2-deficent mice showed that the enzyme absence did not cause developmental abnormalities, and no evident changes were found in the major organs inspected at the histological level (De Laurenzi and Melino, 2001). The authors' explanation was that the presence of other members of the transglutaminase family, like TG1, could possibly compensate for TG2 absence. On the other hand, more recent studies have shown that in a mouse model overexpressing human TG2 in brain, increased levels of TG2 led to higher sensitivity to kainic acid-induced seizures and hippocampal damage (Tucholski et al., 2006). Conversely, the same group also showed that TG2 could play a protective role in the same mouse model, by attenuating ischemic-induced cell death (Filiano et al., 2008; Filiano et al., 2010). More recently, TG2 depletion in normal cortical neurons was shown to affect cell viability, by regulating genes involved in neurite growth and maintenance (Yunes-Medina et al., 2018). Specifically, Gale Johnson group performed TG2 knock down in primary neurons by a shRNA lentivirus and observed a consequent decrease in cell survival, and upregulation of genes involved in extracellular matrix (ECM) function, cytoskeleton integrity pathways and cell signalling, indicating a neurotrophic role for TG2 in physiological conditions (Yunes-Medina et al., 2018). At the same time, increased expression of both TG2 and TG1 following oxidative stress in rat cortical neurons was shown to induce cell death, whereas pharmacological inhibition of both enzymes had a neuroprotective effect (Basso et al., 2012).

Interestingly, TG2 and TG6 have been shown to increase in the hippocampus following incubation of the organotypic cultures with the gliadin peptide 31-43, which was tested in an epilepsy mouse model in the context of gluten-related diseases (Gerace et al., 2017). The deamidating activity of transglutaminases (TGs) was shown to exacerbate the kainic acid-mediated neurotoxic effect of p31-43, thus linking TGs to gluten-related epilepsy (Gerace et al., 2017).

Several studies have shown an increase of TG2 mRNA, protein and activity in models of forebrain ischemia, especially in the hippocampus (Ientile et al., 2004, Tolentino et al., 2004). TG2 was found to increase in blood vessels, microglia and the CA1 hippocampal field following ischemia, and its inhibition by cystamine had a protective effect, delaying neuronal death (Hwang et al., 2009). Downregulation of TG2 activity and protein levels by 17β-Estradiol treatment also protected against hippocampal neuron cell death induced by transient ischemia (Fujita et al., 2006), in apparent contradiction with some of the aforementioned work (Filiano et al., 2008; Filiano et al., 2010; Yunes-Medina et al., 2018).

Other than in neurons, TG2 has also been studied in glial cells, especially in relation to neuroinflammation. Stimuli such as oxidative stress, calcium dysregulation and the production of inflammatory cytokines have been shown to increase TG2 expression and activity in a variety of glial cells models (as reviewed in Ientile et al., 2015). For example, glutamate induced increase of TG2 in primary astrocytes and this was shown to mediate the activation of transcription factor nuclear factor kappa-light (NF-κB), one of the main inducers of immune response and inflammation, by promoting its dimerization and translocation to the nucleus (Caccamo et al., 2005). In turn, NF-κB activation could sustain TG2 expression, in a positive feedback loop (Caccamo et al., 2005). A similar connection had been previously shown in microglial BV2 cells, strengthening the evidence of TG2 involvement in the neuroinflammatory process (Lee et al., 2004).

Gale Johnson's research group from Rochester University (New York, USA) has published in the last decade multiple papers focused on the role of TG2 in both cortical neurons and astrocytes. They illustrated that TG2 ablation is protective in astrocytes, as it promotes their survival under oxygen/glucose deprivation in an ischemic brain mice model, and thus improves their ability to protect neurons (Colak and Johnson, 2012; Feola et al., 2017). However, TG2 inhibition is also a negative factor in repair processes as it affects astrocytes migration, consequently reducing their ability to form a glial scar after brain injury (Monteagudo et al., 2017). This could have both a positive and negative effect, by reducing

inflammation but also impeding neuronal growth (Okada et al., 2006; Renault-Mihara et al., 2008). A similar observation was made in a spinal cord injury mice model, where TG2 KO was shown to attenuate scar formation and increase astrocytes ability to protect neurons from injury, confirming a possible deleterious role of TG2 in astrocytes (Monteagudo et al., 2018).

Pinzón and colleagues have recently demonstrated that astrocytes externalise TG2 under neuroinflammatory conditions that mimic Multiple Sclerosis pathology, both *in vitro* and in a de/re-myelination mice model, affecting ECM deposition and astroglial scarring (Pinzón et al., 2017a,b).

Interestingly, work from Kawabe et al. (2017) has shown that astrocyte-derived TG2 present in the astroglial conditioned media (ACM) was able to accelerate aggregation of Aβ *in vitro* when the freshly prepared peptide was diluted in ACM, and this effect was blocked in the presence of TG2 inhibitor cystamine. In turn, Aβ aggregates added to cultured astrocytes stimulated TG2 expression both intracellularly and in the ACM, highlighting a role for astrocytic TG2 in AD pathology (Kawabe et al., 2017).

In summary, literature data suggest that TG2 could have opposite effects in brain, depending on the type of injury, brain region and cell type considered (Quinn et al., 2018). Although intensive research has been done on this topic, further studies are necessary to understand TG2 role in neurons and astrocytes. Additionally, there is still very limited knowledge on how TG2 is externalised by either cell type, thus promoting any kind of effect on recipient cells.

3.1.1 Aims of this chapter

The general aim of this chapter was to characterise the expression and localisation of TG2 in primary cells isolated from embryonic rat brains, specifically hippocampal neurons and astrocytes. Moreover, the possibility that TG2 could be externalised through astrocytes-derived extracellular vesicles (EVs) was investigated.

3.2 Results

3.2.1 TG2 is localised at neuronal synapses

The presence of TG2 in the brain at tissue and cell level has already been reported, especially in relation to its role in neuroinflammation and brain injury (Martin et al., 2013; Ientile et al., 2015; Quinn et al, 2018). However, most published data about TG2 in neuronal cells is focused to cortical neurons or tissue sections, and specific information about TG2 localisation in hippocampal neurons is sparse.

For this reason, TG2 was first characterised in the cultures of primary rat embryonic hippocampal neurons, with particular focus on its localisation respect to neuronal synapses. For these experiments, neurons were either isolated from hippocampi freshly dissected from rat fetal brains (at embryonic day 18) or dissociated from brain tissues purchased from BrainBits (E18 Rat Hippocampus kit) and maintained according to standard procedures (as described in Methods chapter 2.2.1). Neurons were plated on surfaces coated with poly-L-Lysine (PLL) (either tissue culture plates or glass coverslips) and grown up to 22 days-in-vitro (DIV). Images shown in **Fig. 3.1** are an example of neurons growing in a standard 2-dimentional (2D) culture up to 11 DIV, characterised by progressive differentiation and outgrowth of axons and dendrites, and formation of an intricate network of synaptic connections.

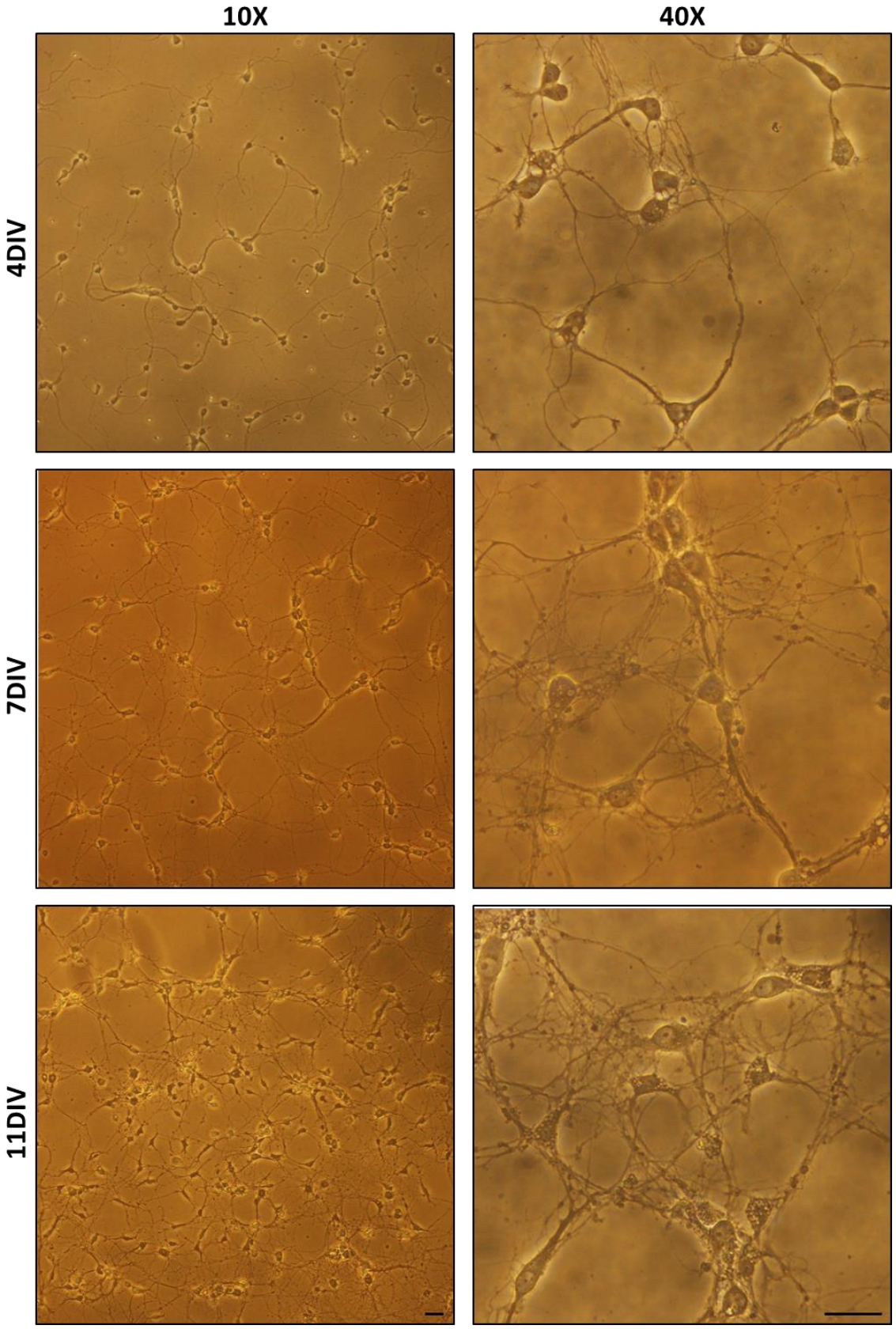

Figure 3.1. Culture of primary rat embryonic hippocampal neurons. *Primary rat embryonic hippocampal neurons were disassociated according to BrainBits protocol and plated on PLL-coated 6-well plates. Cells were maintained in Neurobasal-B27 medium and visualised by Ts100 Eclipse Optical Microscope (Nikon) using 10X and 40X objectives. Scale bars 20 µm.*

The expression of TG2 was initially investigated using immunofluorescence and confocal microscopy. Neurons were differentiated *in vitro* for 22 days (22 DIV), fixed, permeabilised and TG2 was identified by a previously characterised mouse monoclonal antibody (IA12) specific for rat/mouse TG2 (Scarpellini et al., 2014). TG2 (green) showed a punctate pattern widely spread in the perikaryon, dendritic and axonal processes, while no nuclear staining was observed (**Fig. 3.2A**). In order to understand if TG2 was also present at synaptic sites specifically, a co-staining for pre-synaptic marker VGLUT1 (blue) and post-synaptic marker SHANK2 (red) was performed (**Fig. 3.2A**). By quantification of the number of TG2-positive green puncta that were co-localised with either VGLUT1 or SHANK2, it was found that the overall percentage of synaptic TG2 was about 21.2% of the total TG2 signal. Synapses were identified by co-localisation of red and blue signals, as the proximity of a pre- and post-synaptic marker characterises synaptic sites. Moreover, TG2 showed higher localisation at pre-synapses (calculated as number of IA12-VGLUT1 positive puncta normalised on total VGLUT1 puncta) compared to post-synapses (calculated as number of IA12-SHANK2 positive puncta normalised on total SHANK2 puncta), however the difference was not significant (**Fig. 3.2A**, co-localisation indicated by arrows). To confirm TG2 presence at neuronal synapses, crude synaptosomes were isolated from adult mouse brain homogenates and both low speed supernatants (LSS) and synaptosomes (SYN) were analysed by western blotting. TG2 signal, which was normalised to β-tubulin loading control, was 2.4-fold higher at synaptic contacts compared to LSS (**Fig. 3.2B**), confirming TG2 localisation at synapses. In these experiments, crude synaptosomes preparations were validated by probing with synaptic markers glutamate NMDA receptor subtype 2B (NR2B), postsynaptic density protein 95 (PSD-95), vesicular GABA transporter (VGAT) and vesicular glutamate transporter 1 (VGLUT1), which were enriched in SYN samples compared to LSS.

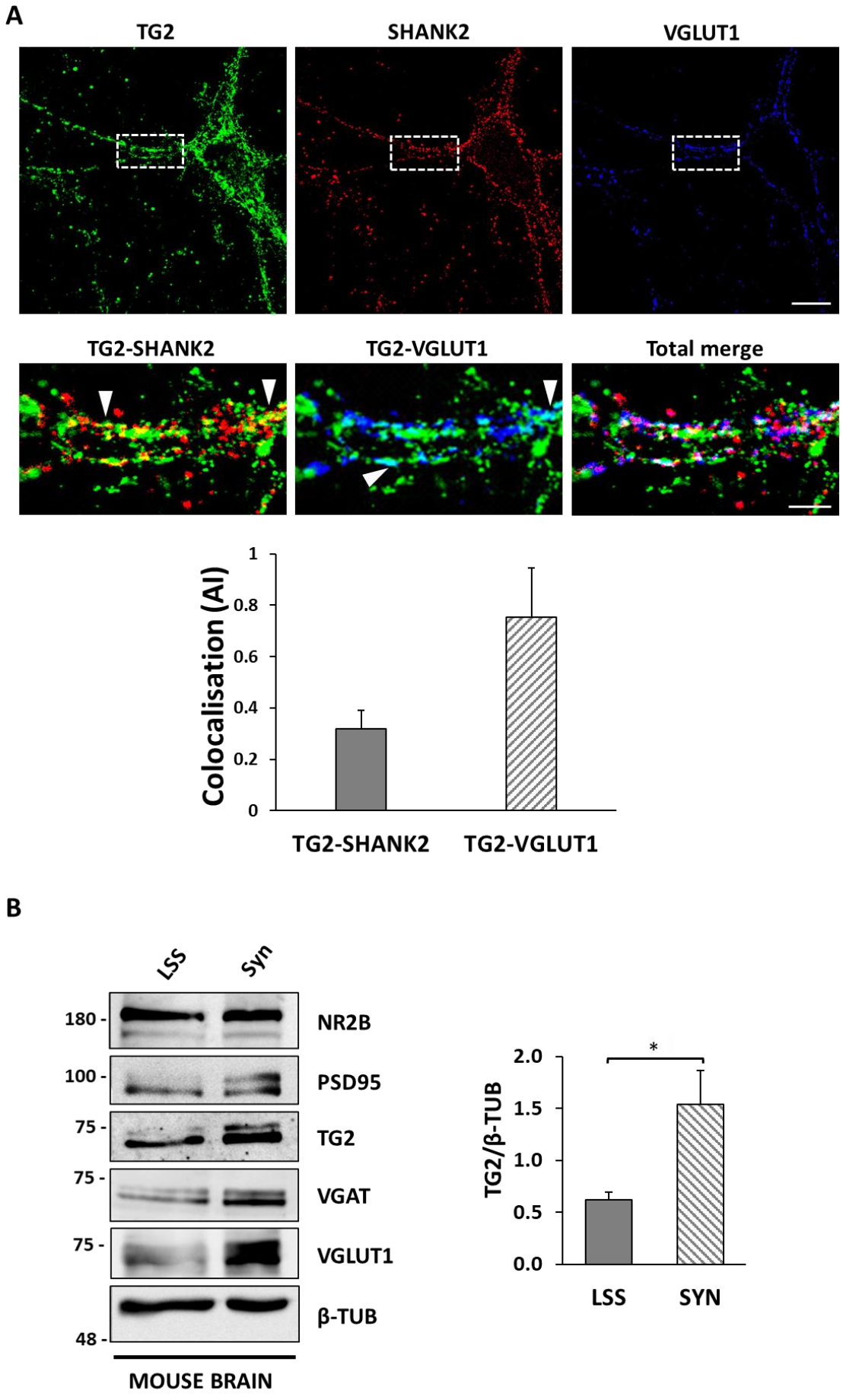

Figure 3.2. TG2 localisation in primary hippocampal neurons and synaptosomes.

Figure 3.2. TG2 localisation in primary hippocampal neurons and synaptosomes. A) *Immunofluorescence staining of primary hippocampal neurons at 22 DIV (standard). Cells were fixed in 4% paraformaldehyde - 4 % sucrose (w/v), permeabilised and stained with anti-TG2 IA12 (green), anti-SHANK2 (red), anti-VGLUT1 (blue) antibodies and DAPI. Coverslips were visualised by laser scanning Leica SP5 confocal microscope using 63X oil immersion objective. Successive serial optical sections (0.5 µm) were recorded over 5 µm planes. Co-localisation puncta were calculated as described in Methods chapter 2.2.2. TG2-VGLUT1 positive puncta: 0.75±0.19; TG2-SHANK2 positive puncta: 0.32±0.07 (values are expressed as mean number of TG2-SHANK2 (or TG2-VGLUT1) positive puncta normalised to total number of Shank2 (or VGluT1) puncta ± SE) (N=3 fields, p=NS). Scale bar 20 µm (low magnification) and 5 µm (high magnification). White arrow heads highlight points of co-localisation.* ***B)*** *Western blotting of crude synaptosomes isolated from adult mouse brain and probed with synaptic markers and polyclonal rabbit anti TG2 antibody. Densitometry analysis shows intensity of TG2 immune-reactive bands normalised to β-tubulin. Ratio TG2 SYN/LSS: 2.4±0.3, *p≤0.05. Data is expressed as mean ± SE (N=4).*

To investigate whether TG2 was present and active on the cell surface, primary hippocampal neurons were analysed using a previously developed plate-assay which involves growing cells in the presence of a biotinylated TG substrate (Scarpellini et al., 2009; as described in Methods chapter 2.2.5.2). Briefly, freshly isolated neurons (0 DIV) were incubated for 2 hours on a fibronectin-coated surface in Neurobasal complete medium and biotin-cadaverine. A specific inhibitor of TG2 transamidating activity (ZDON) was used to distinguish TG2-specific activity from background noise originated by aspecific binding of biotin-cadaverine or by crosslinking from other transglutaminases. As ZDON vehicle is 100% DMSO, a control condition including DMSO (0.1%) was added. TG2 activity was detectable on neurons' surface, however cells appeared to be very sensitive to DMSO, as shown from the drop in activity in the CTR+DMSO condition (**Fig. 3.3A**). ZDON treatment reduced TG2 activity, even if not at a significant level (compared to both CTR and CTR+DMSO) (**Fig. 3.3A**). Considering these results, it was possible that analysing neurons on the day of dissection could be too early to detect surface activity, as cells would have undergone digestion treatment, which could affect the presence of surface molecules, as opposed to neurons

left to grow in culture for multiple days. As described in Methods chapter 2.2.5.2, this assay requires the incubation of cells on FN-coated plates for 2 hours and generally cells monolayers are either trypsinised or detached with EDTA 5 mM in PBS pH 7.4 before addition to the plate. Because it is not possible to trypsinise neurons grown in culture on PLL-coated surfaces, TG2 cell surface activity was evaluated in neurons left to grow on FN for 7 days, followed by 2 hours incubation with biotin-cadaverine. As shown in **Fig. 3.3B**, no significant differences were observed among the tested conditions. Further attempts were made to confirm the results shown in Fig. 3.3A, but because of issues with the transport of tissues from the supplier (BrainBits US), the following delivered tissues were not suitable for analysis.

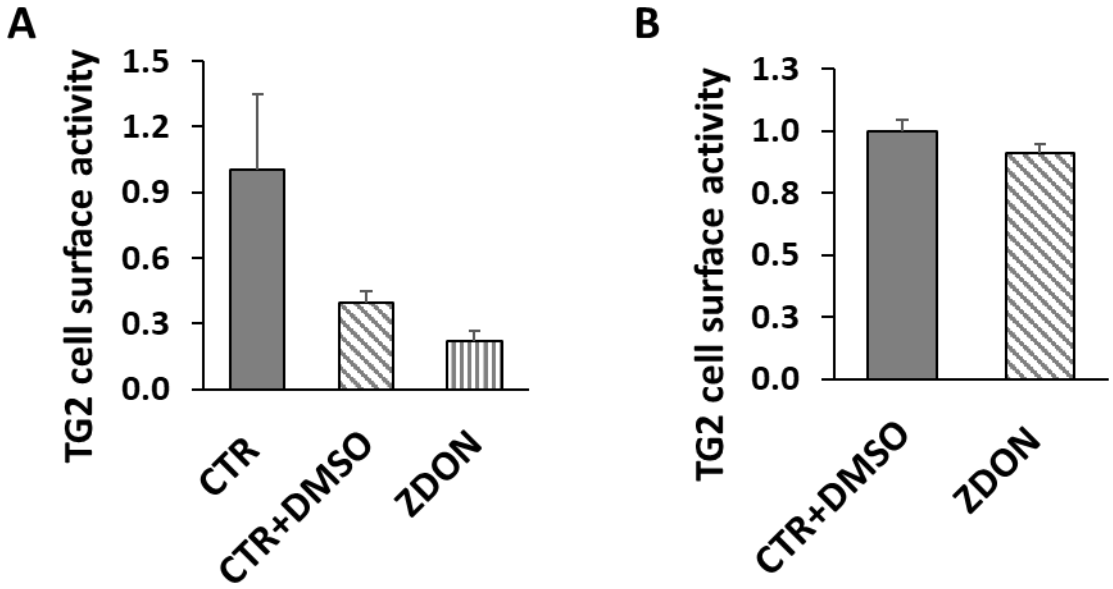

Figure 3.3. TG2 cell surface activity in neurons. A) *Cell surface TG2 activity was quantified in primary hippocampal neurons (BrainBits) on the day of tissue dissociation (0 DIV) by a cell surface activity assay (as described in Methods chapter 2.2.5.2), using TG2 inhibitor ZDON (100 µM) to validate TG2 specific activity. Data is shown as mean ± SE, normalised to CTR (N=1, each condition in triplicate). p=NS. Raw absorbance values minus background: CTR: 0.140±0.049; CTR+DMSO: 0.055±0.008; ZDON: 0.031±0.007.* ***B)*** *Neurons were grown 7 days in FN-coated plated prior to addition of biotin-cadaverine for 2 hours. Data is shown as mean ± SE, normalised to CTR (N=1, each condition in triplicate). p=NS. Raw absorbance values minus background: CTR+DMSO: 0.053±0.003; ZDON: 0.048±0.002.*

In conclusion, TG2 was detectable on neurons surface, but due to the limitation that neurons cannot be trypsinised after being plated and that analysing cells on the day of tissue dissociation is not ideal, the next step was the investigation of TG2 activity in neurons using a different approach.

3.2.2 *In situ* TG2 activity in neurons is not affected by synaptic transmission

In the previous section it was shown that TG2 localises at neuronal synapses and attempts to assess its activity levels on the cell surface were performed with limited success. For this reason a different approach was used based on incubating neurons with a FITC-labelled substrate of TG2, FITC-cadaverine (FITC-cad), as described in Methods chapter 2.2.5.1. Moreover, considering TG2 localisation at synapses, it was interesting to investigate whether TG2 activity was influenced by synaptic activity.

Neurons at 15 DIV were incubated with FITC-cad and treated 16 hours with either ZDON, to inhibit TG2 specific activity, or tetrodotoxin (TTX), an inhibitor of synaptic activity, or bicuculline (BIC), a blocker of GABA inhibitory action which enhances excitatory synaptic transmission. The initial hypothesis was that TG2 activity might decrease in the presence of TTX, a neurotoxin that blocks sodium channels, consequently stopping the calcium oscillations that characterise neural activity. On the other hand, it was speculated that treatment with BIC might increase TG2 activity, as the block of GABA receptors leads to epileptic-like seizures and increase of intracellular calcium concentration ($[Ca^{2+}]_i$).

In the absence of treatment, neurons displayed FITC-cadaverine incorporation in the cells' soma and processes, similar to TG2 protein distribution showed in Fig. 3.1A, and a signal was also detected at nuclear level (**Fig. 3.4A**). Stronger green puncta were observed along dendritic filaments and extracellularly compared to a more diffuse and lower signal in the cell body. A reduction in TG2 activity was visible in the presence of TG2 inhibitor ZDON, however image analysis did not show a significant difference (**Fig. 3.4B**). It was hypothesised that the remaining activity observed in the presence of ZDON may be due to other members of the TG family. TTX treatment quenched the level of TG2 activity visible *in situ*, but quantification of FITC-cad intensity did not show this difference to be significant (**Fig. 3.4B**). Contrary to the initial expectations, neurons incubated with BIC did not show

increased TG2 activity but actually displayed lower intensity compared to untreated neurons, although not at significant level (**Fig. 3.4B**). Western blotting analysis of similarly treated neurons did not show changes in TG2 protein levels (**Fig. 3.4C**). In conclusion, *in situ* TG2 activity was diffused in untreated hippocampal neurons over 16 hours culture, but more intense along neural dendrites and in the extracellular space. Pharmacological alteration of synaptic activity did not result in significant alterations of TG2 activity.

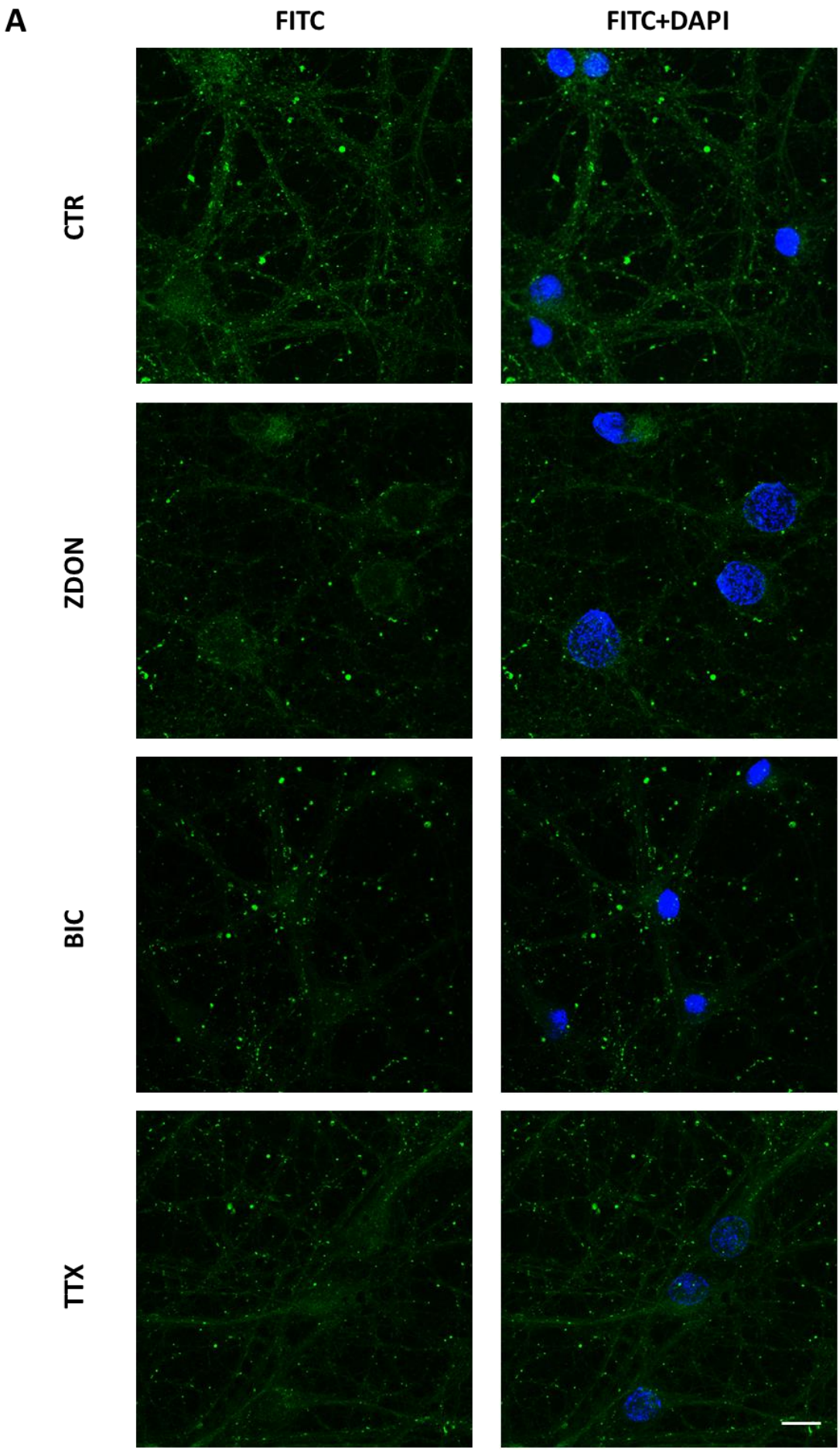
A
FITC
FITC+DAPI
CTR
ZDON
BIC
TTX

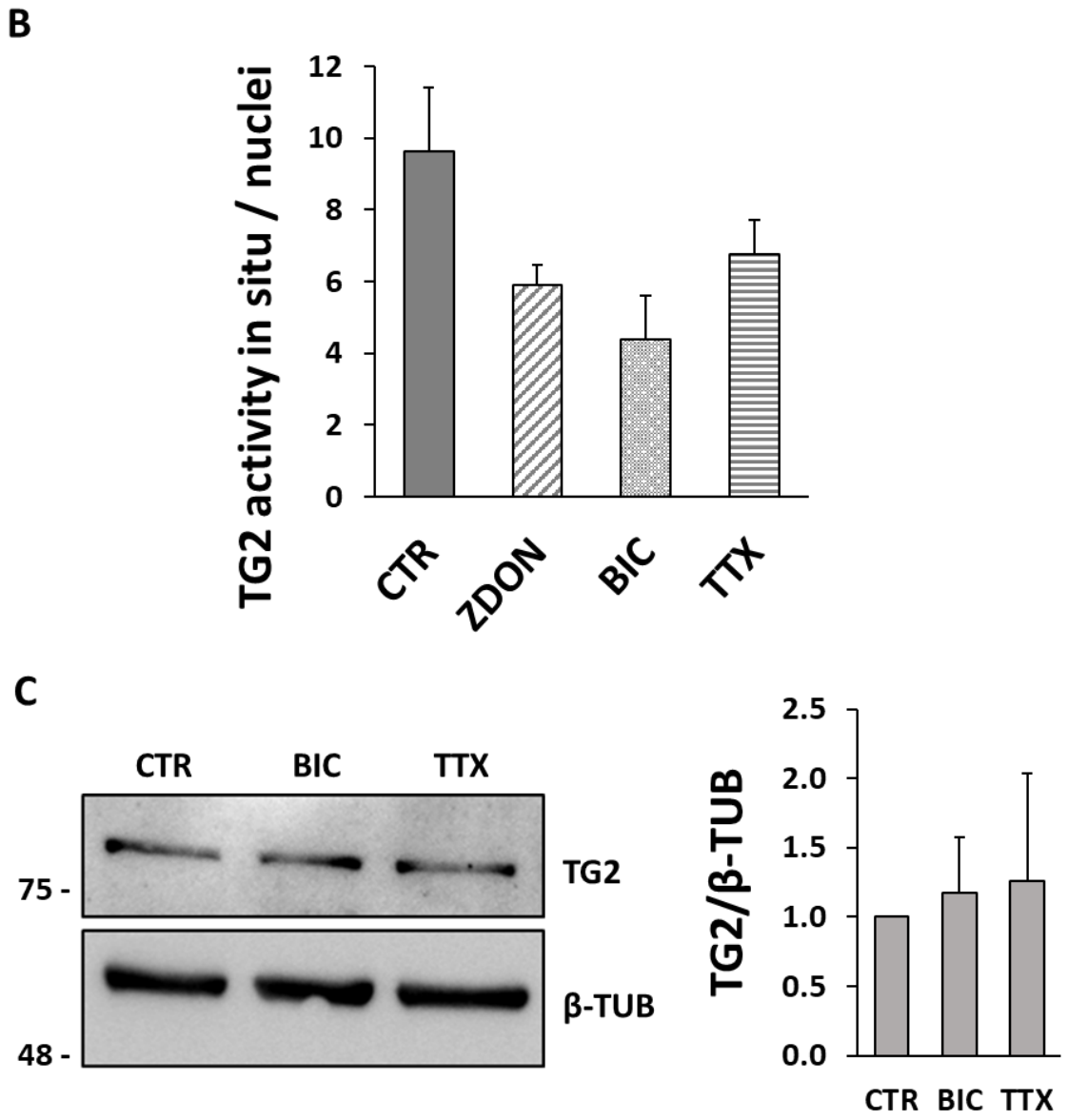

Figure 3.4. TG2 activity in situ is not significantly affected by variations in hippocampal neuron synaptic activity. *Neurons at 15 DIV (standard) were incubated 16 hours at 37ºC with 0.4 mM FITC-Cad and ZDON (100 µM), a specific inhibitor of TG2 activity, or synaptic activity inducer Bicuculline (BIC, 50 µM), an antagonist of inhibitory GABA receptors, or synaptic activity inhibitor Tetrodotoxin (TTX, 1 µM), a blocker of voltage-gated sodium channels, and analysed by activity in situ assay or western blotting.* ***A)*** *After 16 hours incubation, cells were fixed in 90% methanol (v/v in PBS), stained with DAPI and mounted. Coverslips were visualised by laser scanning Leica SP5 confocal microscope using 63X oil immersion objective. Successive serial optical sections (0.5 µm) were recorded over 5 µm planes. Scale bar 20 µm.* ***B)*** *FITC signal was quantified from maximum projection of z-stack image series and normalised by the number of nuclei (>50). Data is expressed as mean of FITC-cad intensity ± SE (N=3). P=NS. Raw intensity values: CTR: 44.0±5.1; ZDON: 34.9±2.3;*

BIC: 23.65±2.0; TTX: 37.3±4.7. ***C)*** *After 16 hours incubation, cells were lysed and analysed by western blotting for detection of TG2. Densitometry analysis shows intensity of TG2 immune-reactive bands normalised on β-tubulin (N=4, p=NS).*

3.2.3 TG2 is present and active in primary astrocytes

Up to this point of the investigation, data have shown the presence of TG2 particularly located at neuronal synapses. However, TG2 is known to be also present in other brain cell types, among which glial cells. This is particularly relevant because the role of TG2 in the diseased brain has been linked to neuroinflammation and in the CNS the cell types which are mostly involved in the inflammatory process are in fact astrocytes and microglia, the so called "immune system" of the brain (Ientile et al., 2015). As astrocytes have a role in extracellular support and repair, functions that are also attributed to TG2 at the molecular level, it was envisaged that astrocytes could be a main source of TG2 in brain. Indeed, recent evidence has shown externalisation of TG2 by astrocytes under neuroinflammatory conditions (Pinzón et al., 2017b), while TG2 presence in astrocytes has also been shown to have a neurotoxic role after ischemic injury (Colak and Johnson, 2012; Feola et al, 2017; Monteagudo et al., 2018).

TG2 was initially analysed in a variety of primary cells isolated from rat brain, namely hippocampal neurons, astrocytes, microglia and total brain homogenates. Western blotting analysis showed that TG2 protein was detectable in all cell types considered, with lower intensity in microglial cells (**Fig. 3.5A**). The expression levels of TG2 full length mRNA (TG2_V1) and the other spliced isoforms (TG2_V2, TG2_V3 and TG2_V4) were quantified by real-time PCR (qPCR) in primary rat microglia and astrocytes. Both TG2_V1 and TG2_V4 were more expressed in astrocytes compared to microglia (**Fig. 3.5B**). TG2_V2 and TG2_V3 were not included as relative quantifications were not consistent, and the Ct values of the selected housekeeping gene (*GAPDH*) were statistically different between the two cell types (*p≤0.05), hence they could not be compared. Indeed, to be able to compare two groups by qPCR, a necessary condition is that the respective reference gene quantifications are not statistically different.

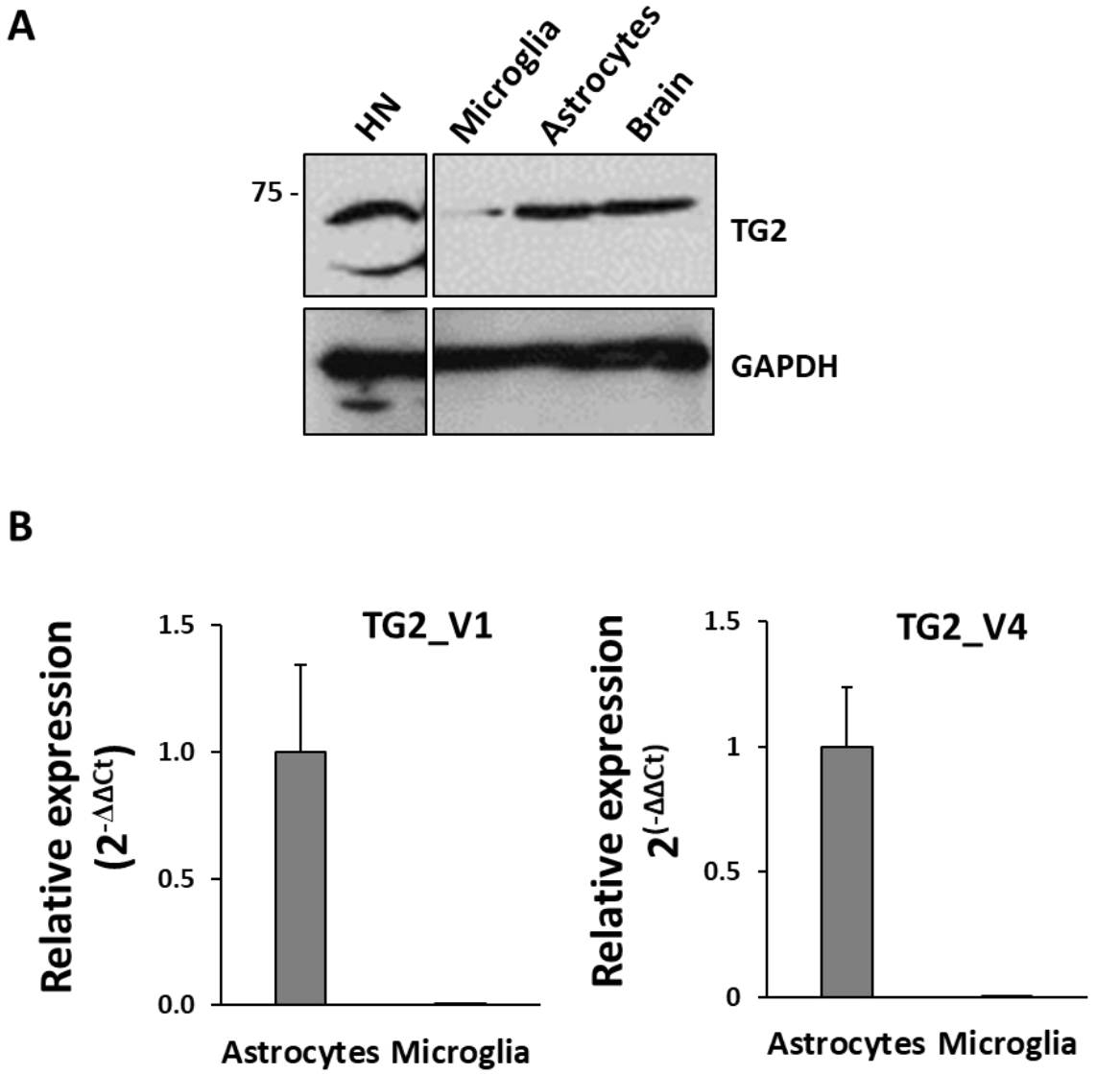

Figure 3.5. Characterisation of TG2 in neural cells. A) *TG2 protein levels were analysed in the total lysates of primary rat hippocampal neurons (HN), microglia, astrocytes and total brain homogenate (standard). Blots were probed with rabbit polyclonal anti-TG2 (Ab421) and anti-GAPDH (N=2). I thank Dr Ilaria Prada from the CNR Institute of neuroscience (Milan, Italy) for providing these blots.* ***B)*** *Relative mRNA expression of TG2 using quantitative qRT-PCR in primary astrocytes and microglia. Relative quantifications were according to Livak and Schmittgen 2001. GAPDH was used as house-keeping gene (N=3, Mann-Whitney test, p=NS).*

Seeing that TG2 was confirmed to be more present in astrocytes compared to microglia, as already shown by Pinzón et al., it was decided to focus the next experiments solely on astrocytes (Pinzón et al., 2017b).

Primary astrocytes were either isolated from freshly dissected cortices from rat fetal brains (at embryonic day 21-22) or dissociated from brain tissues purchased from BrainBits (E18 Rat cortex kit) and maintained according to standard procedures (as described in Methods chapter 2.2.1). Dissociated cells were plated on PLL-coated tissue culture plates or flasks and grown up to 60 DIV. Images shown in **Fig. 3.6** are an example of astrocytes growing in a standard 2-dimentional (2D) culture up to 40 DIV.

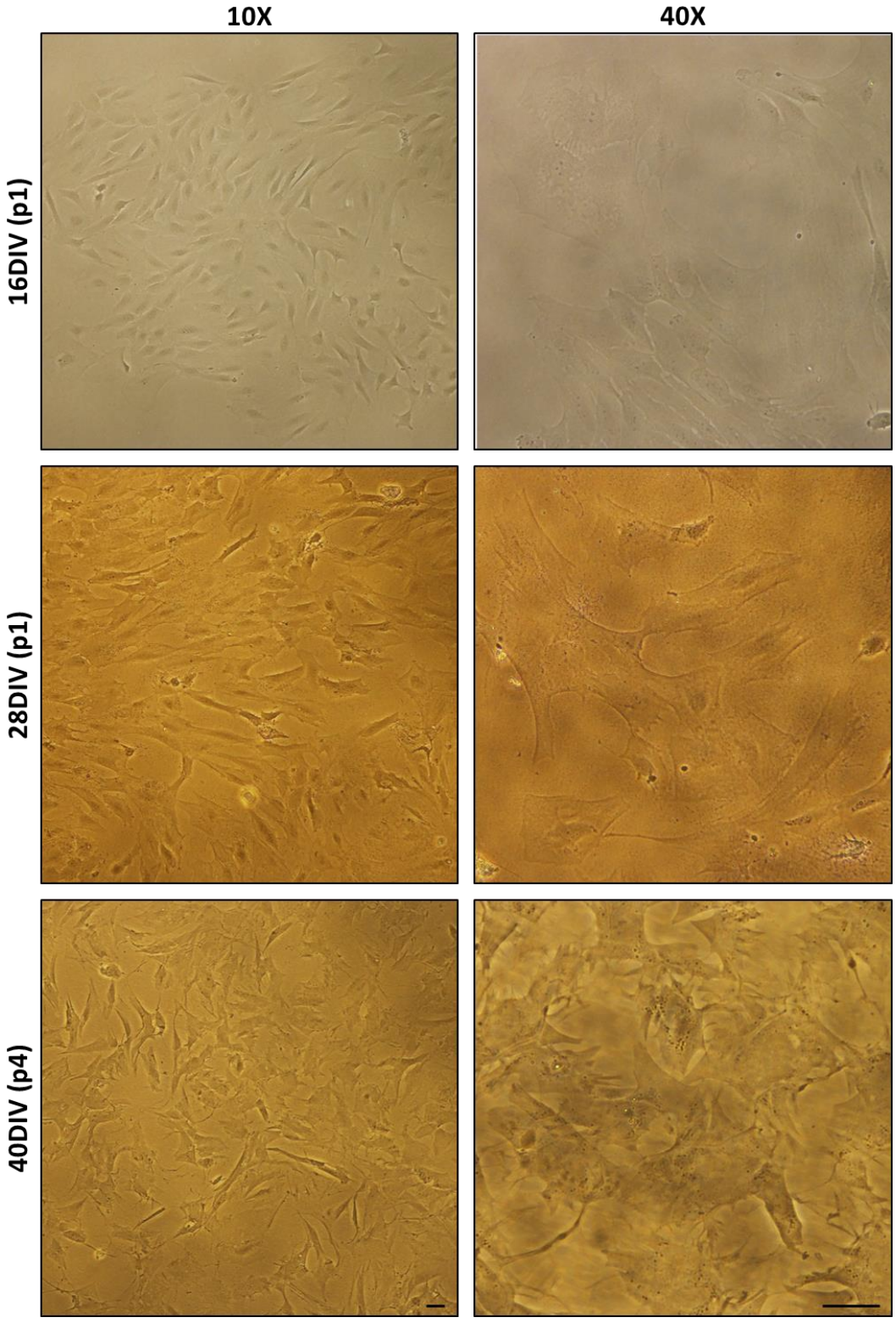

Figure 3.6. Culture of primary rat embryonic astrocytes. *Primary rat embryonic cortical astrocytes were disassociated according to BrainBits protocol and plated on PLL-coated T75 flasks. Cells were maintained in EMEM complete glial medium and visualised by Ts100 Eclipse Optical Microscope (Nikon) using 10X and 40X objectives. Cells were imaged after initial plating (p1) or following consecutive passages by trypsinisation (p4). Scale bars 20 µm.*

TG2 was then characterised by immunofluorescence. Astrocytes grown *in vitro* for 18 days (trypsinised on day 9, plated on PLL-coated coverslip and left to grow until day 18), were fixed, permeabilised and probed for TG2 (IA12 antibody, green) and astrocytic marker Glial fibrillary acidic protein (GFAP, red) (**Fig. 3.7A**). TG2 signal showed a vesicular-like dotted staining, which was mainly localised in the cytoplasm and partially co-localised with GFAP (**Fig. 3.7B**, co-localisation indicated by the white arrow). Analysis of similarly stained cells, but without permeabilisation, showed a similar vesicle-like distribution of TG2, suggesting that the protein is also localised extracellularly (**Fig. 3.7C**).

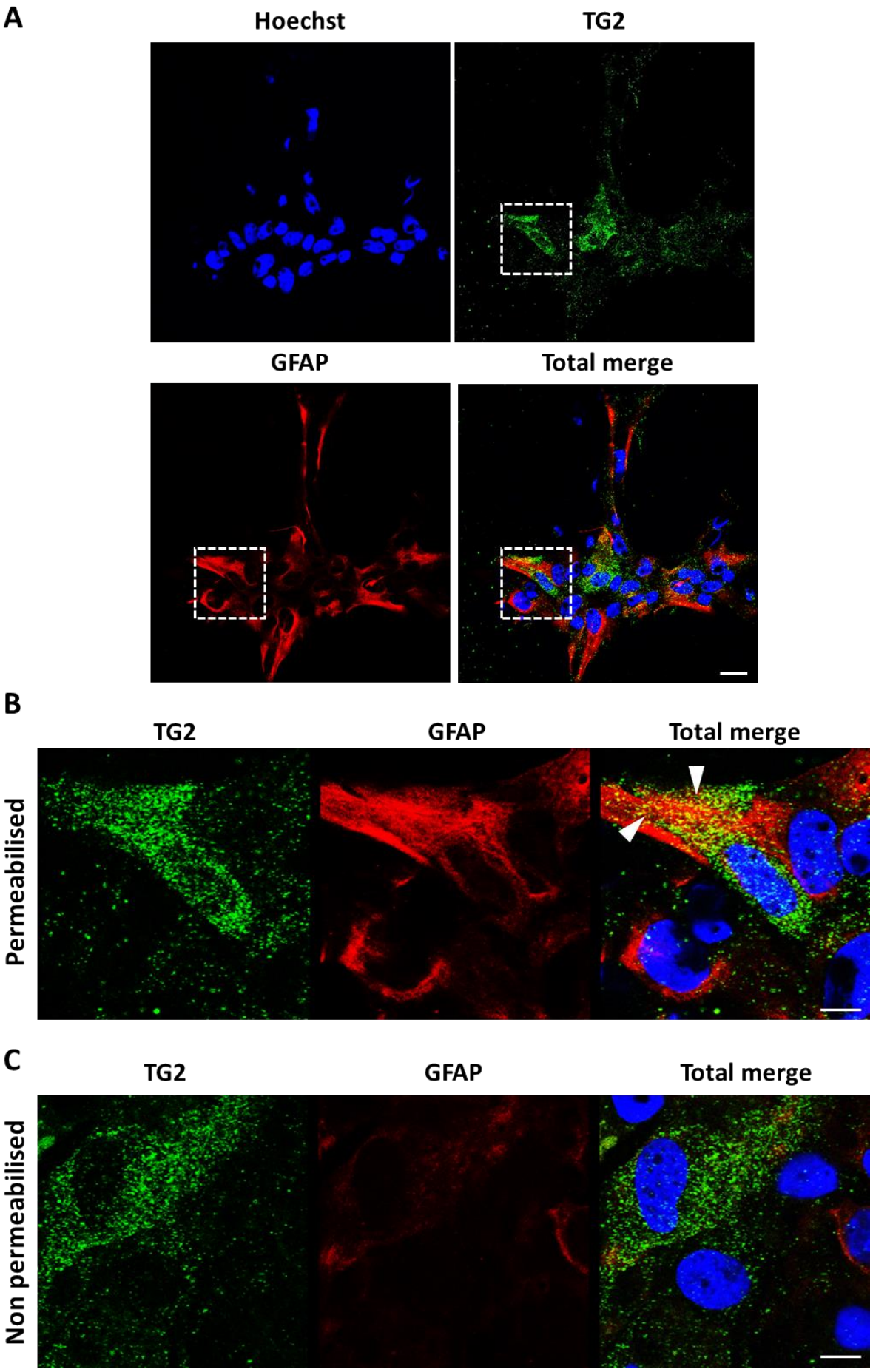

Figure 3.7. TG2 localisation in primary astrocytes.

Figure 3.7. TG2 localisation in primary astrocytes. A) *Immunofluorescence staining of astrocytes at 18 DIV (standard). Cells were fixed in 4% paraformaldehyde - 4 % sucrose (w/v), permeabilised and stained with anti-TG2 IA12 (green), Hoechst (blue) and astrocytic marker anti-GFAP (red). Coverslips were visualised by laser scanning Leica SP5 confocal microscope using 63X oil immersion objective. Successive serial optical sections (0.5 µm) were recorded over 5 µm planes. Scale bar 20 µm.* ***B)*** *Zoom-in of the white dotted line-enclosed section showing details of co-localisation between TG2 and GFAP (highlighted by the white arrow heads). Scale bar 10 µm.* ***C)*** *Zoom-in of astrocytes treated as explained in A, but without permeabilisation. Scale bar 10 µm.*

TG2 often co-localises with Fibronectin (FN), an important substrate and binding partner in the ECM (Akimov et al., 2000; Akimov and Belkin, 2001). To explore this, dual staining was performed with TG2 and ECM marker FN (red) (**Fig. 3.8**). TG2 showed a partial co-localisation with FN, but the cytoplasmic signal was more prominent in comparison to the extracellular signal, suggesting that under control condition (absence of any treatment), TG2 is not highly externalised (**Fig. 3.8**, co-localisation indicated by white arrow heads). This is in line with already published data, where it was shown that astrocytic TG2 accumulates in the ECM in response to pro-inflammatory stimuli, while very low signal was observed in the absence of treatment (Pinzón et al., 2017b).

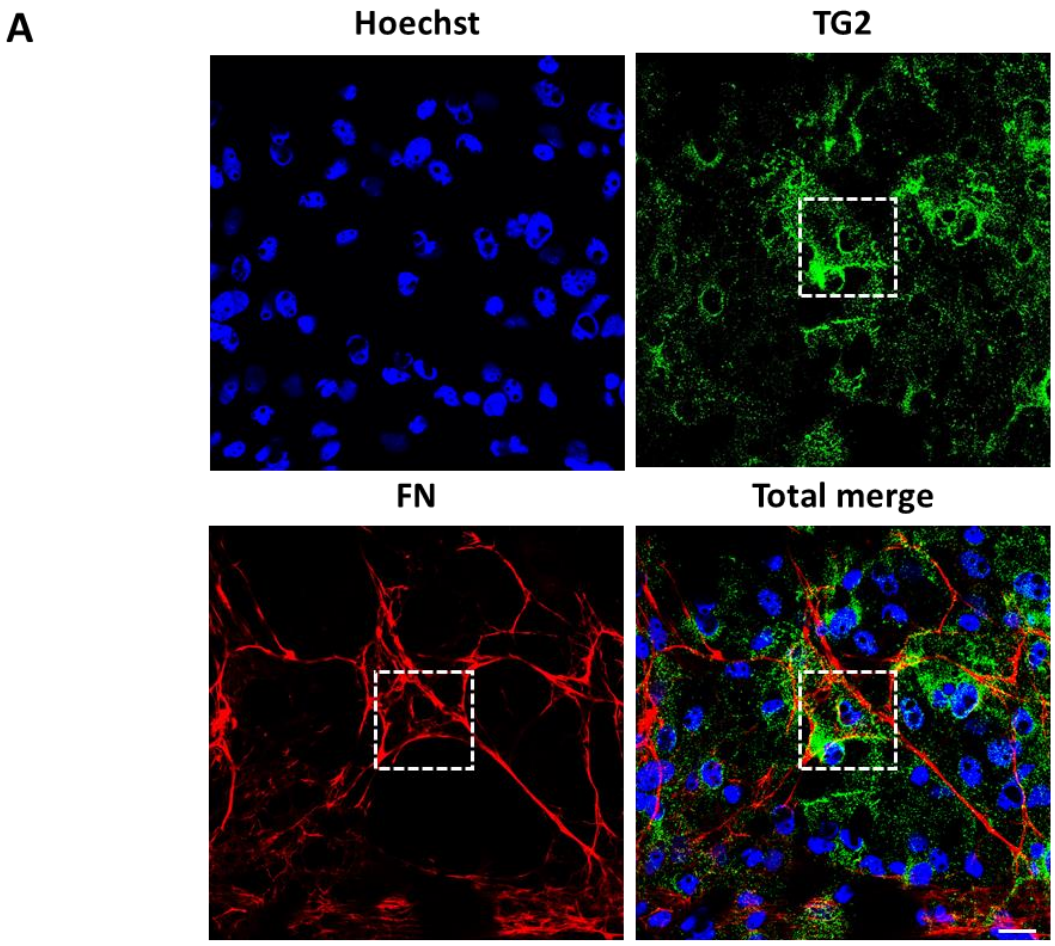

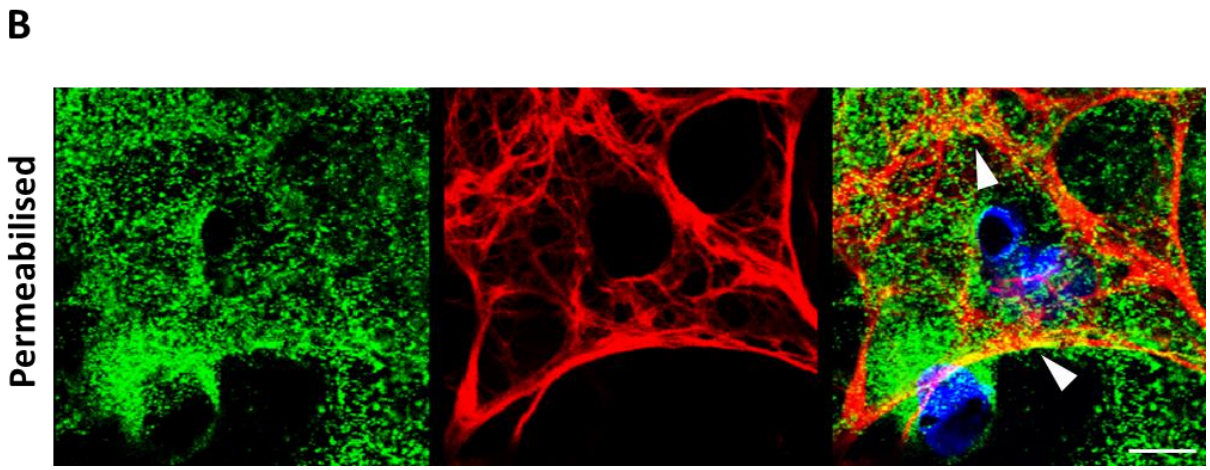

Figure 3.8. TG2 localisation in the extracellular matrix. A) *Immunofluorescence staining of astrocytes at 18 DIV (standard). Cells were fixed in 4% paraformaldehyde - 4% sucrose (w/v), permeabilised and stained with anti-TG2 IA12 (green), Hoechst (blue) and extracellular matrix marker Fibronectin (FN, red). Coverslips were visualised as explained in Fig. 3.7. Scale bar 20 µm.* ***B)*** *Zoom-in of the white dotted section showing details of co-localisation between TG2 and FN (highlighted by the white arrows). Scale bar 10 µm.*

To investigate whether TG2 was present and active on the surface of astrocytes, the cell surface activity assay already presented in section 3.2.1 was used. Astrocytes from 14 DIV up to 44 DIV were trypsinised, resuspended in serum-free media and incubated for 2 hours on a fibronectin-coated plate in the presence of calcium, biotin-cadaverine and ZDON (100 µM). Control condition included DMSO (0.1% v/v). Using this assay, TG2 specific activity was detectable on the surface of astrocytes and was significantly reduced of about 42% by treatment with ZDON (**Fig. 3.9**).

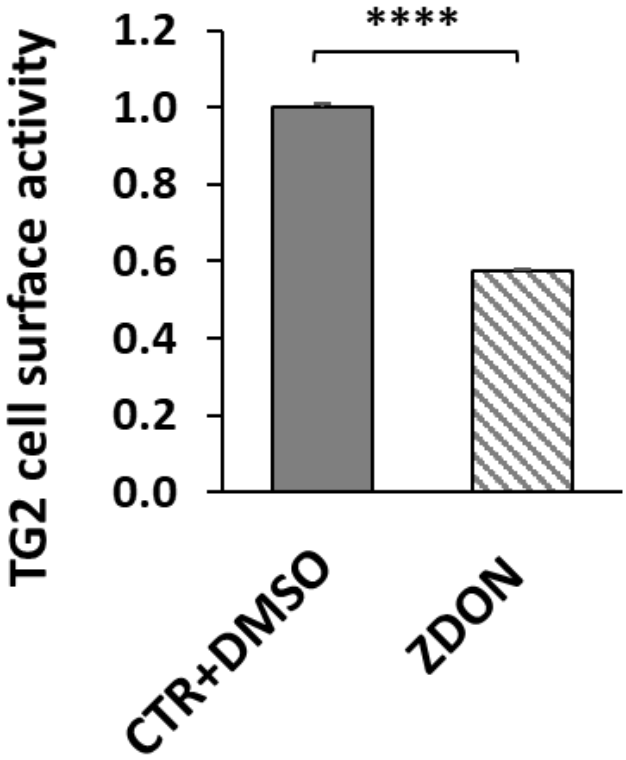

Figure 3.9. TG2 cell surface activity in primary astrocytes. *Cell surface TG2 activity was quantified in primary astrocytes (BrainBits) up to 44 DIV by a cell surface activity assay (as described in Methods chapter 2.2.5.2), using TG2 inhibitor ZDON (100 µM) to validate TG2 specific activity. Cells were resuspended in complete Neurobasal medium and plated on a FN-coated 96-well plate for 2 hours in the presence of biotin-cadaverine. Data is shown as mean ± SE, normalised to CTR in the presence of 0.1% DMSO (N=3, ****p<0.00001). Raw absorbance values minus background: CTR+DMSO: 0.120±0.009; ZDON: 0.067±0.007.*

To summarise these findings, TG2 was found to be expressed in primary astrocytes and to be active at the cell surface level. Moreover, TG2 was shown to be partially externalised and to co-localise with FN in the ECM. Because the mechanism underlying TG2 release by astrocytes is still unclear, the next objective was to investigate this process.

3.2.4 TG2 is released by astrocyte-derived exosomes upon pro-inflammatory stimuli

As already mentioned, previous work has suggested that TG2 is released by astrocytes and accumulates in the surrounding ECM (Pinzón et al., 2017b). However, the hypothesis that TG2 could be externalised via extracellular vesicles (EVs), as recently reported in other cell systems (Furini et al., 2018), was not explored. EVs are important mediators of neuron-glia communication under physiological conditions and stress responses (Proia et al., 2008; Luarte et al., 2017), and thus represent a likely vehicle for TG2 transport. Given this scenario, it was explored whether TG2 may be released in the extracellular environment by astrocytes in association with EVs.

EVs were isolated from primary astrocytes after 24 h incubation in media without serum. To simulate inflammatory stress conditions, cells were also incubated with Lipopolysaccharide (LPS) as previously shown (Bianco et al., 2005; He et al., 2018; Pena-Altamira et al., 2018). Two concentrations were initially tested (0.1 µg/ml and 1 µg/ml) and then, seeing that the higher concentration had major effect, LPS 1 µg/ml was used in the following experiments. Large and small EVs were isolated using serial centrifugations (as described in Methods chapter 2.2.9.1) and characterised by Nanoparticle Tracking Analysis (NTA) (**Fig. 3.10**). Large EVs showed a diameter of about 177 nm and a concentration of $5.7x10^8$ particles/ml, while small EVs were about 140 nm with a concentration of $3.8x10^9$ particles/ml, which are within the expected range. LPS treatment did not affect particle size or concentration (**Fig. 3.10**).

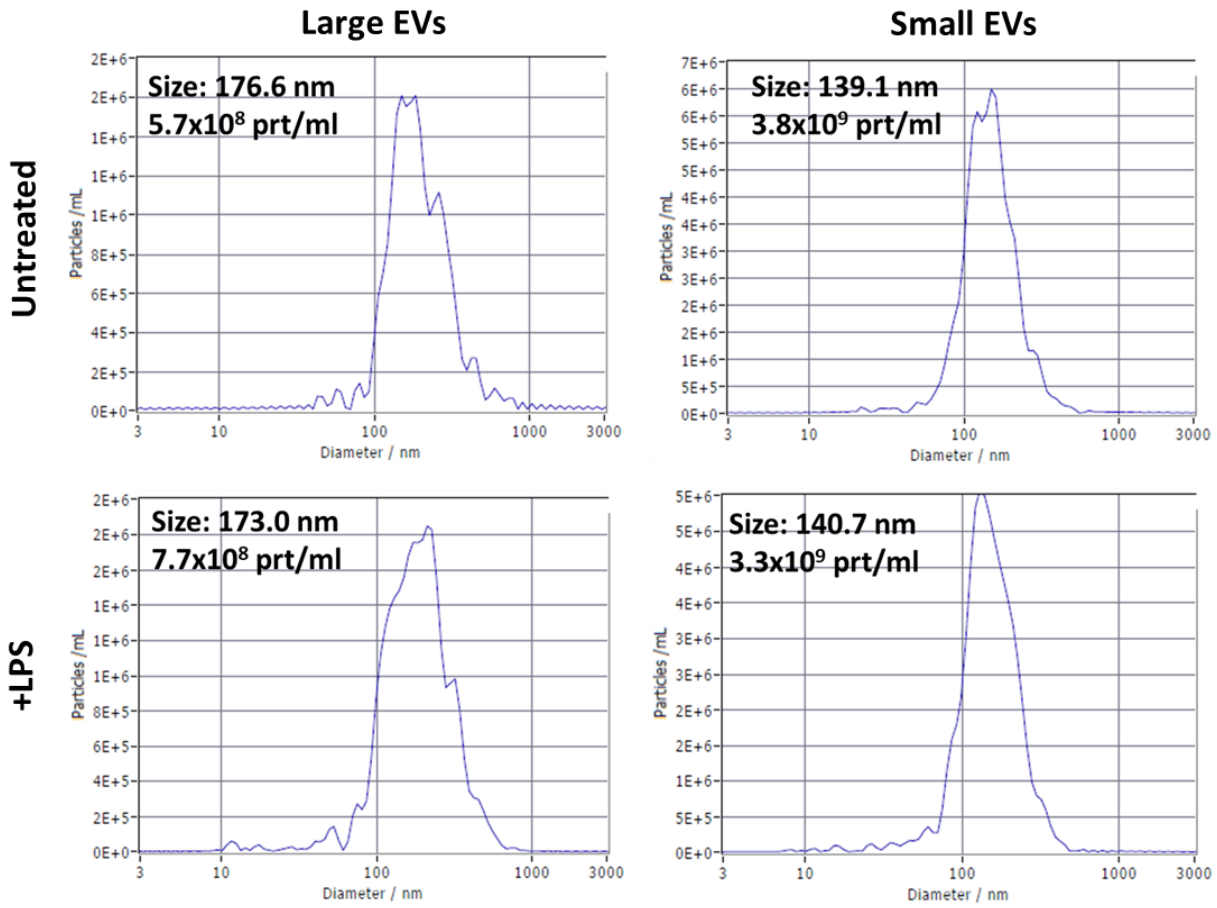

Figure 3.10. EVs characterisation by Nanoparticle Tracking analysis. *Size and concentration distribution of large and small EVs by nanoparticle tracking analysis (ZetaView, Particle Metrix). EVs isolated from both untreated and LPS-treated astrocytes (BrainBits) were isolated, resuspended in particle-free PBS and immediately analysed (N=3).*

Western blotting analysis of total cell lysates revealed that TG2 expression increased upon pro-inflammatory stimuli induced by LPS administration to astrocytes, with consequent deposition of TG2 in the extracellular matrix, which became evident upon LPS stimulation (**Fig. 3.11A**). The EV-free supernatants, following protein precipitation by trichloroacetic acid (TCA), did not show any TG2, regardless of LPS treatment (**Fig. 3.11A**). Western blotting analysis of large and small EVs lysates revealed TG2 enrichment in small EVs, but not in large EVs, isolated from LPS-treated astrocytes conditioned medium (**Fig. 3.11B**). EVs were characterised by expression of specific markers FLOT-2 and ALIX and absence of cytoplasmic astrocytic protein GFAP, other than by NTA, as showed in **Fig. 3.10**.

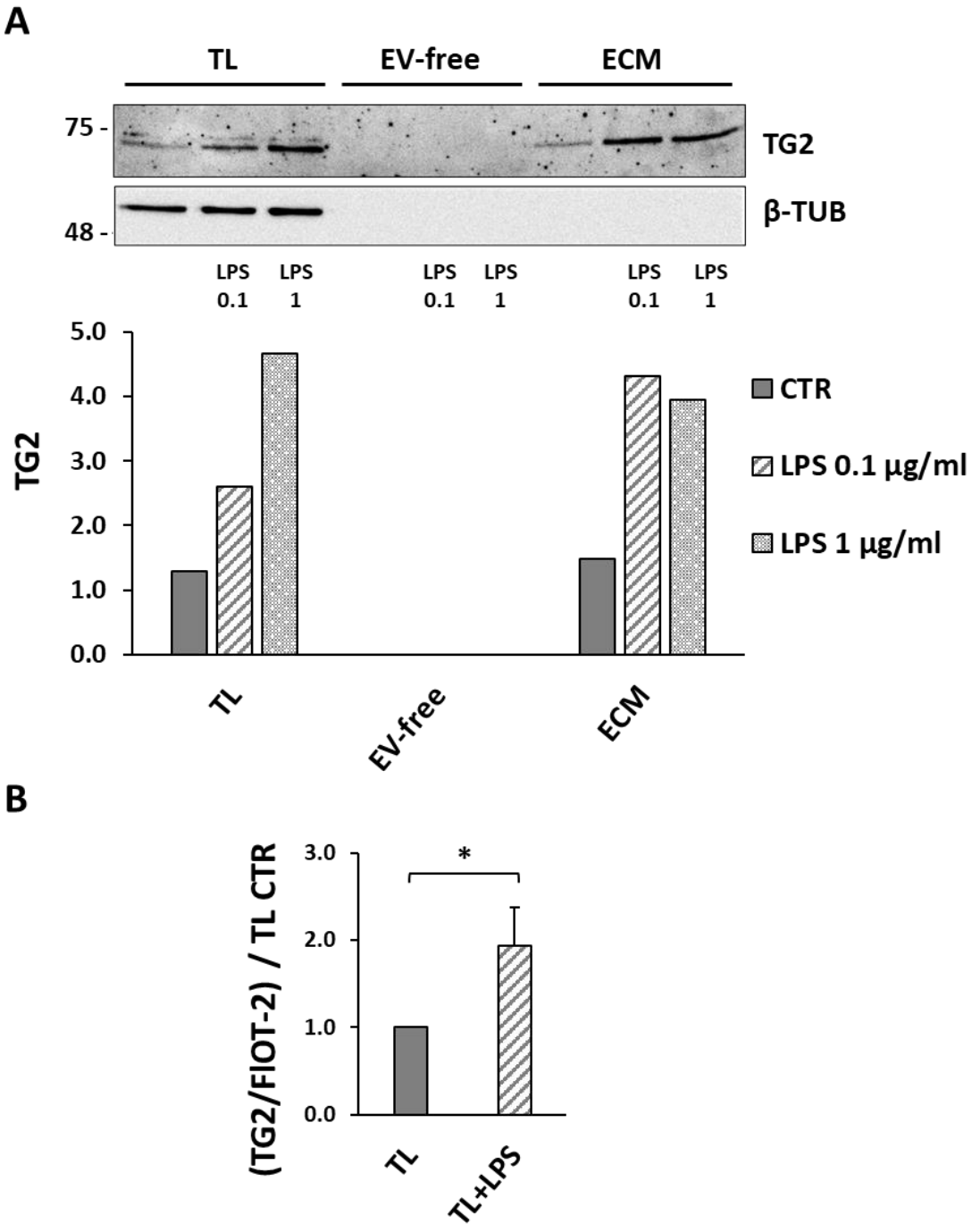
A
TL
EV-free
ECM
75 -
48 -
TG2
β-TUB
LPS 0.1
LPS 1
LPS 0.1
LPS 1
LPS 0.1
LPS 1
TG2
5.0
4.0
3.0
2.0
1.0
0.0
CTR
LPS 0.1 µg/ml
LPS 1 µg/ml
TL
EV-free
ECM
B
(TG2/FIOT-2) / TL CTR
3.0
2.0
1.0
0.0
*
TL
TL+LPS

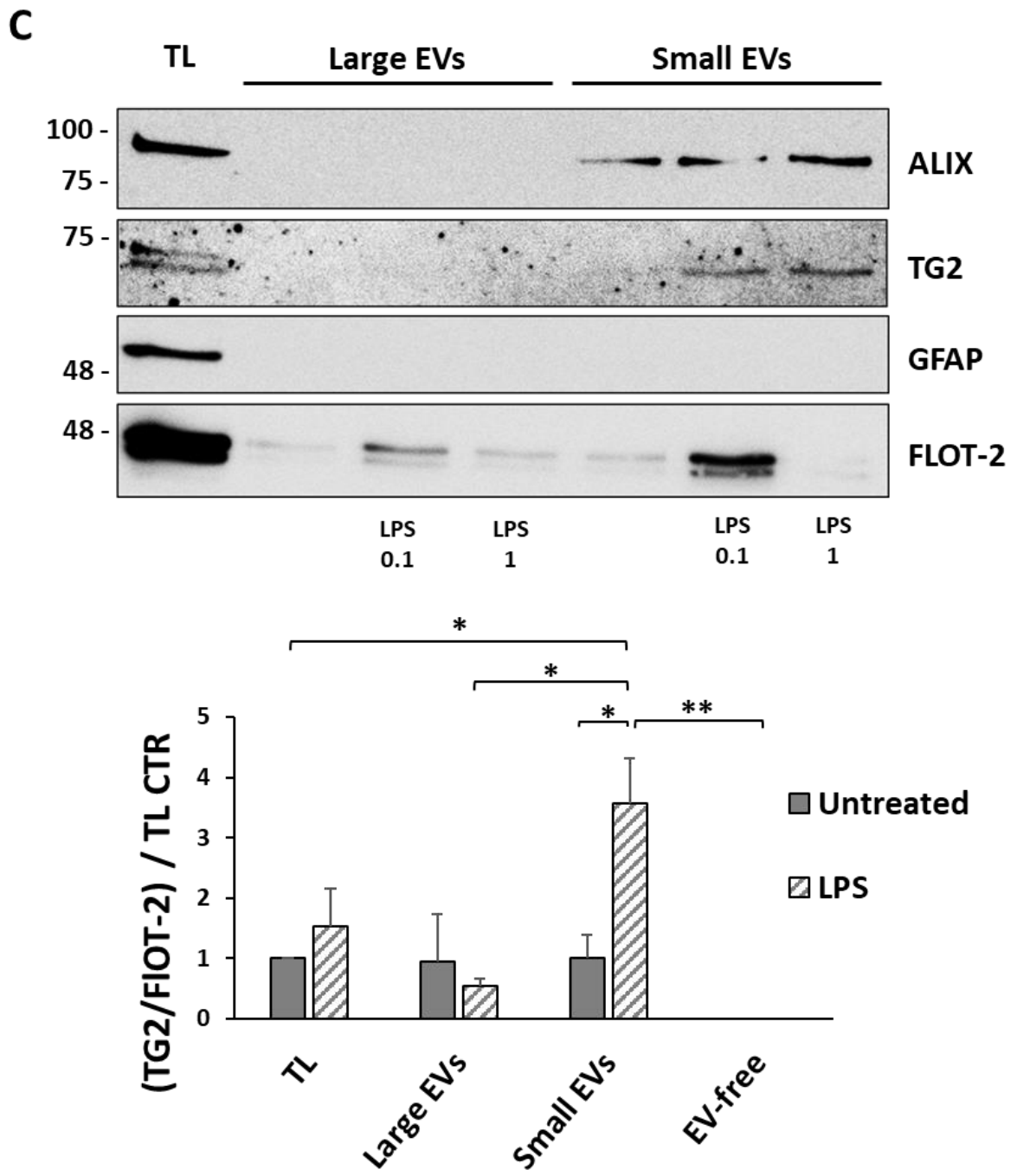

Figure 3.11. Analysis of TG2 in LPS-treated primary astrocytes and EVs. *Cells (BrainBits) were primed with LPS (0.1 µg/ml or 1 µg/ml) for 24 hours in serum-free medium before EVs isolation.* ***A)*** *Western Blotting analysis of astrocytes total lysates (TL), proteins TCA-precipitated from EV-free supernatants (EV-free) and extracellular matrix (ECM). β-tubulin was used as loading control. Densitometry analysis below the blot shows mean intensity of TG2 immune-reactive bands (N=1).* ***B)*** *Densitometry analysis showing mean intensity ± SE of TG2 immune-reactive bands normalised on FLOT-2 and then to TL control values (N=4, *p≤0.05). Raw intensity values TG2/FLOT2: TL CTR: 0.84±0.55; TL LPS: 2.23±1.61.* ***C)*** *Western blotting analysis of lysed EVs (large and small EVs) and detection of EVs markers ALIX and*

*FLOTILLIN-2, glial marker GFAP and of TG2. Densitometry analysis shows mean intensity ± SE of TG2 immune-reactive bands normalised to FLOT-2 and then to TL control values (N=3, *p≤0.05, **p≤0.01). Raw intensity values TG2/FLOT2: TL CTR: 0.50±0.15; TL LPS: 0.69±0.20; Large EVs CTR: 0.37±0.26; Large EVs LPS: 0.31±0.15; Small EVs CTR: 0.46±0.15; Small EVs LPS: 1.86±0.76; EV-free CTR & LPS: 0.0±0.0.*

At present it is not yet known if TG2 is carried in the lumen of astrocytic EVs, as opposed to being exposed on the surface and thus able to directly interact with molecules in the extracellular milieu and cell plasma membrane. In our recent work we were able to demonstrate that vesicular TG2 originating from NRK52E cells (rat renal tubular epithelial cells) was enriched on the surface of small EVs (Furini et al., 2018). Therefore, it would be interesting to investigate if this was also the case for astrocyte-associated vesicular TG2.

In conclusion, these findings suggest that TG2 can be released by astrocytes as a cargo of small EVs under neuroinflammatory conditions, a novel mechanism that has never been described before (**Fig. 3.12**).

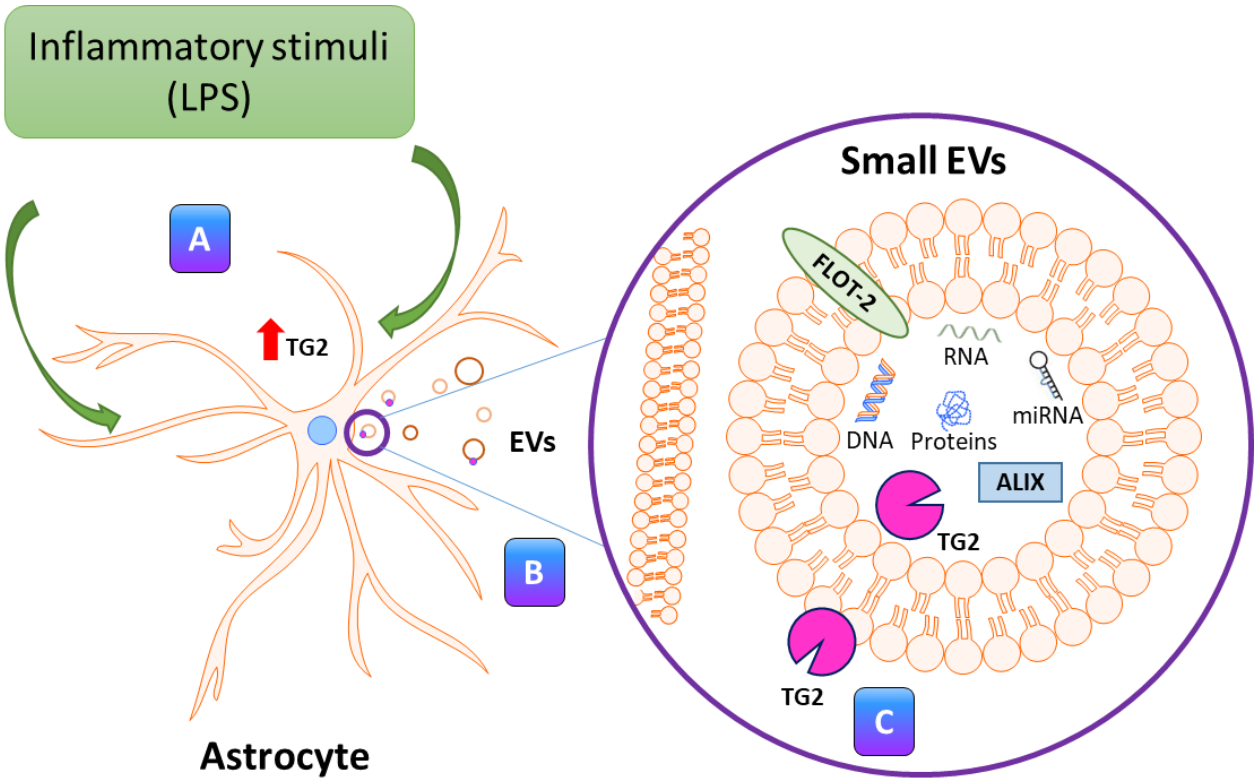

Figure 3.12. Schematic representation of TG2 externalisation by EVs trafficking. A) *Astrocytes activated by Lipopolysaccharides (LPS), an endotoxin which causes inflammatory response, show increased levels of TG2.* ***B)*** *Astrocytes release large and small EVs, which are loaded with nucleic acids (DNA, RNA, miRNAs), proteins and lipids. Among these, small EVs were positive for specific protein markers FLOT-2 (transmembrane) and ALIX (luminal).* ***C)*** *Small EVs isolated from LPS-treated astrocytes contain TG2, either in the vesicle lumen or as a membrane-associated protein. This image was generated with Motifolio (https://www.motifolio.com/).*

3.3 Discussion

The main findings described in this chapter are that in rat primary cell cultures TG2 is present at neuronal synapses and in astrocytes, from which it can be externalised through small EVs under neuroinflammatory conditions.

TG2 has already been described in hippocampal neurons, but neither in detail, nor by using a specific antibody such as mouse monoclonal anti-TG2 IA12 used in this work, which is known to be highly specific for detection of mouse and rat TG2 (Scarpellini et al., 2014). For example, Appelt and colleagues performed TG2 immunostaining of rat hippocampal neurons using an antibody against FXIII, another member of the TG family, and observed a widespread distribution in the cell soma and dendritic processes (Appelt et al., 1996). They also analysed human hippocampal tissue sections and confirmed TG2 presence in the perikaryon and neurites, especially in AD brain compared to controls (Appelt et al., 1996). Other groups have characterised TG2 at the histological level, by western blotting analysis, *in vitro* activity assay or RT-PCR of homogenates from different brain regions (e.g. prefrontal cortex, cerebellum and hippocampus) (Gilad and Varon, 1985; Johnson et al., 1997; Kim et al., 1999), or by immunostaining of tissue sections of either TG2 protein or TG2 transamidation by-product EGGL peptide (Perry and Haynes, 1993; Perry et al., 1995; Kim et al., 1999; Andringa et al., 2004). Some groups also analysed isolated primary cerebellar granule or cortical neurons, confirming TG2 presence in these cell types (Mahoney et al., 2000; Filiano et al., 2010). These studies highlighted the presence of TG2 in different brain tissues and cells, including neurons and brain vasculature, but did not investigate its cellular localisation in detail. Other works aimed at understanding TG2 role in neural development revealed that TG2 localisation in immortalised neuroblastoma cell lines was predominantly cytoplasmic, present both in the cell perikaryon and neurites, and that only about 7% was nuclear (Lesort et al., 1998; Zhang et al., 1998a; Tucholski et al., 2001).

It was shown here for the first time that about 21% of the total TG2 present in hippocampal neurons co-localises with either post- or pre-synaptic markers (**Fig. 3.2A**). Even though TG activity has been detected in synaptosomal preparations (Gilad and Varon, 1985), no one has ever shown that TG2 protein localises specifically at synaptic sites (**Fig. 3.2A-B**).

Because the most commonly studied TG2 function in both physiology and pathology is the transamidation of protein substrates, and this is Ca^{2+}-activated, an attempt to assess whether TG2 activity was present on neurons' surface was made, where activating

concentrations of calcium are likely in the mM range (interstitial fluid $[Ca^{2+}]$: ~1.2 mM) (Jones and Keep, 1988; Carafoli, 1987). The data employing a live cell assay (Jones et al., 1997) suggest that there is active extracellular TG2 in hippocampal neurons. This observation was corroborated by the reduction in TG2 activity in the presence of the widely used TG2 inhibitor ZDON (**Fig. 3.3A-B**). ZDON is a side chain-modified peptide, carrying an electrophilic "DON" group (6-diazo-5-oxo-L-norleucine) which undergoes nucleophilic attack by TG2 residue Cys(277) and is consequently irreversibly bound to TG2 active site in a stable thioether adduct, thus blocking TG2 activity (McConoughey et al., 2010). Among technical limitations, the TG cell surface activity assay used for this experiment, which was developed to analyse cells allowed to attach for 2 hours on FN (Methods chapter 2.2.5.2, Jones et al., 1997), was applied in neurons growing directly on FN for a week prior to performing the assay, as neurons cannot survive proteolytic detachment. Alternatively, freshly disassociated cells (0 DIV) were employed, however high sensitivity to DMSO (0.1%) used as vehicle for the inhibitor (ZDON) was another limitation.

TG2 activity was also measured *in situ* in adherent neurons, grown in the presence of a FITC-labelled TG2 substrate. It was hypothesised that, being located at synaptic sites, TG2 activity could be affected by synaptic transmission. In fact, it is known that TG2 activity is affected by $[Ca^{2+}]_i$ and that in many neurodegenerative diseases, characterised by calcium dysregulation, TG2 activity is enhanced (Smethurst and Griffin, 1996). Contrary to the initial expectations, TG2 did not show changes in response to variations in synaptic activity, at neither the protein nor the activity level (**Fig. 3.4A-C**). It was reasoned that more than the neuronal endogenous TG2, which does not seem to be highly active, it might be the extracellularly localised enzyme which could have a more relevant role in neurons function. Literature data suggest that glial cells, specifically astrocytes, might be a source of extracellular TG2 in brain (Pinzón et al., 2017a,b). Campisi and colleagues were the first group to demonstrate the presence of TG2 activity in primary rat glial cell homogenates (Campisi et al., 1992), while other groups showed that astrocytes express TG2 mRNA (Monsonego et al., 1997), and that TG2 protein, mainly located in the cytosol, present variable levels between cells (van Strien et al., 2011). Therefore, it was shown here that TG2 is expressed in primary glial cells, and that it is present at higher levels in astrocytes compared to microglia (**Fig. 3.5A-B**). TG2 localisation was mainly cytoplasmic, showing a vesicle-like distribution (**Fig. 3.7-3.8**). Interestingly, the same was observed in not permeabilised cells, suggesting that part of the enzyme could be localised at the cell surface,

in vesicular structures (**Fig. 3.7C**). A similar distribution was shown by van Dam's research group, which highlighted the presence of cell-surface TG2 in astrocytes, especially in response to inflammatory stimuli (van Strien et al., 2011). TG2 showed partial co-localisation with ECM marker FN (**Fig. 3.8**), as previously observed in fibroblasts and other cell systems (Verderio et al., 1999; Gaudry et al. 1999; Akimov and Belkin 2001), including astrocytes, where a direct interaction between FN and TG2 has been described (van Strien et al., 2011; Pinzón et al., 2017a,b). In this study, the presence of active enzyme on the astrocytes' surface was confirmed by using a cell surface activity assay (**Fig. 3.9**), which strengthened the hypothesis of a surface localisation. Pinzón and colleagues have also shown TG2 expression in astrocytes, however it was very low in control conditions, whereas it significantly increased upon neuroinflammatory stimuli (i.e. TNF-α + IL-1β treatment), consequently accumulating in the ECM (Pinzón et al, 2017b). In contrast, here abundant TG2 seemed to be detected in astrocytes in comparison. It is possible that mouse anti-TG2 ab1 antibody (clone CUB7402) used in Pinzón's report, which is known to detect human TG2, but less mouse or rat TG2, may have limited experimental data, as in the experiments described here untreated astrocytes displayed a clear TG2 signal observed using the monoclonal mouse anti-TG2 (IA12) antibody (Scarpellini et al., 2014; Burhan et al., 2017). On the other hand, only low TG2 ECM signal was observed in the absence of treatment, confirming that externalisation of TG2 is regulated by stress stimuli, such as inflammation. Seeing that no possible mechanism for TG2 externalisation was proposed in Pinzón's report, this was an extremely interesting question to investigate.

Our research group has recently published a work in the area of kidney fibrosis, showing that TG2 is secreted by EVs during fibrosis progression (Furini et al., 2018). This gave rise to the hypothesis that the same mechanism could be present in astrocytes under inflammatory conditions.

In order to investigate this process, astrocytes were treated with lipopolysaccharide (LPS), a well-known pro-inflammatory molecule, which has been previously shown to increase TG2 expression and activity levels in a variety of cell, among which macrophages and BV2 mouse microglia (Harris et al., 1984; Park et al., 2004; Kawabe et al., 2015; Ding et al., 2017). As expected, LPS treatment increased TG2 protein levels in the total lysates (**Fig. 3.11A-B**) and also induced an increase of TG2 externalisation and accumulation in the ECM (**Fig. 3.11A**). This was consistent with what was initially expected, as also Pinzón and colleagues had observed higher co-localisation of TG2 and ECM marker FN in response to

inflammation (Pinzón et al., 2017). EVs recovered from serum-free conditioned medium of untreated and LPS-treated astrocytes were then analysed, and it was observed that TG2 was enriched in small EVs only upon LPS stimuli (**Fig. 3.11C**). This study demonstrated for the first time that TG2 is released in association with EVs in primary astrocytes. Previous work had detected TG2 in EVs of kidney epithelial cells, mouse embryonic fibroblasts (MEF) and cancer cells (Furini et al., 2018; Diaz-Hidalgo et al., 2016; Antonyak et al., 2011).

Recent literature suggests a significant role for EVs in cell-cell communication. In brain, EVs have a largely unexplored role in cross-talk among neurons, astrocytes and microglia, the immune cells of the CNS (Chaudhuri et al., 2018). TNFα and IL-1β, pro-inflammatory cytokines known to activate glial cells, have been shown to affect astrocytic EVs cargo with an impact on neurotrophic signalling, which resulted in decreased neuronal survival and synaptogenesis (Chaudhuri et al., 2018). Astrocyte-derived EVs isolated from plasma of AD patients were shown to carry high levels of complement effector proteins compared to healthy controls, suggesting that they could promote the spreading of inflammatory signals (Goetzl et al., 2018). In a mouse model of inflammatory brain injury, EVs shed from astrocytes following acute cytokine response (mediated by IL-1β) promoted leucocyte transmigration to the brain and consequent production of cytokines in liver, corroborating evidence of a role for astrocytic EVs as mediators of the communication between astrocytes and neurons, but also between the brain and the peripheral immune system (Dickens et al., 2017). The presence of TG2 in astrocytes-derived EVs could have multiple effects, apart for the most direct externalisation of the enzyme. To date there is no published information on this topic, especially what effect vesicular TG2 could have on neighbouring cells, such as neurons.

In conclusion, it was shown here for the first time that TG2 is released by astrocytes in association with small EVs under inflammatory conditions, and consequently that it accumulates in the ECM above physiological levels during the inflammation process. Because it has been reported that overexpression of TG2 in mice brain potentiates calcium-induced hippocampal damage, suggesting a possible role of TG2 in excitotoxicity-induced neuronal cell death (Tucholski et al., 2006), the next step was to investigate whether the increase of extracellular TG2 could affect synaptic activity and calcium homeostasis in neurons.

CHAPTER 4:

Extracellular TG2 modulates calcium homeostasis in hippocampal neurons

4.1 Introduction

Rise in intracellular calcium concentrations ($[Ca^{2+}]_i$) in neurons is the major trigger of neurotransmitter release from nerve endings, hence it is at the core of neuronal communication (Marambaud et al., 2009). Basal calcium levels are tightly regulated within a narrow physiological range, below 100-200 nM, while extracellularly the concentration is about 1-2 mM (Jones and Keep, 1988, Carafoli, 1987). Calcium influx through permeable channels at the plasma membrane is buffered by a large set of proteins able to bind calcium and by the action of calcium membrane transporters. In particular, the Plasma Membrane Ca^{2+} ATPase (PMCA) and the Na^+/Ca^{2+} exchanger (NCX) are the two main system involved in calcium efflux through the plasma membrane. Perturbations in calcium homeostasis have been reported in several neurodegenerative diseases, including Alzheimer's disease (AD), the most common form of human dementia in the elderly (Marambaud et al., 2009). Alterations in $[Ca^{2+}]_i$ have deleterious consequences for neurons, leading to neuron cell death by necrosis or apoptosis. In particular, a large body of evidence documents a connection between disruption of calcium homeostasis and AD. Cortical neurons established from AD transgenic mice have been shown to exhibit abnormally elevated $[Ca^{2+}]_i$ and quantitative calcium imaging *in vivo* indicated a significant increase in the fraction of spines and dendrites of cortical neurons characterized by calcium overload (Kuchibhotla et al., 2008). Similarly, neurons from HD mouse models (e.g. YAC128) have shown increased NMDA toxicity, due to the huntingtin (htt)-mediated disruption of mitochondrial function and consequent impairment of calcium buffering system, which led to the elevation of $[Ca^{2+}]_i$ (Fernandes et al., 2007). Interestingly, TG2 inhibition in the YAC128 model was shown to protect striatal neurons from NMDA-mediated toxicity both in the presence and absence of mutant htt (McConoughey et al., 2010). Elevated levels of TG2 in HD led to the decrease of mitochondrial proteins such as peroxisome proliferator-activated receptor-γ coactivator-1α (PGC-1α) and cytochrome c levels, causing mitochondrial disfunction. Inhibition of TG2 activity by specific inhibitor ZDON was able to de-repress their expression, thus positively affecting neurons survival under toxic stress (McConoughey et al., 2010).

Overexpression of human TG2 in mice brain was shown to potentiate calcium-induced hippocampal damage, suggesting a possible role of TG2 in excitotoxicity-induced neuronal cell death (Tucholski et al., 2006). The authors hypothesised that this process could be mediated by the TG2-dependent modification of dual leucine zipper-bearing kinase (DLK)

and consequent potentiation of cell death through the c-Jun amino terminal kinase (JNK) pathway. Moreover, they postulated that TG2 could also increase $[Ca^{2+}]_i$, and thus enhance neurons excitability, however they did not provide any detail of a possible mechanism (Tucholski et al., 2006).

Given the key role of calcium in neuronal pathophysiology, the question whether extracellular TG2, either soluble or carried by EVs (including astrocytic EVs, as shown in chapter 3), could be involved in calcium homeostasis was investigated. TG2 itself is calcium activated, therefore it is not unreasonable to think that it could perturbate calcium concentrations, thus affecting its intracellular role as well as neuronal function, via a positive feedback loop. Notably, it has been shown that EVs derived from stimulated microglial cells are in fact able to affect basal $[Ca^{2+}]_i$ in primary astrocytes and neurons, likely by spreading inflammatory signals from the source to the recipient cells (Verderio et al., 2012; Joshi et al., 2014).

4.1.1 Aims of the chapter

The general aim of this chapter was to clarify whether extracellular TG2 could influence calcium homeostasis in neurons, thus affecting their ability to communicate. Firstly, the effect of the enzyme on $[Ca^{2+}]_i$ in rat embryonic hippocampal neurons was investigated, by addition of TG2 in soluble form to the neuronal medium. Moreover, the role of TG2 overexpression in neurons by transient transfection was also examined. Finally, initial experiments with EVs isolated from primary glial cells were centred at looking at the role of EVs and vesicular TG2 on calcium homeostasis in neurons. For this chapter, only neurons and astrocytes prepared according to the standard protocol were used.

4.2 Results

4.2.1 Exogenous TG2 increases cytoplasmic calcium concentration in neurons

In order to understand if extracellular TG2 may directly affect calcium homeostasis in neurons, calcium concentration was detected by analysing the F340/380 fluorescence ratio in fura-2-loaded neurons (as described in Methods chapter 2.2.11). Differentiated neuronal cultures often exhibit synchronous calcium oscillations, with reflecting burst of neuronal firing. Addition of soluble TG2 (10-30 µg/ml) to neurons maintained in Krebs–Ringer's HEPES solution (KRH) (**Fig. 4.1**), characterized by low frequency spontaneous oscillations, promoted the onset of a synchronous calcium spike and increased the interspike intracellular calcium concentration ($[Ca^{2+}]_i$), expressed as ΔF340/380 (ΔF340/380 = 0.126±0.014). This led to blockage of oscillatory activity (**Fig. 4.1**, first red arrow from the left). Upon TG2 removal (**Fig. 4.1,** wash), interspike $[Ca^{2+}]_i$ decreased to pre-treatment values and spontaneous calcium oscillations re-started, indicating that the action of exogenous TG2 was reversible (**Fig. 4.1,** right). These findings suggested that exogenous TG2 alters interspike $[Ca^{2+}]_i$ thereby influencing synchronous calcium oscillations.

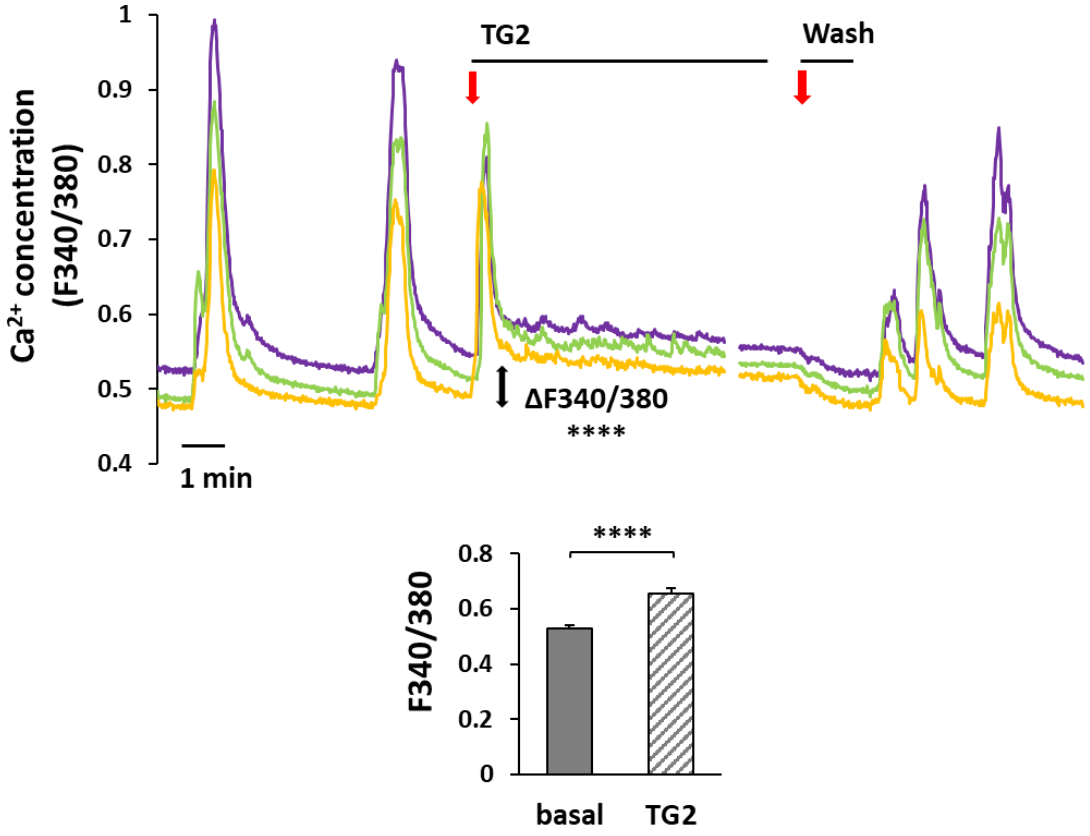

Figure 4.1. Exogenous TG2 blocks spontaneous calcium oscillations and increases basal calcium concentration in neurons*. Temporal analysis of synchronous calcium oscillations,*

*spontaneously occurring in 14 DIV hippocampal neurons in KRH (without TTX), were measured as variation in the F340/380 fluorescence ratio (expressed as ΔF340/380). Addition of exogenous TG2 (10 µg/ml) promoted a calcium spike followed by a sustained plateau, with a block of spontaneous calcium oscillations and a significant increase in intracellular calcium concentration ($[Ca^{2+}]_i$). Data is expressed as mean ± standard error (Basal $[Ca^{2+}]_i$: 0.53±0.01; $[Ca^{2+}]_i$ after TG2 addition: 0.65±0.02; N=23, Student's t-test: ****p<0.00001). Upon TG2 removal (wash with KRH) synchronous calcium oscillations re-started. Three representative traces of neuronal $[Ca^{2+}]_i$ are shown in three different colours.*

To further examine the action of TG2 on calcium homeostasis, neurons were exposed to exogenous TG2 in the presence of TTX (1 µM), which prevents synaptic and synchronous network calcium activity. In virtually all neurons tested, addition of TG2 led to a significant increase in $[Ca^{2+}]_i$ (ΔF340/380 = 0.058±0.005) (**Fig. 4.2A**, first red arrow from the left). Interestingly, upon removal of the protein from the extracellular medium, neurons recovered basal $[Ca^{2+}]_i$, suggesting that the action of TG2 is reversible (**Fig. 4.2A**, wash). This finding is intriguing, as it would imply that the observed process might not be due to transamidation, which leads to a covalent irreversible modification of protein substrates and should not disappear once TG2 is removed. To explore this further, an enzymatically inactive mutant form of TG2 (recombinant human TG2 carrying the active site Cys(277)Ser mutation) was tested (**Fig. 4.2B**). No changes in resting $[Ca^{2+}]_i$ were induced by the inactive TG2 enzyme used in the same concentration as the gplTG2 (**Fig. 4.2B**), suggesting that TG2 activity might be necessary to induce calcium changes.

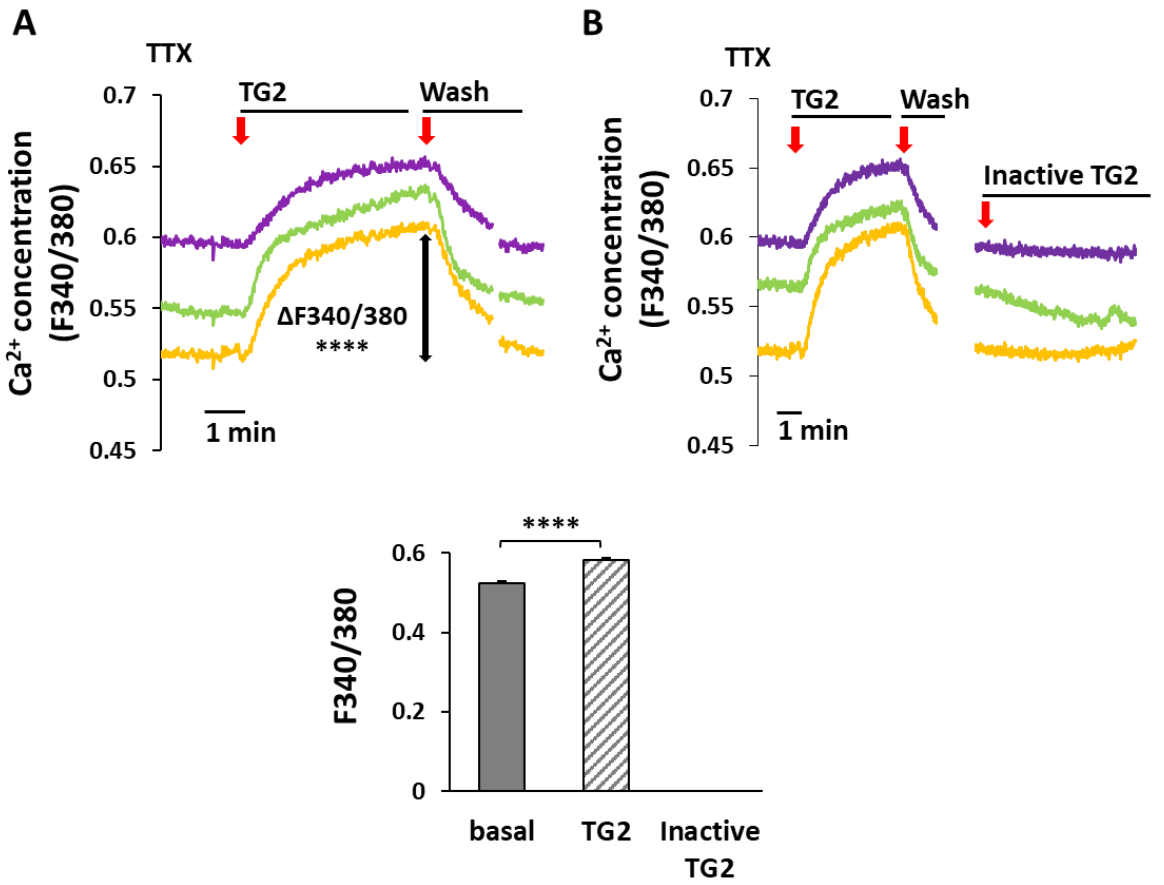

Figure 4.2. Exogenous active TG2 increases cytoplasmic calcium levels in 14-20 DIV hippocampal neurons exposed to TTX*. Temporal analysis of $[Ca^{2+}]_i$ changes in presence of TTX, expressed as ΔF340/380.* ***A)*** *Addition of exogenous TG2 (10 µg/ml) in presence of TTX (1 µM) showed a similar effect as described in Fig. 4.1. Three representative traces of neuronal $[Ca^{2+}]_i$ are shown. Data is expressed as mean ± standard error (Basal $[Ca^{2+}]_i$: 0.52±0.01; $[Ca^{2+}]_i$ after TG2 addition: 0.58±0.01; N=33, Student's t-test: ****p<0.00001).* ***B)*** *Inactive TG2, up to 30 µg/ml, did not affect calcium concentration (N=19).*

4.2.2 Exogenous TG2 causes an influx of calcium from the extracellular environment

Calcium influx through the plasma membrane is a major determinant of basal $[Ca^{2+}]_i$ in cells. Therefore, it was investigated whether TG2, and in particular the extracellular protein, may control basal calcium levels by enhancing calcium influx into neurons. To test this possibility neurons were exposed to soluble TG2 in calcium-free medium. Under this condition no rise in basal $[Ca^{2+}]_i$ occurred (**Fig. 4.3A**, red arrow), while TG2-dependent calcium rises were clearly recorded from the same neurons after addition of 2 mM Ca^{2+} as $CaCl_2$ to the extracellular medium (**Fig. 4.3B**). These findings revealed that calcium influx through the plasma membrane mediates the $[Ca^{2+}]_i$ rise evoked by exogenous TG2.

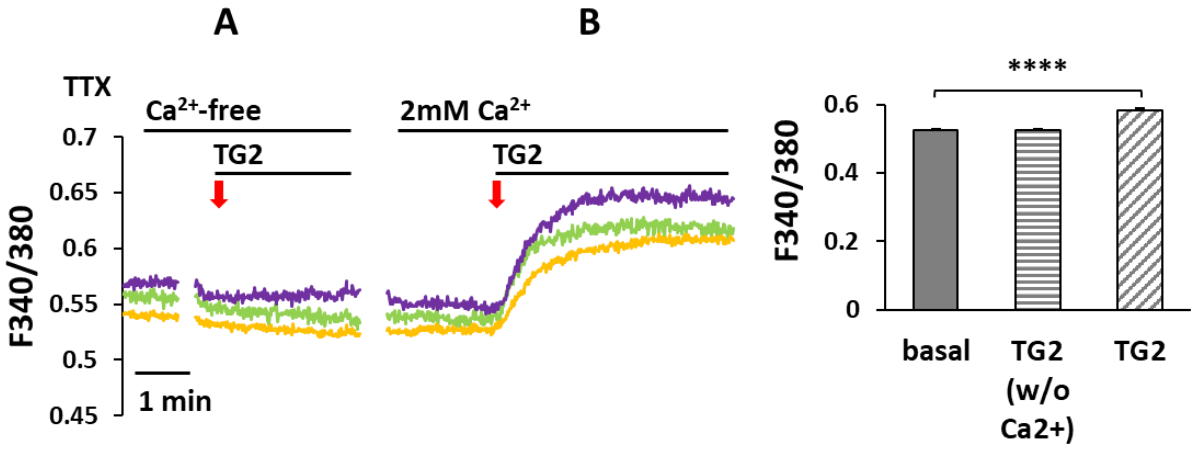

Figure 4.3. Exogenous TG2 does not affect $[Ca^{2+}]_i$ in the absence of extracellular calcium. *Temporal analysis of $[Ca^{2+}]_i$ changes in 14-20 DIV neurons exposed to exogenous TG2 (10 µg/ml) in the absence **(A)** or in the presence **(B)** of extracellular calcium. TG2 was first added to neurons in calcium-free KRH, then washed and finally added again after supplementation of KRH with 2 mM $CaCl_2$. Addition of TG2 in absence of extracellular calcium did not lead to changes in cytoplasmic calcium (N=31).*

4.2.3 Is soluble TG2 catalytically active?

To investigate whether soluble TG2 was catalytically active, the activity levels of gplTG2 in KRH buffer were tested *in vitro*, mimicking the conditions of the calcium imaging experiments described in section 4.2.1. Using a plate-based assay (as described in Methods chapter 2.2.5.3), TG2 was active when KRH was supplemented with the reducing agent dithiothreitol (DTT, 10 mM) (**Fig. 4.4A**). However, the absence of DTT resulted in a significant decrease in TG2 activity which dropped to low background levels (**Fig. 4.4A**). As the neuronal medium in the experiments described in section 4.2.1 was KRH without DTT, this experiment suggests that exogenous TG2 added to hippocampal neurons during calcium imaging recordings was in fact prevalently inactive. This is not surprising, as Verderio et al. had already suggested that soluble extracellular TG2 needs to be in a reduced state to be able to crosslink protein substrates (Verderio et al., 2003). Moreover, this is consistent with current thinking about TG2 activity being tightly regulated by the redox conditions of the extracellular environment (Stamnaes et al., 2010).

It was next hypothesised that TG2 protein conformation could be responsible for the effect of extracellular TG2 on neuronal calcium oscillations. This hypothesis was tested by using

the TG2 inhibitor NC9, which was kindly donated by its developer, Dr. Jeffrey Keillor (University of Ottawa, Canada). NC9 is cell permeable and it is known to block not only TG2 transamidating activity but also GTP-binding and to lock TG2 in the open conformation (Akbar et al, 2017). This is the conformation that TG2 is expected to assume outside the cell where calcium concentration is higher compared to the intracellular levels, although TG2 would most likely fluctuate between open and close conformations, depending also on the redox state (as illustrated in **Fig. 1.9** in Chapter 1). As shown in **Fig. 4.4B**, approximately 30 µM NC9 was sufficient to inhibit 50% of purified enzyme when 12.6 nM of TG2 in Tris-HCl buffer pH 7.4 was used. When the enzyme was pre-incubated with NC9 in KRH buffer pH 7.4 and 10 mM DTT at the same concentration used in the calcium imaging experiments, up to 500 µM NC9 was able to inhibit only about 50% of TG2 (**Fig. 4.4C**, round marker). However, when the assay was repeated in the absence of DTT, 200 µM NC9 completely blocked TG2 activity (**Fig. 4.4C**, triangular marker), hence this concentration of NC9 was chosen to modulate extracellular TG2 in calcium imaging recordings, where DTT would not be present.

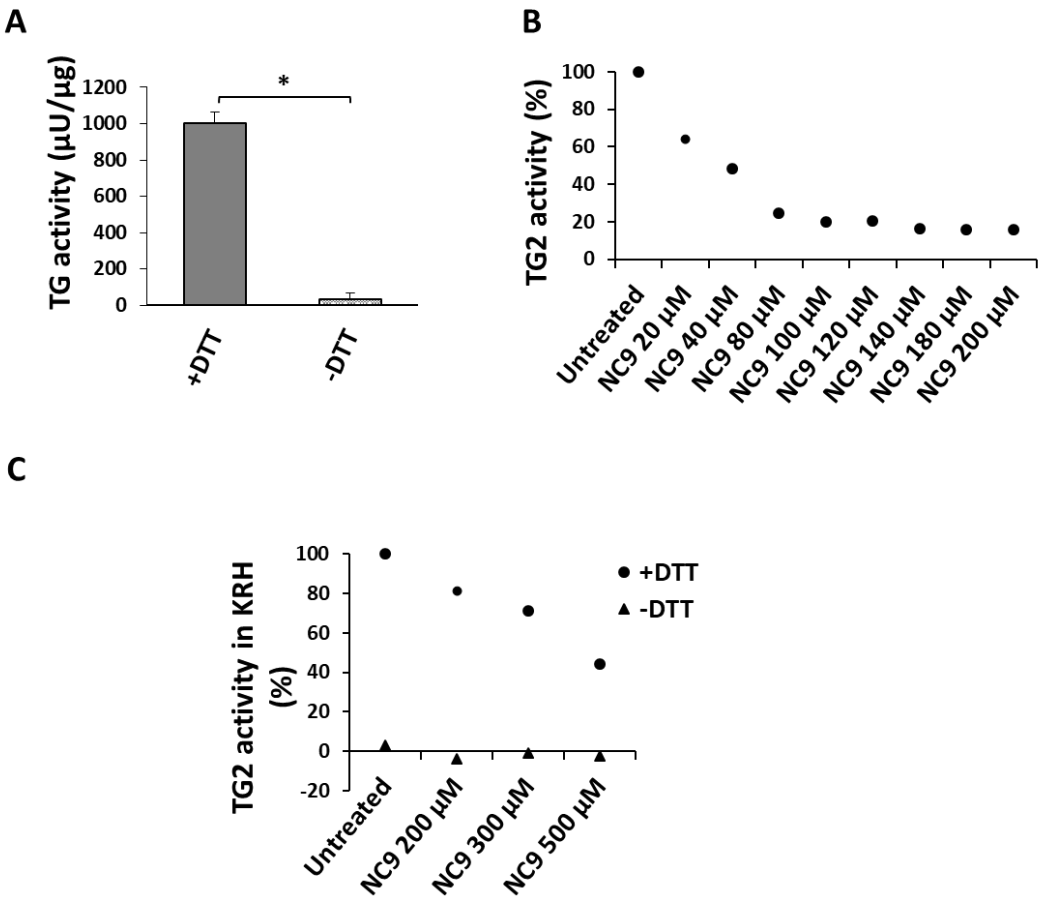

Figure 4.4. TG2 is significantly less active in the absence of reducing agent (DTT).

Figure 4.4. TG2 is significantly less active in the absence of reducing agent (DTT). *Total TG activity assay assessing TG2 activity levels in vitro expressed as µU/µg of protein.* ***A)*** *gplTG2 was incubated in KRH buffer pH 7.4 (which contains 2 mM calcium) in the presence or absence of DTT 10 mM. Data is expressed as mean ± standard error (TG2+DTT: 1004.9±57.8; TG2-DTT: 31.5±34.9. N=1, each condition in duplicate. Student's t-test: *p<0.01).* ***B)*** *Dose-dependent inhibition of TG2 activity by TG inhibitor NC9. The assay was performed with 12.6 nM of gplTG2 in Tris-HCl buffer pH 7.4 and in standard reaction buffer containing 10 mM DTT and 5 mM calcium. The enzyme was pre-incubated 30 minutes with NC9 at room temperature prior to addition to the wells.* ***C)*** *Dose-dependent inhibition of TG2 activity by NC9 in the presence or absence of DTT. The assay was performed with 60 µg/ml (equal to 759 nM) of TG2 in KRH buffer pH 7.4 and reaction buffer containing 5 mM calcium and with or without 10 mM DTT. After 30 minutes pre-incubation at room temperature, samples were diluted in KRH to fall within the assay detection range (24 ng/well) prior to addition to the wells and consequent addition of reaction buffer. TG2+DTT curve (round markers), untreated: 1004.9±57.8; NC9 200 µM: 816.3±9.8; NC9 300 µM: 716.6±36.5; NC9 500 µM: 442.4±73.0. TG2-DTT curve (triangular markers), untreated: 31.5±34.9; NC9 200 µM: -36.6±0.5; NC9 300 µM: -8.8±1.1; NC9 500 µM: -21.9±8.7.*

Pre-incubation of TG2 with the TG inhibitor NC9 (200 µM) in KRH before addition to the neurons led to a 1.6-fold increase in calcium influx compared to TG2 pre-treated with DMSO (vehicle) alone (**Fig. 4.5A**). Calcium influx was expressed as Area Under the Curve (AUC) calculated for 30 seconds after addition of any stimulus (as described in Methods chapter 2.2.11). When NC9 was added directly to neurons in the absence of TG2 to investigate the role of endogenous TG2, an increase in $[Ca^{2+}]_i$ was also detected, whereas addition of DMSO alone (vehicle) did not show any effect (**Fig. 4.5B**).

These data seem to suggest that the conformation of TG2 is important for neuronal calcium changes induced upon supplementation of extracellular soluble TG2 enzyme. They also support a role for endogenous TG2 when in the open conformation.

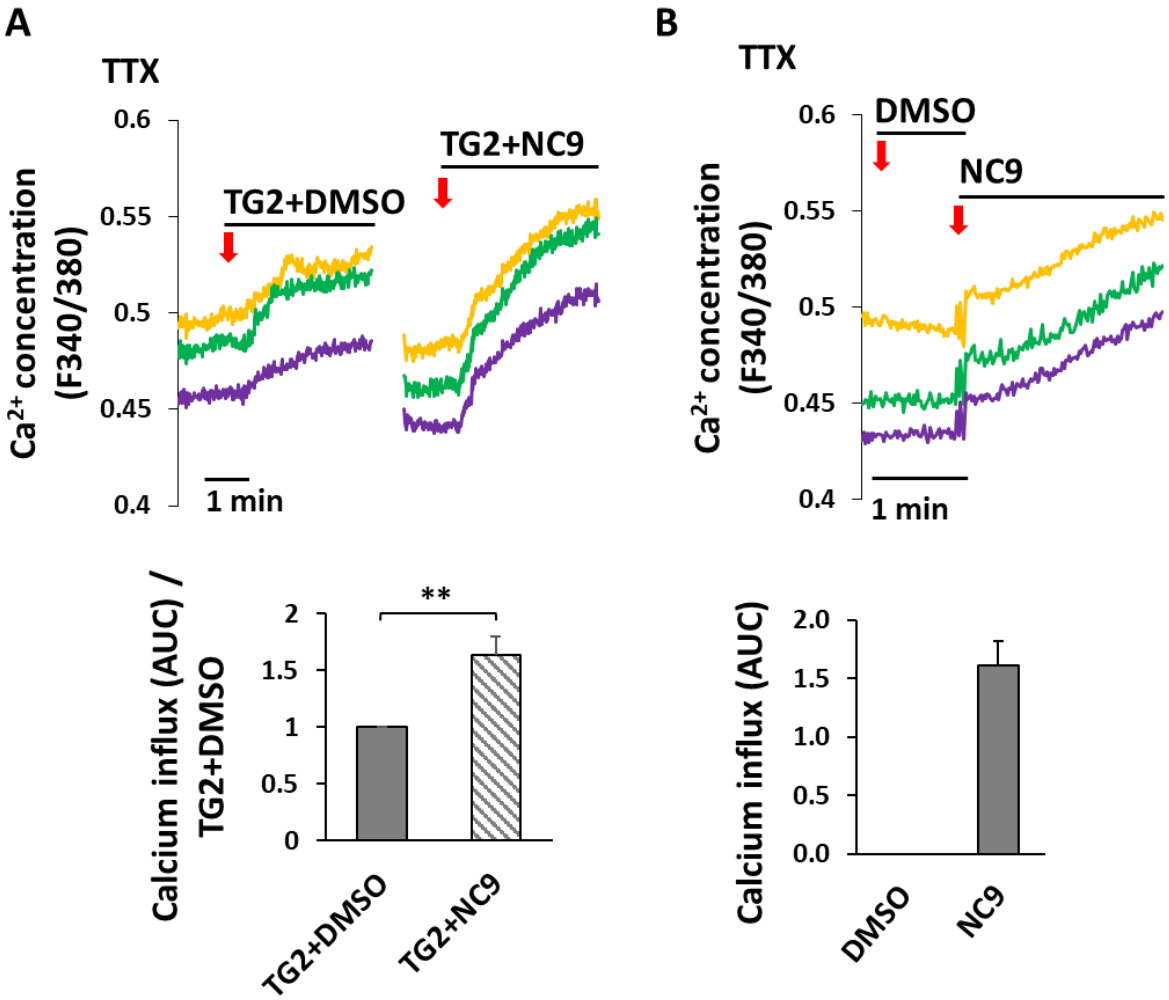

Figure 4.5. Calcium rise is enhanced by TG2 in open conformation. *Temporal analysis of $[Ca^{2+}]_i$ changes in the presence of TTX, expressed as Area Under the Curve (AUC).* ***A)*** *Neurons were first exposed to exogenous TG2 (30 µg/ml) pre-treated with DMSO (vehicle, 0.4% v/v), then washed and finally exposed to TG2 pre-treated with NC9 200 µM. Soluble TG2 was pre-treated at a concentration of 60 µg/ml, then added to neurons in KRH to reach a final concentration of 30 µg/ml. Data is expressed as mean AUC ± standard error normalised to TG2+DMSO (AUC TG2+DMSO: 0.43±0.05; TG2+NC9: 0.63±0.05; N=16, Student's t-test: **p<0.001).* ***B)*** *Neurons were exposed to DMSO (vehicle, 0.4% v/v) or NC9 alone (200 µM). Data is expressed as mean AUC ± standard error (AUC NC9 alone: 1.61±0.21, N=25; AUC DMSO alone: null; N=25).*

4.2.4 Overexpression of TG2 increases calcium concentration in neurons

Since NC9 was able to induce a calcium influx by modulating endogenous TG2, it became necessary to understand whether the effect of TG2 on neuronal $[Ca^{2+}]_i$ was exclusively promoted by extracellular TG2 released by non-neuronal sources (such as astrocytes), or whether neuronal TG2 itself could mediate $[Ca^{2+}]_i$ rise, as suggested by changes produced by NC9 (**Fig. 4.5B**). To this aim, EGFP-tagged TG2 or EGFP alone were overexpressed in neurons at 8 DIV. EGFP-TG2 was expressed ubiquitously in the cell body and processes, as shown by the widely spread green fluorescence (**Fig. 4.6A**). Some of the expressed TG2 was externalised, as revealed by confocal fluorescence microscopy of fixed and not permeabilised neurons incubated with anti-EGFP antibody, which was detected by a secondary Alexa-555-conjugated antibody (red fluorescent dye) (**Fig. 4.6A**). The staining of EGFP-tagged TG2 resembled that of endogenous TG2 (Fig. 3.2A in Chapter 3), showing similar cellular localisation, however this was stronger and did not show a punctuate pattern, suggesting a more widespread diffusion due to overexpression. When analysed by calcium imaging, neurons transfected with pEGFP-N1-TG2 showed a significant increase in resting $[Ca^{2+}]_i$ compared to neurons transfected with pEGFP-N1 vector, with a mean ΔF340/380 of 0.12 (**Fig. 4.6B**). The difference in $[Ca^{2+}]_i$ was abolished when EGFP-TG2 neurons were incubated with the TG2 inhibitor ZDON (mean ΔF340/380 = 0.085) (**Fig. 4.6C**), which similarly to NC9 is cell permeable and able to trap TG2 in open conformation (Pinkas et al., 2007; Lindeman, 2011). Interestingly, ZDON decreased resting $[Ca^{2+}]_i$ also in EGFP-transfected control neurons (mean ΔF340/380 = 0.058). These data suggest a role for endogenous TG2 in the control of basal $[Ca^{2+}]_i$ (**Fig. 4.6C**). They also reinforce the notion that TG2 conformation (also affected by ZDON) or alternatively TG2 activity, could be critical in this process.

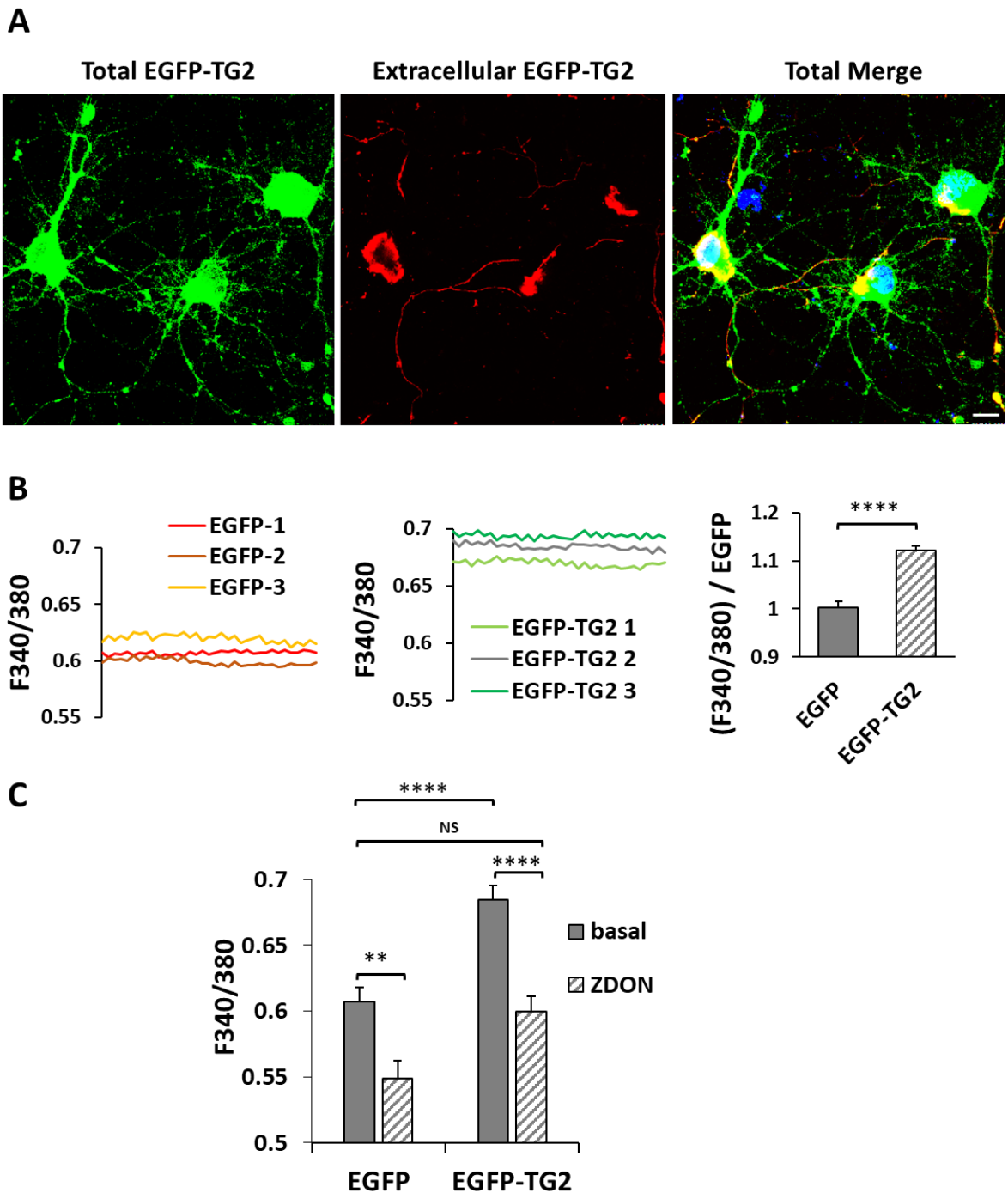

Figure 4.6. Overexpression of TG2 increases calcium concentration in neurons. A) *Neurons at 8 DIV were transfected with pEGFP-N1-TG2 or pEGFP-N1 vector, fixed without permeabilisation 48 hrs after transfection and stained with anti-EGFP (red) to visualise extracellular EGFP-TG2 and Hoechst (blue) to visualise the nuclei. Coverslips were visualised by laser scanning Leica SP5 confocal microscope using 63X oil immersion objective. Scale bar 10 µm.* ***B)*** *Temporal analysis of $[Ca2^{+}]_i$ changes in transfected neurons. ΔF340/380 was calculated between the mean F340/380 of EGFP-TG2 neurons and EGFP neurons. Three representative traces of EGFP and EGFP-TG2 neuronal $[Ca^{2+}]_i$ are shown. Data is expressed as mean ± standard error normalised to EGFP (EGFP: 0.548±0.008, N=103; EGFP-TG2:*

*0.604±0.006, N=158. ****p<0.00001).* ***C)*** *A subgroup of transfected neurons was treated with TG2 inhibitor ZDON (100 µM), which led to a significant reduction of $[Ca^{2+}]_i$ in both EGFP and EGFP-TG2 transfected neurons. Data is expressed as mean ± standard error (EGFP basal: 0.61±0.01, N=36; EGFP+ZDON: 0.55±0.01, N=30; EGFP-TG2 basal: 0.69±0.01, N=39; EGFP-TG2+ZDON: 0.60±0.01. **p<0.001; ****p<0.00001).*

To further explore the capability of endogenous TG2 to influence neuronal calcium homeostasis, 21-22 DIV neurons exhibiting intense oscillatory activity and increased $[Ca^{2+}]_i$ in response to bicuculline (50 µM), were incubated with ZDON. This setup was chosen, as it would mimic a condition of increased $[Ca^{2+}]_i$ and possibly consequent activation of endogenous TG2. Addition of the TG2 inhibitor about 4 minutes after bicuculline stimulus led to a significant decrease in the frequency of calcium oscillations, calculated as number of peaks/second (Hz), from 0.14 Hz to 0.06 Hz (**Fig. 4.7**, second red arrow from the left). Moreover, ZDON significantly decreased the interspike basal $[Ca^{2+}]_i$ (mean ΔF340/380 = 0.304) (**Fig. 4.7**), which is consistent with what was observed in transfected neurons, as shown in **Fig. 4.6C**.

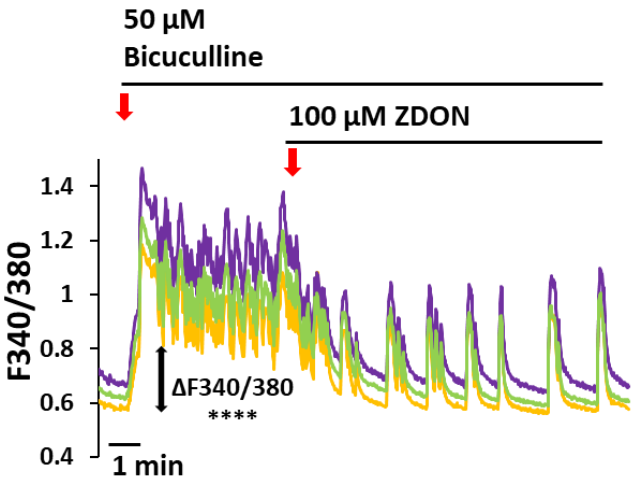

Figure 4.7. Endogenous TG2 inhibition decreases basal intracellular calcium concentrations and oscillation rates evoked by Bicuculline. *Temporal analysis of $[Ca^{2+}]_i$ changes in 21-22 DIV neurons in KRH (without TTX) stimulated with Bicuculline (50 µM), an antagonist of GABA receptors, which induced an intense oscillatory activity. Calcium minimum values in presence of Bicuculline were significantly reduced to basal levels after TG2 inhibition with 100 µM ZDON (minimum $[Ca^{2+}]_i$ with bicuculline: 0.93±0.04; minimum $[Ca^{2+}]_i$ after ZDON addition: 0.63±0.02; N=16, Student's t-test: ****p<0.00001).*

Taken together these findings suggest that also neurons produce and release TG2, which contributes to set $[Ca^{2+}]_i$ at higher levels as observed for exogenous TG2. It is still unclear if this effect is mediated by TG2 conformation or activity, as the inhibitors NC9 and ZDON, which both locks the enzyme in open conformation and blocks its transamidating activity, have shown to trigger opposite responses in neurons.

4.2.5 Involvement of L-type VOCCs in TG2-dependent $[Ca^{2+}]_i$ changes

To clarify the mechanisms underlying TG2-dependent calcium influx through the plasma membrane, neurons were stimulated with soluble TG2 in the presence of blockers of the main Ca^{2+} entry pathways in neurons, namely glutamate receptors (NMDARs, AMPARs and KARs), voltage-operated calcium channels (VOCCs) and the sodium-calcium exchanger (NCX). Firstly, NMDARs and AMPARs/KARs were blocked by supplementing the neuronal medium (KRH with TTX) with the antagonists APV and CNQX respectively. In the absence of these blockers, extracellular TG2 led to increased $[Ca^{2+}]_i$ as previously observed (**Fig. 4.8A**), however in the presence of the antagonists, TG2 addition was still able to elicit calcium increase (**Fig. 4.8B**). The calculated ΔF340/380 in the presence or absence of APV and CNQX were not statistically different (mean ΔF340/380 control: 0.058±0.003; mean ΔF340/380 with blockers: 0.062±0.006), ruling out the involvement of these ligand-gated calcium permeable receptors in mediating TG2-induced $[Ca^{2+}]_i$ changes.

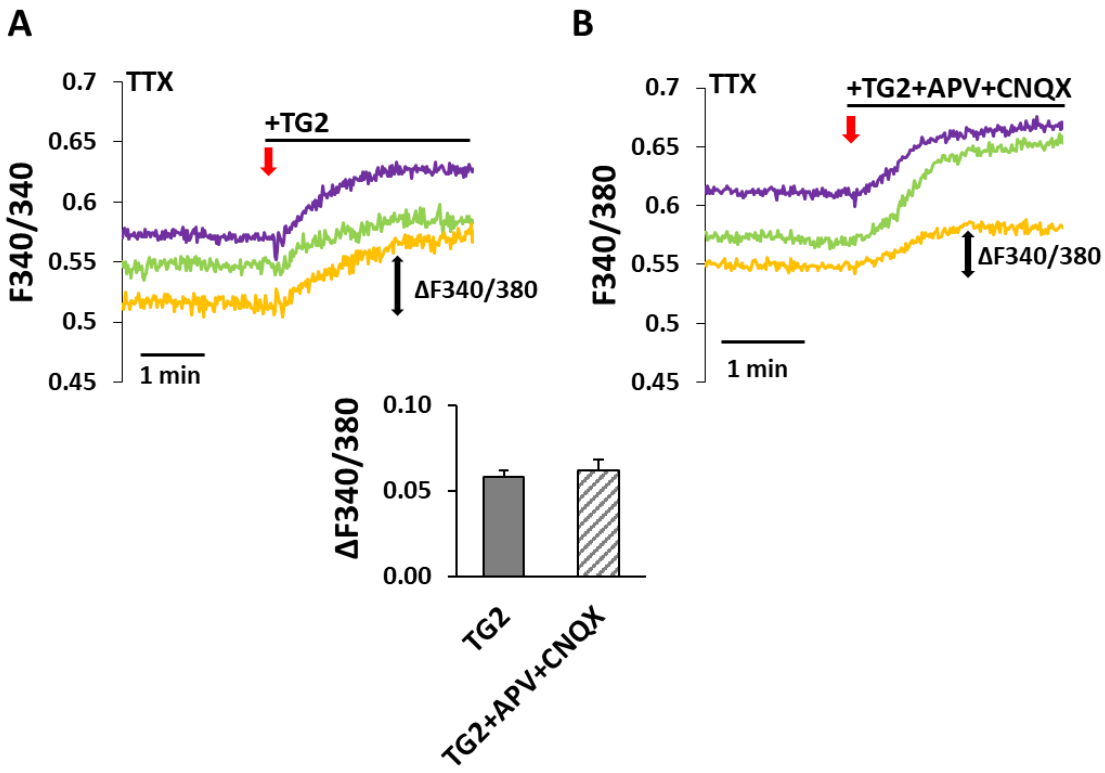

Figure 4.8. Exogenous TG2 increases $[Ca^{2+}]_i$ in the presence of NMDAR and AMPAR/KARs antagonists. *Temporal analysis of $[Ca^{2+}]_i$ changes in 14-20 DIV neurons exposed to exogenous TG2 (10 µg/ml) in the absence **(A)** or in the presence **(B)** of APV (NMDARs antagonist) and CNQX (AMPARs/KARs antagonist). TG2-dependent calcium rise was not affected by either blocker (mean ΔF340/380 control: 0.058±0.003, N=46; mean ΔF340/380 in presence of blockers: 0.062±0.006, N=9. Student's t-test: p=NS).*

Next, to analyse the possible contribution of VOCCs, a selection of pharmacological inhibitors of these channels was used. Pre-treatment with cadmium, a general blocker of VOCCs, reduced TG2-dependent Ca^{2+} responses by about 82.4% (**Fig. 4.9A**) and caused an almost complete recovery (88.3%) of $[Ca^{2+}]_i$ towards basal levels when applied during the plateau phase of calcium response induced by exogenous TG2 (**Fig. 4.9B**). Similarly, pre-treatment with nickel, a more specific inhibitor of T-type VOCCs, decreased TG2-dependent Ca^{2+} rises by 66.2% (**Fig. 4.9A**), and it caused a drop of $[Ca^{2+}]_i$ below basal level (about 151% inhibition) when applied during the plateau phase induced by TG2 (**Fig. 4.9B**). The involvement of VOCCs was corroborated by the observation that calcium transients evoked by 15 mM KCl, a stimulus known to depolarise neurons and cause VOCCs opening (Bading et al., 1993), rose faster and reached higher peak in the presence of TG2, with a significant 2-fold increase in average calcium influx (**Fig. 4.9C**).

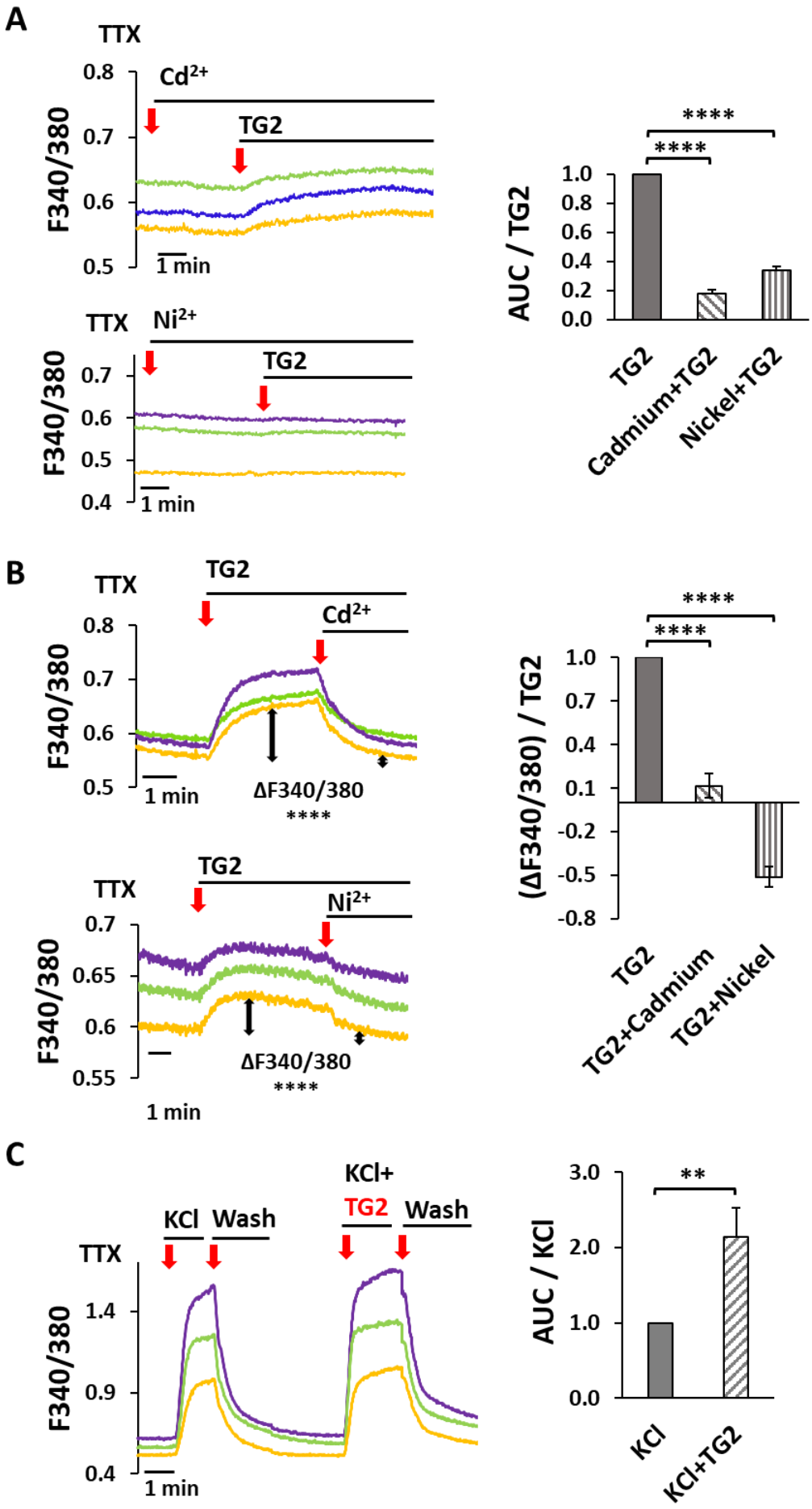

Figure 4.9. Extracellular TG2 mediates calcium influx in neurons through L-type VOCCs.

Figure 4.9. Extracellular TG2 mediates calcium influx in neurons through L-type VOCCs. *Temporal analysis of $[Ca^{2+}]_i$ changes in 14-20 DIV neurons exposed to exogenous TG2 (10 µg/ml) and VOCCs blockers.* ***A)*** *Pre-treatment with cadmium, a general blocker of calcium channels, and nickel, a blocker of T-type VOCCs, reduced TG2-dependent Ca^{2+} responses of about 82.4% and 66.2% respectively. Data is expressed as mean area under the curve (AUC) normalised to TG2 alone treatment (ratio AUC cadmium+TG2/TG2 = 0.18±0.03, N=7; ratio AUC nickel+TG2/TG2 = 0.34±0.03, N=15. ****P<0.00001).* ***B)*** *Addition of cadmium and nickel during the plateau phase of calcium response induced by exogenous TG2 led to a recovery of $[Ca^{2+}]_i$ towards basal levels, corresponding to about 88.3% and 151% inhibition respectively. Data is expressed as difference between $[Ca^{2+}]_i$ after each treatment and basal $[Ca^{2+}]_i$, normalised to TG2 alone treatment (mean ΔF340/380 TG2+cadmium/TG2 = 0.12±0.07, N=18; mean ΔF340/380 TG2+nickel/TG2 = -0.51±0.08, N=25. ****P<0.00001).* ***C)*** *Calcium transients induced by 15 mM KCl in the presence of NMDAR and AMPAR/KAR blockers APV and CNQX, revealed that $[Ca^{2+}]_i$ rose faster and reached higher peak in the presence of TG2, with a 2-fold increase in average calcium influx. Data is expressed as mean AUC normalised to KCl alone treatment (AUC KCl = 5.8±0.6; AUC KCl+TG2: 8.6±0.5; N=22, **P<0.01).*

Among the VOCCs controlling calcium transport through the plasma membrane, L-type VOCCs are highly abundant in the somatodendritic region of hippocampal neurons (Pravettoni et al., 2000; Condliffe et al., 2010; Leitch et al., 2009). Therefore, the possible contribution of these channels to calcium influx in the neuronal soma evoked by exogenous TG2 was explored. Calcium responses to TG2 were reduced by about 36% in neurons pre-treated with the selective of VOCCs L-type blocker nifedipine (NF) (**Fig. 4.10A**). In addition, the drug caused a partial recovery of $[Ca^{2+}]_i$ towards resting levels when applied during the plateau phase of calcium response induced by TG2 (**Fig. 4.10B**), suggesting that TG2 dependent calcium influx partially occurs through L-type VOCCs.

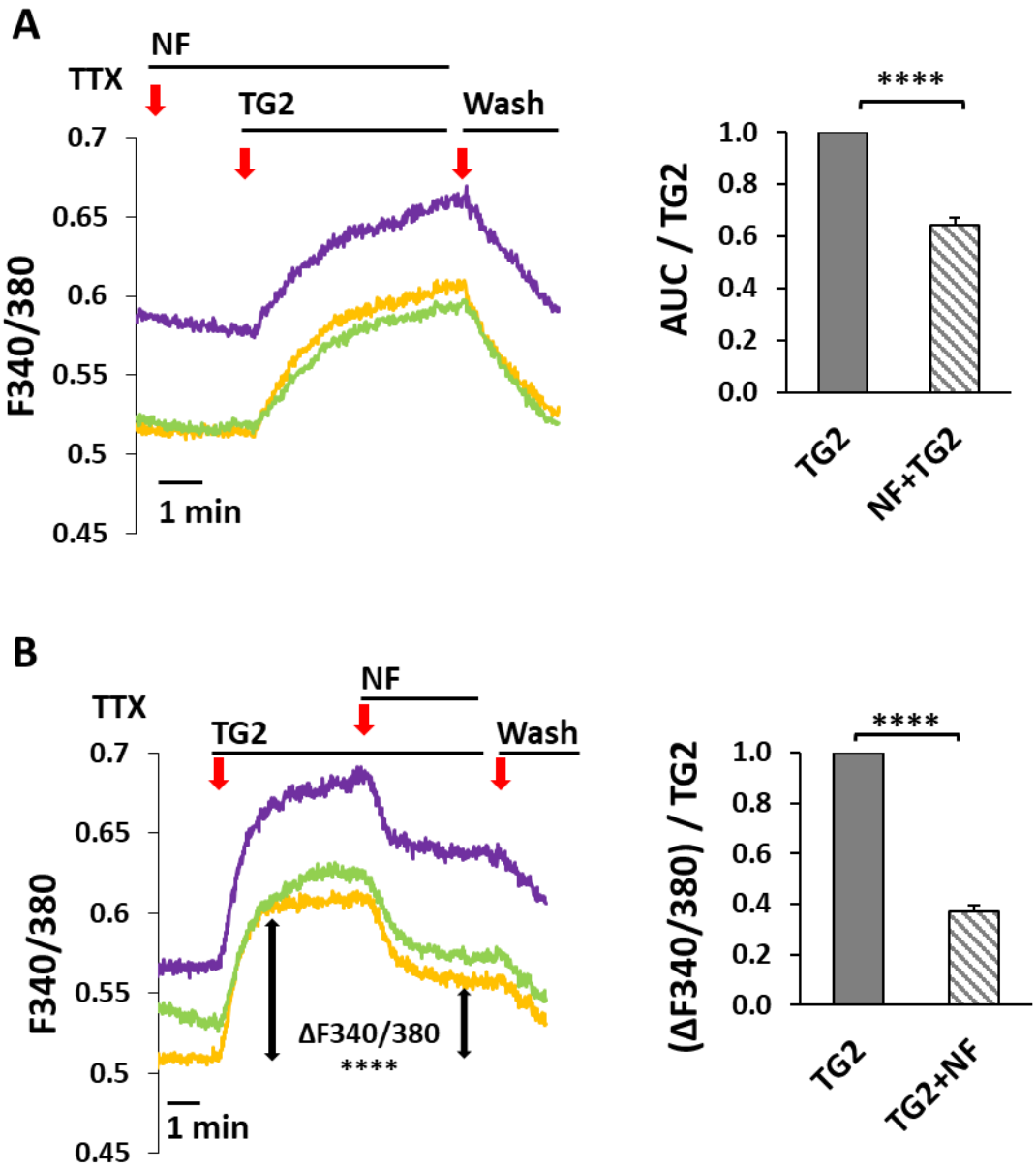

Figure 4.10. Nifedipine reduces TG2-dependent calcium influx. *Temporal analysis of $[Ca^{2+}]_i$ changes in 14-20 DIV neurons exposed to exogenous TG2 (10-30 µg/ml) and L-type VOCCs blocker Nifedipine (NF).* ***A)*** *Calcium responses to TG2 were reduced of about 36% in neurons pre-treated with NF (AUC TG2: 0.57±0.06; AUC NF+TG2: 0.36±0.03; N=21; ****P<0.00001).* ***B)*** *NF caused a partial recovery of about 63% of calcium concentration towards resting levels when applied during the plateau phase of calcium response induced by exogenous TG2 (mean ΔF340/380 TG2: 0.077±0.006; mean ΔF340/380 TG2+NF: 0.030±0.004; N=25; ****P<0.00001).*

Collectively, data obtained with NF suggest that TG2-induced calcium influx partially occurs through L-type VOCCs channels. This could be caused either by a direct interaction of TG2 with the channels, or as a secondary effect following a membrane depolarisation, which is the signal leading to voltage-gated channels opening.

4.2.6 Exogenous TG2 induces membrane depolarisation and the generation of ionic inward currents

It was hypothesised that extracellular TG2 could lead to $[Ca^{2+}]_i$ via stimulation of membrane depolarisation in neurons. To test this possibility, whole cell patch clamp was performed in the absence and presence of soluble TG2 in 9-15 DIV neurons. These experiments were carried out in the laboratory of Prof. Mazzanti (Department of Biosciences, Laboratory of Cellular and Molecular Physiology, University of Milan, Italy). Neurons were analysed either in voltage or current clamp mode, to study the effect of TG2 addition on both membrane potential and currents. In current clamp (I=0), TG2 addition induced a slow membrane depolarization (of about 20 mV) (**Fig. 4.11A**). In the same configuration, TG2 promoted excitatory postsynaptic currents (EPSCs), consistent with the activation of an inward calcium current (**Fig. 4.11B**). In this set of experiments, TG2 was added directly to the neuronal medium during the recordings (manual mode). Afterwards, a perfusion system was installed in Prof. Mazzanti laboratory, hence in the following experiments TG2 was added in perfusion mode. Voltage clamp experiments, expressed as current/voltage relationship (I/V curves) before and after addition of soluble TG2 are shown in **Fig. 4.11C**. To understand which VOCCs were involved in this process, a protocol for isolation of L-type VOOCs was used (pre-pulse of 40 mV and a Δ10 mV step from -30 to 0 mV, as described in Methods chapter 2.2.12). Perfusion of TG2 (**Fig. 4.11C** left panel, red I/V curve) led to an increased inward current compared to control (black I/V curve).

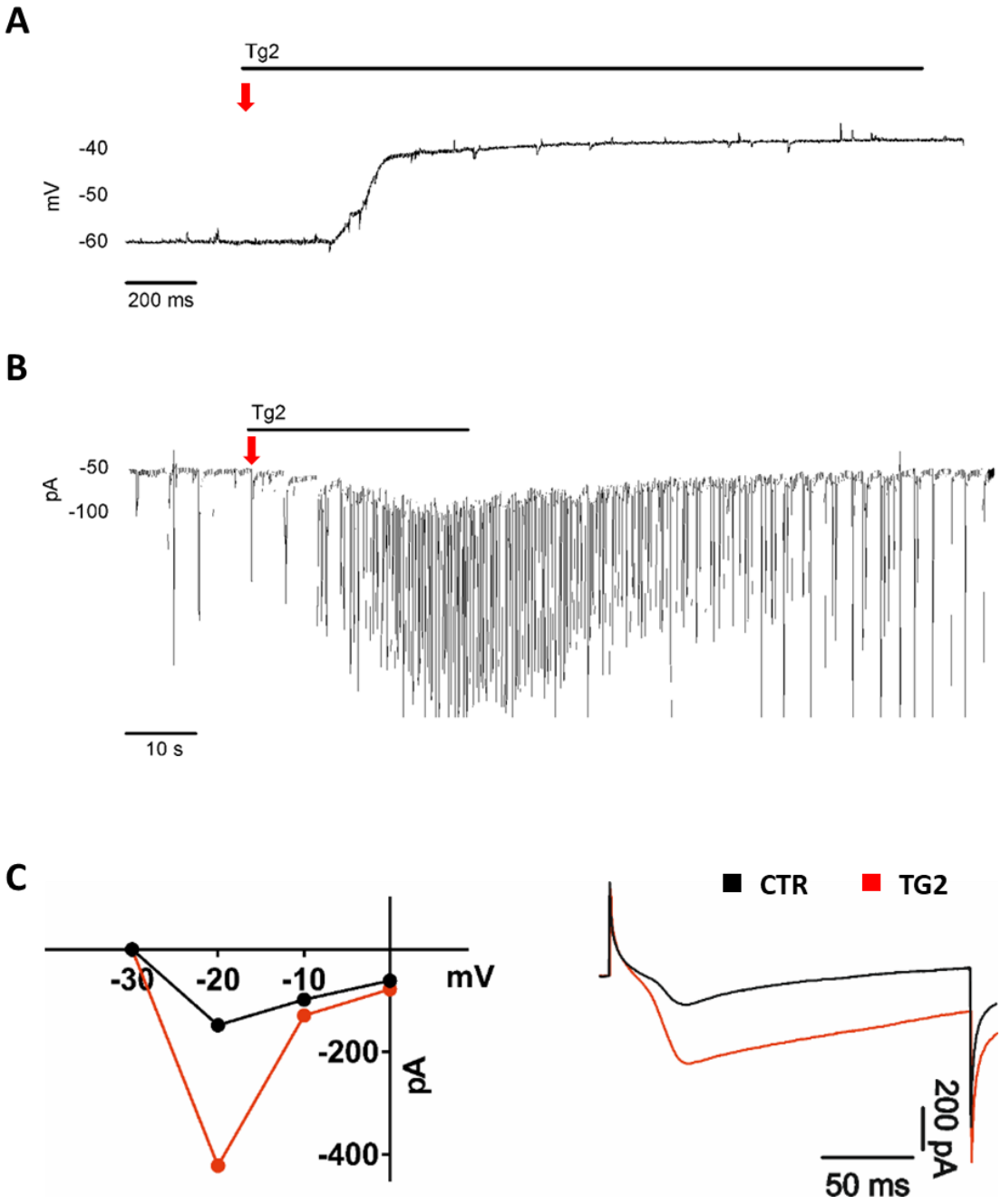

Figure 4.11. Whole-cell patch-clamp recordings of 9-15 DIV neurons exposed to TG2. *These experiments were performed by Ivan Verduci (University of Milan, Italy).* ***A)*** *Whole cell current clamp. Addition of TG2 (manual mode) induced a slow membrane depolarization of about 20 mV (N=3).* ***B)*** *Whole cell current clamp. Addition of TG2 (manual mode) promoted excitatory postsynaptic currents (EPSCs) consistent with the activation of an inward Ca^{2+} current (N=3).* ***C)*** *Whole cell voltage clamp results expressed as current/voltage (I/V) curves. Perfusion of TG2 (red I/V curve, left panel) led to an increased inward current compared to control (black I/V curve). Right panel shows the current recordings of the same experiment at -20 mV. The protocol for isolation of L-type VOCCs was applied as described in Methods chapter 2.2.12.*

To confirm the involvement of VOCCs in this process, nickel ability to block TG2-depended depolarisation was tested. Whole cell current clamp recordings (I=0) confirmed that nickel reverted the slow membrane depolarisation evoked by TG2 (**Fig. 4.12A**). Moreover, Nifedipine (NF) was used to block L-type VOCCs specifically during voltage clamp recordings performed as in **Fig. 4.11C**. The TG2-dependent inward current was completely prevented by NF (**Fig. 4.12,** red I/V curve).

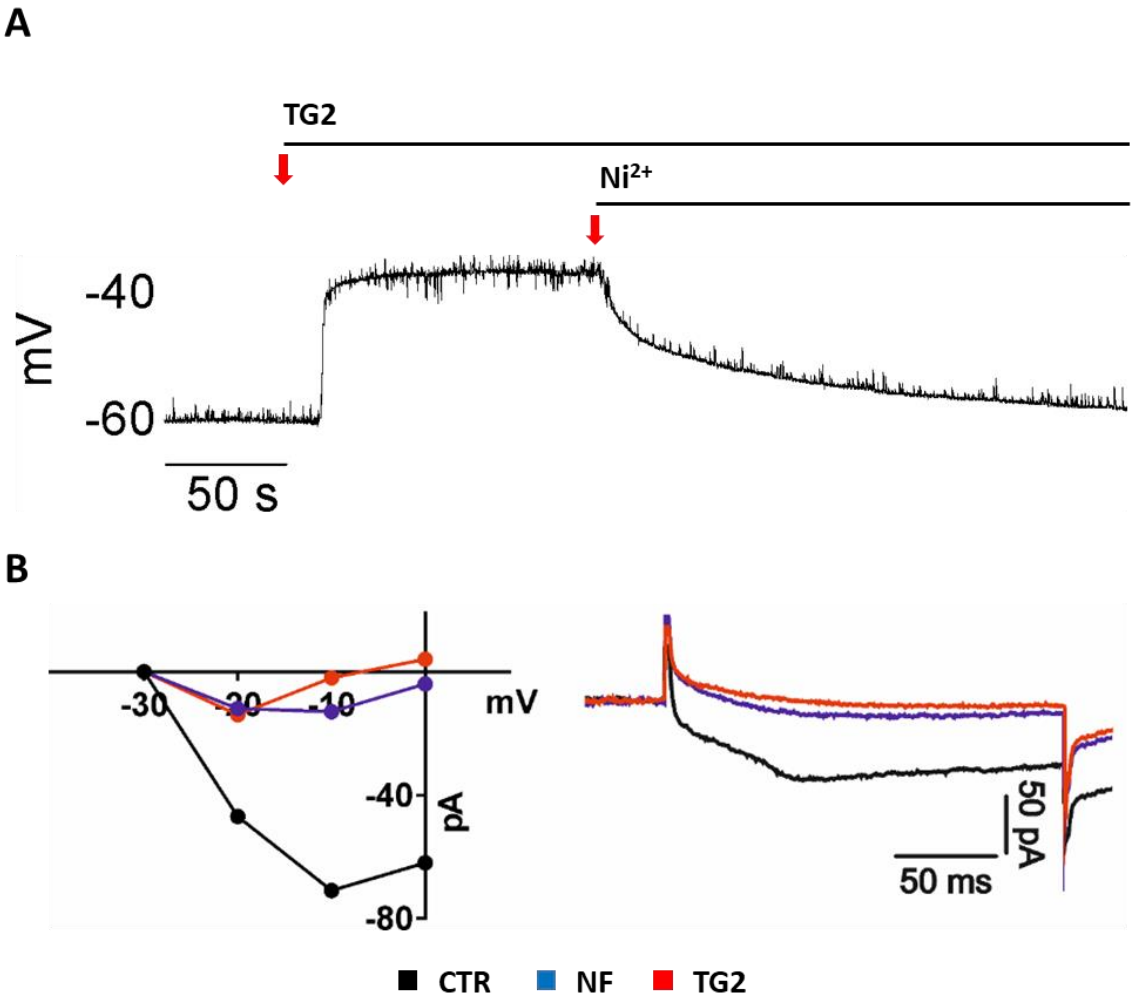

Figure 4.12: Effect of TG2 on membrane potential and currents in presence of VOCCs blockers. *Neurons at 8-16 DIV were analysed by whole cell patch clamp.* ***A)*** *Whole cell current clamp. Addition of Nickel after TG2 (manual mode) repristinated resting membrane potential.* ***B)*** *Whole cell voltage clamp results expressed as current/voltage (I/V) curves. Perfusion of TG2 in presence of NF (red I/V curve, left panel) did not lead to increased inward current compared to control (black I/V curve). Right panel shows the current recordings of the same experiment at -20 mV (N=3). The protocol for isolation of L-type VOCCs was applied as described in Methods chapter 2.2.12.*

Collectively these data suggest for the first time a role for TG2 in membrane depolarisation and identify L-type VOCCs as one of the possible targets of TG2 responsible for dysregulation of basal calcium concentration in neurons.

4.2.7 TG2-dependent calcium response is also mediated through the sodium/calcium exchanger (NCX)

Despite electrophysiological recordings indicating complete inhibition of inward calcium current evoked by TG2 under block of L-type VOCCs (**Fig. 4.12**), a residual Ca^{2+} response was observed in calcium imaging experiments, largely sensitive to both cadmium and nickel (**Fig. 4.10B**). In addition to VOCCs, both cadmium and nickel inhibit the activity of the NCX, a key regulator of calcium transport through the plasma membrane (Blaustein and Lederer, 1999). Therefore, a possible involvement of the exchanger in Ca^{2+} dysregulation caused by the enzyme was hypothesised. NCX normally removes Ca^{2+} from neurons in exchange for Na^+, which enters the neuron down its gradient across the plasma membrane (Blaustein and Lederer, 1999). However, perturbation of the Na^+ gradient leads to operation of the exchanger in the reverse mode, causing Ca^{2+} influx into the neurons (Blaustein and Lederer, 1999). To promote NCX reverse mode, extracellular Na^+ and K^+ were removed from the neuronal medium (Na^+/K^+-free KRH). In these conditions, the response to exogenous TG2 was strikingly increased (about 8-fold increase) (**Fig. 4.13A**), suggesting that NCX may amplify TG2-dependent Ca^{2+} entry. Addition of the NCX inhibitor YM-244769 significantly decreased TG2-dependent Ca^{2+} influx in both normal and Na^+/K^+-free medium, of about 48.4% and 37.3% respectively (**Fig. 4.13B**). These data indicate that not only VOCCs, but also NCX contributes to elevate $[Ca^{2+}]_i$ in neurons exposed to extracellular TG2.

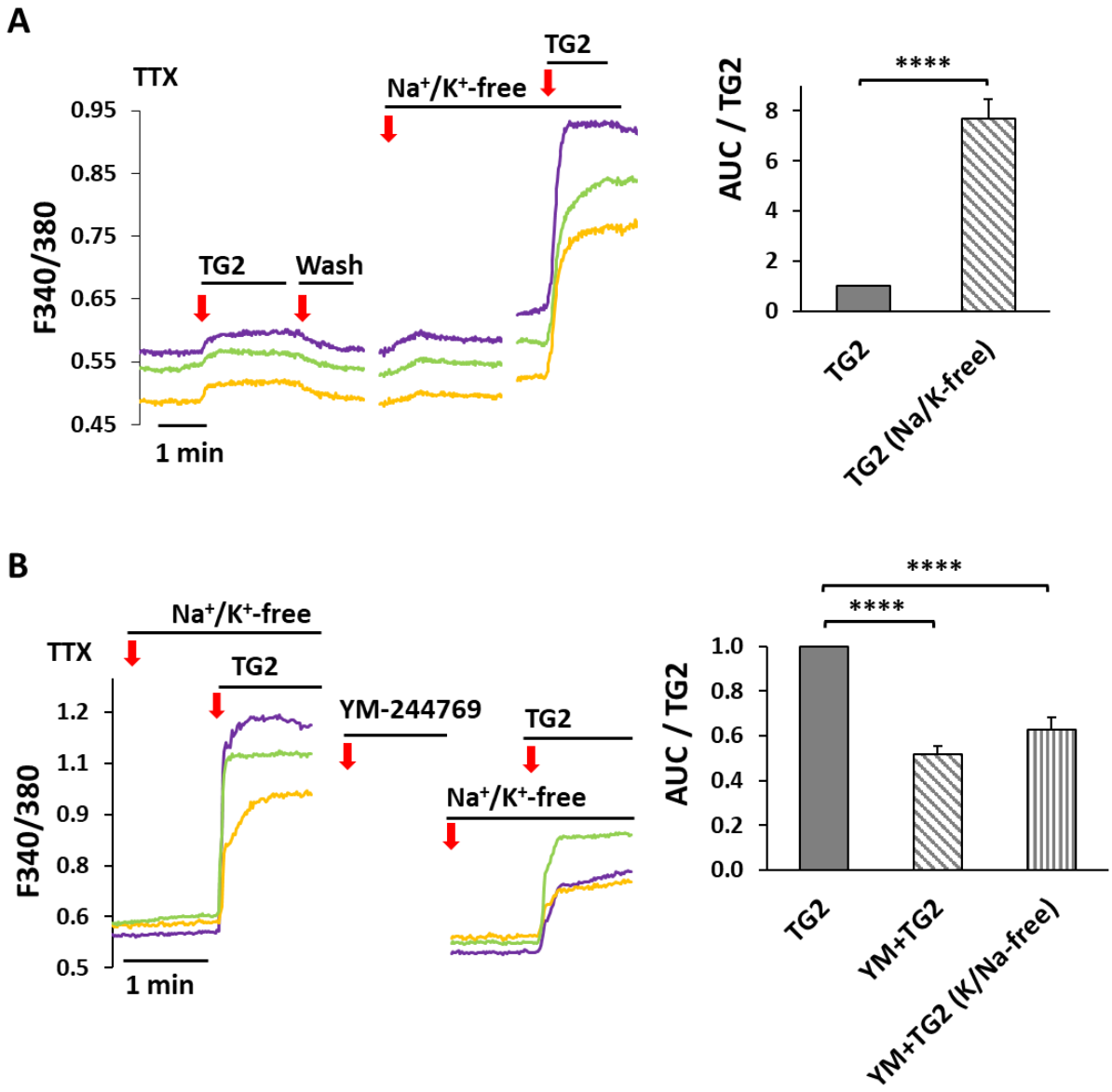

Figure 4.13. Contribution of NCX to TG2-dependent calcium rise*. Temporal analysis of $[Ca^{2+}]_i$ changes in 14-20 DIV neurons exposed to exogenous TG2.* ***A)*** *Addition of TG2 in Na^+/K^+-free KRH led to a 8-fold increase in average calcium influx compared to normal KRH (AUC TG2: 0.82±0.14, N=20; AUC TG2 in Na^+/K^+-free KRH: 6.27±1.04, N=20; ****P<0.00001). Data is expressed as mean ± standard error normalised to TG2 AUC values.* ***B)*** *Incubation with NCX inhibitor YM-244769 (10 minutes) led to a significant decrease in calcium influx, both in Na^+/K^+-free KRH (AUC TG2 in Na^+/K^+-free KRH: 7.56±1.08, N=21; AUC TG2+YM244769 in Na^+/K^+-free KRH: 3.82±0.48, N=21. ****P<0.00001) and normal KRH (AUC TG2: 0.55±0.04, N=25; AUC TG2+YM244769: 0.028±0.02, N=25; ****P<0.00001). Data is expressed as mean ± standard error normalised to TG2 AUC values.*

4.2.8 TG2-rich glial EVs increase $[Ca^{2+}]_i$ in neurons

Taking into consideration the results obtained so far, the next step was to investigate if the addition of extracellular EVs-associated TG2 would affect $[Ca^{2+}]_i$ similarly to the soluble form that had been used in the previous sections. As described in Chapter 3, it had been previously demonstrated that EVs isolated from LPS-treated astrocytes carried TG2 and could therefore be a source of extracellular TG2 in brain under neuroinflammatory conditions (**Fig. 3.11C**).

EVs were isolated from primary mixed glial cocultures (primary astrocytes and microglia isolated from E18 embryonic rat cortices, as described in Methods chapter 2.2.1.2) under the same conditions as shown in Chapter 3 (section 3.2.4). Specifically, glial cells were washed with KRH pH 7.4 and incubated in serum-free media supplemented with 1 μg/ml LPS for 24 hours prior to EVs isolation. To pellet both large and small EVs in a single pellet, the 10,000xg centrifugation was omitted. Because ATP has been shown to be present in glial-derived EVs and to induce calcium responses in glial cells (Verderio and Matteoli, 2001; Coco et al., 2003), the vesicle pellet was resuspended in KRH containing 30 U/ml apyrase, an enzyme that hydrolyses ATP to AMP (Verderio and Matteoli, 2001). EVs isolated from two confluent T75 flasks (about $20x10^6$ cells) were added to fura-2-loaded hippocampal neurons in the presence or absence of monoclonal anti-TG2 antibody (IA12) (**Fig. 4.14**), and neuronal $[Ca^{2+}]_i$ were recorded in several fields of the same slide prior to EVs addition (basal calcium) and 20 minutes after, in order to allow EVs to deposit and interact with the neurons. TG2-rich EVs were able to induce a significant increase in $[Ca^{2+}]_i$ compared to basal ($\Delta F340/380 = 0.012$, N>80, tested on 3 slides) (**Fig. 4.14**). Inhibition of vesicular TG2 by pre-treatment of EVs with the antibody IA12 enhanced this effect, leading to a 2.5-fold higher $\Delta F340/380$ compared to untreated EVs ($\Delta F340/380 = 0.031$, N>30, tested on 1 slide) (**Fig. 4.14**).

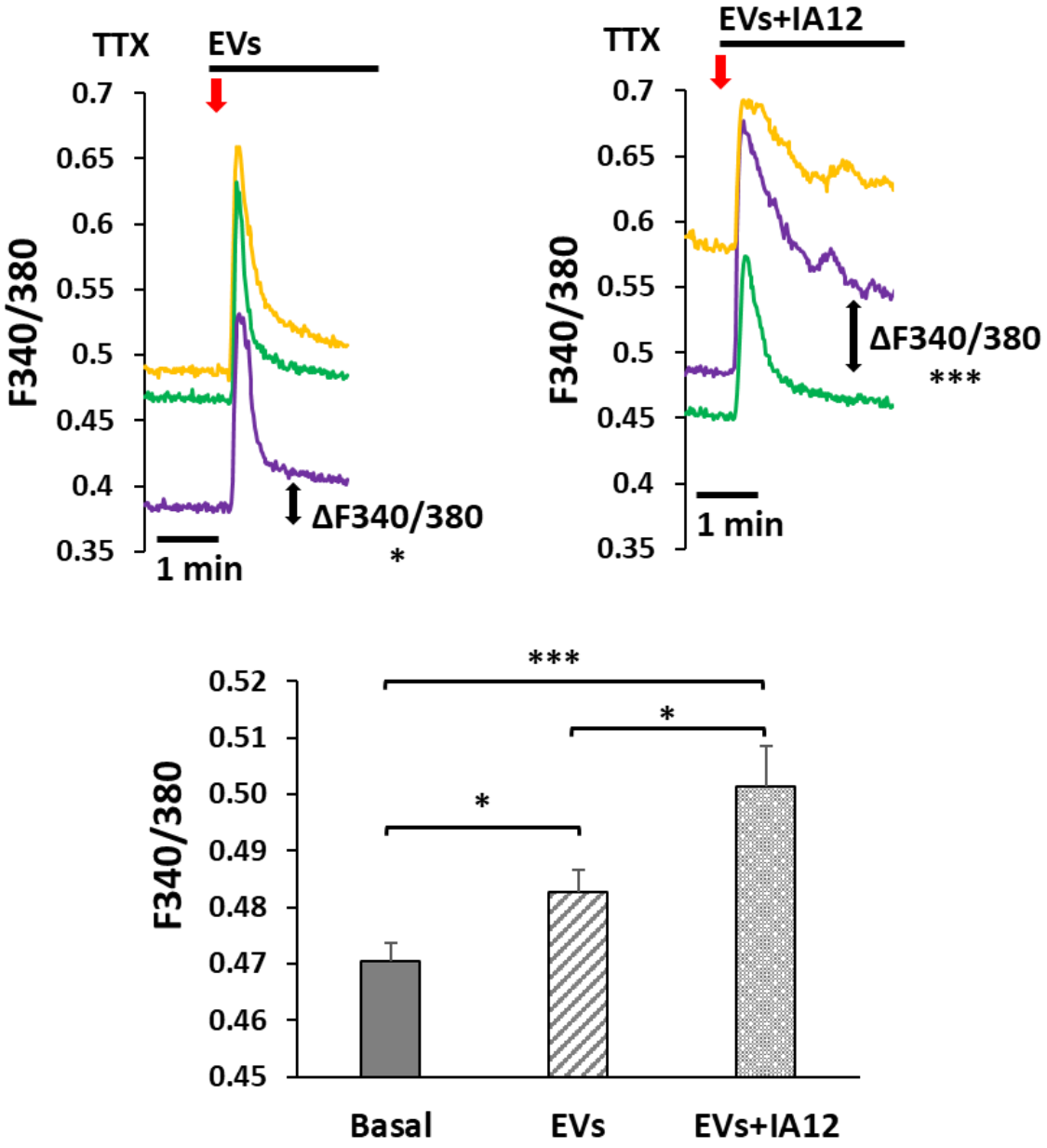

Figure 4.14. Glial EVs increase $[Ca^{2+}]_i$ in neurons. *Temporal analysis of $[Ca^{2+}]_i$ changes in 15 DIV neurons stimulated with EVs isolated from glial cells treated with LPS (about $20x10^6$ cells), measured as variation in the F340/380 fluorescence ratio. EVs were isolated after incubation with LPS (1 µg/ml) for 24 hours in serum-free media and resuspended in KRH supplemented with 30 U/ml of apyrase and with or without monoclonal anti-TG2 antibody (IA12, 1:100). The 10,000xg centrifugation was omitted, so large and small EVs were isolated together and used for this set of experiments. Three representative traces of neuronal $[Ca^{2+}]_i$ are shown. Data is expressed as mean ± standard error (Basal $[Ca^{2+}]_i$: 0.470±0.003, N=130; $[Ca^{2+}]_i$ EVs: 0.483±0.004, N=88; $[Ca^{2+}]_i$ EVs+IA12: 0.501±0.007, N=31. *p<0.05; ***p<0.0001).*

These results indicate that vesicular TG2, as a cargo of glial-derived EVs, contributes to alter calcium homeostasis in neurons under neuroinflammatory conditions.

In conclusion, it was demonstrated here for the first time that extracellular TG2, either added in soluble form, carried by glial-derived EVs or externalised by neurons, was able to increase $[Ca^{2+}]_i$ in primary hippocampal neurons (**Fig. 4.15A-B**). Calcium influx could be a consequence of membrane depolarisation induced by TG2 (**Fig. 4.15C**), through the activation of L-type VOCCs (**Fig. 4.15D**). Alternatively, TG2 might interact with other molecules and mediate calcium influx via VOCCs and NCX (**Fig. 4.15D-E**). Calcium overload is a hallmark of various neurodegenerative diseases and activates a variety of mechanisms leading to cell death (Marambaud et al, 2009). At the same time, increase in $[Ca^{2+}]_i$ could potentially activate intracellular TG2, enhancing the transamidation of endogenous targets and formation of neurotoxic protein aggregates, which could contribute to neuronal death (**Fig. 15F**).

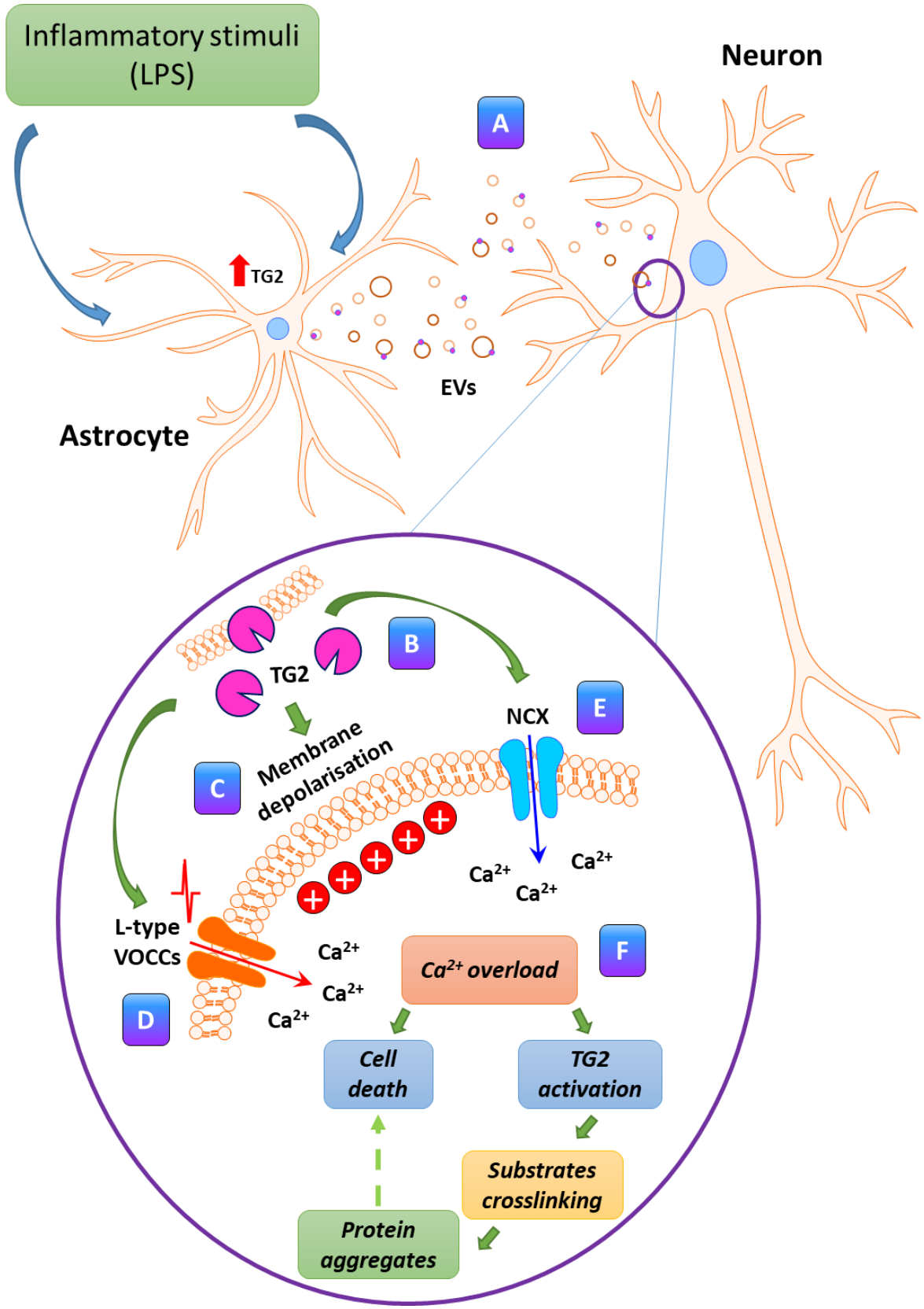

Figure 4.15. Schematic representation of Chapter 4 results. A) *Astrocytes activated by Lipopolysaccharides (LPS), an endotoxin which causes inflammatory response, release EVs carrying TG2.* ***B)*** *Extracellular TG2 (in soluble form or vesicle-bound) interacts with neurons, inducing a calcium influx that increases intracellular calcium levels ($[Ca^{2+}]_i$).* ***C)*** *Extracellular TG2 causes a membrane depolarisation (of about 20 mV) and activates an inward calcium*

current. ***D)*** *Calcium influx is mediated by L-type Voltage Operated Calcium Channels (VOCCs) and* ***E)*** *the Sodium/calcium exchanger (NCX).* ***F)*** *Increase of intracellular calcium levels is neurotoxic and can lead to cell death. At the same time, higher* $[Ca^{2+}]_i$ *can activate intracellular TG2, which could in turn crosslink endogenous substrates, leading to the formation of neurotoxic protein aggregates and cell death. This image was generated with Motifolio (https://www.motifolio.com/).*

4.3 Discussion

This study has established for the first time that extracellular TG2 affects calcium homeostasis in neurons. It does so by inducing an influx of calcium ions through L-type VOCCs and NCX, possibly following membrane depolarisation. Moreover, it was proved that also endogenous TG2 is capable of inducing an increase of $[Ca^{2+}]_i$ when transiently overexpressed in hippocampal neurons.

The regulation of $[Ca^{2+}]_i$ is a fundamental biological process, especially in neurons, being calcium signalling at the basis of synaptic plasticity, neurons survival and their ability to communicate (Marambaud et al., 2009). Hence, neurons are especially sensitive to changes in $[Ca^{2+}]_i$ and their function is heavily impacted by dysregulation of calcium homeostasis. This is the case of many neurodegenerative and neuroinflammatory diseases, where calcium regulation is impaired, leading to an overload of intracellular Ca^{2+} and consequent activation of the apoptotic pathway and increase of neurons excitotoxicity (Marambaud et al., 2009).

Many studies have highlighted that in patients affected by neurodegeneration, TG2 protein and activity levels are increased (as reviewed in Martin et al., 2013 and Wilhelmus et al., 2014). TG2 involvement in the neurodegenerative process has been traditionally associated to its enhanced ability to crosslink target proteins (e.g. Amyloid β, tau and α-synuclein), leading to their aggregation. However, a direct link between TG2 and the pathogenesis of these diseases has not been identified yet.

More recently, new insights on TG2 regulatory mechanisms have suggested that the enzyme conformation could be equally important to mediate both physiological and pathological effects (Katt et al., 2018). Open TG2 was in fact shown to have cytotoxic effects in NIH 3T3 fibroblasts and in human cancer cells (HeLa), independently from its crosslinking activity (Datta et al., 2007). Similarly, in mouse striatal cells transfected with mutant forms of TG2, the open conformation mutant increased the cells susceptibility to oxygen/glucose deprivation-mediated cell death compared to cells expressing wild-type TG2 or the catalytically inactive form [Cys(277)Ser mutant] (Colak et al., 2011; Singh et al., 2016). TG2 conformation and cellular localisation were also shown to have opposite effects on hypoxic/hypoglycemic-induced cell death in HEK-293A cells (Gundemir et al., 2013). To date, there is little understanding regarding this process and which cellular functions TG2 conformation might affect.

Here it was shown that extracellular TG2, both exogenous and endogenous, is able to affect $[Ca^{2+}]_i$ in hippocampal neurons, a novel function that has never been attributed to TG2 before (**Fig. 4.1** and **4.2**). Interestingly, calcium was restored to basal levels upon removal of TG2 from the neuronal medium, revealing that this was a reversible process. This finding led to the idea that the transamidating activity of TG2 might not be involved, as it would be expected that the covalent crosslinking of a substrate would lead to irreversible effects. Hence, the next step was to ask whether TG2 conformation might be responsible instead and this hypothesis was tested firstly by checking if the soluble TG2 used in these experiments was catalytically active. The *in vitro* simulation of the TG2 microenvironment when $[Ca^{2+}]_i$ increases were recorded in neurons, revealed that TG2 was capable of a low level of Ca^{2+}-dependent transamidation (**Fig. 4.4A**). Although the simulation *in vitro* might be imperfect not reflecting fully the state of live cells (as it was performed in the absence of cells and thus could not take into account physiological redox conditions), it is known that TG2 needs to be in a reduced state to be able to exert its crosslinking activity (Verderio et al., 2003). Sollid's research group has extensively investigated this aspect, showing that TG2 activity is regulated by the state of a redox sensitive cysteine triad located in the catalytic core, specifically Cys(230), Cys(370) and Cys(371) (Stamnaes et al., 2010). They demonstrated that TG2 is inactivated when Cys(230) is oxidized and forms disulphide bonds with the other two Cys residues. Moreover, calcium was able to prevent the formation of these bonds, confirming that not only the redox environment, but also calcium concentration are equally fundamental modulators of TG2 activity (Stamnaes et al., 2010). Knowing that active TG2 would be able to crosslink a variety of substrates in the ECM, which would lead to the pathological accumulation of ECM proteins and tissue fibrosis, it is not surprising that the enzyme activity would be finely regulated in the extracellular milieu. It is in fact suggested that TG2 continuously changes between different conformational structures, going from the close (inactive), to the open but oxidized (inactive) and open reduced (active) (Pinkas et al., 2007; Jin et al., 2011; illustrated in **Fig. 1.9**). The presence of guanine nucleotides (i.e. GTP/GMP) is also important for TG2 regulation, however this is more relevant in the intracellular space where calcium concentration is lower. In this environment, TG2 can bind and hydrolyse GTP and be stabilised in a closed inactive conformation (Achyuthan et al., 1987; Liu et al., 2002). On the other hand, in the extracellular space where calcium concentration is higher, GTP-binding to TG2 is reduced and TG2 regulation relies more on the redox state and binding to other molecules, such as

heparan sulfate proteoglycans (HSPG) (Liu et al., 2002; Lortat-Jacob et al., 2012). Confirming this perspective, oxidised extracellular TG2 was found to be activated by recombinant human thioredoxin (Trx) in fibroblasts, and also by Trx derived from monocytic cells exposed to IFN-γ (Jin et al., 2011). Recently, the TG2 interactome elucidated by our group in a model of chronic kidney fibrosis revealed a cluster of redox regulatory proteins significantly more associated with TG2 in fibrotic kidney compared to controls, suggesting that the hyperactivation of TG2 during fibrosis is partially due to its association with these reducing partners (Furini et al., 2018).

Specific TG2 inhibitors were used to block TG2 activity and lock it in open conformation. Two inhibitors were available, namely NC9 (from Dr Keillor) and ZDON (supplied by Zedira). NC9 carries an electrophilic acrylamide warhead linked to a lysine side chain, which is attacked by TG2 active site cysteine residue [Cys(277)] and forms and irreversible complex (Keillor et al., 2008; Clouthier et al., 2012). ZDON is a side chain-modified peptide, carrying an electrophilic "DON" group (6-diazo-5-oxo-L-norleucine) which undergoes nucleophilic attack by Cys(277) and is consequently irreversibly bound to TG2 active site in a stable thioether adduct (McConoughey et al., 2010). Surprisingly, the two inhibitors ZDON and NC9 had opposite effects on neurons when they were added during calcium imaging recordings. NC9 was able to enhance TG2-mediated Ca^{2+} influx, both when pre-incubated with exogenous TG2 (**Fig. 4.5A**), and even to a greater extent when added to neurons alone to inhibit endogenous TG2 (**Fig. 4.5B**). Conversely, addition of ZDON to EGFP-TG2 overexpressing neurons characterised by higher calcium levels, led to a decrease of $[Ca^{2+}]_i$, seemly promoting a protective effect by recovering physiological basal calcium (**Fig. 4.6C**). It cannot be excluded that in this cell system overexpressing and externalising TG2, the protein would be more active compared to the soluble exogenous TG2 added to the medium in purified form. In conclusion it cannot be said for certain whether ZDON effect was mediated by TG2 activity or conformation and the dilemma of whether or not TG2 activity is involved in increasing basal $[Ca^{2+}]_i$ still remains. A combination of both TG2 PTM and TG2 protein conformation may also be likely. Interestingly, a decrease in $[Ca^{2+}]_i$ after ZDON addition was also observed in EGFP control neurons (**Fig. 4.6C**), suggesting that the inhibitor had an effect on endogenous TG2 too. Moreover, ZDON had protective effect in neurons presenting epileptic-like oscillatory activity induced by bicuculline (**Fig. 4.7**). These data are in agreement with previous findings in an HD mouse model (YAC128), where ZDON was shown to have a protective effect on striatal neurons (McConoughey et al., 2010).

Specifically, pre-treatment of neurons with ZDON prior to NMDA addition protected both control and YAC128 neurons from toxicity, through the upregulation of the mitochondrial protein PGC-1α (McConoughey et al., 2010).

From these findings it was concluded that the observed calcium influx is a reversible effects mediated specifically by TG2, however it is not possible to say yet if this depends on activity, conformation or both.

Another possible explanation for the reversibility of TG2 function on $[Ca^{2+}]_i$ raise may be that TG2 target could be a molecule present in the neuronal medium, which would be removed together with TG2 during the washing step. Indeed, a less characterised function of TG2 is the transamidation of monoamine neurotransmitters, a reaction called monoaminylation (as recently reviewed in Muma et al., 2018). Firstly, serotonin was shown to be an intracellular substrate of TG2 transamidation to small GTPases in platelets during activation (serotonylation) (Dale et al., 2002; Walter et al., 2003). Consequently, other signalling molecules were identified to be substrates of TG2 PTM, e.g. histamine in mastocytoma cells (Vowinckel et al., 2012), while extracellular dopamine and noradrenaline were shown to be transamidated to plasma FN *in vitro* and in glioma C6 cells (Hummerich et al., 2010-2012). TG2-mediated monoaminylation and activation of the small GTPase rac1 has been shown to affect dendritic plasticity and morphology in rat embryonic cortical neurons (Mi et al., 2017). These findings open a new perspective for TG2 modification of neurotransmitters, especially the potential of their incorporation into soluble proteins like plasma FN. Therefore, in the light of this study, the possibility that extracellular TG2 could modify a neurotransmitter and this produce an increase in $[Ca^{2+}]_i$ cannot be excluded.

In order to clarify the mechanism underling TG2-dependent effect on $[Ca^{2+}]_i$, a series of channels antagonists and blockers were employed, targeting the main calcium transporters in neuronal cells. Calcium influx was not affected by blockage of NMDARs and AMPARs/KARs (**Fig. 4.8**). On the other hand, it was significantly reduced in the presence of L-type VOCCs blocker Nifedipine (**Fig. 4.10**) and completely nullified by more general VOCCs blockers like Nickel and Cadmium (**Fig. 4.9**). Additionally, also NCX appeared to be involved, as TG2 addition in the presence of NCX blocker YM-244769 significantly decreased TG2-dependent Ca^{2+} influx (**Fig. 4.13**).

Patch clamp experiments were performed to investigate the effect of TG2 on membrane currents and potential. They revealed that when TG2 was added in perfusion mode to neurons, a membrane depolarisation of about 20 mV and a correspondent inward current

were induced (**Fig. 4.11**), thus showing that TG2 could either directly cause depolarisation and consequently the opening of voltage gated channels, or first affect channels that would then induce depolarisation. The involvement of L-type VOCCs by patch clamp was shown by addition of extracellular TG2 in the presence of NF, which blocked the TG2-induced current (**Fig. 4.12**).

Activation of L-type VOCCs is important in hippocampal neurons for LTP and synaptic plasticity (Grover and Teyler, 1990; Raymond and Redman, 2002), together with NMDAR activity (Collingridge et al., 1983; Tsien et al., 1996) and Store Operated Calcium Channels (SOCCs) (Behnisch and Reymann, 1995; Harvey and Collingridge, 1992). Alterations in VOCCs activity have been reported in neurodegeneration, such as in AD (as reviewed in LaFerla 2002 and Nimmrich and Eckert 2013), and they have been proposed as possible therapeutic targets (Yagami et al., 2012; Cataldi, 2013). For example, $A\beta_{1-40}$ has been shown to induce calcium influx through L- and N-type VOCCs in rat synaptosomes, thus promoting the apoptotic pathway (MacManus et al., 2000). Moreover, $A\beta_{25-35}$ was shown to cause Ca^{2+} influx and excitatory potentials in hippocampal neurons by affecting both NMDAR and L-type VOCCs (Brorson 1995, Kim and Rhim, 2011). Notably, the use of specific VOCCs blocker S-312-d has shown neuroprotective effects (Yagami et al., 2004), as well as new compounds with multitarget-directed ligands targeting VOCCs and Ser/Thr phosphatase (Lajarín-Cuesta et al., 2016) or VOCCs and phosphoprotein phosphatase 2A (PP2A) (Gonzalez et al., 2018).

Similarly to VOCCs, CNX in fundamental for the regulation of calcium concentrations and activation of the reverse mode (Ca^{2+} influx) has been associated with neuropathic pain caused by nerve-injury (Jaggi and Singh, 2011), ischemic damage (Matsuda et al., 2001), increased oxygen/glucose deprivation-mediated neuronal damage and infarct injury (Secondo et al., 2015).

It is evident that perturbation of the Ca^{2+} transport and buffering systems is deleterious for neuronal survival. In this picture, TG2-dependent calcium influx could represent an additional mechanism which participates to the general dysregulation of calcium homeostasis in neurodegenerative conditions.

This study has shown that astrocytes are a rich source of TG2 and that this can be secreted via EVs. It was also shown that glial-derived EVs increase calcium concentration in neurons and preliminary data have suggested that TG2 might be involved. In fact, when EVs were pre-incubated with monoclonal anti-TG2 antibody IA12 before addition to neurons, calcium influx was significantly increased (**Fig. 4.14**). It is likely that IA12, which binds TG2 in the

catalytic domain and blocks its activity, might also force TG2 in open conformation, and thus corroborate the findings obtained with the NC9 inhibitor that indicate a role for open TG2 in mediating calcium influx. EVs are known to be mediators of cell-cell communication and thus it is feasible to hypothesise that TG2 might be carried by EVs, accumulate in the extracellular space and in this way affect neuronal function.

Overall, data in this chapter have highlighted a TG2-specific effect on calcium homeostasis, specifically the triggering of a Ca^{2+} influx through both L-type VOCCs and NCX. TG2 might interact directly with this channels, or indirectly by causing membrane depolarisation or affecting signalling molecules such as neurotransmitters. Additionally, it is not yet possible to say if this effect is mediated by the enzyme activity, conformation or a combination of both, which is probably the most likely scenario.

In order to improve the understanding of the mechanism undelaying TG2-dependent calcium influx in neurons, a mass spectrometry based approach was next used to identify TG2 partners in a context of neuroinflammation and neurodegeneration.

CHAPTER 5:

TG2 "transamidome" in a cell model simulating Alzheimer's disease

5.1 Introduction

TGs involvement in the pathological progression of neurodegenerative diseases has been traditionally associated with their ability to crosslink a variety of brain substrates *in vivo* and *in vitro* (Benilova et al., 2012; Martin et al., 2013). Increased TGs activity in brain under stress conditions has been shown to participate to the formation of protein aggregates that characterise proteinopathies such as AD, PD and HD, as demonstrated by the presence of TGs-mediated crosslinks in senile plaques, neurofibrillary tangles and disease inclusion bodies (Nemes et al., 2004; Wilhelmus et al., 2009; Appelt et al., 1996; Bonelli et al., 2002). In order to clarify the mechanism underlying this process and identify the targets of TGs-mediated crosslinking, a variety of studies focusing on diverse diseases have relied on proteomic approaches. The most common modus operandi for the determination of TGs substrates has been the incubation of cells and tissue lysates with labelled general amine substrates (e.g. biotin-cad) or more isozyme specific targets (e.g. biotin-K5 and biotin-T26 peptides for TG1 and TG2 respectively), followed by isolation of labelled protein complexes and LC-MS/MS analysis or amino acid sequencing. In fact, each TGs have been shown to have preferential *in vivo* and *in vitro* substrates, and that the transamidation reaction can be restricted to specific sequences (as reviewed in Hitomi and Tatsukawa, 2015). For this reason, specific glutamine- (acyl donor) and lysine- (acyl acceptor) donor substrates have been employed to identify targets of TGs PTM (reviewed in Savoca et al., 2018). For example, this approach has been used to identify TGs targets in human intestinal epithelial cells as a model of celiac disease (Orrú et al., 2003), in liver and kidney fibrosis (Tatsukawa et al., 2017-2018) and recently also in brain (André et al., 2017), as summarised in **Table 5.1**. However, these studies have all the same limitation that identify *in vitro* TGs substrates which would not necessarily be targets of TGs-catalysed crosslinking *in vivo*, where Ca^{2+} and redox state are controlled and may result in TG2 inactivation. Instead the *in vitro* assays were carried out in activating conditions (high calcium and DTT), thus forcing the system so that TGs would be activated and crosslink all available substrates. Conversely, only few studies have used a different approach, by first incubating the labelled peptides with live cells and lysing the samples only afterwards, thus capturing TGs-mediated incorporation of potential substrates "*ex vivo*". To our knowledge, this was done only in rat embryonic cardiomyoblast-derived H9c2 cells (Vyas et al., 2016-2017-2018).

Table 5.1. Representative proteomic studies on the identification of TGs crosslinking targets in cells and tissue lysates in vitro.

Tissue/cell type	Pathology	Method	References
Human intestinal epithelial cells	Coeliac disease	Incorporation of biotinylated glutamine donor F11KA (FXIII specific) and T26 (TG2 specific) – MALDI TOF MS/MS	Orrù et al., 2003
Differentiating osteoblastic cell line	Normal	Incorporation of biotinylated amine donor BPNH2 and amine acceptor A25 peptides – MALDI TOF MS/MS	Watanabe et al., 2013
Blood cloth	Normal	FXIII Incorporation of biotinylated 5-(biotinamido)pentylamine (BPA) – LC MS/MS	Nikolajsen et al., 2014
Human keratinocytes	Normal	Incorporation of biotinylated glutamine donor K5 (TG1 specific) – MALDI TOF MS/MS	Yamane et al., 2016
Mouse Liver	Liver fibrosis	Incorporation of biotinylated glutamine donor K5 (TG1 specific) and T26 (TG2 specific) – MALDI TOF MS/MS	Tatsukawa et al., 2017
Mouse Kidney	Kidney fibrosis	Incorporation of biotinylated glutamine donor K5 (TG1 specific) and T26 (TG2 specific) – MALDI TOF MS/MS	Tatsukawa et al., 2018
	Normal	Incorporation of biotinylated glutamine donor T26 (TG2 specific) – LC MS/MS	Ito et al., 2018
Mouse and human brain	CTR mice, human HD	Incorporation of biotinylated amine donor BPNH2 and amine acceptor A25 peptides – MALDI TOF MS/MS	André et al., 2017

In the light of the previous findings described in Chapter 4, TG2 substrates in rat embryonic hippocampal neurons were investigated to reveal possible partners that could participate to TG2-mediated alteration of calcium homeostasis. A proteomic approach that our group recently published for the detection of TG2 binding partners in kidney fibrosis was employed (Furini et al., 2018) and adapted for the detection of TG2 transamidation substrates, which has been henceforth named TG2 "transamidome". In order to mimic a neuropathological environment which would enhance TG2 activity, the neurons were incubated with TG2 substrate FITC-cad in the presence of Amyloid β peptide ($A\beta_{1-42}$) alone or in conjunction with TG2 inhibitor ZDON, and this *ex vivo* model of AD was used to study TG2 targets under neurodegenerative conditions.

5.1.1 Aims of this chapter

The general aim of this chapter was the identification of TG2 crosslinking substrates in hippocampal neurons under neurodegenerative-like conditions induced by Aβ. The neuronal proteome under physiological and pathological conditions was also studied, highlighting TG2 activity-dependent changes in protein expression levels. For this chapter, only neurons prepared according to the standard protocol were used.

5.2 Results

5.2.1 Aβ treatment increases TG2 activity *in situ* in neurons

Firstly, a test to investigate whether TG2 activity may change under pathological conditions was performed. To simulate an AD environment *ex vivo*, primary hippocampal neurons were exposed to the synthetic peptide $A\beta_{1-42}$ (4 μM) along with the fluorescent amino substrate FITC-cad (Verderio et al., 1998). This treatment does not affect neurons viability, as the aggregated Aβ used for these experiments (directly dissolved in vehicle DMSO) is known to be less neurotoxic compared to the oligomeric form (Ruiz et al., 2014; Joshi et al., 2014). In untreated neurons, TG2 showed a punctuate pattern distributed along the edges of cell somata and especially in the processes, with a low intensity indicating background activity (**Fig. 5.1**). Conversely, Aβ treatment for 8 hours induced a significant 2.2-fold increase of TG-dependent FITC-Cad crosslinking into endogenous substrates, which increased to 6-fold in the case of 16 hours treatment (**Fig. 5.1**). FITC signal was increased and widely distributed in the treated neurons, nucleus included, losing the punctuate pattern that characterised the control condition (**Fig. 5.1**).

Knowing that Aβ treatment enhanced TG2 crosslinking activity, this *ex vivo* model of AD was used to study TG2 substrates in live neurons under neurodegenerative conditions.

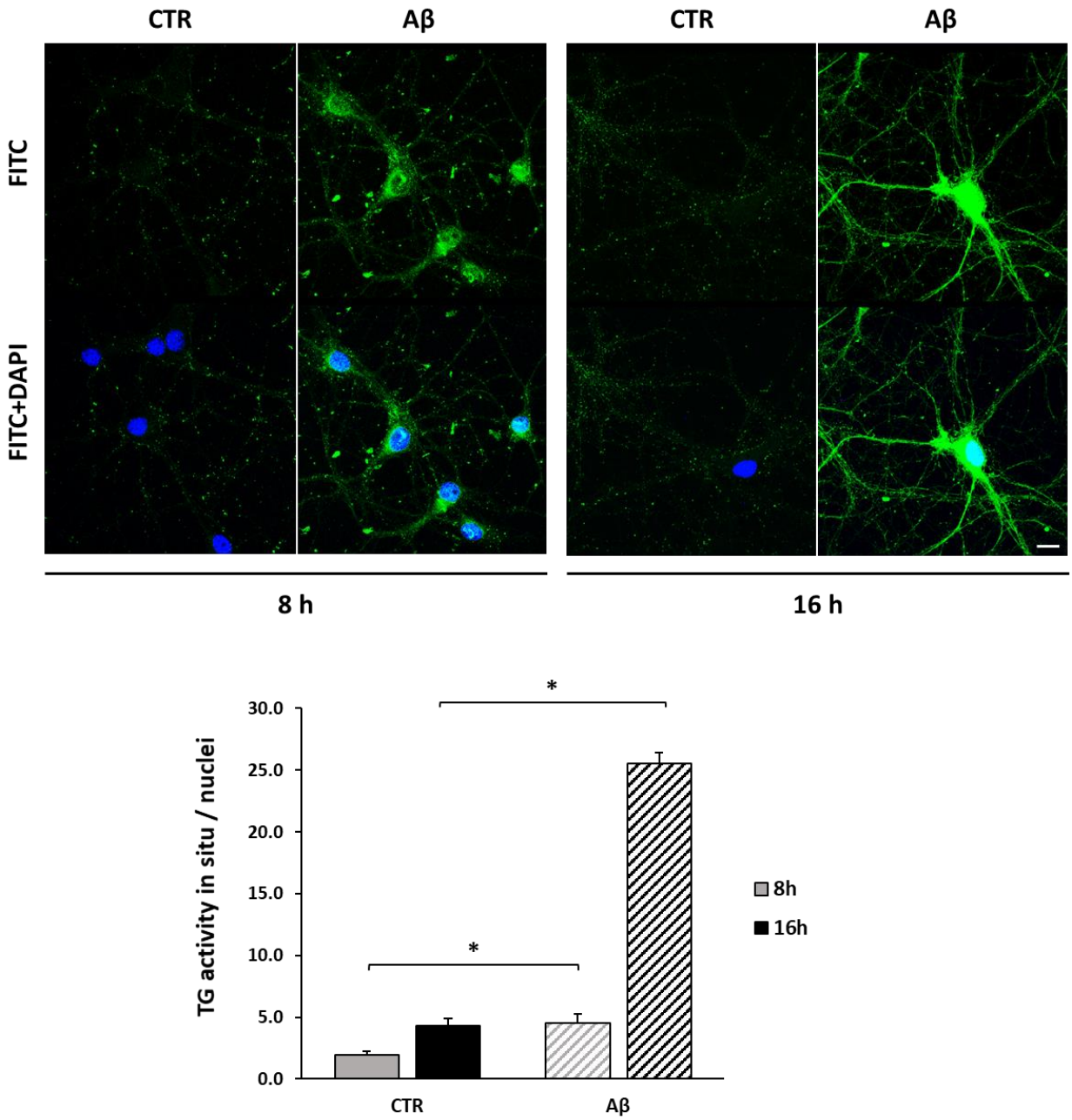

Figure 5.1. Neuronal TG2 activity in situ increases in response to Aβ treatment. *Primary rat embryonic hippocampal neurons at 15 DIV were incubated with FITC-cad (0.4 mM) in the absence or presence of Aβ peptide (4 µM) as described in Method. After 8 or 16 hours incubation, cells were fixed in 90% methanol (v/v in PBS), stained with DAPI and mounted. Coverslips were visualised by laser scanning Leica SP5 confocal microscope using 63X oil immersion objective. Successive serial optical sections (0.5 µm) were recorded over 5 µm planes. Scale bar 10 µm. FITC signal was quantified from maximum projection of z-stack image series and normalised by the number of nuclei. Data is expressed as mean of FITC-cad intensity ± SE (N=5 fields of one slide). Raw intensity values: 8 h, CTR: 2.0±0.3; Aβ: 4.53±0.70; *p≤0.05; 16 h, CTR: 4.3±0.6; Aβ: 25.5±0.9; *p≤0.05.*

5.2.2 Identification of TG2 transamidation targets in neurons exposed to Aβ

In order to identify the range of TG2 molecular targets in hippocampal neurons, under physiological and stress conditions, a quantitative Mass Spectrometry (MS) approach was employed. Differently from already published data (Vyas et al., 2016-2018), FITC-labelled primary amine cadaverine (FITC-cad) was used as lysine-donor (acyl acceptor) as it was shown to be more cell permeable compared to biotin-cad (Verderio et al., 1998). Neurons at 9 DIV were incubated with FITC-Cad (0.4 mM) with or without Aβ peptide (4 µM) and Aβ peptide with TG2 inhibitor ZDON (100 µM) as control for 8 hours (N=3 replicas). This time point was chosen based on preliminary *in situ* visualisation of TG activity to avoid any cell death that may occur after prolonged exposure to Aβ. At this stage, any protein with suitable glutamine-bound γ-carboxamide group would have been modified by transamidation to incorporate the primary amino group of FITC-labelled cadaverine (as illustrated in **Fig. 1.7** in Chapter 1). Total cell lysates were immunoprecipitated (IP) with an anti-fluorescein monoclonal antibody to analyse the FITC-covalently bound proteins, i.e. the TG2 transamidation substrates, collectively referred to as TG2 "transamidome" (as described in Methods chapter 2.2.14.1). The flowchart in **Fig. 5.2** illustrates the experimental approach that was used.

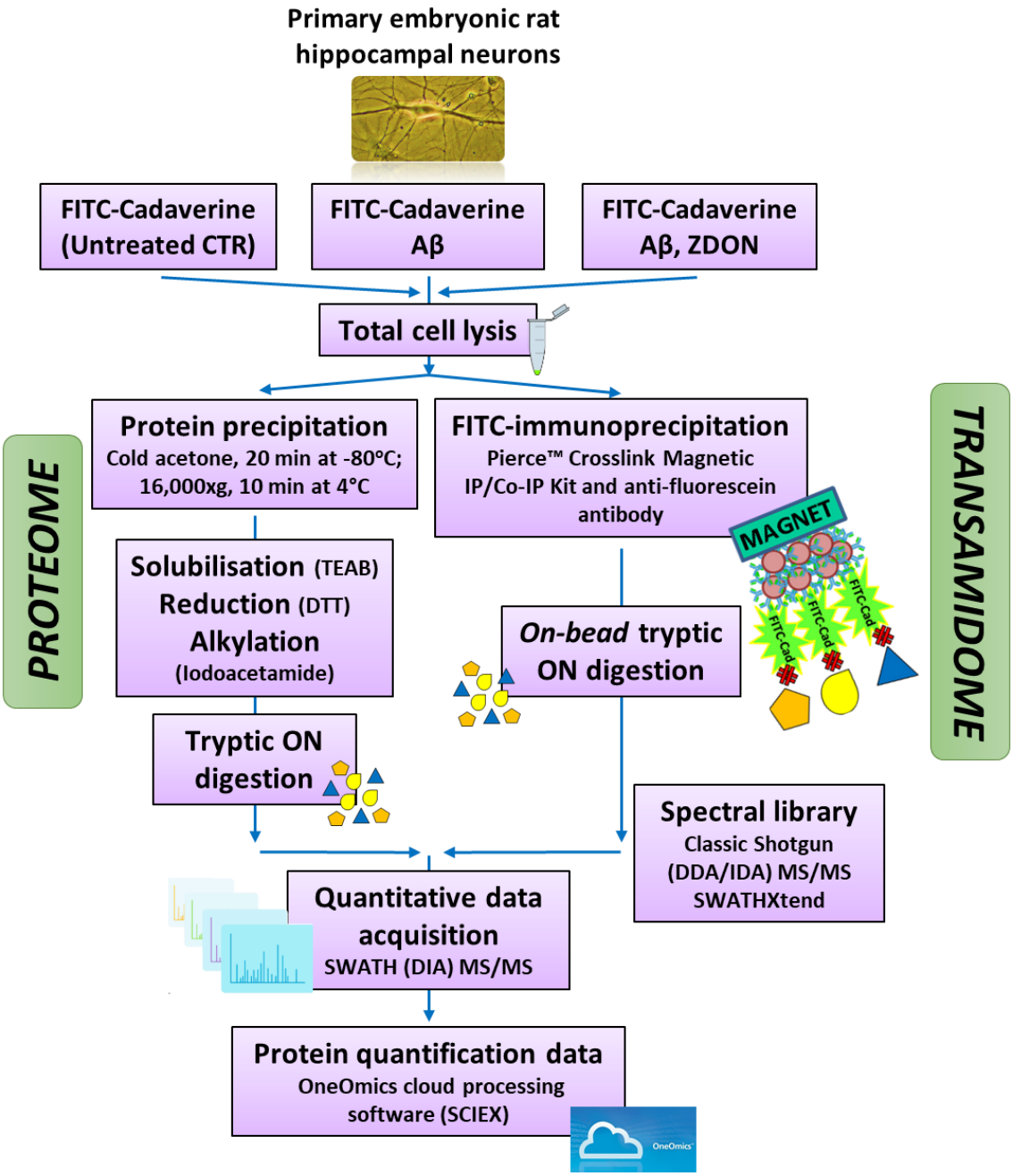

Figure 5.2. Schematic representation of the experimental procedure for the identification of TG2 crosslinking targets in neurons. *Neurons at 9 DIV, obtained from the hippocampi of E18 fetal rats (13 embryos), were incubated 8 hours at 37°C with FITC-Cad (0.4 mM) with or without ZDON (100 µM) and Aβ peptide (4 µM) and lysed in Pierce™ Crosslink Magnetic IP/Co-IP Kit lysis buffer. All conditions were carried out in triplicates (about 0.52x10^6 neurons each). FITC-Cad associated proteins were immunoprecipitated from the total cell lysates (14 µg), using magnetic beads coated with an anti-fluorescein monoclonal antibody. Magnetic beads – associated protein complexes were subjected to "on-bead" trypsin digestion (0.02 mg/ml MS grade trypsin) at 37°C for 14 hours in the presence of 0.01% (w/v) ProteaseMAX™ Surfactant. Magnetics beads were then removed using a magnetic stand,*

trypsin was inactivated by addition of 0.5% TFA and samples were vacuum concentrated to dryness and resuspended in 20 µl of 5% (v/v) acetonitrile/0.1% (v/v) formic acid for IDA/DDA shotgun and quantitative DIA SWATH-MS/MS analysis.

Firstly, all samples were analysed by classic shotgun DDA/IDA MS for the generation of a spectral library (Gillet et al., 2012) (Methods chapter 2.2.14; **Fig. 5.2**). More than 1000 proteins were identified (i.e. 1135 proteins in total), and about 5-fold more proteins were detected in the total lysates (TL) compared to FITC-IP samples. These are listed in **Fig. 5.3**.

Samples	Proteins at 1% FDR	Peptides at 1% FDR	Spectra at 1% FDR
TL_Aβ1	915	5329	8883
TL_Aβ2	790	4570	7171
TL_Aβ3	722	3532	5264
TL_CTR1	831	4512	7114
TL_CTR2	801	4450	7022
TL_CTR3	200	860	1069
TL_Aβ+ZDON1	827	4669	7601
TL_Aβ+ZDON2	869	4855	7552
TL_Aβ+ZDON3	850	5437	8234
FITC-IP_Aβ1	180	774	1338
FITC-IP_Aβ2	150	586	1109
FITC-IP_Aβ3	222	1055	1839
FITC-IP_CTR1	149	629	1092
FITC-IP_CTR2	98	523	1163
FITC-IP_CTR3	255	1181	1964
FITC-IP_Aβ+ZDON1	149	617	1135
FITC-IP_Aβ+ZDON2	139	495	973
FITC-IP_Aβ+ZDON3	108	463	791
Pool of all samples	874	6861	6992

Figure 5.3. Summary of identified proteins by shotgun IDA/DDA. *Spectral library generated by shotgun IDA/DDA MS. Samples were analysed singularly (triplicates), as well as pooled together. Table shows the number of identified proteins, peptides and spectra with a cut-off for false discovery rate (FDR) of 1%. TL_CTR and FITC-IP_CTR denotes untreated neurons, TL_Aβ and FITC-IP_Aβ denotes neurons incubated with Aβ alone, TL_Aβ+ZDON and FITC-IP_Aβ+ZDON denotes neurons incubated with both Aβ and TG2 inhibitor ZDON. Total lysates (TL); FITC-immunoprecipitates (FITC-IP).*

FITC-immunoprecipitates were then analysed by comparative quantitative proteomics (SWATH MS/MS) (Gillet et al., 2012). In order to identify TG2 targets that were transamidated with FITC-cad after Aβ stimulus, fold change (FC) variations were calculated for neurons incubated with Aβ either compared with untreated neurons (CTR) or compared with Aβ+ZDON treated neurons. FC analysis was performed with the SCIEX OneOmics processing software as described in Methods chapter 2.2.14. A total of 877 proteins were identified in the FITC-IP (TG2 transamidome), of which 10 were quantitatively significantly altered in the Aβ-treated sample compared to control with a confidence ≥ 60% (**Table 5.1** and **Fig. 5.4**). A list of proteins significantly altered with confidence above ≥ 50% is included in the supplementary data (Table S.1). Six proteins were more targets of TG2 in the presence of Aβ compared to CTR (positive $\log_2$(FC) and FC>1 values), hence in conditions where TG2 was more active: Transmembrane channel-like protein 5 (TMC5), two ribosomal proteins (RS18 and RS25), β-enolase (ENOB), Keratin type I cytoskeletal 40 (K1C40) and Amyloid β A4 (A4) (**Fig. 5.4**, right). Among these, the increase of Aβ was an expected result, as Aβ was added in high quantity to the neurons to mimic neurodegeneration and it is a known target of TG2 crosslinking (Hartley et al., 2008; Benilova et al., 2012). On the other hand, 5 proteins were significantly reduced (negative $\log_2$(FC) and FC<1 values), hence became less TG2 substrates in Aβ-treated neurons compared to CTR. These were Prenylcysteine oxidase (PCYOX), Synaptobrevin homolog (YKT6), Sorting and assembly machinery component 50 homolog (SAM50), Anionic trypsin-1 (TRY1) and Ig γ-2A chain C region (IGG2A) (**Fig. 5.4**, left). These proteins were more bound to FITC-cad in untreated neurons compared to Aβ, suggesting that they could be better target of TG2 in physiological conditions.

Table 5.1: List of proteins substrates of TG2 upon Aβ exposure compared to untreated controls (CTR), with confidence ≥60%. *Proteins that were more target of TG2 are highlighted in gold (FC>1), while proteins that were less targets of TG2 upon Aβ are highlighted in green (FC<1).*

Aβ/CTR transamidome					
Protein ID			$Log_2(FC)$	FC	Confidence
Q5EGY4	YKT6	Synaptobrevin homolog YKT6	-2.42	0.19	91.3%
P20760	IGG2A	Ig gamma-2A chain C region	-0.45	0.73	83.0%
P62271	RS18	40S ribosomal protein S18	2.11	4.30	80.0%
Q5M7W4	TMC5	Transmembrane channel-like protein 5	1.08	2.11	76.1%
P00762	TRY1	Anionic trypsin-1	-1.02	0.49	74.1%
P15429	ENOB	Beta-enolase	2.01	4.02	73.2%
P62853	RS25	40S ribosomal protein S25	1.26	2.40	69.1%
Q6AXV4	SAM50	Sorting and assembly machinery component 50 homolog	-2.28	0.21	67.6%
Q6IFW2	K1C40	Keratin, type I cytoskeletal 40	3.01	8.04	67.4%
P08592	A4	Amyloid beta A4 protein	3.35	10.18	61.4%
Q99ML5	PCYOX	Prenylcysteine oxidase	-3.32	0.10	61.1%

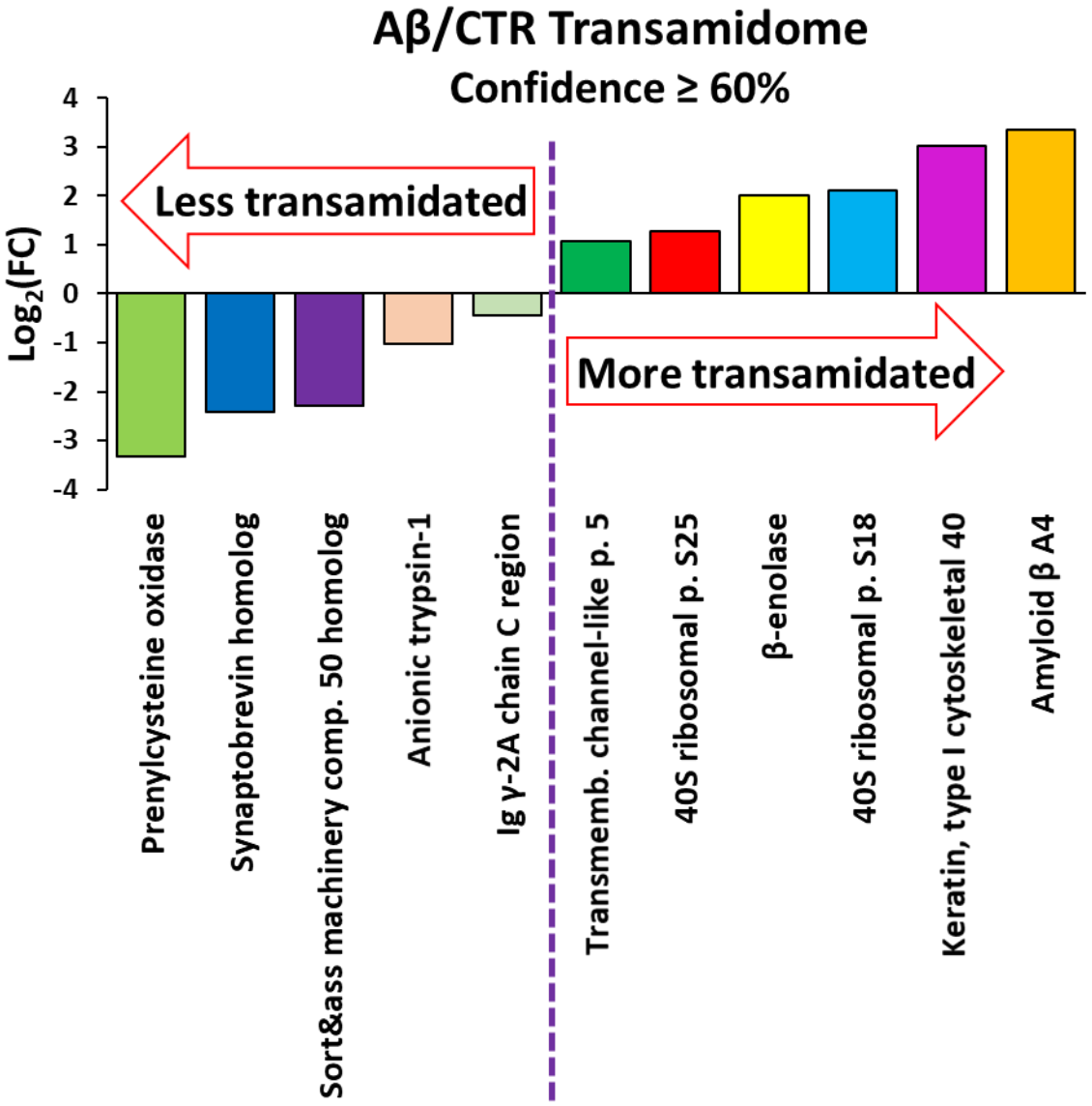

Figure 5.4. Protein targets of TG2 transamidation upon Aβ stimulus in neurons. *Histogram shows proteins target of TG2 transamidation in neurons upon Aβ exposure compared to control, plotted according to increasing log_2(FC) values (N=3 replicas). Data were obtained by quantitative SWATH-MS/MS analysis and expressed as log_2(FC), where negative values represent proteins which were less target of TG2 transamidation, while positive values represent proteins which were increased substrates of TG2 in the presence of Aβ. Only variations with confidence ≥ 60% were included.*

In order to rule out issues with unspecific IP proteins, specific targets of TG2 transamidation were identified by comparing the transamidome of neurons with the transamidome of similarly Aβ-treated cells but in the presence of TG2 inhibitor ZDON (Aβ+ZDON). Proteins showing positive log_2(FC) values (FC>1), indicating that they were less bound to FITC-cad in the presence of Aβ+ZDON compared to Aβ alone, would be considered highly specific substrates of TG2. A total of 8 proteins were found to be specific transamidation targets with a confidence ≥ 60% (gold rows in **Table 5.2,** and **Fig. 5.5**, right). A list of proteins significantly altered with confidence above ≥ 50% is included in the supplementary data (Table S.2).

Table 5.2: List of proteins substrates of TG2 upon Aβ exposure compared to Aβ+ZDON, with confidence ≥60%. *Proteins that are highly specific targets of TG2 are highlighted in gold (FC>1), while proteins that are not specific substrates of TG2 are highlighted in green (FC<1).*

Aβ/Aβ+ZDON transamidome					
Protein ID			Log_2(FC)	FC	Confidence
Q07647	GTR3	Solute carrier family 2, facilitated glucose transporter member 3	-4.85	0.03	89.2%
Q62745	CD81	CD81 antigen	3.80	13.96	88.1%
P62864	RS30	40S ribosomal protein S30	1.35	2.55	84.3%
P62271	RS18	40S ribosomal protein S18	1.27	2.42	78.1%
P62853	RS25	40S ribosomal protein S25	1.06	2.09	75.2%
P20760	IGG2A	Ig gamma-2A chain C region	-0.46	0.73	75.0%
P15429	ENOB	Beta-enolase	2.87	7.29	72.0%
Q6IFW6	K1C10	Keratin, type I cyt keletal 10	-1.16	0.45	71.1%
P97612	FAAH1	Fatty-acid amide hydrolase 1	2.46	5.49	70.6%
Q9WU34	SEPT3	Septin-3	-1.59	0.33	67.8%
Q9JI92	SDCB1	Syntenin-1	-1.92	0.26	65.7%
P41562	IDHC	Isocitrate dehydrogenase NADP cytoplasmic	-4.27	0.05	65.3%
Q01728	NAC1	Sodium/calcium exchanger 1	-0.68	0.62	64.2%
P11506	AT2B2	Plasma membrane calcium-transporting ATPase 2	2.91	7.53	61.8%
P13471	RS14	40S ribosomal protein S14	0.88	1.85	61.2%
Q4V8B7	HSDL1	Inactive hydroxysteroid dehydrogenase-like protein 1	-4.53	0.04	60.2%

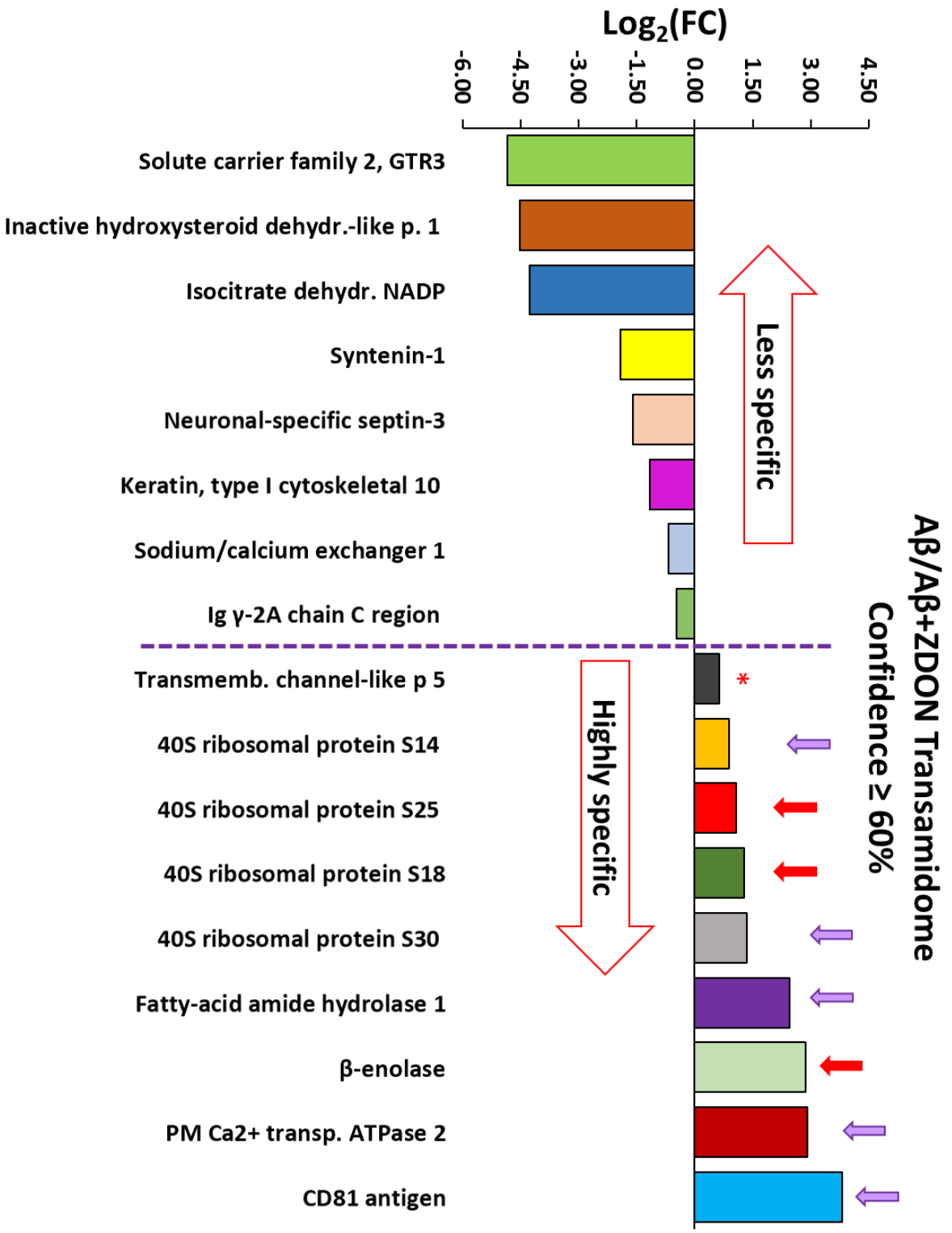

Figure 5.5. Specific protein targets of TG2 transamidation in neurons. *Histogram shows proteins substrates of TG2 transamidation in neurons upon Aβ exposure compared to Aβ+ZDON, plotted according to increasing log_2(FC) values (N=3 replicas). Data were obtained by quantitative SWATH-MS/MS analysis and is expressed as log_2(FC), where positive values represent proteins which were highly specific targets of TG2, while negative values represent proteins which were less specific target of TG2 transamidation. Only variations with confidence ≥ 60% were included, apart from TMC5 (* confidence = 44%).*

Red arrows highlight the 3 proteins that were confirmed as specific substrates among the ones identified in the Aβ/CTR transamidome comparison. Purple arrows highlight the new highly specific substrates which emerged from the Aβ/Aβ+ZDON transamidome comparison.

Only 3 out of the 6 proteins that had been previously identified as increased targets of TG2 upon Aβ stimulus (**Fig. 5.4, right**), were confirmed here as specific substrates, namely ENOB and ribosomal proteins RS18 and RS25 (**Fig. 5.5**, red arrows). ENOB is involved in the glycolysis process, suggesting a possible effect of TG2 modification on metabolism in the stressed neurons. Ribosomal proteins have been previously identified as TGs substrates, especially RS19 which was shown to be oligomerised by Factor XIIIa crosslinking and act as a chemoattractant for macrophages and monocyte by interacting with the C5a receptor (Nishiura et al. 1996; Chen et al., 2013-2014). TMC5, which is a putative ion channel (Keresztes et al., 2003), was identified as a specific substrate but with a lower confidence (44%) (**Fig. 5.5**, red asterisk). Despite this, it remains an interesting substrate, particularly in the light of findings described in Chapter 4, as it might represent a previously unknown target of TG2 able to affect ionic homeostasis in neurons under stress conditions. Other proteins emerged from this analysis as specific targets, i.e. CD81 antigen, Fatty-acid amide hydrolase 1 (FAAH1), Plasma membrane Ca^{2+} transporting ATPase 2 (AT2B2) and ribosomal proteins RS14 and RS30 (**Fig. 5.5**, purple arrows). CD81 is a member of the tetraspanin family and a cell-surface glycoprotein; it mediates signal transduction events and it is used as a EVs marker. Notably, CD81 was not an increased substrate in the Aβ/CTR transamidome comparison (FC: 0.4; confidence: 47%), nevertheless it is a specific target of TG2 crosslinking in neurons independently from Aβ. FAAH1 hydrolyses bioactive fatty acid amides (e.g. endogenous cannabinoid, oleamide, anandamide), thereby terminating their signalling functions. FAAH1 was also increased in the Aβ versus CTR transamidome, but at lower confidence (FC: 12.6; confidence: 53.3%; Supplementary table S.1). AT2B2 (also called PMCA2) is an ionic pump which pushes calcium ions outside from the cell going against concentration gradients, and as such plays an important role in maintaining calcium homeostasis. Similarly to FAAH1 and ENOB, AT2B2 was increased in the Aβ/CTR transamidome comparison, although not significantly (FC: 6.5; confidence: 38%). This

pump is interesting as it could be another element participating to TG2-dependent increase of neuronal calcium $[Ca^{2+}]_i$. On the other hand, 8 proteins were identified which had not reduced their incorporation of FITC-cad by TG2 inhibition (negative log_2(FC) values and FC<1), so they were not regarded as specific substrates (green rows in **Table 5.2** and **Fig. 5.5**, left). Among these, the Na^+/Ca^{2+} exchanger (NAC1 or NCX1) was particularly intriguing, as it was previously shown that TG2 is able to mediate calcium entrance in neurons through NCX (Chapter 4, **Fig. 4.13**). The fact that specific TG2 inactivation did not affect NCX transamidation to FITC-cad may indicate that the crosslinking could be also due to another transglutaminase. It also cannot be ruled out that TG2 was not completely inhibited by ZDON under the experimental conditions.

In conclusion, TG2 specific substrates were identified in neurons exposed to Aβ, and among these TMC5 and AT2B2 stood out as ionic channels and transporters possibly involved in TG2-dependent alteration of calcium homeostasis. Other substrates emerged, such as CD81, suggesting an activity of TG2 PTM of surface vesicular proteins, and Aβ, which was already known as a TG2 target. Finally, a number of ribosomal proteins emerged as clear substrates of TG2 transamidation, together with other proteins involved in cell metabolism.

5.2.3 Proteome of neurons exposed to Aβ: comparison with TG2 Transamidome

At this stage it was interesting to evaluate whether the substrates of TG2 PTM in neurons exposed to Aβ were also affected in expression by the treatment. In the same way it was interesting to considerate if the ZDON treatment employed to inhibit TG2 was able per se to change the proteome of Aβ-treated cells. Moreover, to date there is no report profiling the proteome of hippocampal neurons modelling AD pathology *ex vivo* by Aβ exposure.

In order to investigate changes in protein expression due to Aβ treatment, the same cell lysates which had been used for FITC-IP were analysed by SWATH-MS/MS as described in the previous section. Specifically, the lysates were divided into two parts, one for FITC-IP and one for evaluation of the total proteome, and then processed as described in Methods chapter 2.2.14.2. The whole hippocampal neurons proteome consisted of about 1100 proteins in total, of which 24 were significantly altered in the Aβ proteome compared to CTR (**Table 5.3** and **Fig. 5.6**), with a confidence ≥ 70%. Specifically, 17 overexpressed and 7

downregulated proteins were discovered (**Fig. 5.6**). The complete list of proteins changed in the Aβ/CTR proteome with a confidence above ≥ 50% is included in the supplementary data (**Table S.3**).

Among the proteins that had been identified as TG2 substrates in the previous section, only CD81 and Aβ were significantly changed in the Aβ/CTR proteome. Specifically, CD81 was downregulated (FC: 0.5, confidence: 98%), suggesting that TG2 interaction with CD81 was highly specific, while Aβ was upregulated (FC: 45.4, confidence: 73%), as expected, in the presence of treatment (**Fig. 5.6**, red arrows). A cluster of Aβ upregulated mitochondrial proteins emerged (NAKD2, PRDX3, MDHM, NDUV2, C1QBP and TIM13), which suggested an Aβ-driven dysregulation of mitochondrial functions, which is a largely reported hallmark of neurodegeneration (Beal, 1998; Markesbery, 1999) (**Fig. 5.6**, red asterisks). Among the downmodulated proteins, a cytoskeleton-associated cluster was identified (TAGL, K1C10, K2C1 and K2C1B) (**Fig. 5.6**, red triangles).

Table 5.3: List of proteins significantly changed upon Aβ exposure compared to CTR, with confidence ≥70%. *Proteins that were increased by Aβ compared to CTR are highlighted in gold (FC>1), while proteins that were decreased upon Aβ are highlighted in green (FC<1).*

Aβ/CTR proteome					
Protein ID			Log_2(FC)	FC	Confidence
Q62745	CD81	CD81 antigen	-1.102	0.466	0.979
Q4KM98	MFF	Mitochondrial fission factor	-3.883	0.068	0.933
P38983	RSSA	40S ribosomal protein SA	0.656	1.576	0.847
O35796	C1QBP	Complement component 1 Q subcomponent-binding protein, mitochondrial	1.250	2.378	0.843
P04636	MDHM	Malate dehydrogenase, mitochondrial	0.843	1.793	0.840
Q6IFW6	K1C10	Keratin, type I cytoskeletal 10	-1.899	0.268	0.831
Q5U2U2	CRKL	Crk-like protein	4.707	26.125	0.827
P31044	PEBP1	Phosphatidylethanolamine-binding protein 1	0.736	1.665	0.790
Q6IMF3	K2C1	Keratin, type II cytoskeletal 1	-2.280	0.206	0.788
P10960	SAP	Sulfated glycoprotein 1	0.597	1.512	0.776
P19234	NDUV2	NADH dehydrogenase ubiquinone flavoprotein 2, mitochondrial	0.653	1.572	0.771
P63331	PP2AA	Serine/threonine-protein phosphatase 2A catalytic subunit alpha isoform	0.752	1.684	0.761
P62076	TIM13	Mitochondrial import inner membrane translocase subunit Tim13	0.488	1.403	0.752
P47868	SCG3	Secretogranin-3	1.670	3.181	0.741
Q6IG01	K2C1B	Keratin, type II cytoskeletal 1b	-3.862	0.069	0.738
P08592	A4	Amyloid beta A4 protein	5.505	45.398	0.733
P35704	PRDX2	Peroxiredoxin-2	0.670	1.591	0.728
Q5XIG4	OCAD1	OCIA domain-containing protein 1	1.707	3.265	0.724
Q1HCL7	NAKD2	NAD kinase 2, mitochondrial	1.145	2.212	0.720
P07335	KCRB	Creatine kinase B-type	0.638	1.557	0.720
Q07936	ANXA2	Annexin A2	-0.825	0.564	0.718
Q9Z0V6	PRDX3	Thioredoxin-dependent peroxide reductase, mitochondrial	1.105	2.151	0.711
Q923W4	HDGR3	Hepatoma-derived growth factor-related protein 3	2.696	6.481	0.705
P31232	TAGL	Transgelin	-0.958	0.515	0.704

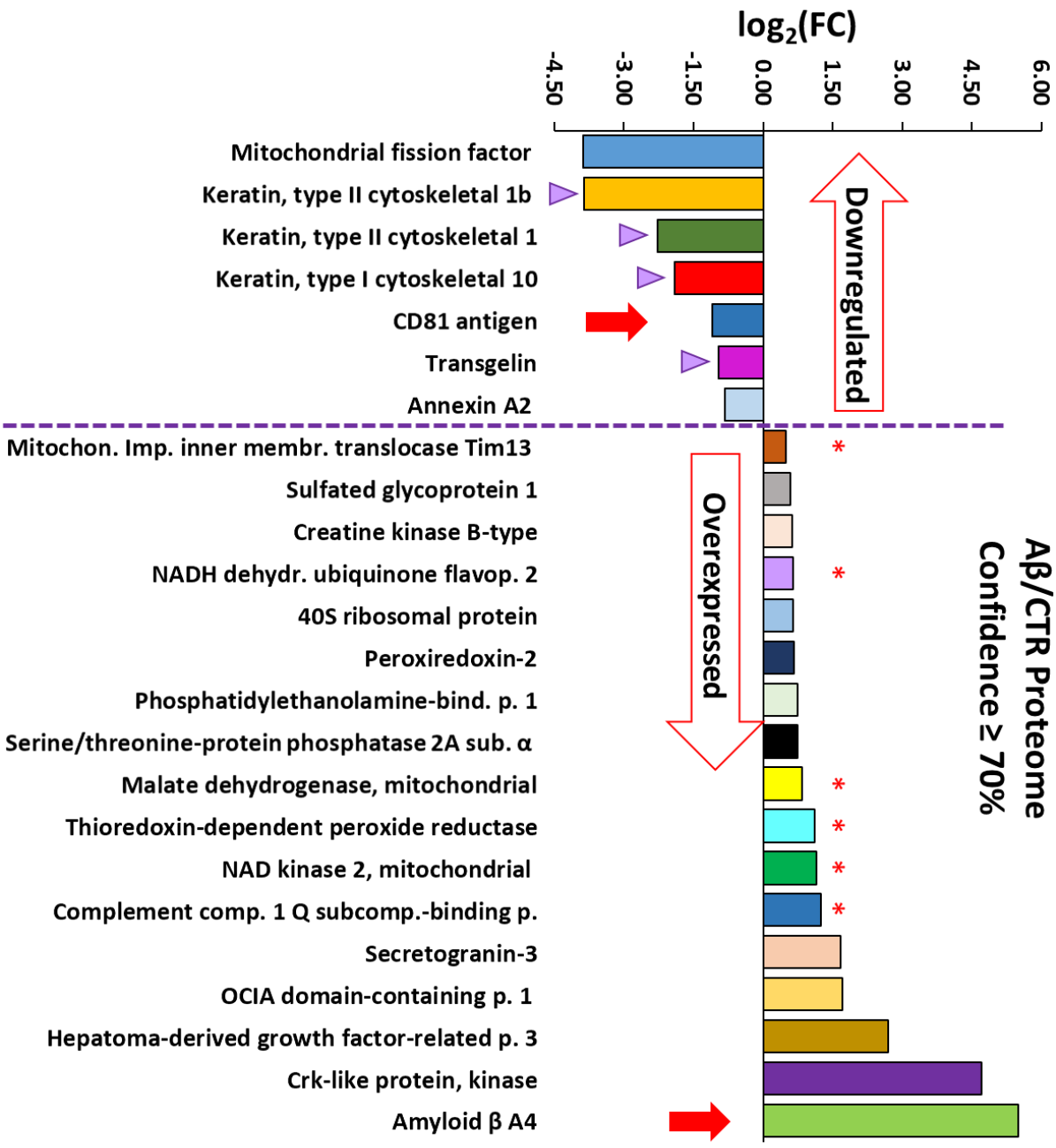

Figure 5.6. Altered proteins in the proteome of Aβ treated neurons compared to untreated CTR. *Histogram shows proteins significantly changed in neurons upon Aβ exposure compared to CTR, plotted according to increasing log_2(FC) values (N=3 replicas). Data were obtained by quantitative SWATH-MS/MS analysis and expressed as log_2(FC), where negative values represent proteins which were downregulated, and positive values proteins which were overexpressed following Aβ treatment. Only variations with confidence ≥ 70% were included. Red arrows highlight the substrates which were previously identified in the TG2 transamidome. Red asterisks underline an upregulated mitochondrial cluster, and purple triangles highlight a downregulated cytoskeleton associated cluster.*

The PANTHER online classification system was used to characterise the significantly changed proteins according to their "Protein class", "Molecular function", "Biological Process" and "Cellular Component" (Panther GO Slim features) (**Table 5.4A** and **A continued** for the Aβ upregulated and **Table 5.4B** for the Aβ downregulated proteins). In terms of "Molecular function" GO classification of the pool of Aβ upregulated proteins (**Table 5.4A** and **A cont.**), the most represented category was "Ion binding" (GO:0043167), which included 9 proteins among which serine/threonine-protein phosphatase 2A catalytic subunit α isoform (PP2AA), mitochondrial import inner membrane translocase subunit Tim13 (TIM13) and mitochondrial NADH dehydrogenase [ubiquinone] flavoprotein 2 (NDUV2) (**Fig. 5.7**, red square). The other top functional categories were "Catalytic activity" (GO:0003824) with 8 proteins such as Peroxiredoxin-2 (Prdx2), followed by "Enzyme binding" (GO: 0019899) with 7 proteins, such as Aβ (A4) and mitochondrial complement component 1 Q subcomponent-binding protein (C1QBP) (**Fig. 5.7**).

Table 5.4: Gene Ontology (GO) annotation terms and PANTHER functional analysis of Aβ/CTR proteome. *Functional analysis was performed by PANTHER (http://www.pantherdb.org) using the annotation terms ontologies for GO-slim "Biological Process", "Molecular Function", "Cellular Component" and "Protein Class". When the GO-slim analysis didn't include any term, a more comprehensive analysis was performed (GO database complete feature), for which corresponding GO codes were not provided.* ***A)*** *Analysis of upregulated proteins.* ***B)*** *Analysis of downregulated proteins.*

A

Upregulated proteins (70% confidence)					
Mapped IDs	**Gene Name; Gene Symbol**	**PANTHER Protein Class**	**PANTHER GO-Slim Molecular Function**	**PANTHER GO-Slim Biological Process**	**PANTHER GO-Slim Cellular Component**
SAP	Prosaposin; Psap		adenylate cyclase activity(GO:0004016); enzyme activator activity (GO:0008047); receptor binding(GO:0005102)	G-protein coupled receptor signaling pathway (GO:0007186); biosynthetic process (GO:0009058); cell differentiation (GO:0030154); cyclic nucleotide metabolic process (GO:0009187); growth (GO:0040007); intracellular signal transduction (GO:0035556); lipid metabolic process (GO:0006629); nitrogen compound metabolic process (GO:0006807); regulation of nucleobase-containing compound metabolic process (GO:0019219); regulation of phosphate metabolic process (GO:0019220); reproduction (GO:0000003); response to stimulus (GO:0050896); single-multicellular organism process (GO:0044707); system development (GO:0048731)	cytoplasm (GO:0005737); extracellular space (GO:0005615); lysosome (GO:0005764); membrane (GO:0016020); vacuole (GO:0005773)
MDHM	Malate dehydrogenase, mitochondrial; Mdh2	dehydrogenase (PC00092)	oxidoreductase activity(GO:0016491)	carbohydrate metabolic process (GO:0005975); generation of precursor metabolites and energy (GO:0006091); tricarboxylic acid cycle (GO:0006099)	cytoplasm (GO:0005737); mitochondrial matrix membrane
SCG3	Secretogranin-3; Scg3	peptide hormone (PC00179)	Protein binding	protein localization to secretory granule	secretory granule membrane; cytoplasmic vesicle
PP2AA	Serine/threonine-protein phosphatase 2A catalytic subunit alpha isoform; Ppp2ca	calcium-binding protein(PC00060); protein phosphatase (PC00195)	calcium ion binding (GO:0005509); phosphoprotein phosphatase activity (GO:0004721)	cell cycle (GO:0007049); glycogen metabolic process (GO:0005977); mRNA processing (GO:0006397); protein phosphorylation (GO:0006468); regulation of carbohydrate metabolic process (GO:0006109); regulation of nucleobase-containing compound metabolic process (GO:0019219); response to stress (GO:0006950); transcription from RNA polymerase II promoter (GO:0006366)	centromeric region; nucleus; cytoplasm (GO:0005737); postsynaptic density membrane raft; synapse
NDUV2	NADH dehydrogenase [ubiquinone] flavoprotein 2, mitochondrial; Ndufv2	dehydrogenase (PC00092); reductase (PC00198)	oxidoreductase activity (GO:0016491)	cellular process (GO:0009987); respiratory electron transport chain (GO:0022904)	plasma membrane (GO:0005886); protein complex (GO:0043234)
KCRB	Creatine kinase B-type; Ckb	amino acid kinase (PC00045)	amino acid kinase activity (GO:0019202)	brain development; phosphorylation; cellular chloride ion homeostasis; phosphocreatine biosynthetic process	extracellular space; nucleus; cytoplasm (GO:0005737); dendrite; neuronal cell body

A continued

Upregulated proteins (70% confidence)					
Mapped IDs	**Gene Name; Gene Symbol**	**PANTHER Protein Class**	**PANTHER GO-Slim Molecular Function**	**PANTHER GO-Slim Biological Process**	**PANTHER GO-Slim Cellular Component**
C1QBP	Complement component 1 Q subcomponent-binding protein, mitochondrial; C1qbp		mRNA binding; protein kinase C binding; hyaluronic acid binding; translation activator activity; adrenergic receptor binding; mitochondrial ribosome binding	negative regulation of transcription; positive regulator of apoptotic process; immune response (negative regulation of IFN γ and IL-12); complement activation; positive regulation of protein kinase B signaling; positive regulation of dendritic cell chemotaxis	nucleus; cytoplasm; mitochondrion; plasma membrane; presynaptic active zone; GABA-ergic synapse
TIM13	Mitochondrial import inner membrane translocase subunit Tim13; Timm13		metal ion binding	protein targeting (GO:0006605); protein insertion into mitochondrial inner membrane; chaperone-mediated protein transport	mitochondrion
PEBP1	Phosphatidylethanolamine-binding protein 1; Pebp1	protease inhibitor	serine-type endopeptidase inhibitor activity; ATP binding receptor serine/threonine kinase binding	regulation of neurotransmitter levels; response to oxidative stress; response to toxic substance; hippocampus development; negative regulation of MAPK cascade; response to calcium ion	cytoplasm (GO:0005737)
PRDX2	Peroxiredoxin-2; Prdx2	peroxidase(PC00180)	oxidoreductase activity (GO:0016491); peroxidase activity (GO:0004601)	response to oxidative stress; removal of superoxide radicals; response to lipopolysaccharide; negative regulation of neuron apoptotic process	cytosol (GO:0005829)
NAKD2	NAD kinase 2, mitochondrial; Nadk2		NAD+ kinase activity; ATP binding	NADP biosynthetic process	mitochondrion
RSSA	40S ribosomal protein SA; Rpsa		structural constituent of ribosome (GO:0003735)	RNA localization (GO:0006403); biosynthetic process (GO:0009058); cellular component biogenesis (GO:0044085); cellular process (GO:0009987); nitrogen compound metabolic process (GO:0006807); nuclear transport (GO:0051169); nucleobase-containing compound transport (GO:0015931); organelle organization (GO:0006996); rRNA metabolic process (GO:0016072); translation (GO:0006412)	cytosol (GO:0005829); organelle (GO:0043226); ribosome (GO:0005840)

A continued

Upregulated proteins (70% confidence)					
Mapped IDs	**Gene Name; Gene Symbol**	**PANTHER Protein Class**	**PANTHER GO-Slim Molecular Function**	**PANTHER GO-Slim Biological Process**	**PANTHER GO-Slim Cellular Component**
RSSA	40S ribosomal protein SA; Rpsa		structural constituent of ribosome (GO:0003735)	RNA localization (GO:0006403); biosynthetic process (GO:0009058); cellular component biogenesis (GO:0044085); cellular process (GO:0009987); nitrogen compound metabolic process (GO:0006807); nuclear transport (GO:0051169); nucleobase-containing compound transport (GO:0015931); organelle organization (GO:0006996); rRNA metabolic process (GO:0016072); translation (GO:0006412)	cytosol (GO:0005829); organelle (GO:0043226); ribosome (GO:0005840)
HDGR3	Hepatoma-derived growth factor-related protein 3; Hdgfrp3	growth factor (PC00112); transcription cofactor (PC00217)	growth factor activity (GO:0008083); sequence-specific DNA binding transcription factor activity (GO:0003700); transcription cofactor activity (GO:0003712)	cell-cell signaling (GO:0007267); regulation of transcription from RNA polymerase II promoter (GO:0006357); signal transduction (GO:0007165); neuron projection development; microtubule polymerization	nucleus; cytoplasm
CRKL	Crk-like protein; Crkl		phosphotyrosine residue binding; identical protein binding	cellular process (GO:0009987); neuron and glia migration; synapse assembly; dendrite development; brain development; retinoic acid receptor signaling pathway	cytosol (GO:0005829); neuromuscular junction; extrinsic component of postsynaptic membrane
PRDX3	Thioredoxin-dependent peroxide reductase, mitochondrial; Prdx3	peroxidase (PC00180)	oxidoreductase activity (GO:0016491); peroxidase activity (GO:0004601)	response to oxidative stress; mitochondrion organization; response to lipopolysaccharide; negative regulation of kinase activity; negative regulation of apoptotic process; regulation of mitochondrial membrane potential; cellular oxidant detoxification	cytosol (GO:0005829); mitochondrion
A4	Amyloid beta A4 protein; App	signalling molecule (PC00207)	receptor binding(GO:0005102)	cellular process (GO:0009987); intracellular protein transport (GO:0006886)	
OCAD1	OCIA domain-containing protein 1; Ociad1	major histocompatibility complex antigen (PC00149)		regulation of stem cell differentiation	endosome

B

Downregulated proteins (70% confidence)					
Mapped IDs	**Gene Name; Gene Symbol**	**PANTHER Protein Class**	**PANTHER GO-Slim Molecular Function**	**PANTHER GO-Slim Biological Process**	**PANTHER GO-Slim Cellular Component**
TAGL	Transgelin; Tagln	non-motor actin binding protein (PC00165)	actin binding (GO:0003779); structural constituent of cytoskeleton (GO:0005200)	muscle contraction (GO:0006936)	actin cytoskeleton (GO:0015629); intracellular (GO:0005622)
K1C10	Keratin, type I cytoskeletal 10; Krt10	intermediate filament (PC00129); structural protein (PC00211)	structural constituent of cytoskeleton (GO:0005200)	cellular component morphogenesis (GO:0032989); cellular process (GO:0009987)	intermediate filament cytoskeleton (GO:0045111); intracellular (GO:0005622)
K2C1	Keratin, type II cytoskeletal 1; Krt1	intermediate filament (PC00129); structural protein (PC00211)	structural constituent of cytoskeleton (GO:0005200)	cellular component morphogenesis (GO:0032989); cellular process (GO:0009987)	intermediate filament cytoskeleton (GO:0045111); intracellular(GO:0005622)
MFF	Mitochondrial fission factor; Mff		protein binding, GTPase binding	mitochondrial fission during apostosis; release of cytochrome c from mitochondria; regulation of mitochondrion organization; positive regulation of synaptic vesicle endocytosis	mitochondrion
ANXA2	Annexin A2; Anxa2		cytoskeletal protein binding; structural constituent of epidermis	fatty acid metabolic process (GO:0006631); keratinocyte development cellular response to calcium ion	ubiquitous
K2C1B	Keratin, type II cytoskeletal 1b; Krt77	intermediate filament (PC00129); structural protein (PC00211)	structural constituent of cytoskeleton (GO:0005200)	cellular component morphogenesis (GO:0032989); cellular process (GO:0009987)	intermediate filament cytoskeleton (GO:0045111); intracellular(GO:0005622)
CD81	CD81 antigen; Cd81	cell adhesion molecule (PC00069); membrane-bound signaling molecule (PC00152); receptor (PC00197)	integrin binding; cholesterol binding; MHC class II protein binding	cell surface receptor signaling pathway (GO:0007166); regulation of biological process (GO:0050789); response to stimulus (GO:0050896); positive regulation of inflammatory response to antigenic stimulus; receptor internalization; regulation of macrophage migration	integral to membrane (GO:0016021); plasma membrane (GO:0005886)

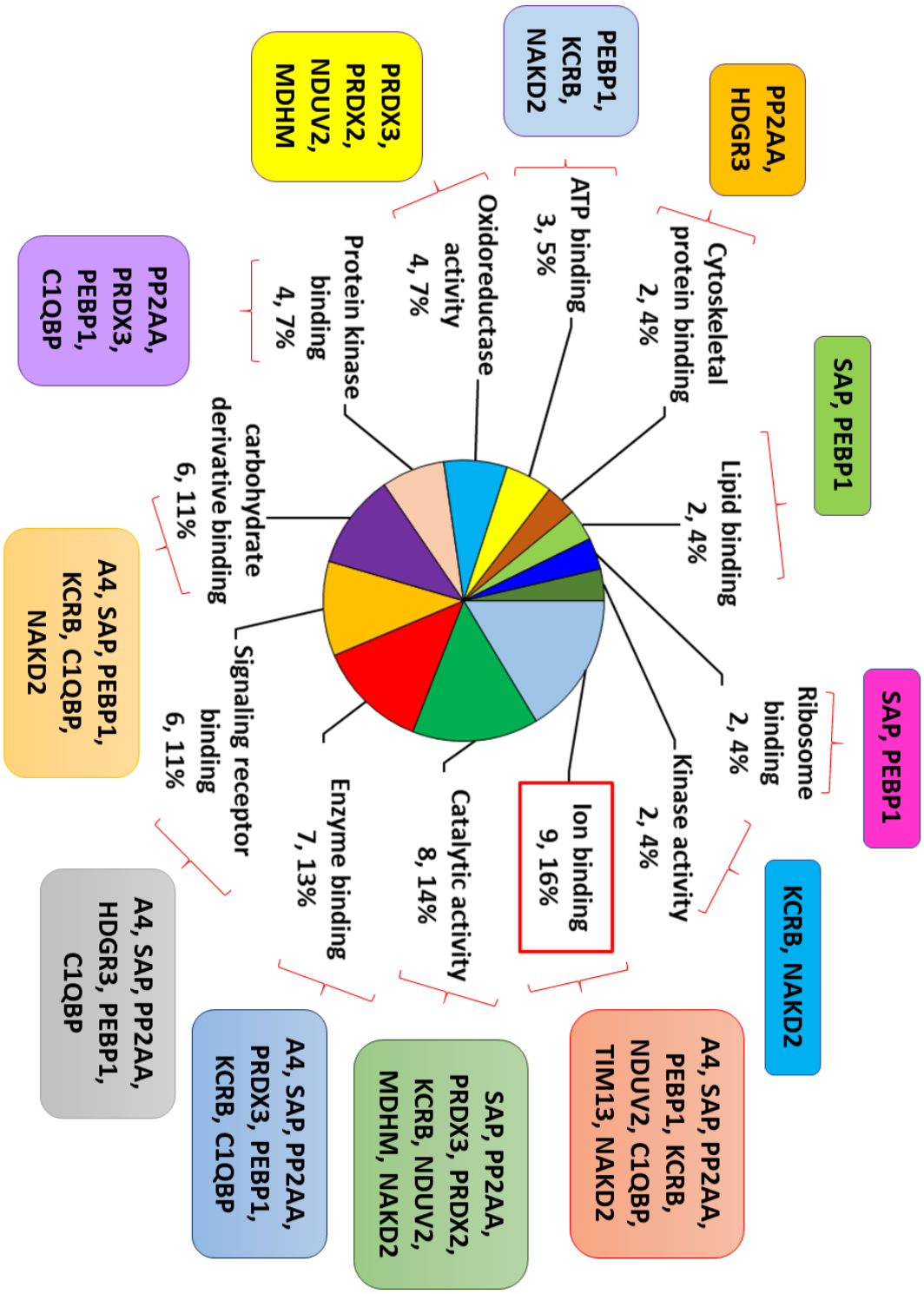

Figure 5.7. PANTHER GO-Slim Molecular Function of proteins upregulated in Aβ vs CTR proteome. *Functional analysis of was performed by PANTHER (http://www.pantherdb.org) using the annotation terms ontologies for GO-slim Molecular Function. A selection of the more relevant molecular functions was made from a total of 349 identified functions. Labels show in this order: Category accession name, number of proteins in that category and % of proteins belonging to the category over the total number of category hits. The red square highlights the most represented category.*

In order to identify the proteins which levels were specifically affected by TG2 activity, the Aβ proteome was compared with that of cells treated with Aβ in the presence of TG2 inhibitor ZDON (Aβ+ZDON). Considering a confidence ≥ 70%, 14 proteins emerged as significantly changed (**Table 5.5** and **Fig. 5.8**). The complete list of proteins changed in the Aβ/Aβ+ZDON proteome with a confidence above ≥ 50% is included in the supplementary data (**Table S.4**). Eight proteins had a significant lower expression when neurons were cultured in the presence of ZDON, which is denoted by FC>1 and positive log_2FC values (**Fig. 5.8,** right). These were glia maturation factor β (GMFB), which acts as a brain growth factor and is known to induce neuronal and glial differentiation (Lim et al., 1989), and protein CutA (CUTA), a copper-related protein believed to be a putative membrane anchor for acetylcholinesterase and that has been shown to interact with BACE1 and inhibit generation of Aβ peptides (Hou et al., 2015). Other proteins which were decreased by TG2 inhibition are involved in neuronal growth and migration: CRKL, an adapter protein participating in neurons migration and synapses formation (Chen et al., 2004; Hallock et al., 2010); GIT1, also reported to be involved in neuritogenesis (Turner et al., 2001; Li et al., 2016); GBLP (also called Rack1), a multifunctional ribosomal scaffolding protein, which also plays a role in axon growth (Kershner and Welshhans, 2017). The decrease of neurotrophic proteins in response to TG2 inactivation suggest a possible neuroprotective role for active TG2 in neurons. Ribosomal proteins were also included (RS7 and RS24), as well as pro-apoptotic factor BAX, which had been previously shown to be a target of TG2 transamidation (Rodolfo et al., 2004). Among the proteins that were overexpressed in the presence of ZDON (meaning that they are usually repressed by active TG2), which is denoted by FC<1 and negative log_2FC values (**Fig. 5.8,** left), a cluster of cytoskeleton-associated proteins was found, including K1C10, which had been previously shown to be reduced in the FITC-IP Aβ/Aβ-ZDON sample too (**Fig. 5.5**). ZW10 interactor (ZWINT), a kinetochore protein, was decreased, as well as brain acid soluble protein 1 (BASP1), which is a calmodulin-binding protein localised at pre-synaptic membrane rafts and has been recently shown to be involved in membrane dynamics (Maekawa et al., 1993; Ueno et al., 2018).

Table 5.5: List of proteins significantly changed upon Aβ exposure compared to Aβ+ZDON, with confidence ≥70%. *Proteins that were decreased in response to TG2 inhibition by ZDON (meaning that they are induced by TG2 activity in physiological conditions) are highlighted in gold (FC>1), while proteins that were increased upon ZDON addition (meaning that they are inhibited by TG2 activity in physiological conditions) are highlighted in green (FC<1).*

Aβ/Aβ+ZDON proteome					
Protein ID			Log_2(FC)	FC	Confidence
Q6MGD0	CUTA	Protein CutA	2.626	6.174	0.868
Q6IG01	K2C1B	Keratin, type II cytoskeletal 1b	-3.779	0.073	0.835
Q63690	BAX	Apoptosis regulator BAX	3.273	9.668	0.811
Q63228	GMFB	Glia maturation factor beta	2.083	4.236	0.803
Q6IMF3	K2C1	Keratin, type II cytoskeletal 1	-1.659	0.317	0.792
Q6IFW6	K1C10	Keratin, type I cytoskeletal 10	-1.415	0.375	0.789
P62083	RS7	40S ribosomal protein S7	0.543	1.457	0.786
P62850	RS24	40S ribosomal protein S24	2.020	4.057	0.781
Q8VIL3	ZWINT	ZW10 interactor	-1.989	0.252	0.748
P68035	ACTC	Actin, alpha cardiac muscle 1	-1.643	0.320	0.743
Q05175	BASP1	Brain acid soluble protein 1	-0.820	0.567	0.718
Q5U2U2	CRKL	Crk-like protein	3.531	11.561	0.717
Q9Z272	GIT1	ARF GTPase-activating protein GIT1	2.093	4.266	0.711
P63245	GBLP	Guanine nucleotide-binding protein subunit beta-2-like 1	0.717	1.644	0.707

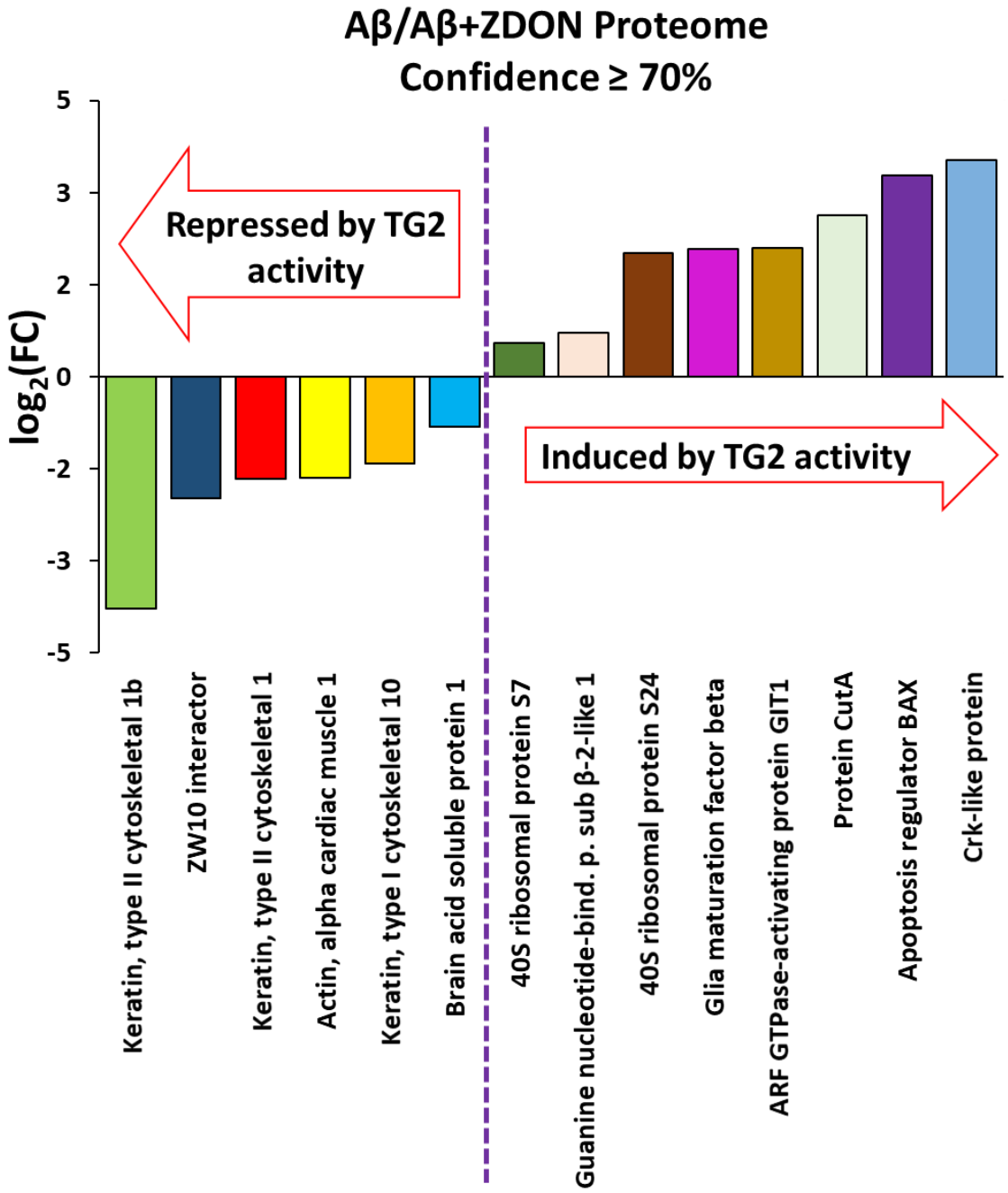

Figure 5.8. Altered proteins in the proteome of Aβ treated neurons compared to Aβ+ZDON. *Histogram shows proteins significantly changed in neurons upon Aβ exposure compared to Aβ+ZDON (TG2 inhibition), plotted according to increasing log_2(FC) values (N=3 replicas). Data was obtained by quantitative SWATH-MS/MS analysis and is expressed as log_2(FC), where negative values represent proteins which were reduced by TG2 activity (higher values in Aβ+ZDON compared to Aβ), and positive values represent proteins which were induced by TG2 activity (higher values in Aβ compared to Aβ+ZDON). Only variations with confidence ≥ 70% were included.*

In conclusion, 11 proteins which were targets of TG2 under Aβ-driven neurodegenerative conditions were identified, among which TMC5 and AT2B2 could represent previously unknown partners of TG2 playing a role in the regulation of calcium homeostasis in neurons (**Fig. 5.9**). Moreover, the analysis of the Aβ/Aβ+ZDON proteome revealed the alteration of proteins linked to neuronal growth and survival, but also to the apoptosis pathway, suggesting a dual role for TG2.

Figure 5.9. Schematic representation of overall results. A) *Astrocytes activated by Lipopolysaccharides (LPS), an endotoxin which causes inflammatory response, release EVs carrying TG2.* ***B)*** *Extracellular TG2 (in soluble form or vesicle-bound) interacts with neurons, inducing a calcium influx that increases intracellular calcium levels ($[Ca^{2+}]_i$).* ***C)*** *Extracellular TG2 causes a membrane depolarisation (about 20 mV) and activates an inward calcium current.* ***D)*** *Calcium influx is mediated by L-type Voltage Operated Calcium Channels (VOCCs) and* ***E)*** *the Sodium/calcium exchanger (NCX).* ***F)*** *Increase of intracellular calcium levels is neurotoxic and can lead to cell death. At the same time, higher $[Ca^{2+}]_i$ can activate intracellular TG2, which could in turn crosslink endogenous substrates, leading to the formation of neurotoxic protein aggregates and cell death.* ***G)*** *Aβ stimulus induces $[Ca^{2+}]_i$ increase and consequent activation of neuronal endogenous TG2.* ***H)*** *Activated TG2 crosslinks a variety of endogenous substrates, including AT2B2 and TMC5, which might participate to the dysregulation of calcium homeostasis in neurons under neurodegenerative-like conditions. This image was generated with Motifolio (https://www.motifolio.com/).*

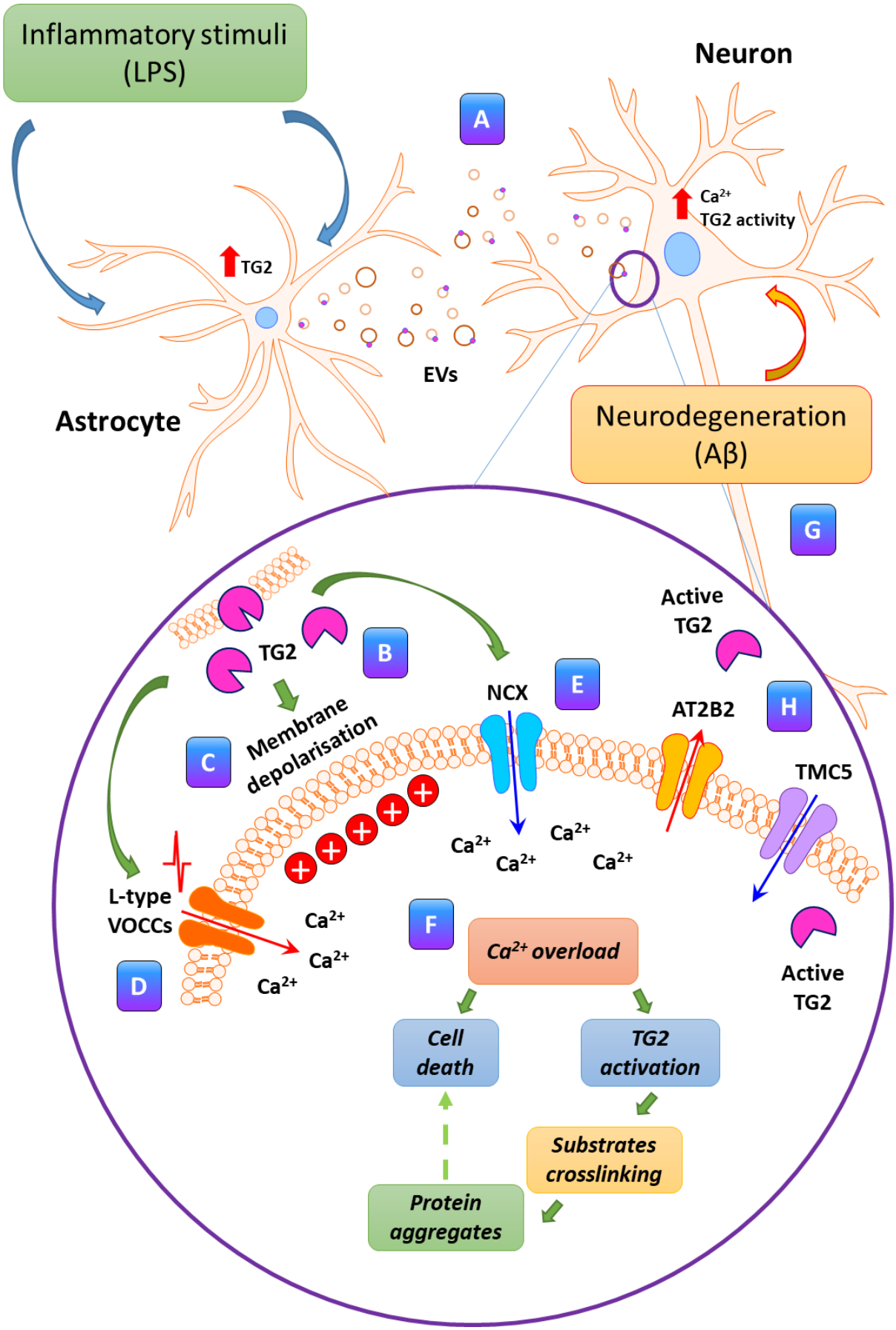
Inflammatory stimuli (LPS)
Neuron
A
Ca2+
TG2 activity
TG2
EVs
Astrocyte
Neurodegeneration (Aβ)
G
Active TG2
TG2
B
NCX
E
AT2B2
H
C
Membrane depolarisation
TMC5
Ca2+
Ca2+
Ca2+
Ca2+
L-type VOCCs
Ca2+
Ca2+
Ca2+
F
Ca2+ overload
D
Active TG2
Cell death
TG2 activation
Substrates crosslinking
Protein aggregates

5.3 Discussion

TG2 ability to crosslink protein substrates and generate insoluble protein aggregates has been associated with a variety of neurodegenerative diseases. Indeed, proteins such as Aβ, tau, α-synuclein and huntingtin are known targets of TG2 transamidation, which is generally found to be increased in brain disorders (Benilova et al., 2012; Martin et al., 2013). However, there is limited information and agreement on whether TG2 activity is elevated *in vivo* and whether other proteins are target of TG2 PTM concurring to pathogenesis. Here a global approach was adopted to identify all specific TG2 substrates in a cell model simulating AD based on treating primary hippocampal neurons with $A\beta_{1-42}$, thus mimicking the increase of extracellular $A\beta_{1-42}$ that characterises both fAD and sAD (Scheuner et al., 1996; Mark et al., 1997; Portelius et al., 2010). This was achieved by using comparative proteomics (Gillet et al., 2012), to compare substrates of TG2 (highlighted by FITC-cad incorporation into endogenous substrates) with and without TG2 inhibition by ZDON, one of the most specific TG2 inhibitors. Changes in Aβ proteome identified by ZDON-mediated inhibition of TG2 were also investigated. Collectively, thanks to this approach, the first TG2 "transamidome" was generated in a cell model simulating AD.

When primary hippocampal neurons were incubated with Aβ in the presence of the fluorescein-labelled primary amine cadaverine, a 6-fold increase of TG2 activity *in situ* was observed, measured by incorporation of FITC-cad into endogenous substrates (**Fig. 5.1**), suggesting that TG2 is hyper-activated in a Aβ-driven neurodegenerative context. This is in line with current thinking, as both TG2 activity and its by-product EGGL have been found to be increased in neurodegenerative conditions (Nemes et al., 2001; Bonelli et al., 2002; Vermes et al., 2004; Jeitner et al., 2001-2008). A total of 11 proteins emerged as TG2 specific substrates. These included Aβ, a known TG2 substrate (Hartley et al., 2008; Benilova et al., 2012), although Aβ was endogenously provided in this model. Given the importance of Aβ aggregation during the development of AD, this is a further confirmation that TG2 participates to the neurodegenerative process (Wilhelmus et al., 2009; Benilova et al., 2012; Marin et al., 2013). Interestingly, two proteins involved in ion transport were also found among TG2 targets, namely AT2B2 and TMC5. AT2B2 (also called PMCA2) is part of the Plasma Membrane Calcium-Transporting ATPase family of pumps and mediates the efflux of Ca^{2+} from the cytoplasm across the plasma membrane. Inhibition of PMCAs activity has been observed in the aging brain and in association with both Aβ and tau/p-tau accumulation in AD brain membranes (Mata et al., 2011; Berrocal et al., 2009-2015),

confirming that PMCAs play an important role in maintaining calcium homeostasis. TMC5 belongs to a family of transmembrane proteins possibly involved in ion transport (Keresztes et al., 2003). TMCs are ubiquitously expressed in most organs, however not much is known about their functions. Because mutations in TMC1 are responsible for some familial forms of hearing disorders, which are characterised by altered potassium currents, it was hypothesised that these proteins are likely involved in ion transport (Kurina et al., 2002; Keresztes et al., 2003). Notably, recent work showed that TMC5 is increased in prostate cancer (PCa) patients and that TMC5 KO in PCa cell lines reduced cell proliferation by blocking the cell cycle, revealing a possible role for this protein in cell development (Zhang et al., 2019). In the light of the findings described in Chapter 4, AT2B2 and TMC5 emerged as possible partners of TG2 which might be involved in TG2-mediated modulation of calcium homeostasis in neurons.

Other TG2 targets were ENOB, involved in the glycolysis pathway, K1C40 (Keratin type I cytoskeletal 40) and FAAH1, which hydrolyses bioactive fatty acid amides. Enolase had already been reported as a glutamine donor for TG2 transamidation in *C. elegans* (Madi et al., 2001). Interestingly, ENOB was not only increased as a substrate by Aβ exposure compared to control neurons, but was also confirmed as a specific substrate in the Aβ/Aβ+ZDON transamidome, suggesting that the PTM of ENOB by TG2 might be a significant modification induced by Aβ. The dysregulation of cell energy metabolism is a known factor involved in neurodegeneration (Beal, 1998; Markesbery, 1999) and enolases have been shown to be inactivated in the AD hypometabolic and oxidised environment (Butterfield et al., 2006; Butterfield and Lange, 2009). It is plausible that TG2 could lead to aggregates of ENOB as indicated by primary amine incorporation, resulting into its inactivation.

CD81, a tetraspanin and cell-surface glycoprotein involved in a variety of functions, was significantly decreased in the Aβ/CTR proteome, yet it was still highly increased in the Aβ/Aβ+ZDON transamidome, suggesting that it is a specific target of TG2 independently from Aβ. CD81 has been involved in the processing pathway of the amyloid precursor protein (APP) together with other members of the tetraspanin family (Seipold and Saftig, 2016), moreover, CD81 is a well-known EVs marker (Thery et al., 2018). It is tempting to suggest that TG2-mediated PTM might have a role in EVs trafficking.

Four ribosomal proteins (RS14, RS18, RS25 and RS30) were among TG2 substrates, suggesting a possible effect of TG2 at the transcriptional level. Consistently, another

ribosomal protein, namely RS19, has been reported as a target of Factor XIIIa (Nishiura et al. 1996; Chen et al., 2013-2014), supporting the idea that ribosomal proteins are targets of TGs-mediated crosslinking, which might have an impact on protein synthesis. Indeed, ribosome dysfunction has been reported as an early event in the etiopathogenesis of AD (Ding et al., 2005).

The proteome of Aβ treated neurons (**Fig. 5.6** and **Table 5.6**) identified a cluster of mitochondrial proteins which were upregulated following Aβ stimuli, namely NAKD2, PRDX3, MDHM, NDUV2, C1QBP and TIM13. These are all linked to energy imbalance and mitochondrial dysfunction, which are common hallmarks of AD (Beal, 1998; Markesbery, 1999). This was seen in animal and cellular models of AD, all showing clear sings of metabolic dysfunction at the mitochondrial level (Martire et al., 2016). Consistent with this finding, when the mitochondrial proteome of cortical neurons incubated with $A\beta_{25-35}$ peptide was investigated, Aβ-driven metabolic dysfunction was also revealed (Lovell et al., 2005). Incubation of brain endothelial cells with $A\beta_{1-40}$ led to the alteration of calcium homeostasis, inducing ER stress and activation of the apoptotic pathway (Fonseca et al., 2013). Among this cluster of Aβ induced proteins, NAKD2 is mitochondrial kinase that catalyses the phosphorylation of NAD to NADP. Mutations in this gene are associated with a rare autosomal recessive disorder that can cause dienoyl-CoA reductase deficiency (DECRD) and hyper-lysinemia, which also presents peripheral neuropathy (Pomerantz et al., 2018). PRDX3 and PRDX2 are respectively a mitochondrial and cytoplasmic peroxide reductase and are activated in response to apoptotic signals and oxidative stress (Hu et al., 2018). Consistent with the proteome obtained in this study, members of the peroxiredoxin family have been found altered in patients affected by AD and other neurological conditions, like PD, HD and Down Syndrome (Kim et al., 2001; Krapfenbauer et al., 2003; Sorolla et al., 2008). The expression of PRDX3 had neuroprotective effects in a *Drosophila* model of neurodegeneration, improving mitochondrial and neurons integrity (Angeles et al., 2014). Similarly, activation of PRDX2 by sulfiredoxin-mediated denitrosylatation (removal of an -NO group) protected human-induced pluripotent stem cell (hiPSC)-derived neurons and dopaminergic cells lines from NO-induced oxidative stress (Sunico et al., 2016). Protein levels of mitochondrial C1QBP (equally called p32) were also increased upon Aβ. This is a multifunctional protein involved in diverse functions, including energy homeostasis and immune response (Barna et al., 2019). Notably, it was shown to be enriched in synaptic mitochondria (Volgyi et al., 2015) and to directly interact with $GABA_AR$, possibly modulating

the receptor biosynthesis or functions in physiological conditions (Schrarer et al., 2001). Although C1QBP overexpression induced apoptosis in fibroblasts (Meenakshi et al., 2003; Chowdhury et al., 2008), its KO in mice was shown to be deleterious, leading to axon degeneration and progressive loss of oligodendrocytes, with consequent de-myelination of white matter fibres (Yagi et al., 2017). Interestingly, according to the Gene Ontology classifier "Biological process", mitochondrial protein C1QBP is a positive regulator of protein kinase B (KCRB) signalling (**Table 5.4A** continued), which was also found to be significantly overexpressed following Aβ exposure. KCRB is a creatine kinase (KC) which regulates ATP levels in neurons and is a fundamental mediator of the cell response to bioenergetic stress (Aksenov et al., 2000). In AD and other dementias, CKs activity is inhibited by protein oxidation, which participates to the deterioration of neuronal homeostasis (Aksenov et al., 2000). Active KCRB was shown to interact with human tau *in vitro*, whereas the oxidised form which is present in AD brains lost this ability (Hernandez et al., 2019).

Furthermore, PP2AA is another pro-apoptotic protein that was increased upon Aβ. This is one of the major serine phosphatases, mainly involved in the regulation of microtubule-associated proteins (MAPs). It is associated with stress responses to cytokines inflammatory stimuli and mediates pro-apoptotic signals, thus PP2AA activation has been recently suggested as a possible strategy for anti-cancer treatment (Carratu et al., 2016; Clark and Ohlmeyer, 2019). At the same time, PP2AA has been proposed as a therapeutic target for neurodegenerative and inflammatory diseases, thanks to its ability to reduce inflammatory responses by modulating the Toll like receptor 4 (TLR4)/NF-kB pathway (Clark and Ohlmeyer, 2019). PP2AA is known to play a central role in maintaining tau functions by mediating its de-phosphorylation (Sontag et al., 1999) and in AD tissues its activity was found to be impaired, leading to tau hyper-phosphorylation and formation of NFT (Sontag and Sontag, 2014). For these reasons, it is possible to hypothesise that the increase of PP2AA in the Aβ proteome might be due to the activation of an anti-inflammatory response in stressed neurons.

A number of neurotrophic and pro-survival proteins were increased in response to Aβ, such as CRKL, SCG3, HDGR3 and SAP, which are involved in neuronal growth, dendrite and brain development. For example, SCG3 participates to the biogenesis of secretory granules and is expressed in intraneuronal vesicles (Ottiger et al., 1990; Hosaka et al., 2002), while HDGR3 was shown to be a motor neurons trophic factor (Marubuchi et al., 2006).

On the other hand, among the Aβ downmodulated proteins a cytoskeleton-associated cluster could be identified, likely indicating a structural dysfunction of the stressed neurons, and mitochondrial fission factor (MFF). MFF mediates mitochondrial organisation, and its downmodulation was shown to impair mitochondrial ability to divide, leading to increased size and ability to uptake calcium, with consequent reduction of $[Ca^{2+}]_i$ and decrease in pre-synaptic activity (Lewis et al., 2018).

Collectively, these data showed that neurons incubated with Aβ presented an altered bioenergetic metabolism, and activated both pro-apoptotic signals and neurotrophic factors in a compensatory fashion.

By comparing the Aβ proteome with the Aβ proteome in conditions of TG2 inhibition (ZDON), Aβ-stimulated proteins also targets of TG2 PTM could be identified (**Table 5.5** and **Fig. 5.8**). Some proteins involved in neuronal growth and migration were selectively decreased following TG2 inactivation, namely GMFB, CRKL, GIT1 and GBLP. The decrease of neurotrophic proteins in response to TG2 inactivation suggest a possible neuroprotective role for active TG2. These findings are in line with previous observations describing TG2 ability to protect neurons from oxygen and glucose deprivation (OGD) stress after ischemic insult (Filiano et al., 2008; Filiano et al., 2010). Consistent with these data, downmodulation of TG2 in cortical neurons by a shRNA lentivirus was deleterious was neuronal survival (Yunes-Medina et al., 2018). TG2 was shown to contribute to the correct assembly of respiratory complexes at the mitochondrial level, and lack of TG2 caused energy impairment (Mastroberardino et al., 2006). Moreover, TG2 is known to be involved in the development of the CNS, promoting synaptogenesis and neurite outgrowth (Maccioni and Seeds, 1986; Mahoney et al., 2000; Tucholski et al., 2001; Singh et al., 2003; Bailey and Johnson, 2004). Although data from this study and others have linked TG2 with cell survival, a large body of data also support a neurotoxic role for TG2 in neurons. For example, overexpression of TG2 in mouse brain led to hippocampal damage and increased sensitivity to kainic acid-induced seizures (Tucholski et al., 2006). Similar observations were made in rat cortical neurons exposed to oxidative stress, where TGs overexpression induced increased cell death, whereas pharmacological inhibition of both TG1 and TG2 was neuroprotective (Basso et al., 2012). Moreover, ablation of TG2 was shown to decrease neuronal death in a mouse model of HD (Mastroberardino et al., 2002). Lastly, the evidence that TG2 participates to the progression of neurodegeneration by crosslinking endogenous substrates also support its negative role in disease (Martin et al., 2013).

In this work, apoptotic factor BAX was also found to be downregulated by TG2 inhibitor ZDON, suggesting that active TG2 supports BAX expression and pro-apoptotic signals. Notably, TG2 has been shown to be involved in BAX translocation to mitochondria and consequent release of cytochrome c, thus mediating a pro-apoptotic pathway (Yoo et al., 2012; Rodolfo et al., 2004). At the same time, the opposite was also described by Cho and colleagues, who demonstrated that overexpression of TG2 downmodulated BAX protein levels and inhibited apoptosis, whereas TG2 downregulation induced BAX expression and cell apoptosis (Cho et al., 2010).

Given the ample variety of processes that TG2 is involved in, both at the physiological and pathological level, it is likely that TG2 may play different roles at different stages of disease and activate both pro- and anti-apoptotic signals in cells under stressing conditions. So it is not overly surprising to find contrasting literature on the topic. In fact, in the *ex vivo* model of AD used in this work, the activation of opposing pathways was observed, as TG2 seemed to mediate both neuroprotective proteins involved in neuronal survival and also promote cell death by regulation of BAX.

CHAPTER 6:

Detection of TG2 in biological samples from patients affected by dementia

6.1 Introduction

Transglutaminases (TGs) have been implicated with neurodegenerative conditions for the past 30 years, and numerous attempts have been made to link their expression or activity with these conditions.

Independent studies have reported that TGs transcripts, enzymatic activity and antigen were significantly elevated in Alzheimer's disease (AD) patients compared to controls, e.g. in the prefrontal cortex (Citron et al., 2001; Johnson et al., 1997, Kim et al., 1999) and cerebrospinal fluid (CSF) (Bonelli et al., 2002; Nemes et al., 2001) (**Table 1.2**). TG2 was found to be co-localised with tau in neurofibrillary tangles (NFTs) (Citron et al., 2001) and with Aβ in amyloid plaques, where TG *in situ* activity was also detected (Zhang et al., 1998; Wilhelmus et al., 2016). Interestingly, Wilhelmus and colleagues demonstrated that both TG2 and TG1 are expressed in NFTs and senile plaques (SPs) in AD brains (Wilhelmus et al., 2009). Increased levels of TGs-induced crosslinking have been observed in Parkinson's disease (PD) brains, implying a possible involvement of TG2 in aggregation of α-synuclein into Lewy bodies (Andringa et al., 2004; Grosso et al., 2014; Junn et al., 2003; Vermes et al., 2004). TG2 protein and activity were also detected at higher levels in Huntington Disease (HD) brain (Lesort et al., 1999). In fact, huntingtin has been proposed as TGs substrate (due to polyGln expansion), and TG2 activity was found to be elevated in HD CSF compared to healthy controls (Lesort et al., 1999; Jeitner et al. 2001- 2008) (**Table 1.2** in Chapter 1). More recently, TG2 was also found to play a role in Multiple Sclerosis (MS) pathology, and TG2 mRNA was increased in MS patients-derived monocytes compared to controls (van Strien et al., 2015; Sestito et al., 2016).

Although the majority of literature data suggest that TG2 may be considered a promising biochemical marker of AD and other neurodegenerative diseases, Wolf and colleagues have questioned its function as biomarker of dementia, as in their hands neither TG2 concentration nor transamidation activity were significantly increased in AD brain homogenates (Wolf et al., 2013).

Despite this body of work, data remain contradictory and limited by the restrictions posed when using mainly post-mortem brain samples or CSF for these studies.

In the present study, TG2 was investigated as a biomarker of dementia using an approach based on a significant number of patients samples (estimated by power analysis) and on biological fluids that are routinely collected in AD centres, hence more in line with current diagnostic procedures (e.g. analysis of plasma samples and primary fibroblasts). Literature

data support the idea that peripheral tissues can mirror the pathological state of the brain, especially in the case of familial patients, where all cells retain the same genetic background, including the expression of disease-causing gene mutations (Clos et al., 2012). This was observed in HD fibroblasts, which showed ultrastructural damages especially at mitochondrial level, a hallmark of neurodegeneration (Squitieri et al., 2010; Siddiqui et al., 2012). Similarly, cells from both familial and sporadic AD and PD patients showed mitochondrial impairment, altered levels of reactive oxygen species (ROS) and dysregulation in calcium homeostasis compared to control fibroblasts (Gibson et al., 1996; Gray and Quinn, 2015; Zanellati et al., 2015; Lopez-Fabuel et al., 2017; Perez et al., 2018; Braggin et al., 2019; Gonzalez-Casacuberta et al., 2019).

At the same time, a new approach for the early diagnosis of neurodegenerative diseases has risen in recent years, which is the identification of blood-based biomarkers (Zetterberg and Burnham, 2019). Although the detection of brain-related disease markers in blood is challenging, due to the Blood-Brain Barrier (BBB) limiting the passage of molecules into the bloodstream, recent findings suggest that this is a promising alternative to more invasive diagnostic methods like PET or CSF analysis. For example, the detection of plasma Aβ peptides has been shown to have a high predictive power for AD and an accuracy of about 90% compared to PET, which is still one of the golden standards for AD diagnosis (Nakamura et al., 2018). Likewise, neurofilament light (NfL) levels in plasma have shown a strong correlation to respective CSF concentrations and were increased in both sporadic and familial AD plasma compared to controls (Weston et al., 2017; Mattsson et al., 2017). Interestingly, also blood-derived EVs have been proposed as possible biomarkers of disease in neurodegeneration, even if at the moment, the complexity of the isolation protocols represent a limitation to the application in the clinic (Fiandaca et al., 2015; Goetzl et al., 2015-2019, Seongju et al., 2019). These findings support the validity of the approach and the novelty of this investigation, as to our knowledge TG2 has never been characterised in primary fibroblasts from dementia patients and only limited data are in the public domain for plasma (**Table 6.1**).

Here the association of TG2 with pathology was investigated using primary fibroblasts and plasma from a “powerful” number of well characterised dementia patients.

Table 6.1. Detection of TG2 protein and activity in plasma or serum reported in the literature.

Plasma/Serum			
Variable quantified	**Method**	**Disease**	**References**
Protein levels	Multiplex ELISA (MAGPIX, Merk)	EC	Torres et al., 2019
		GO	Becerick et al., 2016
	ELISA (Cusabio Biotech)	CP	Becerick et al., 2017
Enzymatic activity	Plate assay (TG-Covtest kit) *(serum)*	Mastocytosis	Ahn et al., 2015
	Incorporation of ^{3}H-putrescine into dimethyl casein (radioactivity) *(plasma and serum)*	CTR	Fujita et al., 1998
EGGL [Nε(γ-glutamyl)-lysine] isopeptide levels	- Internal standard tracer - Precolumn phenylisothiocyanate derivatization - HPLC separation *(plasma)*	AD, VaD	Nemes et al., 2001
	- HPLC *(plasma)*	CTR	Harsfalvi et al., 1992
γ-Glutamylamines levels	- Reversed phase HPLC - Electrochemical detection (EC) *(plasma)*	CTR	Jeitner et al., 2008

Abbreviations: Endometrial cancer, EC; Gingival Overgrowth, GO; Chronic Periodontitis, CP; Healthy controls, CTR; Alzheimer's Disease, AD; Vascular dementia, VaD.

6.1.1 Aims of this chapter

The general aim of this chapter was to verify if TG2 could be detected in primary fibroblasts and plasma of dementia patients, and be associated with dementia. To achieve this, the analysis of primary fibroblasts from control healthy subjects and sporadic AD patients (sAD), and plasma from controls, sAD, FTLD and MCI subjects was performed. An ELISA-based assay for the detection of TG2 in plasma was optimised and applied for the analysis of plasma-derived EVs. Finally, an attempt to measure the product of TG2 crosslinking was made, namely the ε-(γ-glutamyl)lysine dipeptide, in the patients' plasma. All patients' samples were obtained from the IRCCS-Fatebenefratelli, National Centre for Alzheimer's and Mental Diseases (Brescia, Italy).

6.2 Results

6.2.1 TG2 expression in primary fibroblasts of AD patients compared to controls

In order to verify if TG2 correlates with dementia and can be considered a prognostic marker for AD, primary dermal fibroblast from control and dementia subjects were analysed for detection of TG2 protein and activity.

The calculation of the sample size was carried out in collaboration with statisticians from the IRCCS-Fatebenefratelli institute (Italy), the provider of all the patients' samples used for this project, as described in Methods chapter 2.2.1.4.2. Using a two-tailed test for independent samples, with alpha 0.05 and power 80%, a minimum sample size of 10 subjects was suggested to observe a significant variation. Therefore, a sample size of 15 subjects per group was selected. Patient diagnosis was made following international guidelines by a team of neuropsychologists, neurologists, psychiatrists and nurses, who performed neuropsychological and behavioural assessments (Ghidoni et al., 2014). Fibroblasts details are summarised in **Table 6.2**.

Table 6.2. Demographic characteristics of patients

Diagnosis	Age	Sex (Males / Females)	N
CTR	63.3±6.2	3 / 4	7
sAD	76.0±8.5	3 / 2	5

Abbreviations: Healthy controls, CTR; Sporadic Alzheimer's Disease, sAD.

Fibroblasts were isolated from skin biopsies and maintained as described in Methods chapter 2.2.1.4.3. No morphological difference was noted between healthy and AD fibroblasts allowed to adhere on TCP in complete medium with serum when observed by light microscopy (**Fig. 6.1**). Published data suggest that sAD cells present alterations in mitochondrial metabolism (Moreira et al., 2007; Pérez et al., 2017-2018, Braggin et al., 2019), therefore signs of mitochondrial impairment/apoptosis could be expected, however this was not investigated.

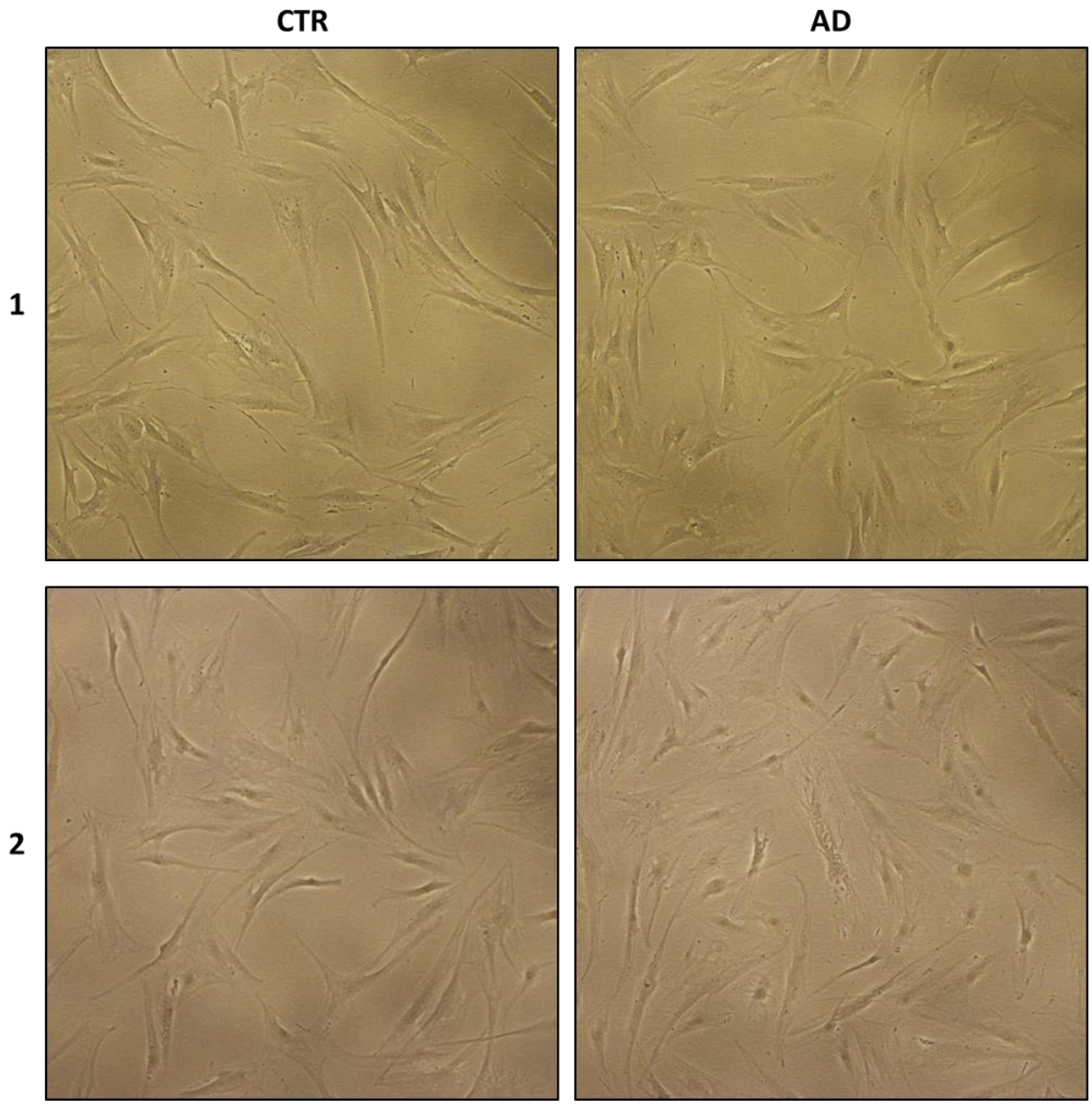

Figure 6.1. Culture of primary human dermal fibroblasts. *Primary human dermal fibroblasts from control (CTR1 and CTR2) and AD (AD1 and AD2) subjects skin biopsies were maintained in EMEM complete media as described in Methods chapter 2.2.1.4.3. Cells at passage 4 were visualised by Ts100 Eclipse Optical Microscope (Nikon) using 10X objective. All samples were obtained under ethical approval as described in Methods chapter 2.2.1.4.1.*

The expression of TG2 was quantified in the total lysates of 7 CTR and 5 sAD fibroblasts by western blotting. Blots were probed with the mouse monoclonal anti-TG2 (CUB7402) antibody, which is known to detect human TG2 with high specificity. The densitometry analysis of the blots revealed a trend increase of TG2 protein in AD patients compared to

controls (**Fig. 6.2A-B**), however this was not at a significant level. Cell lysates from different subjects but from the same cohort presented high variability of TG2 levels, which explains high variation (**Fig. 6.2B**, left plot).

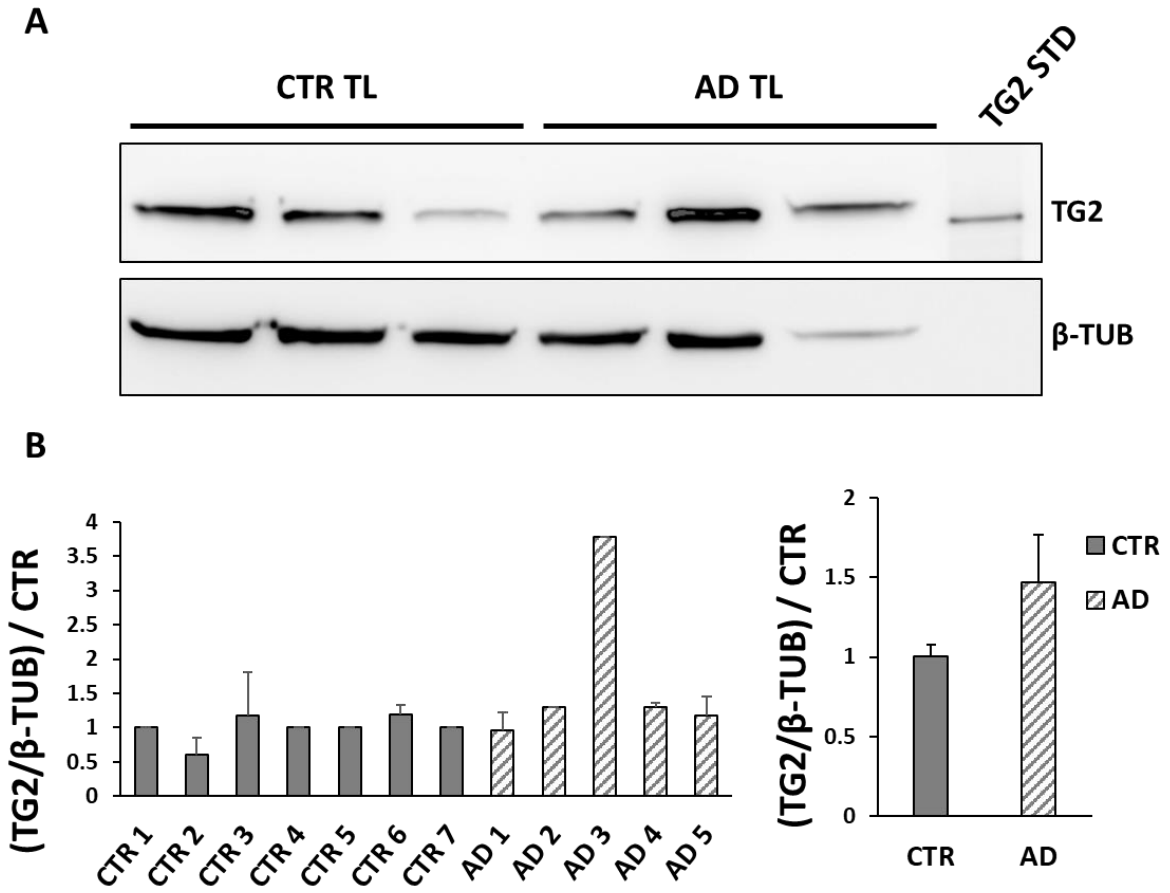

Figure 6.2. Analysis of TG2 in CTR and AD primary fibroblasts by western blot. *Cells at 80% confluence were lysed in RIPA buffer and analysed by western blot.* ***A)*** *Representative blot of fibroblasts' total lysates (TL) of 3 CTR (lanes 1-3) and 3 sAD subjects (lanes 4-6). gplTG2 was used as molecular weight standard. Blots were probed with mouse monoclonal anti-TG2 (CUB7402) and anti-β-Tubulin.* ***B)*** *Densitometry analysis shows mean intensity ± SE of TG2 immune-reactive bands normalised to β-TUB and then to CTR 1. A total of 7 CTR and 5 sAD were tested in 8 independent experiments, each subject tested from 1 up to 3 times. Single patient's quantifications are shown on the left plot, while average values are shown on the right. P=NS.*

TG2 levels were then assessed by immunofluorescence in fixed and permeabilised fibroblasts. In both AD and CTR fibroblasts, TG2 signal was mainly visible in the cytoplasm, and no evident nuclear staining was detected (**Fig. 6.3A-B**). Similarly to the staining of primary rat hippocampal neurons and astrocytes (**Fig. 3.2** and **3.7** in Chapter 3), TG2 presented a dotted-like signal. Image quantification of confocal images showed that TG2 protein was 1.6-fold higher in AD fibroblasts compared to CTR (**Fig. 6.3C**).

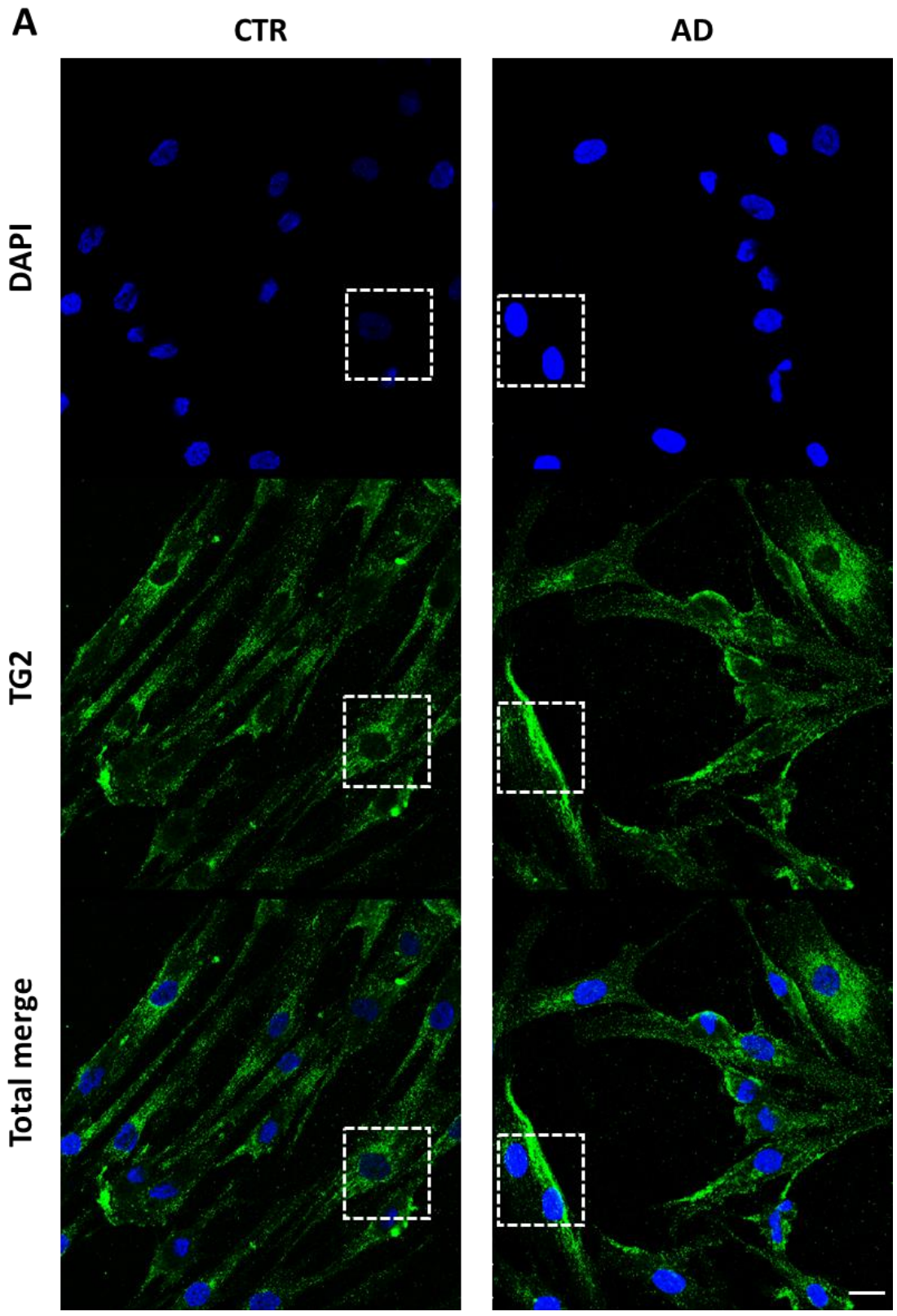
A
CTR
AD
DAPI
TG2
Total merge

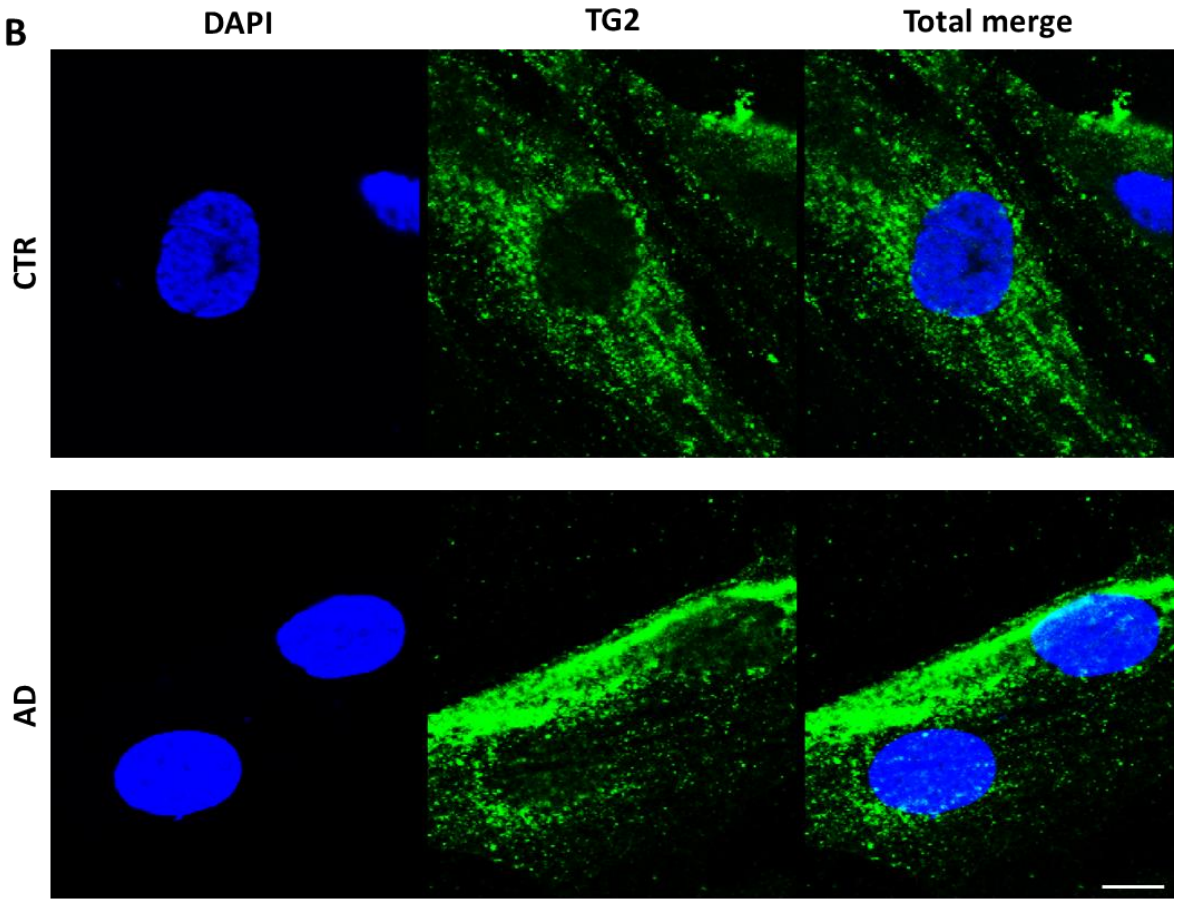

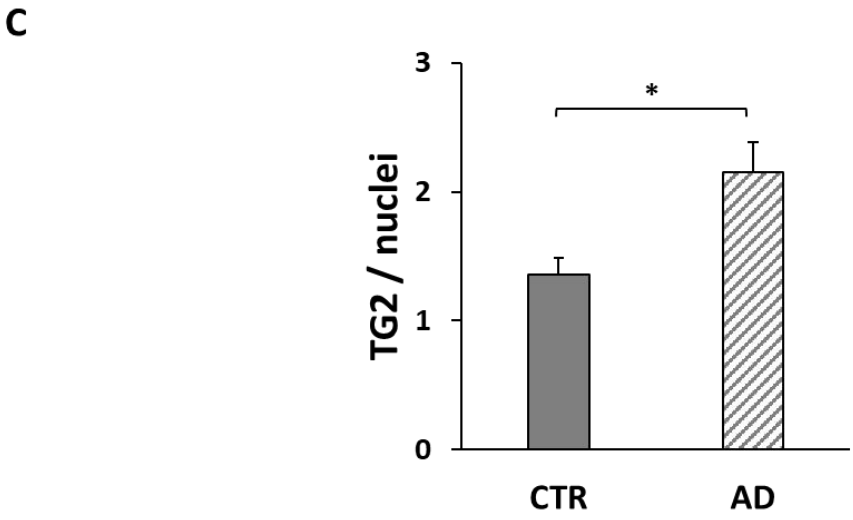

Figure 6.3. TG2 localisation in primary fibroblasts. A) *Immunofluorescence staining of CTR and sAD fibroblasts (p3) plated in a chamber slide. Cells were fixed in 3% paraformaldehyde in PBS pH 7.4 (w/v), permeabilised and stained with DAPI (blue) and anti-TG2 CUB7402 antibody followed by FITC-labelled anti mouse IgGs (green). Slides were visualised by laser scanning Leica SP5 confocal microscope using 63X oil immersion objective. Successive serial optical sections (0.5 µm) were recorded over 5 µm planes. Scale bar 20 µm.* ***B)*** *Zoom-in of the white dotted section of CTR (top) and AD (bottom). Scale bar 10 µm.* ***C)*** *TG2 signal was*

*quantified from maximum projection of z-stack image series and normalised to the number of nuclei. Data is expressed as mean of TG2 intensity ± SE (N=4 fields of one slide representative of CTR and AD, with about 10 cells imaged per field). CTR: 1.36 ± 0.13; AD: 2.15 ± 0.24; *p<0.05.*

TG2 enzymatic activity was measured in fibroblasts total lysates by a plate activity assay (as described in Methods chapter 2.2.5.3). These starting experiments have revealed that TG activity was 2.2-fold higher in sAD compared to healthy controls (**Fig. 6.4**). The presence of mycoplasma contamination in the cells from the remaining subjects hampered the analysis which could not be taken to a conclusion in the available time.

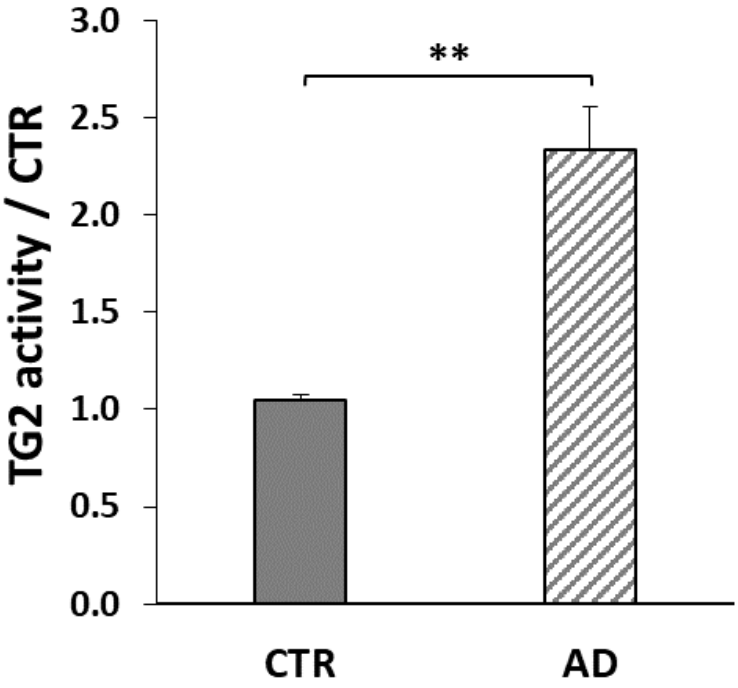

Figure 6.4. Analysis of TG2 activity in CTR and AD primary fibroblasts. *TG2 activity was quantified in the total lysates of primary dermal fibroblasts in sucrose lysis buffer and expressed as µU/µg of lysate (as described in Methods chapter 2.2.5.3). Data is shown as mean activity ± SE, normalised to CTR (N=1 CTR and 2 AD, each tested in duplicate in 2 independent experiments; **p≤0.001). CTR: 0.27±0.09; AD: 0.55±0.14.*

Because the previous results illustrated in this study revealed that TG2 could be released by astrocytes-derived EVs in a context of neuroinflammation, the presence of TG2 in EVs from dermal fibroblasts was tested. Large and small EVs were isolated from the serum-free conditioned medium of healthy and sAD primary fibroblasts by serial centrifugation as described in Methods chapter 2.2.9.2. Particle size distribution of EVs isolated from CTR fibroblasts was obtained by ZetaView analysis as previously described (Methods chapter 2.2.10). This showed small particles around 130.1±2.1 nm and large particles around 266.6±7.0 nm, in line with published data using a similar methodology (Benussi et al., 2016) (**Fig. 6.5**). Quantification of particles concentration showed that small EVs were about one order of magnitude higher than large EVs ($5.3x10^9$ and $5.9x10^8$ respectively) (**Fig. 6.5**).

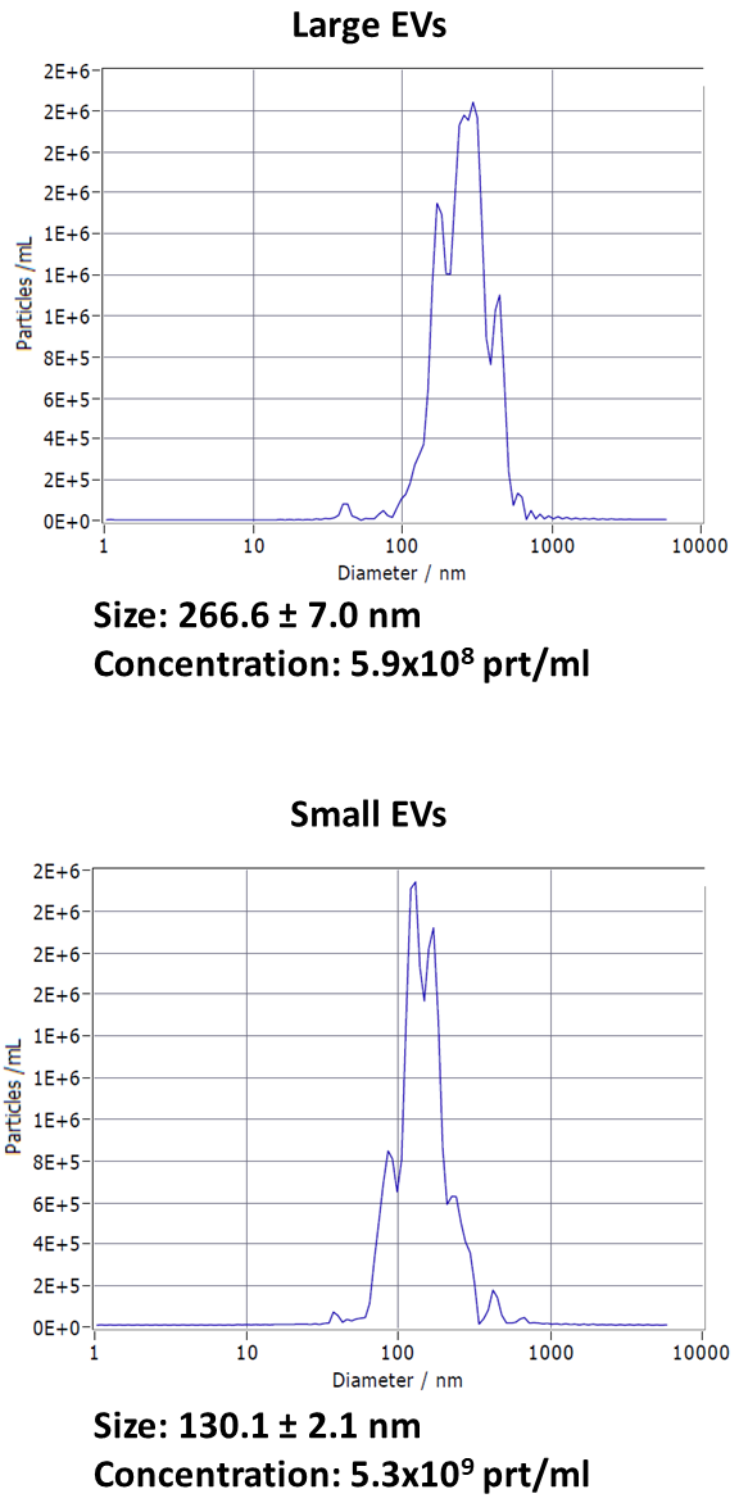

Figure 6.5. NTA analysis of EVs isolated from primary CTR and sAD fibroblasts*. Size and distribution of EVs isolated from CTR fibroblasts were characterised by ZetaView. One representative graph is shown (N=2). Size is expressed as average mode ± SE.*

Western blotting analysis of EVs derived from CTR fibroblasts, revealed that small EVs were more abundant compared to large EVs, as indicated by the enrichment in vesicular markers FLOT-2, TSG101 and ALIX (**Fig. 6.6A**) and confirmed by NTA (**Fig. 6.5**). The presence of TG2 was revealed in the small EVs (**Fig. 6.5A**). Attempts to quantify TG2 in EVs isolated from the conditioned medium of CTR and AD fibroblasts were limited by difficulties of isolating EVs (no or low presence of EVs markers) or low level of TG2 (**Fig. 6.6B**).

In conclusion, these data have shown that TG2 can be detected in primary skin fibroblasts from healthy subjects and dementia patients, and that it is also externalised by EVs. Due to issues with mycoplasma contamination with these primary cell lines, it was not possible to screen a sufficient number of patients and controls for the conclusions to be significant.

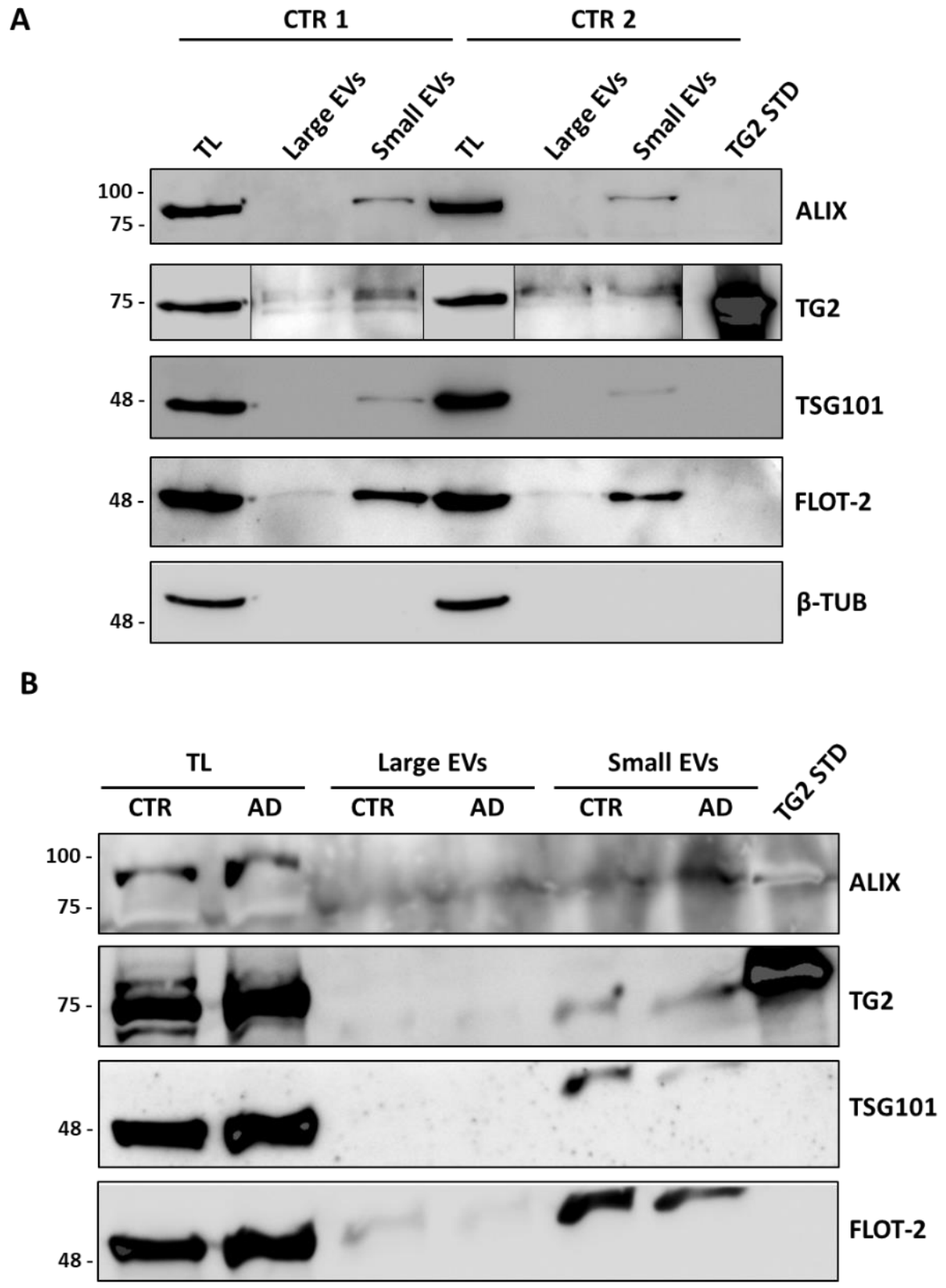

Figure 6.6. Western blotting analysis of TG2 in EVs isolated from CTR and AD primary fibroblasts. *Cells were plated in 3 T75 flasks (0.4-0.5x10^6 cells/flask), left to attach 24 hours and then incubated in serum-free media for 72 hours before EVs isolation, as described in Methods chapter 2.2.9.2. Fibroblasts total lysates (TL, 100 µg), large and small EVs lysates (total amount isolated from 3 flasks, 10-15 µg) were lysed in RIPA buffer and analysed by*

western blot. Blots were probed with mouse monoclonal anti-TG2 (CUB7402) and vesicle marker mouse anti-TSG101, then stripped and re-probed with rabbit anti-ALIX and mouse anti-FLOT-2. In some cases, an additional stripping and re-probing with rabbit anti-tubulin was also performed. ***A)*** *Blot of TL and EVs isolated from one CTR fibroblast, in duplicate. The blot for TG2 detection shows parts of the same membrane at different exposure times, to better appreciate TG2 signal in TL and EVs.* ***B)*** *Blot of TL and EVs isolated from one CTR and one AD fibroblasts.*

6.2.2 Detection of TG2 in human plasma

Plasma represents a very attracting sample to use for diagnosis, mainly because collection is much easier and less invasive compared to CSF, yet not much is known on the presence of TG2 in biological fluids such as plasma. Moreover, concerns exist regarding the plasma high abundance proteins (HAPs) masking rare markers as TG2.

A commercially available ELISA assay and classic laboratory methods were tested to compare sensitivity (summarised in **Table 6.3**) and determine if any of them would be suitable for detection of TG2 in plasma.

Table 6.3. Summary of tested techniques for the detection of TG2 protein/activity in plasma and sensitivity

Approach for TG2 quantification	Detection range (TG2 concentration and molarity)	Principle
Western Blotting	5-40 µg (total proteins)	Primary and secondary antibody; chemiluminescence detection
ELISA (Covalab)	0.02-1 µg/ml (0.2-12.8 nM)	Double monoclonal antibody sandwich: primary ab coating, detection with different primary ab, secondary ab-HRP conjugated, TMB, H_2SO_4, absorbance reading (450 nm)
TG activity assay (Jones et al., 1997; Scarpellini et al., 2009)	0.02-1 µg/ml (0.2-12.8 nM)	FN coating, biotin-cadaverine incorporation, extravidin peroxidase, TMB, H_2SO_4, absorbance reading (450 nm)
ELISA optimised in this study	0.0078-0.5 µg/ml (0.1-6.4 nM)	FN coating, detection with primary monoclonal ab, secondary ab-HRP conjugated, TMB, H_2SO_4, absorbance reading (450 nm)

Firstly, a test to verify if TG2 was detectable in plasma was performed by western blotting (**Fig. 6.7**). Plasma from two healthy subjects was quantified by Bradford assay and diluted in PBS pH 7.4 as previously described (Zhang et al., 2012). A range between 5 and 40 µg was loaded for each sample and blots were probed for TG2 with a classic monoclonal antibody efficient towards human TG2 (CUB7402) and β-actin (as loading control). No TG2 signal was detected in any of the plasma dilutions, contrary to the positive control (total lysate of prostate cancer cell line PC3) and TG2 standard which showed a TG2-specific band (MW ~75 kDa) (**Fig. 6.7**). A large band at around 63 kDa was observed by Red Ponceau staining, which is likely to be serum albumin (**Fig. 6.7**).

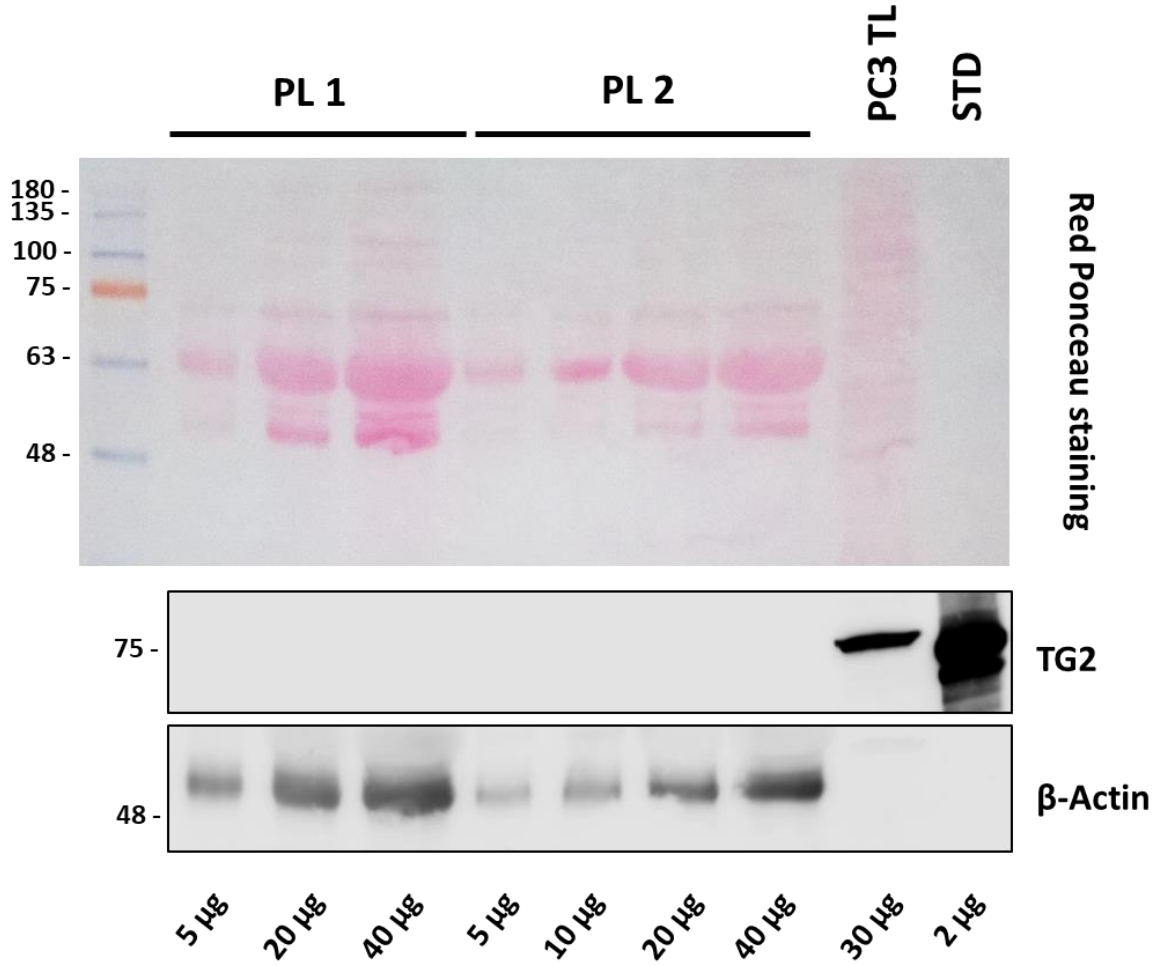

Figure 6.7. Detection of TG2 in plasma by WB. *Plasma from 2 healthy subjects (kindly donated by the John van Geest centre, NTU) was serially diluted in PBS pH 7.4 and resolved in a 12% acrylamide gel as described in Zhang et al., 2012. Plasma total protein concentration was assessed by Bradford assay and was about 75 µg/µl. Total lysate (TL) from PC3 (prostate cancer) cells was used as positive control for detection of human TG2. Red Ponceau staining of the nitrocellulose membrane is shown on top. Blots were probed with mouse monoclonal anti-TG2 (CUB7402) and rabbit polyclonal anti-β-Actin antibodies (N=2).*

Then a commercially available ELISA kit (supplied by Covalab UK) was tested, which had been developed for the detection of human TG2 and gplTG2. This kit is based on a solid phase sandwich ELISA principle, and consists in a 96-well plate coated with an anti-TG2 monoclonal antibody (as described in Methods chapter 2.2.15). A plasma pool from healthy

subjects commercially available was analysed and both undiluted plasma and serial dilutions up to 1:128 were tested, as well as a standard TG2 curve (0-1 µg/ml), as shown in **Fig. 6.8A**. No TG2 was detected in the plasma samples, whose absorbance values were below the background signal given by the sample buffer (**Fig. 6.8B**). The same was observed when even higher plasma dilutions were analysed. These results suggested that the kit was not suitable for detection of plasmatic TG2, possibly for the presence of plasma HAPs which might interfere with the interaction of the TG2 epitope with the monoclonal antibody coating.

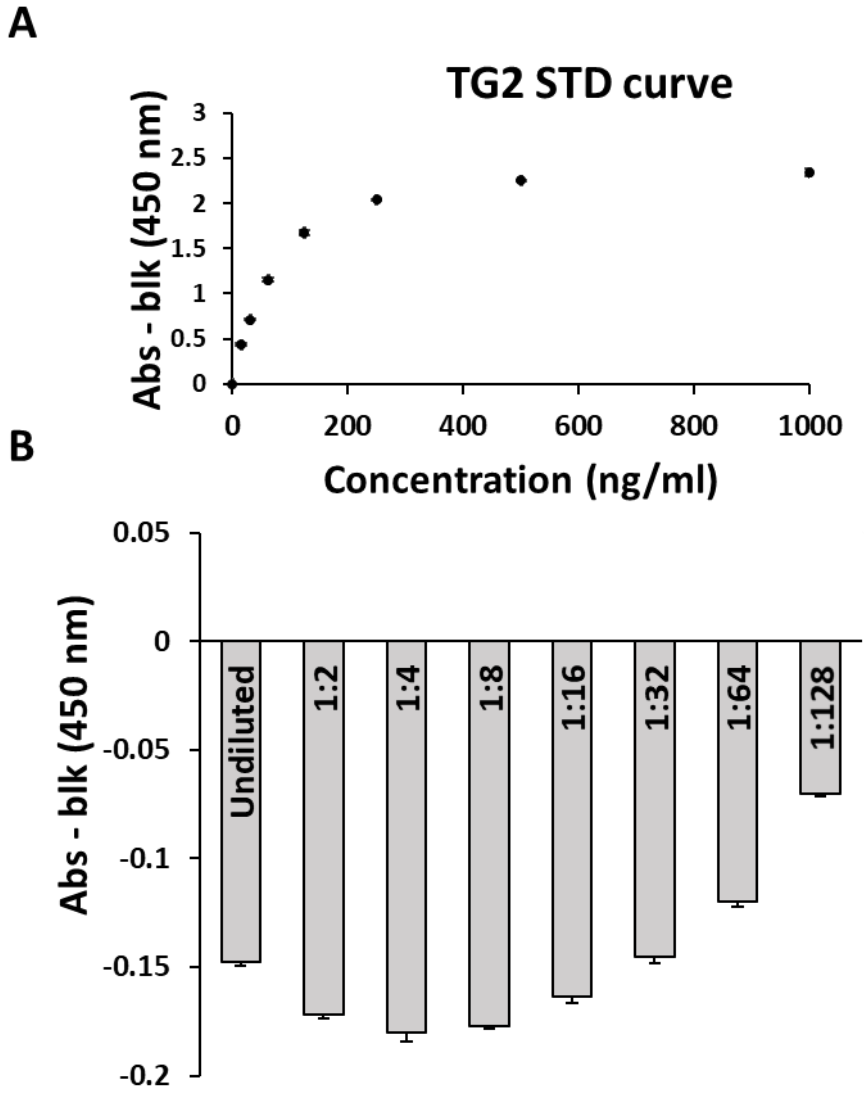

Figure 6.8. Detection of TG2 in plasma by ELISA using a commercial kit (Covalab). *Plasma from a pool of healthy subjects commercially available was serially diluted in sample buffer and analysed by ELISA (Covalab).* ***A)*** *Standard curve of TG2 (purified enzyme provided with the kit) expressed as mean of absorbance readings at 450 nm minus background ± SE (in duplicates).* ***B)*** *Histogram showing absorbance readings at 450 nm (minus blank) of plasma*

samples in a typical experiment (N=2, each point assessed in duplicate). All values were negative (below background level). Data are shown as mean absorbance minus blank ± SE. Sample buffer (blk): 0.230±0.004; undiluted plasma: 0.082±0.002.

6.2.3 Optimisation of an ELISA-based assay for detection of TG2 in plasma

Starting from the protocol described in Verderio et al., 2003, an assay for the detection of plasma TG2 was optimised, seeing that the commercially available kit was not adequate. The assay exploits TG2 capability to interact with FN, thanks to the conserved FN binding site present in TG2 N-terminal domain (Jeong et al., 1995; Hang et al., 2005; **Fig. 1.8** in Chapter 1). The principle (**Fig. 6.9**) is based on the capture of TG2 protein on a fibronectin coated plate and detection of TG2 specific antigen by the monoclonal mouse anti-TG2 antibody (CUB7402), followed by a secondary anti-mouse antibody conjugated to Horse Radish peroxidase (HRP) and classic development with HRP substrate TMB (3,3',5,5'-Tetramethylbenzidine). Details are presented in the Methods chapter 2.2.16.

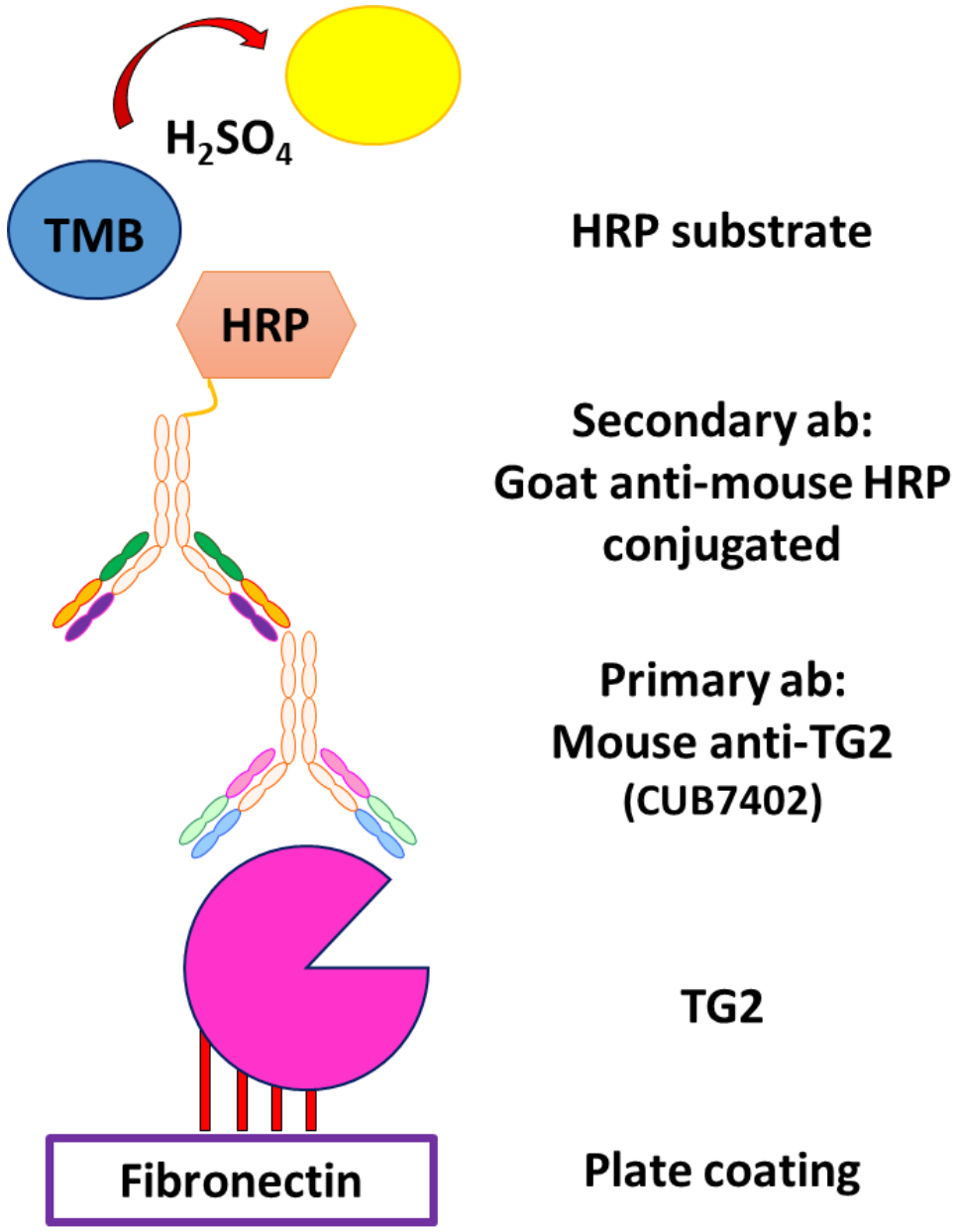

Figure 6.9. Optimisation of an ELISA-based assay for detection of TG2 in plasma. *Workflow representing the assay principle, which was optimised starting from an already published protocol developed by Verderio's research group (Verderio et al., 2003; Scarpellini et al., 2009). Briefly, a 96-well plate is coated with FN 5 µg/ml in Tris-HCl 50 mM pH 7.4 (or BSA as negative control), blocked for 1 hour at 37°C with 3% BSA in Tris-HCl 50 mM pH 7.4 and samples, diluted in blocking buffer, are incubated 2 hours at 37°C. After washing with Tris-HCl, plates are incubated 15 hours at 4°C with the primary antibody (mouse anti-TG2 CUB7402, 1:1000 dilution), then washed (in Tris-HCl 50 mM + 0.05% Tween20) and incubated 2 hours at RT with the secondary antibody (anti-mouse-HRP). After washing, the plate is developed by addition of TMB (7.5% in phosphate citrate buffer and 0.014% H_2O_2) and stopped with H_2SO_4. Absorbance reading was performed at 450 nm.*

Firstly, the maximum detection range of the assay was tested by generating a standard curve with gplTG2, which is efficiently recognised by the monoclonal antibody anti-TG2 CUB7402 (Verderio et al., 2003; Scarpellini et al., 2009) (**Fig. 6.10**). A 96-well plate was coated with 5 µg/ml FN for which TG2 has high affinity and incubated 15 hours at 4°C. After washing and blocking, a standard curve of gplTG2 immobilised on FN could be obtained from 0.0078 to 0.5 µg/ml of TG2 (correspondent to 0.1 nM and 6.4 nM of TG2 respectively). The standard curve was prepared in blocking buffer (BSA 3% in Tris-HCl pH 7.4) and in order to mimic conditions more similar to plasma, 1.22 mM Ca^{2+} was added, which is the average Ca^{2+} concentration in plasma (Martin et al., 2014; Moller et al., 2015). As TG2 is activated by calcium, and this might impact its binding to FN, a chelating agent was added (2 mM EDTA). After addition of the standard curve to the FN-coated plate, the assay was carried out as described in the Methods (chapter 2.2.16, **Fig. 6.9**). As shown in **Fig. 6.10**, when a combination of EDTA and Ca^{2+} was added to the standard curve, TG2 could be detected at a significantly higher sensitivity compared to TG2 in blocking buffer alone (**Fig. 6.10**, yellow and blue curve respectively). The tests performed with supplementation of either EDTA or Ca^{2+} alone, and with higher concentrations of TG2 standard, are available in the supplementary data (**Fig. S.1**). In conclusion, the optimal range for TG2 standard detection was 0.1-6.4 nM, equal to 0.0078-0.5 µg/ml of TG2 (**Fig. 6.10**), an improvement in the minimum detectable TG2 concentration as a result of the optimisation. In addition, the blank absorbance values were reduced from 0.265±0.01 (**Fig. S.1**) to 0.116±0.01 in the optimised assay (**Fig. 6.10**).

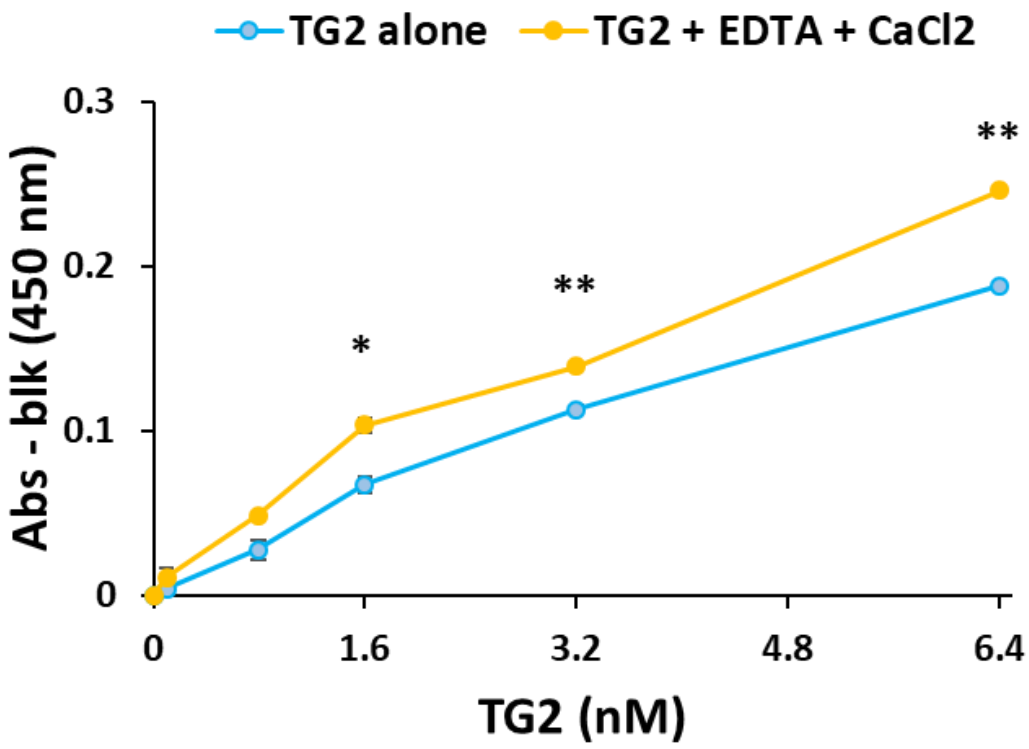

Figure 6.10. Optimisation of TG2 standard curve and assay conditions. *A standard curve of TG2 in blocking buffer alone, or supplemented with 2mM EDTA and 1.22 mM $CaCl_2$ was analysed by ELISA as described in Methods chapter 2.2.16. Data are expressed as mean of absorbance readings at 450 nm minus background ± SE (in duplicates). *p≤0.05; **p≤0.01.*

Different dilutions of a commercially available plasma pool from healthy subjects were analysed using the optimised TG2 ELISA. The pool of plasma was either tested undiluted or diluted up to 1:8 in blocking buffer, in the presence or absence of 2 mM EDTA (**Fig. 6.11A**). Dilutions above 1:2 gave absorbance values at background level (lower than 0.122), hence it was determined that plasma could not be diluted more than 1:2 (**Fig. 6.11A**). Additionally, the presence of 2 mM EDTA improved the precision of the dilution rate (PL/PL 1:2 ratio without EDTA = 3.01; PL/PL 1:2 ratio with EDTA = 2) (**Fig. 6.11B**, left histogram), also significantly increasing the detection of TG2 concentration in the diluted sample (**Fig. 6.11B**, right histogram).

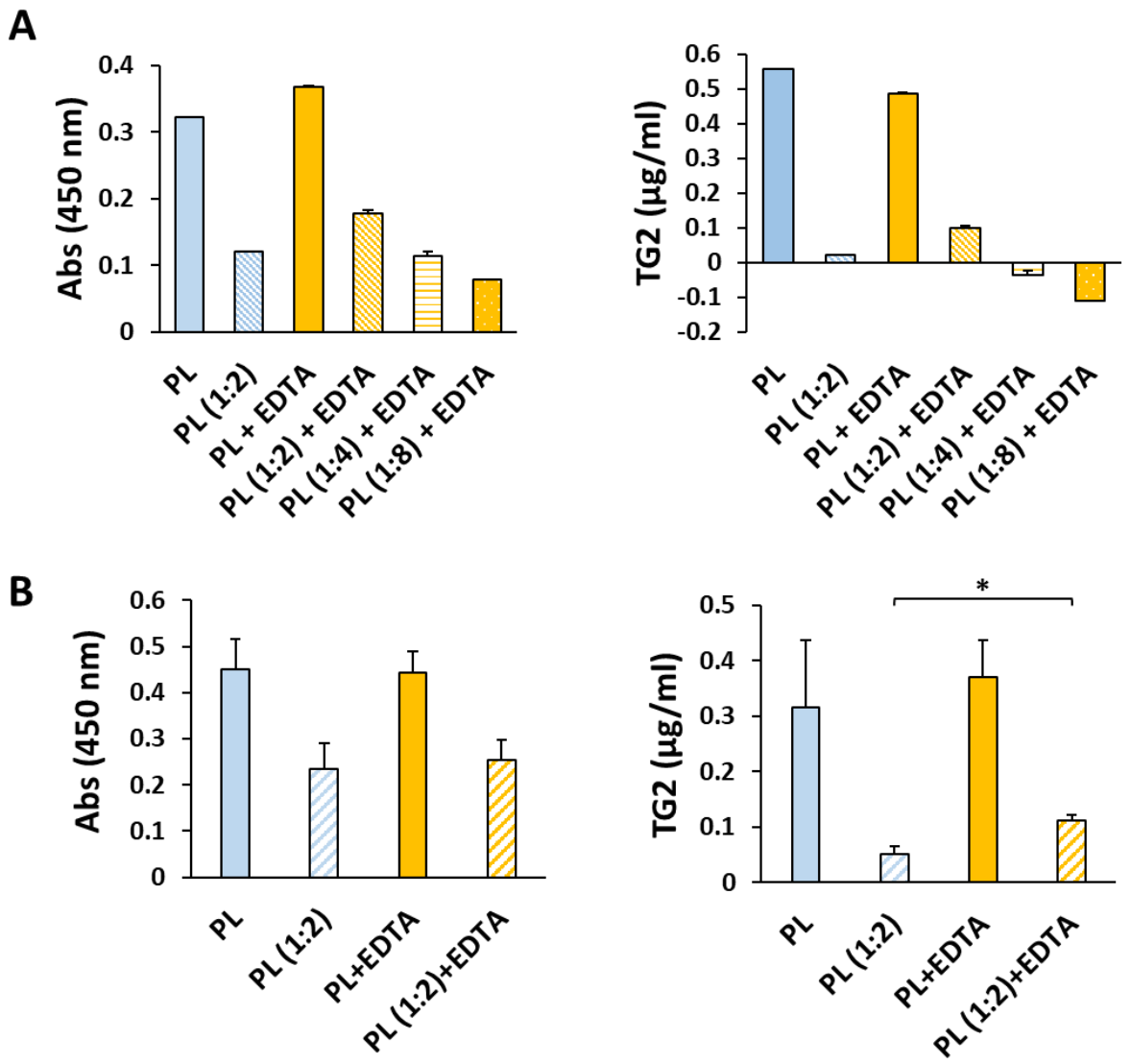

Figure 6.11. Optimisation of plasma dilutions. A) *Serial dilutions of plasma (PL, pool of healthy subjects) in blocking buffer (3% BSA in assay buffer) with or without addition of 2 mM EDTA (50 µl/well). A representative experiment is shown. Plot on the right shows correspondent TG2 mean concentrations ± SE (in duplicates). Absorbance raw values PL: 0.323±0.00; PL 1:2: 0.12±0.00; Blank (Blk): 0.104±0.002; PL+EDTA: 0.367±0.002; PL+EDTA 1:2: 0.179±0.004; PL+EDTA 1:4: 0.114±0.006; PL+EDTA 1:8: 0.078±0.00; Blank+EDTA (Blk): 0.122±0.001. TG2 concentrations were extrapolated from appropriate standard curves.* ***B)*** *Average of 2 independent experiments, confirming better performance of plasma dilutions in the presence of EDTA. Data are presented as mean ± SE of raw absorbance readings (left) or TG2 concentrations (right). *p≤0.05.*

As conclusive proof of the assay specificity for TG2 detection in plasma, the spike-in of increasing concentrations of gplTG2 in plasma was performed to verify how much plasma would interfere with the detection of the antigen. A standard curve of gplTG2 was prepared in blocking buffer (supplemented with 2 mM EDTA and 1.22 mM CaCl2) and in undiluted plasma (pool of healthy controls, supplemented with 2 mM EDTA), from 0.0078 to 0.25 µg/ml (**Fig. 6.12A**). The comparison of the two curves revealed that plasma partially covered the detection of gplTG2, giving lower sensitivity compared to blocking buffer (**Fig. 6.12A**, purple and yellow curve respectively). Then a 1:2 dilution, which was expected to decrease plasma background, was tested to verify if it would perform better compared to undiluted plasma. Hence standard curves were prepared as described in Fig. 12A but in plasma diluted 1:2 in blocking buffer (containing 2 mM EDTA) (**Fig. 6.12B**). A comparison between TG2 in undiluted plasma (purple line) and TG2 in 1:2 diluted plasma (green line) revealed that plasma dilution improved the detection of spike-in TG2, even though in both cases TG2 values were still lower compared to the STD curve in blocking buffer (yellow curve) (**Fig. 6.12B**).

In conclusion, the 1:2 dilution of plasma was the best compromise to diminish plasma background signal and still be able to specifically detect TG2.

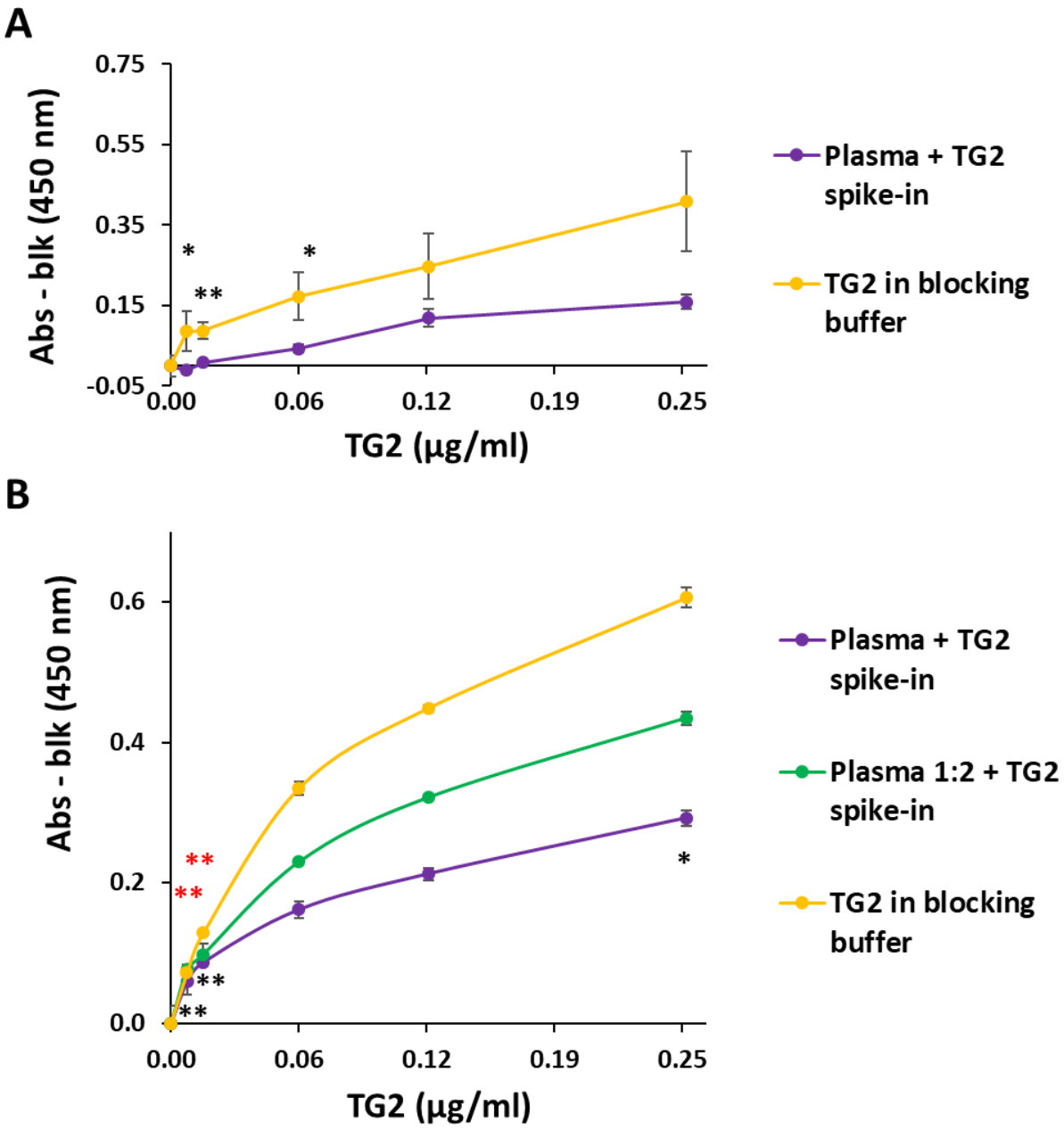

Figure 6.12. Spike-in of TG2 in plasma. A) *TG2 was added at increasing concentrations (from 0.0078 to 0.25 µg/ml) to undiluted plasma (containing 2 mM EDTA) and blocking buffer (containing 2 mM EDTA and 1.22 mM $CaCl_2$). Data are expressed as mean of absorbance readings at 450 nm minus relative blanks (namely blocking buffer for yellow curve and plasma for purple curve) ± SE (in duplicates). *p≤0.05; **p≤0.01.* ***B)*** *TG2 was added at increasing concentrations (from 0.0078 to 0.25 µg/ml) to undiluted plasma and plasma diluted 1:2 in blocking buffer (containing 2 mM EDTA). Data are expressed as mean of absorbance readings at 450 nm minus relative blanks (namely blocking buffer for yellow curve, plasma for purple curve and plasma 1:2 for green curve) ± SE (in duplicates). *p≤0.05; **p≤0.01. Black asterisks refer to plasma spike-in vs TG2 in blocking buffer comparison, while red asterisk refer to plasma 1:2 spike-in vs TG2 in blocking buffer comparison.*

6.2.4 Detection of TG2 in plasma of dementia patients

In order to determine if plasma TG2 levels correlated with dementia, plasma samples from four cohorts were selected: healthy subjects (CTR), and patients affected by sporadic Alzheimer's disease (sAD), Mild cognitive impairment (MCI) and Frontotemporal Lobar Degeneration (FTLD). Power analysis revealed that 10 subjects per cohort would be sufficient to perform a statistically relevant analysis (as described in section 6.2.1), hence 15 samples were included for each group (**Table 6.4**). All blood samples were collected according to standard procedures and with ethical consent, and clinical diagnosis was made following international guidelines as already described in section 6.2.1.

Table 6.4. Demographic characteristics of the patients' cohorts

Diagnosis	Age	Sex (Males/Females)	N
CTR	*69.1±4.1*	*5 / 10*	*15*
AD	*69.0±4.7*	*6 / 8*	*14*
MCI	*70.3±3.8*	*8 / 7*	*15*
FTLD	70.3±4.8	7 / 8	15

CTR: Healthy; AD: Alzheimer's Disease; MCI: Mild Cognitive Impairment; FTLD: Frontotemporal Lobar Degeneration

Samples were analysed by ELISA assay following the settings optimised as explained in section 6.2.3. Data (TG2 antigen) were expressed as concentration (µg/ml) relatively to a standard curve obtained with gplTG2. Statistical analysis of TG2 concentration in the analysed plasma did not show significant differences among the study groups (**Fig. 6.13**). The FTLD group showed a wider variability compared to the others, however CTR and diagnosed patients had similar levels of plasma TG2.

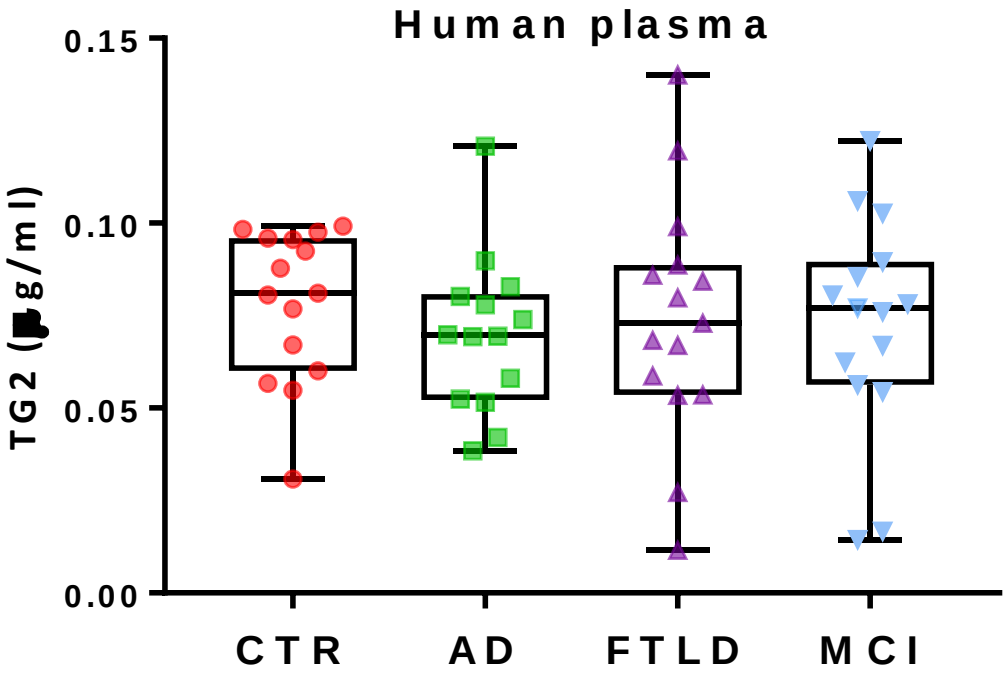

Figure 6.13. Detection of TG2 in plasma of healthy and dementia patients by ELISA. *Plasma from healthy subjects (CTR, N=15 + 1 pool of healthy subjects from Tebu-Bio) and patients affected by Alzheimer's disease (AD, N=14), Frontotemporal dementia (FTLD, N=15) and Mild cognitive impairment (MCI, N=15) were diluted 1:2 in blocking buffer (with 2mM EDTA) and analysed by ELISA (in house optimised protocol). Box plot shows TG2 concentration in plasma, specifically the minimum, mean, maximum, 25th and 75th percentiles. CTR: 0.078±0.005; AD: 0.070±0.006; FTLD: 0.074±0.008; MCI: 0.073±0.008. p: NS (Student's t-test and one-way ANOVA).*

This result confirmed that TG2 could be detected in patients' plasma, however the analysis of whole plasma did not allow for the identification of significant differences among the analysed groups. It was hypothesised that the presence of HAPs in plasma (e.g. albumin), although diluted, could still partially cover TG2 detection and thus hinder the measurement of small variations. Furthermore, it was reasoned that TG2 could be included in EVs in plasma, since it was found bound to EVs in urine in our recent work (Furini et al., 2018). Therefore, the investigation proceeded by exploring if TG2 was detectable in EVs isolated from plasma. If this was the case, the TG2 screening in patients could be conducted in plasma EVs fractions, thus eliminating the issue of HAPs interference.

6.2.5 Detection of TG2 in EVs isolated from plasma

The isolation of EVs was optimised using a commercially available plasma pool of healthy subjects according to a published isolation protocol (Gagni et al., 2015) based on serial centrifugations as schematically shown in **Fig. 6.14A** (described in Methods chapter 2.2.9.3). Plasma (100 µl) was diluted 1:100 in particle-free PBS, centrifuged at low speed to discard large particulates, and the supernatant (SN) passed through a 0.22 µm syringe filter (SN_f). The SN_f was then ultracentrifuged to obtain the EVs P100' pellet, which was either directly analysed, or additionally ultracentrifuged to obtain the EVs P100'' pellet (**Fig. 6.14A**). The inclusion of a washing step of P100' was assayed to test whether it would result into a cleaner EVs preparation without material loss (P100''), which was checked by Nanoparticle Tracking Analysis (NTA). NTA analysis of P100' and P100'' EVs pellets showed a particles size of about 103 and 130 nm respectively, and particle concentration decreased from about $4.4x10^{10}$ to $2.5x10^{9}$ particles/ml respectively (**Fig. 6.14B**). When similarly prepared EVs were analysed by western blotting, a marked decrease of EVs markers in P100'' compared to P100' was observed, namely FLOT-2, TSG101 and HSC70 (**Fig. 6.14C**). The BCA protein quantification confirmed this trend, as P100'' was 7-fold less abundant compared to P100' (mean protein amount P100': 46.1±29.9; P100'': 6.7±4.4; total amount is expressed in µg). Red Ponceau staining of the nitrocellulose membrane showed an intense band at about 63kDa, likely to be albumin, which decreased after the PBS washing, suggesting that the wash step was able to diminish the amount of albumin co-pelleted with the plasma EVs, however possibly also rare markers (**Fig. 6.14C**, comparison between P100' and P100'' lanes). TG2 protein signal, although of limited quality, was present in EVs. This was a new finding, as no one has previously reported TG2 in plasma EVs. As expected, TG2 band was reduced in P100'' pellet (**Fig. 6.14C**, red arrow).

Even if the P100'' was a cleaner preparation presenting less albumin contamination, the loss of EVs due to the further PBS wash was too great for the detection of TG2. Therefore, the analysis of EVs isolated from patients plasma was performed using a single ultracentrifugation step.

A

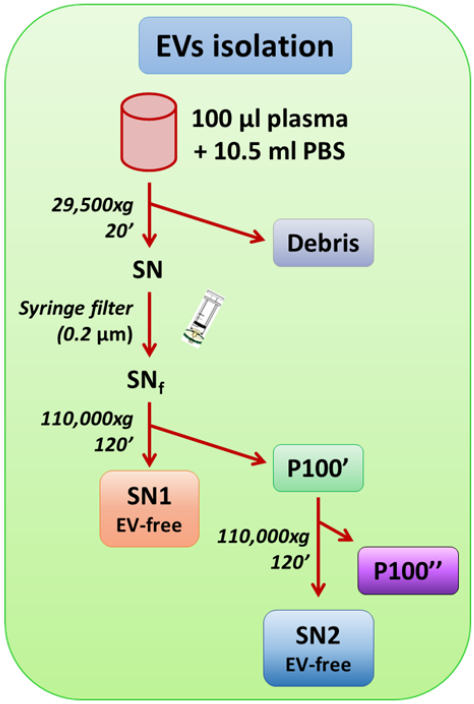

B

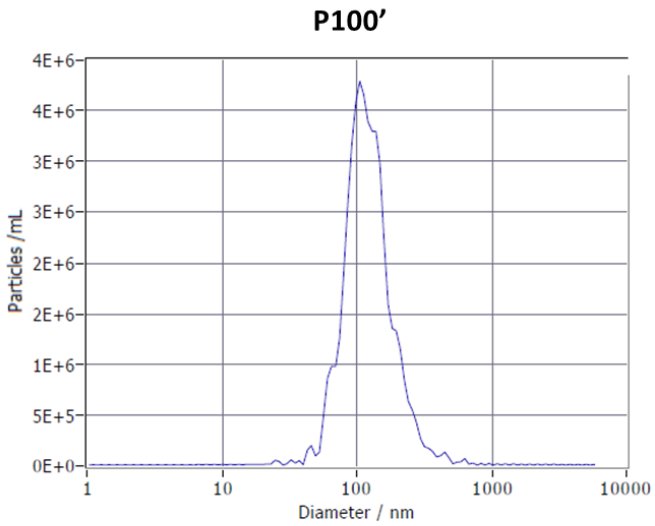

Size: 103.5 ± 2.2 nm
Concentration: 4.4x10^{10} prt/ml

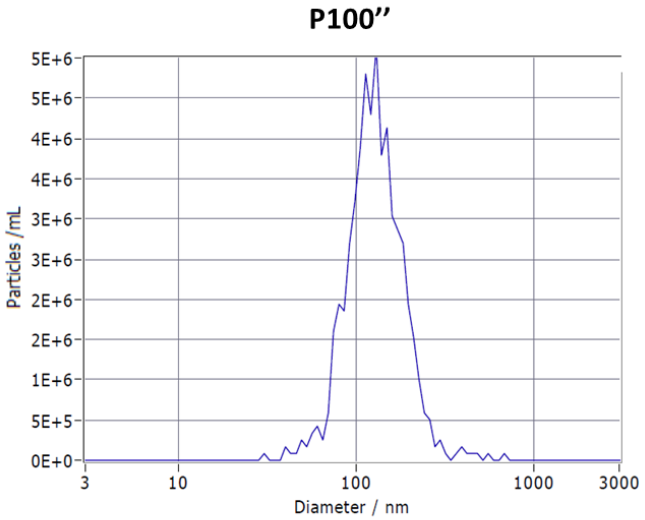

Size: 128.0 ± 4.1 nm
Concentration: 2.5x10^{9} prt/ml

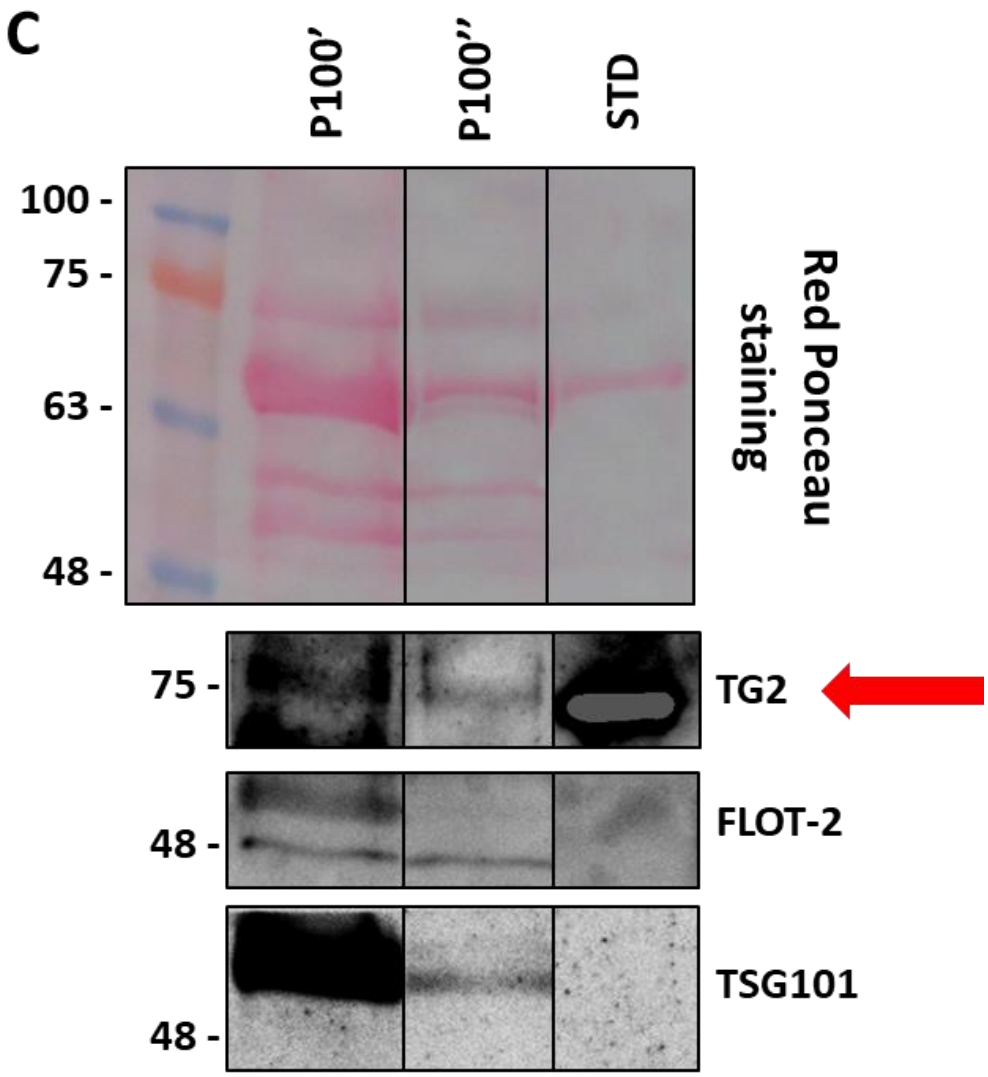

Figure 6.14. Detection of TG2 in small EVs isolated from plasma by WB. *Small EVs were isolated from 100 µl of plasma from a pool of healthy subjects for TG2 detection.* ***A)*** *Graphical representation of EVs isolation protocol from plasma with either one (P100') or two (P100'') ultracentrifugation steps.* ***B)*** *NTA analysis of EVs size and distribution of P100' and P100'' pellets resuspended in 100 µl of PBS by ZetaView. One representative graph for each pellet is shown (N=2).* ***C)*** *Western blotting analysis of EVs from isolations with either one or two ultracentrifugations. Blots were probed for EVs marker FLOTILLIN-2 and for TG2 (CUB7402 antibody), then stripped and re-probed for TSG101 detection (N=3). Human recombinant TG2 was used as positive control (20 ng).*

EVs were isolated starting from 100 µl of plasma from 4 CTR and 4 sAD patents. Western blotting analysis of the P100' pellets showed positive signals for EVs markers FLOT-2 and TSG101 (**Fig. 6.15**). TG2 displayed a double band, one at the MW of the TG2 standard and the other seemed to be below 75 kDa, hence of lower MW compared to the human TG2 standard, suggesting they might be the result of an aspecific binding (**Fig. 6.15**).

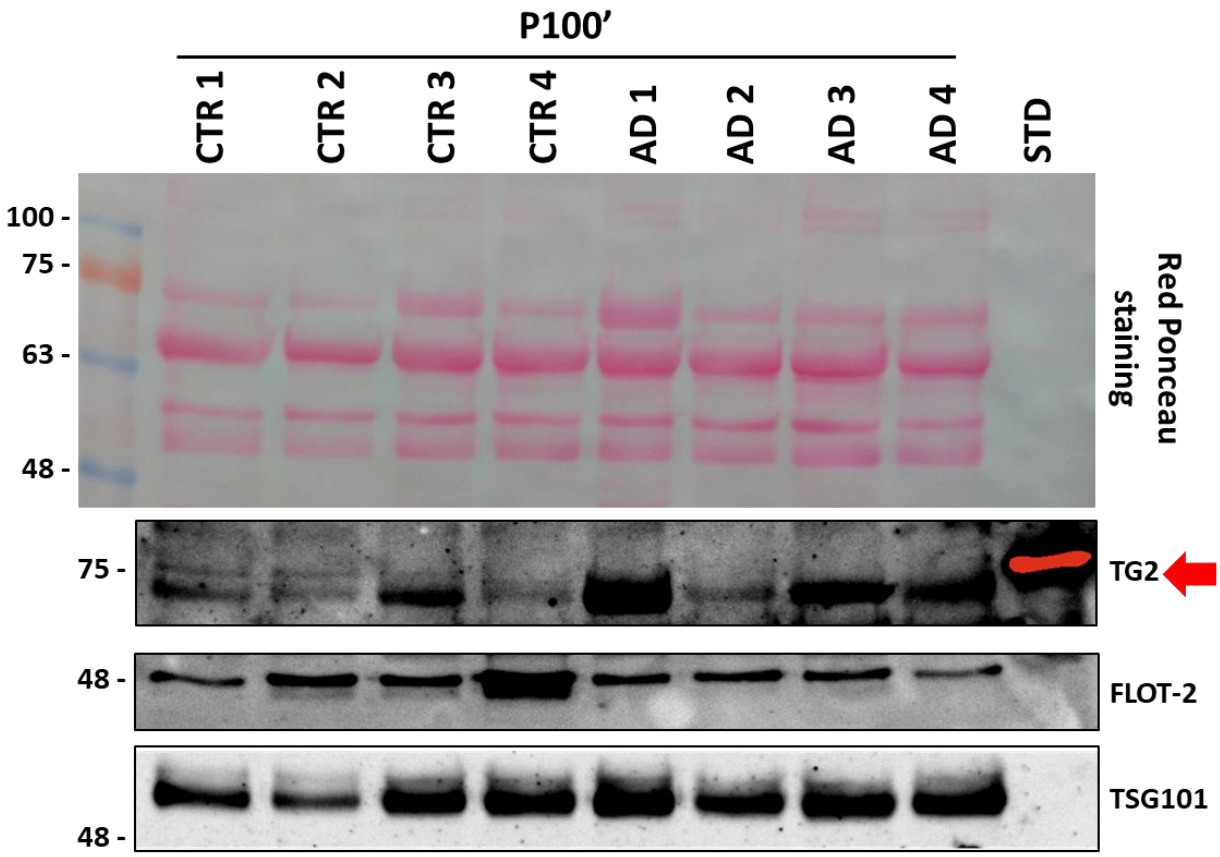

Figure 6.15. Detection of TG2 in small EVs isolated from plasma of CTR and AD subjects by WB. *Small EVs were isolated from 100 µl of plasma (P100') from healthy subjects (CTR, N=4) and Alzheimer's disease affected patients (AD, N=4). Blots were probed for EVs marker FLOTILLIN-2 and for TG2, then stripped and re-probed for detection of TSG101. Human recombinant TG2 was used as positive control (20 ng).*

The blot was of difficult interpretation, given the high background. To investigate if other techniques could be more efficient than western blotting for the detection of TG2 in plasma EVs, the optimised ELISA assay described in section 6.2.3 was employed. TG2 was detected in plasma (diluted 1:2 in blocking buffer containing 2 mM EDTA as previously optimised) and about 32% less in lysed EVs (LB with 2 mM EDTA) (**Fig. 6.16A**). Detection in whole EVs was significantly lower (97% and 95.5% less compared to plasma and lysed EVs respectively), suggesting that TG2 was mainly localised in the plasma EVs lumen. Proteins precipitated from EV-free supernatants were below blank values (**Fig. 6.16A**), which indicated that all detected TG2 was vesicle-bound. Therefore, despite the TG2 value was higher in plasma than in the EVs lysate, taking into account possible loss of material in preparing EVs, these data point at an enrichment of TG2 in EVs in plasma. Initial investigation of TG2 activity in the same samples using an in house TG activity assay (Jones et al., 1997; Scarpellini et al., 2009) revealed a higher TG specific activity in EVs than total plasma (**Fig. 6.16B**).

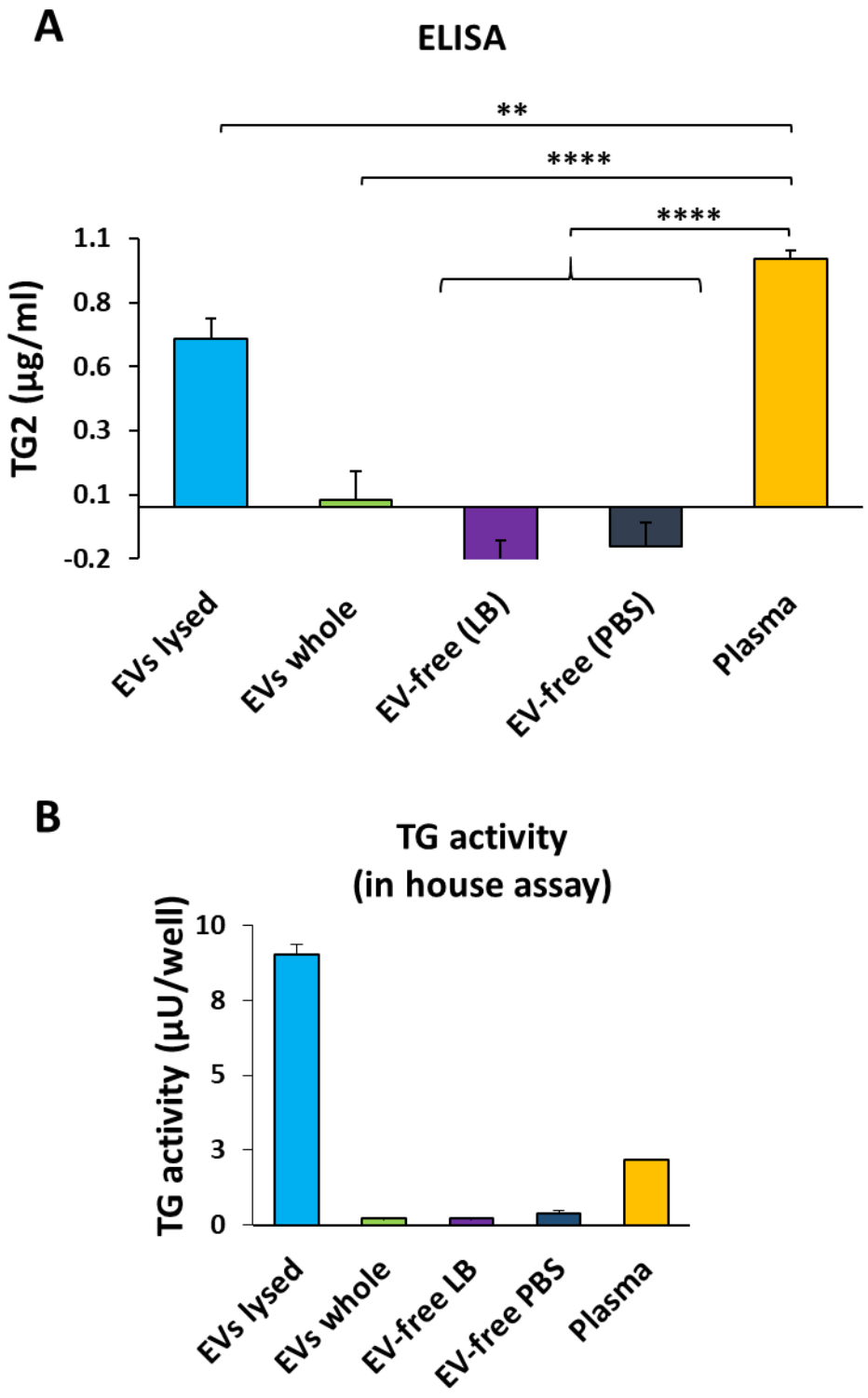

Figure 6.16. Detection of TG2 in small EVs isolated from plasma by plate assays. *Small EVs (P100') were isolated from 100 µl of plasma from a pool of healthy subjects and analysed for TG2 detection whole (PBS) or lysed (sucrose lysis buffer - LB). Also TCA-precipitated proteins from EV-free supernatants were analysed. PBS and LB absorbance values (blanks) were subtracted from whole and lysed EVs values respectively.* ***A)*** *TG2 protein levels in plasma, EVs and EV-free supernatants were analysed by in house developed ELISA. Each sample was analysed in duplicate (N=3). All relative blanks were first subtracted and then*

*values were normalised to plasma TG2 concentration. Plasma was diluted 1:2 in blocking buffer and values were corrected by dilution factor. Data is expressed as mean µg/ml ± SE (mean absorbance plasma diluted 1:2: 0.33±0.05; EVs lysed: 0.38±0.06; EVs whole: 0.28±0.05; EV-free LB: 0.27±0.05; EV-free PBS: 0.25±0.04; PBS: 0.25±0.05; LB: 0.26±0.05). **p≤0.01; ****p≤0.0001.* ***B)*** *TG2 activity levels in plasma, EVs and EV-free supernatants by in house developed enzymatic assay. Each sample was analysed in duplicate (N=1). Data is expressed as mean µU/well ± SE (mean absorbance plasma pool: 0.115±0.00; EVs lysed: 0.34±0.01; EVs whole: 0.06±0.01; EV-free LB: 0.042±0.001; EV-free PBS: 0.062±0.007; PBS: 0.051±0.002; LB: 0.053±0.004).*

6.2.6 Detection of TG2 crosslinking product ε-(γ-glutamyl)-lysine (EGGL)

Another approach to investigate the relevance of TG2 as a biomarker for dementia is the detection of TG2-specific crosslinking by-product, namely the Nε-(γ-L-glutamyl)-L-lysine isopeptide (EGGL). EGGL levels in CSF were found to correlate with dementia in previous studies, being significantly increased in dementia patients (AD, VaD and HD) compared to controls when measured by a HPLC-based approach (Nemes et al., 2001; Jeitner et al., 2008). EGGL have also been identified by immunohistology in brain using a commercially available anti-EGGL antibody (81D4) (Citron et al., 2002; Wilhelmus et al., 2009), however this antibody has never been used to detect TG crosslinking products in biological fluids. In order to develop an immuno-based approach for the detection of crosslinks in plasma using the anti-EGGL antibody 81D4, the antibody efficiency to detect EGGL was explored by generating crosslinking products *in vitro*. TG2 (200 ng) was allowed to react with its substrate FN fragment of 30 kDa (Jeong et al., 1995; Hang et al., 2005) in activating conditions (5 mM $CaCl_2$ and 10 mM DTT) for increasing incubation times at 37^{o}C and resolved by SDS-page in reducing conditions (**Fig. 6.17A**) (as described in Methods chapter 2.2.17 and Fig. 6.17 legend). A chelating agent (EDTA 5 mM) was included as negative crosslinking control to block TG2 catalytic activity and hence inhibit crosslinks generation. In these conditions, the TG2 band (about 75 kDa) was visible only in the presence of EDTA (**Fig. 6.17A**, +EDTA lanes), while in activating buffer it "disappeared" and visibly accumulated at the top of the gel. TG2 processing (polymerisation) of the 30kDa fragment

was evident by its reduction when calcium was available (**Fig. 6.17A**, -EDTA lanes). The reaction occurred as early as 30 seconds time point, the first to be monitored. Lowering the temperature to 4°C and room temperature (RT) did not stop TG2 processing of FN or reduce it to produce a smaller polymer that could be separated by SDS-page and could be used as a positive control of EGGL reaction (**Fig. 6.17B**). When the same samples were analysed by western blotting, EGGL was visible only at the top of the gel, confirming FN polymerisation (**Fig. 6.17C,** left and central blot). TG2 probing with anti-TG2 antibody (CUB7402) showed a specific band both at the expected 75 kDa and in correspondence to the top aggregates, suggesting that also TG2 becomes crosslinked by itself (**Fig. 6.17C,** right blot).

A

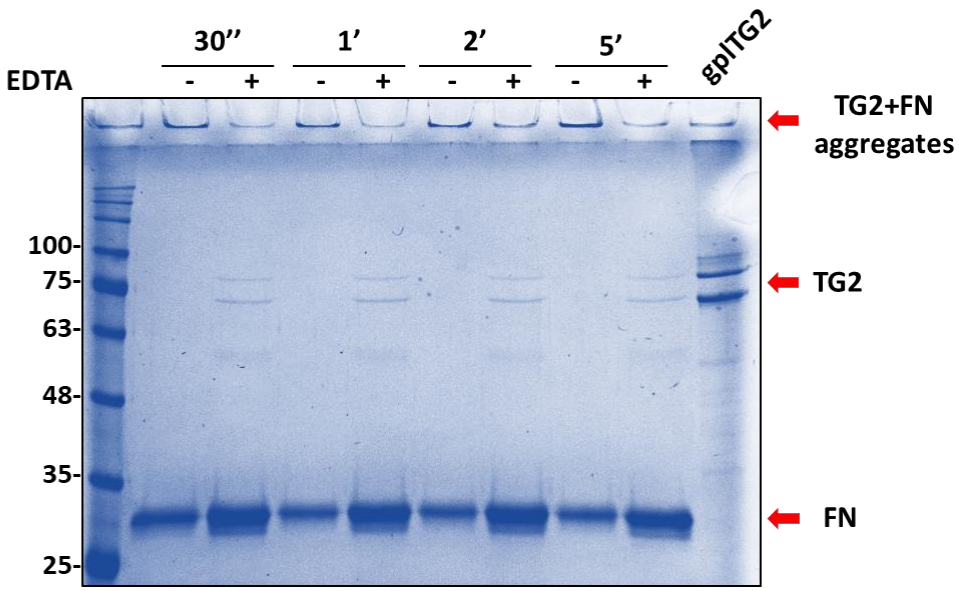

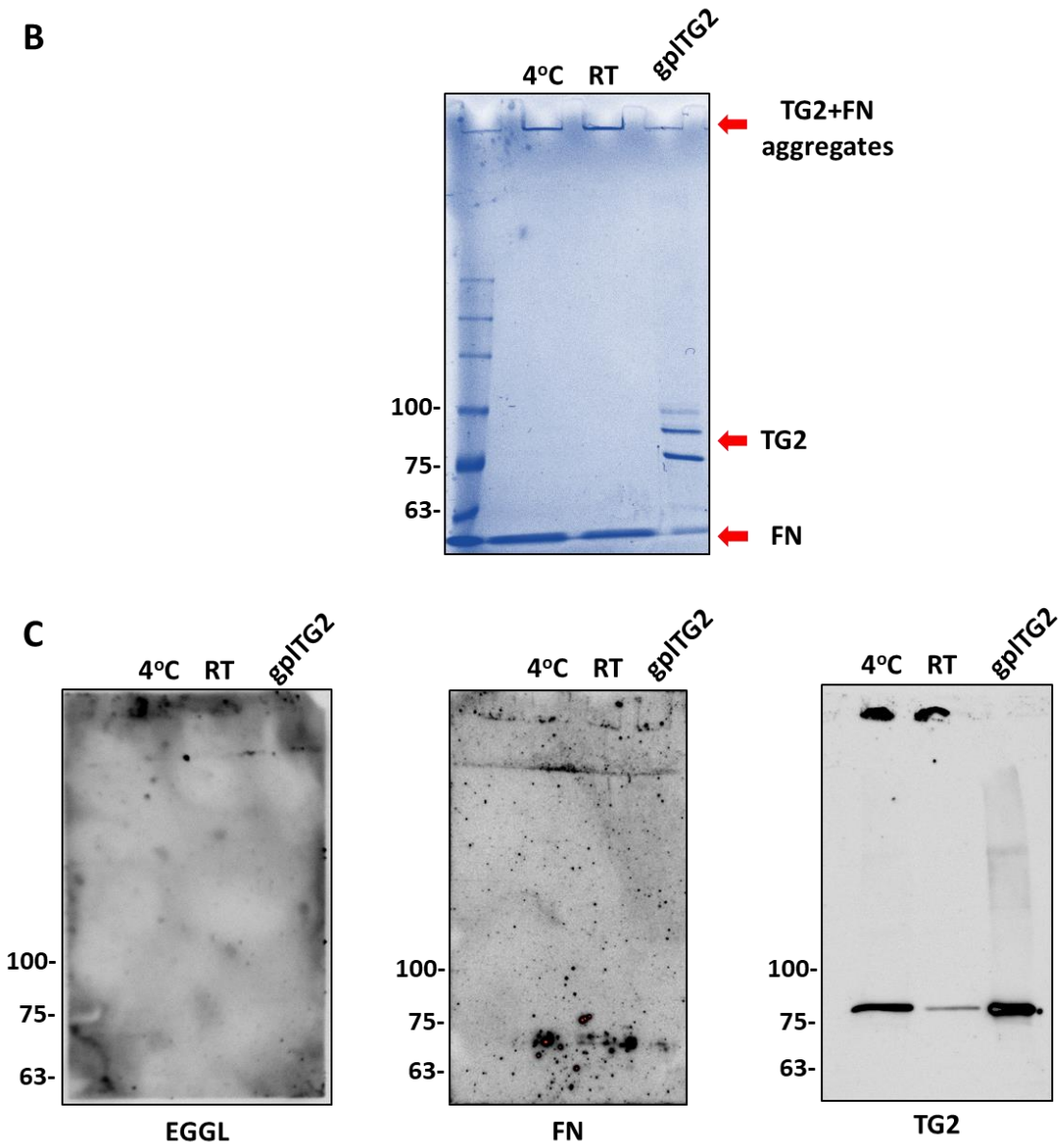

Figure 6.17. Detection of EGGL by SDS page. *EGGL crosslinks were generated by incubation of TG2 (200 ng) with 30 kDa FN fragment (5 µg) in activating conditions (Tris-HCl 50 mM pH 7.4, 5 mM $CaCl_2$ and 10 mM DTT).* ***A)*** *Crosslinks were generated at increasing incubation times at 37°C, in the presence or absence of 5 mM EDTA (to inhibit TG2 activity and EGGL formation). After incubation, samples were diluted with 6X Laemmli buffer, boiled, loaded in a 10% acrylamide gel and run as described in Methods chapter 2.2.3.3. Blue Coomassie stain of separated proteins was obtained by 1 hour incubation with InstantBlue and decolouration with water.* ***B)*** *Crosslinks were generated at 4°C or room temperature (RT) for 15 minutes and analysed as described above in a 6% acrylamide gel.* ***C)*** *Same samples described in B were analysed by western blotting (6% acrylamide gels). Blots were probed with mouse anti-EGGL (Abcam), then stripped and re-probed with Rabbit polyclonal anti-FN (F3648) and mouse monoclonal anti-TG2 (CUB7402).*

Since a crosslinking product of size compatible with gel electrophoresis could not be generated *in vitro*, immunodetection of EGGL could not be optimised in this way. Optimisation was crucial as antibody 81D4 has been often attributed unspecific binding and indeed a positive control is fundamental in all immune assay. As a way forward the dot blot technique was explored. Full length FN was employed as a substrate as its size was no longer an issue in a dot blot. Data showed that the anti-EGGL antibody stained FN dots only when this was incubated with TG2 in activating buffer (**Fig. 6.18**, first red arrow from the left), indicating crosslinking. Anti-EGGL antibody therefore was specific for the crosslinked form of FN. However, some immunoreactivity was also seen when TG2 alone was incubated in activating buffer (**Fig. 6.18**, second red arrow from the left), suggesting that also TG2 is a crosslink substrate. Notably EDTA, which inhibits TG2 activity, led to a background signal in the dot, again suggesting specificity of the anti-EGGL antibody.

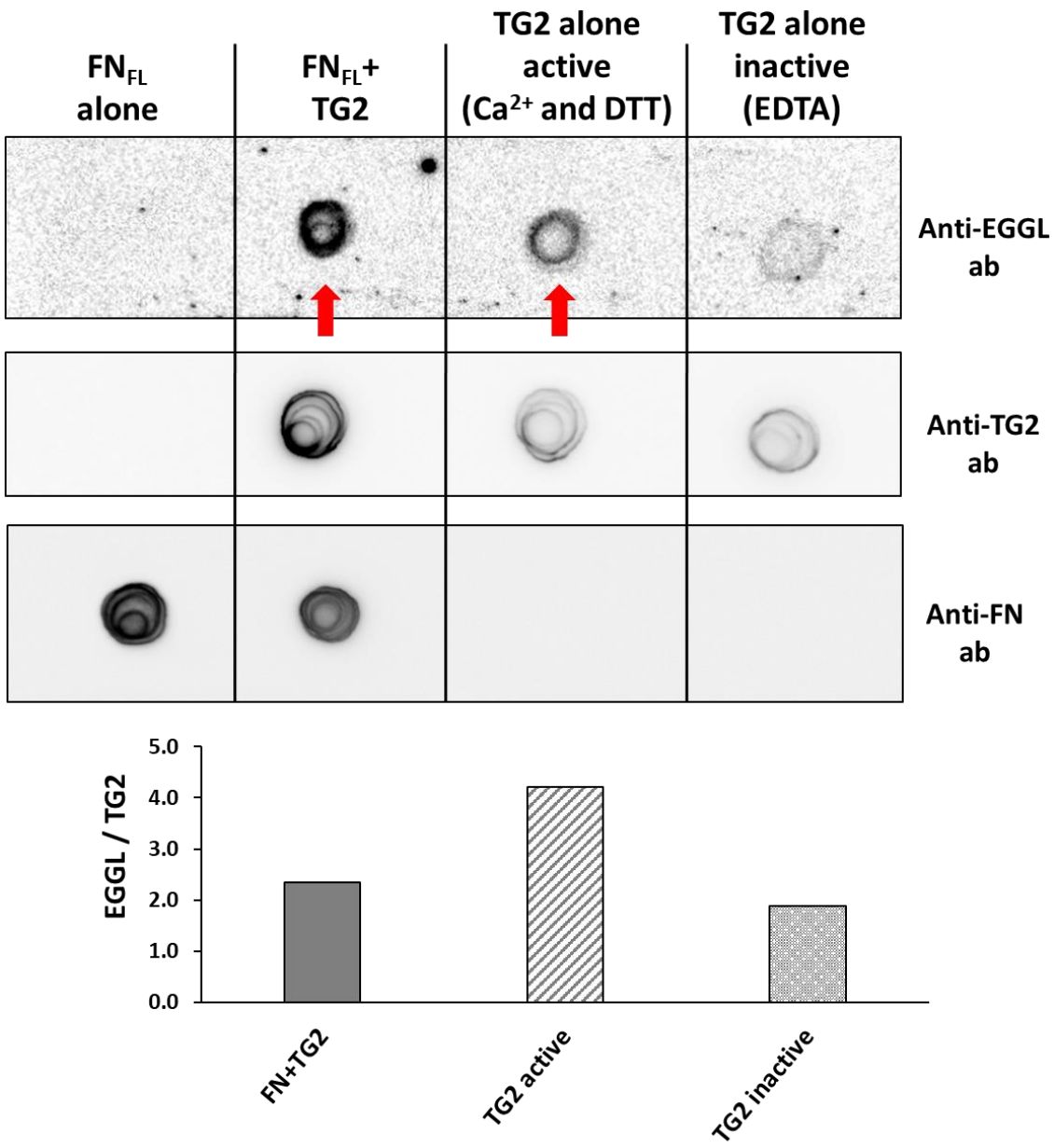

Figure 6.18. Detection of EGGL by dot blot. *EGGL crosslinks were generated by incubation of TG2 (200 ng) with FN (500 ng) in activating conditions (Tris-HCl 50 mM pH 7.4, 5 mM CaCl2 and 10 mM DTT), 15 minutes at room temperature. Controls were FN alone and TG2 alone in activating or deactivating conditions (5 mM EDTA). Samples were then loaded directly on a nitrocellulose membrane (5 µl each) and probed for TG2 (mouse monoclonal CUB7402), FN (rabbit polyclonal F3648) and GGEL dipeptide (mouse monoclonal 81D4), as described in Methods chapter 2.2.3.10. Plot at the bottom shows densitometry analysis of EGGL normalised to TG2.*

Next, the detection of EGGL in plasma was tested by dot blot. Serial dilutions of a plasma pool of healthy subjects in Tris-HCl 50 mM pH 7.4 were spotted directly on nitrocellulose (5 µl each) and probed for EGGL, TG2 and FN (**Fig. 6.19**). FN +/- TG2 were also spotted as positive and negative control respectively. The EGGL generated in the lab were also included as controls, which showed the same trends as in **Fig. 6.18**. EGGL were detected down to 1:500 dilution of plasma, with 1:100 giving the best result (**Fig. 6.19**, red arrow).

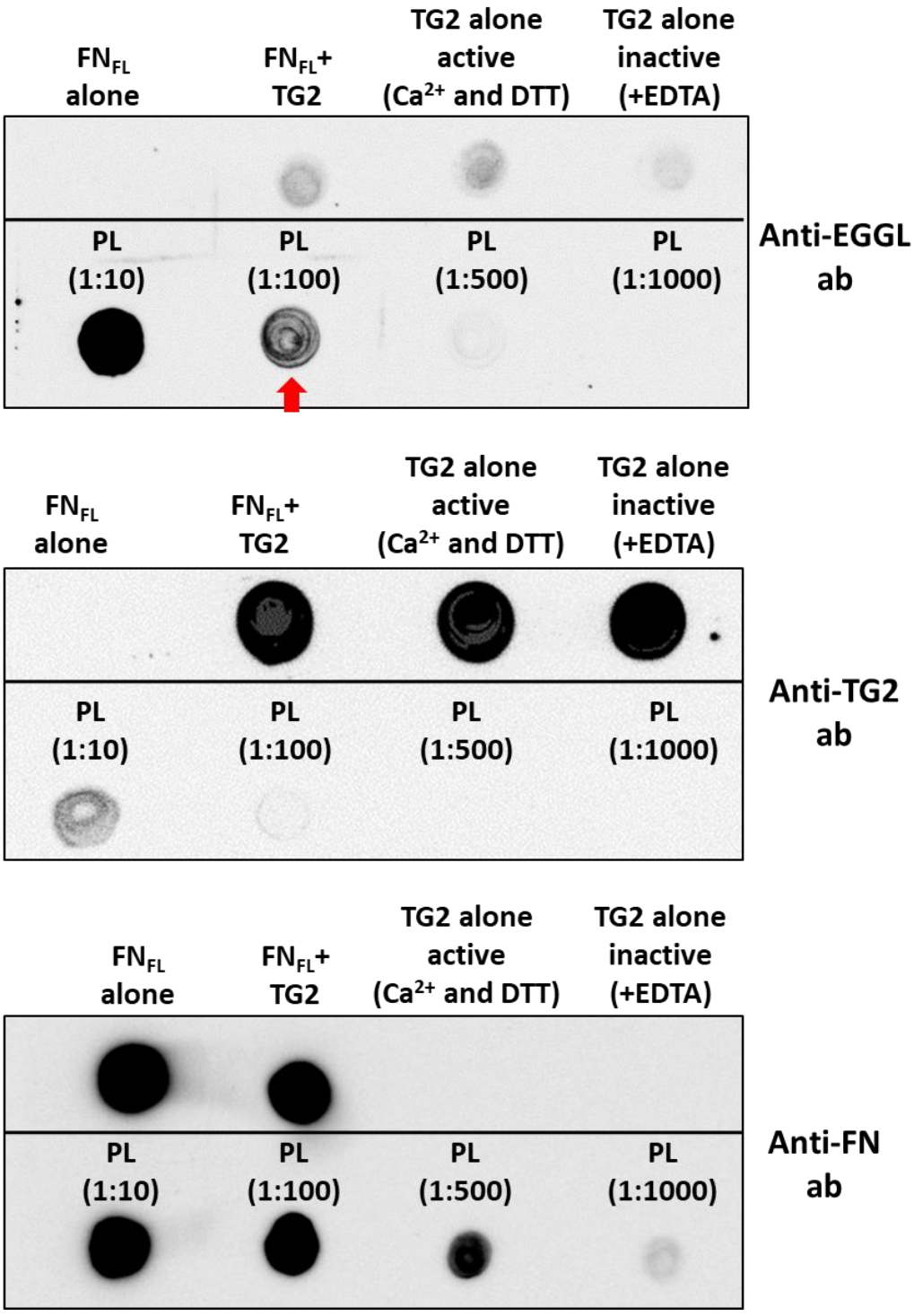

Figure 6.19. Detection of EGGL in plasma by dot blot.

Figure 6.19. Detection of EGGL in plasma by dot blot. *Serial dilutions of plasma in Tris-HCl 50 mM pH 7.4 were loaded directly on a nitrocellulose membrane (5 µl each) and probed for TG2 (mouse monoclonal CUB7402), FN (rabbit polyclonal F3648) and GGEL dipeptide (mouse monoclonal 81D4), as described in Methods chapter 2.2.3.10. The red arrow highlights the best plasma dilution for detection of EGGL (1:100).*

This showed the potential of the approach to identify EGGL crosslinks specifically. The presence of TG2 crosslinks was investigated in plasma of healthy subjects (CTR) and dementia patients (AD, FTLD and MCI). Four samples from each cohort were randomly selected, diluted 1:100 in Tris-HCl 50 mM pH 7.4 and processed as described above. EGGL signal, normalised to FN, was 1.7-fold higher in AD plasma compared to control, albeit not at significant levels (p=0.2) (**Fig. 6.20**). No differences were observed in the other groups (**Fig. 6.20**).

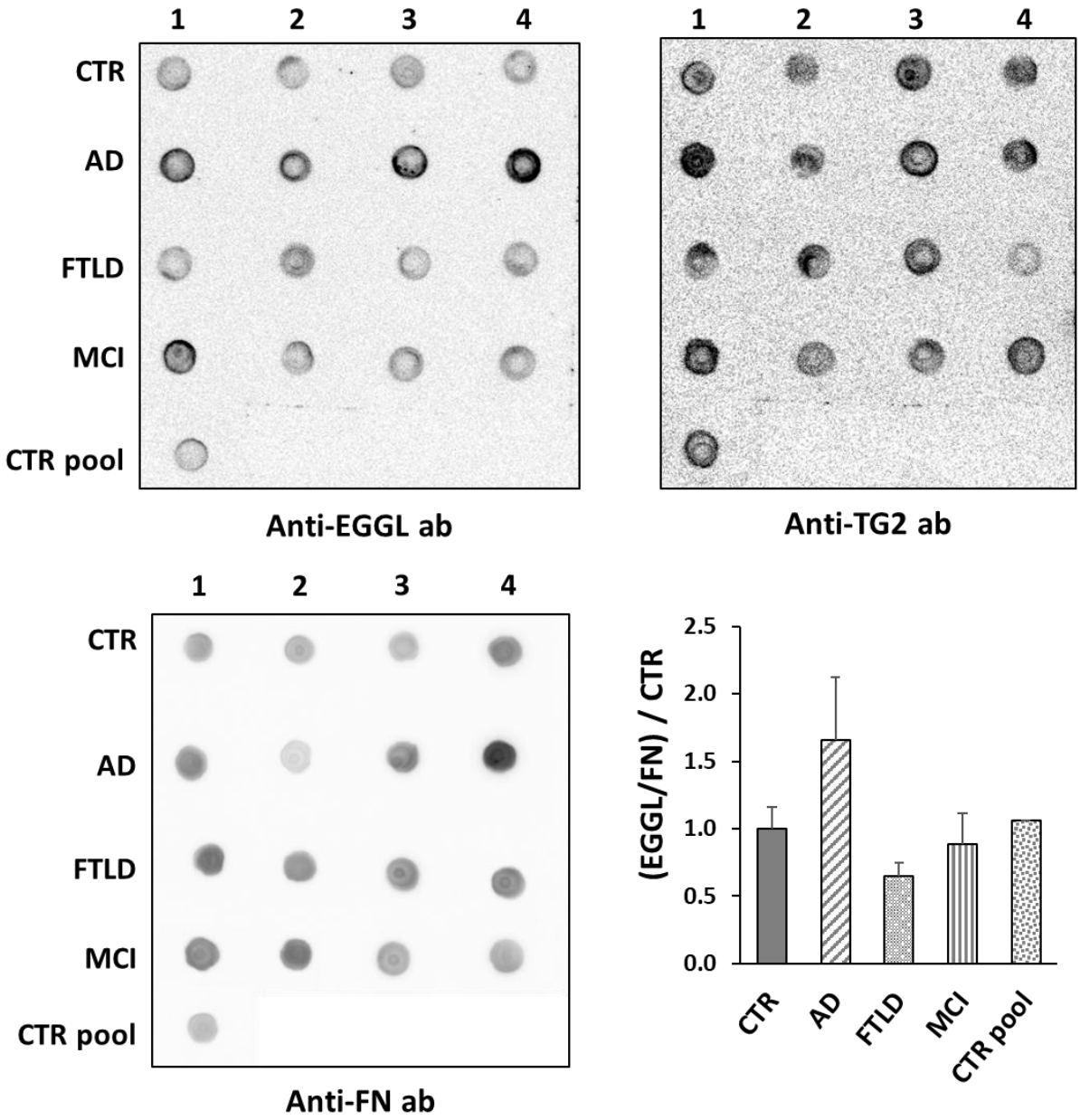

Figure 6.20. Detection of EGGL dipeptides in plasma of control and dementia subjects by dot blot. *Plasma from healthy subjects (CTR, N=4 + commercial CTR pool) and patients affected by Alzheimer's disease (AD, N=4), Frontotemporal dementia (FTLD, N=4) and Mild cognitive impairment (MCI, N=4) were diluted 1:100 in Tris-HCl 50 mM pH 4, and analysed by dot blot (5 µl each). Membranes were probed for TG2, FN and EGGL. Plot on the right shows densitometry analysis of EGGL normalised to FN and then to average CTR value (mean ± SE). EGGL/FN, CTR: 1.11±0.17; AD: 1.84±0.52; FTLD: 0.72±0.22; MCI: 0.98±0.26; CTR pool: 1.03.*

In order to verify the precision of this technique, the same AD plasma (N=4) and control pool were selected and spotted each one in triplicate (**Fig. 6.21**). EGGL signal presented intra-sample variability (**Fig. 6.21A**) as the same was observed when the blot was probed for TG2 (**Fig. 6.21B**) and FN (**Fig. 6.21C**). Evidently, the efficiency of antibody binding was affected by the sample's spotting, which was highly difficult to keep 100% consistent. In conclusion, dot blot was not the best technique to reliably detect EGGL in plasma. This effort has revealed that the anti-EGGL antibody is specific for TG2 crosslinks, however to overcome issues with imprecision of the "dots", an ELISA assay based on the immunodetection of EGGL with the 81D4 antibody would be more quantitative compared to the dot blot.

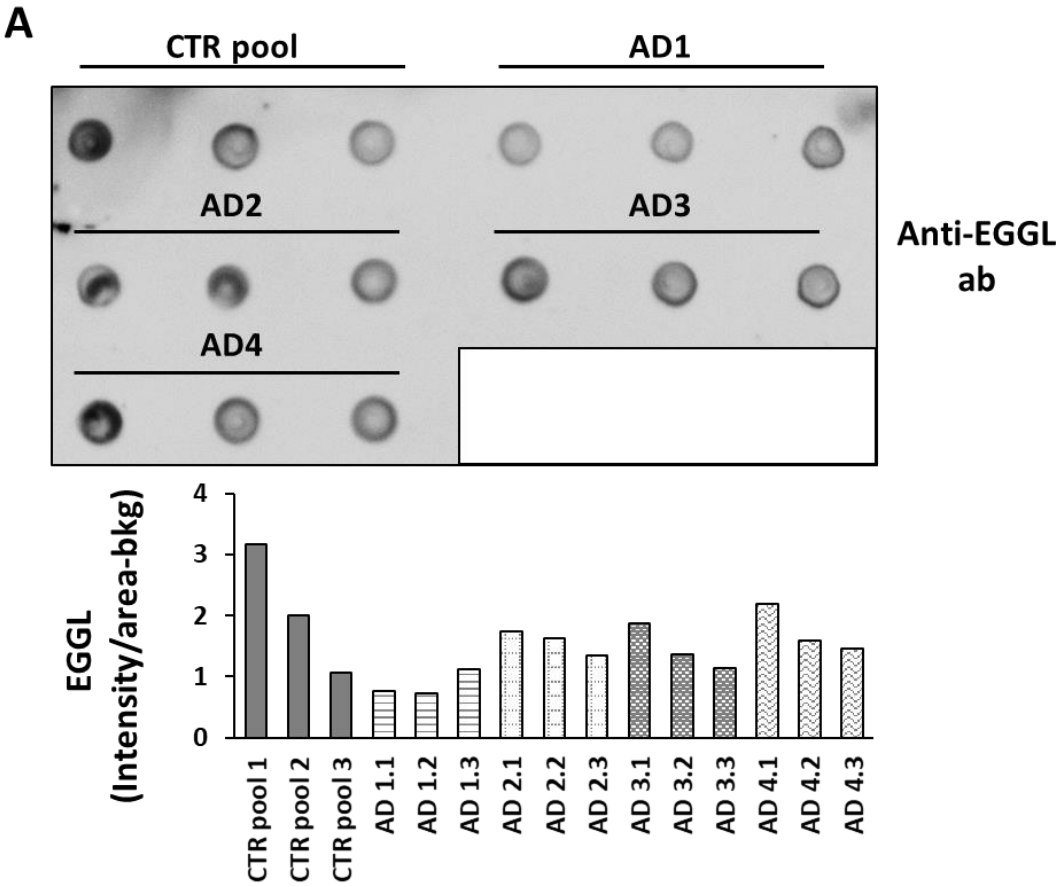

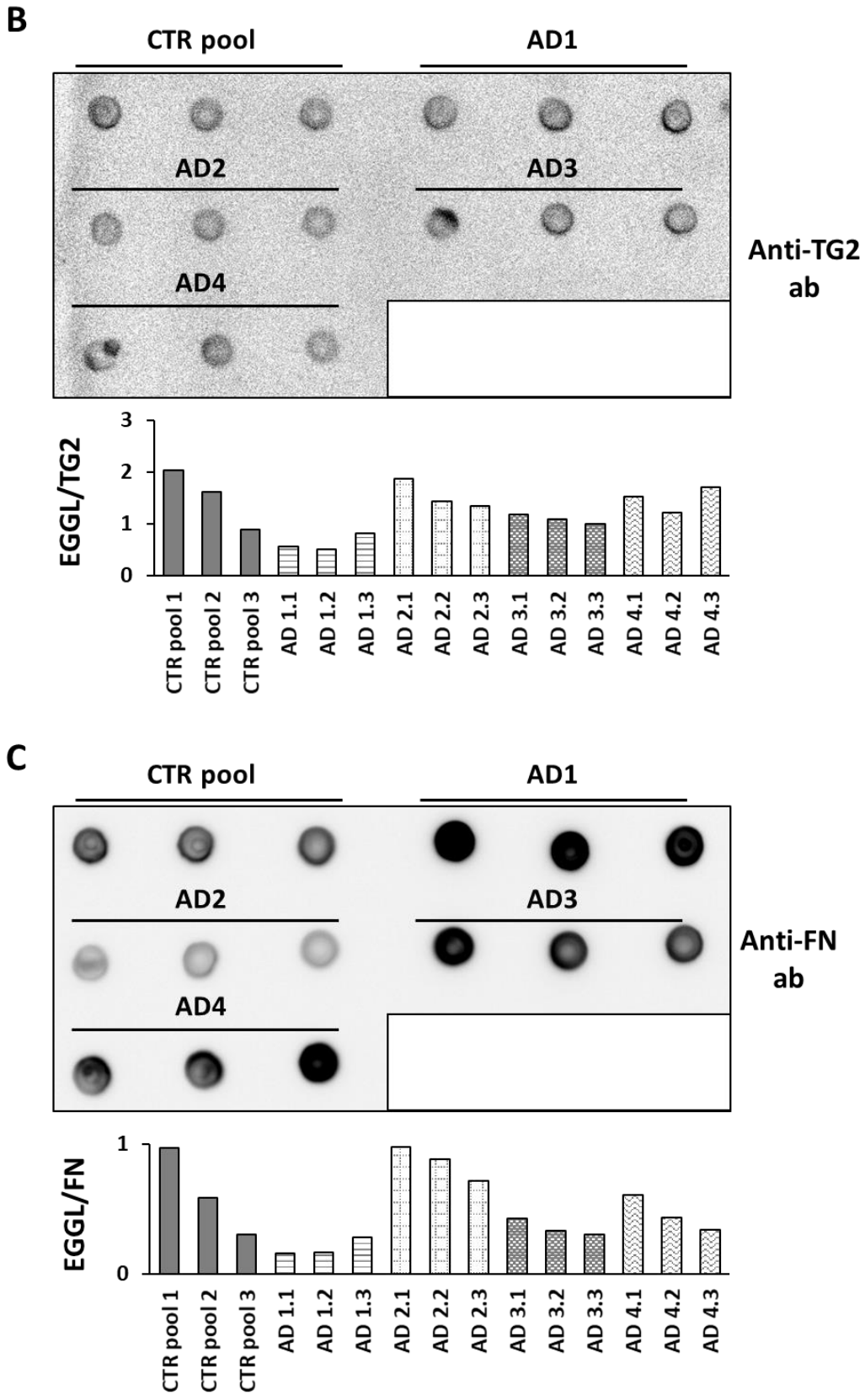

Figure 6.21. Detection of EGGL dipeptide in plasma of control and AD subjects by dot blot. *Plasma from a pool of healthy subjects (CTR pool, Tebu-Bio) and patients affected by Alzheimer's disease (AD, N=4), were diluted 1:100 in Tris-HCl 50 mM pH 4, and analysed by dot blot in triplicates.* ***A)*** *Probing with anti-GGEL (81D4) antibody. Plot shows raw*

densitometry analysis of single EGGL dots, expressed as Intensity/Area-background (a.u./mm^2). ***B)*** *Probing with anti-TG2 (CUB7402) antibody. Plot shows densitometry analysis of EGGL normalised to TG2.* ***C)*** *Probing with anti-FN (F3648) antibody. Plot shows densitometry analysis of EGGL normalised to FN.*

In conclusion, the effort to measure TG2 in patients' cells *ex vivo* and in plasma was limited by technical problems, like mycoplasma contamination or lack of sensitive assays. Collectively, an increase in TG2 expression was shown in the primary fibroblasts of a small number of dementia patients compared to controls. Analysis of whole plasma by optimised ELISA assay revealed no changes between dementia patients and controls, but also a possible masking effect from HAPs. At the same time, new work in this study has shown that TG2 is carried by EVs in plasma, hence quantification of TG2 should be performed in EVs fractions for a more accurate and sensitive evaluation. The only available anti-EGGL antibody (81D4) was also explored validating its specificity, setting the basis for the development of an ELISA test based on 81D4 to quantify the end product of TG2 PTM. In fact, as TG2 is mostly inactive, not so much its expression as its activity (reflected by the presence of crosslinks) is expected to increase in disease.

6.3 Discussion

Nowadays, the clinical diagnosis of neurodegenerative diseases, particularly AD, is the result of a multidisciplinary approach which relies on cognitive assessments and well established biomarkers, such as structural magnetic resonance imaging (MRI) of brain atrophy, positron emission tomographic imaging (targeting Aβ, tau, and brain glucose metabolism), analysis of Aβ peptides and tau levels in CSF (Blennow et al., 2010-2015; Frisoni et al., 2010; Mattsson et al., 2015). However, these techniques are very invasive, expensive and not available in all memory clinics, making the diagnosis of patients more complicated. For these reasons, intensive research efforts have been focused on the identification of alternative and less invasive approaches, e.g. blood-derived biomarkers (Zetterberg and Burnham, 2019).

Following from past literature giving contradictory results on the link between TG2 levels and dementia (Martin et al., 2013; Wolf et al., 2013), an attempt was made to investigate whether TG2 could be correlated with dementia in biological samples from healthy subjects and dementia patients that are routinely collected in AD centres (plasma and skin biopsies). TG2 levels were analysed in plasma, which represent an easily accessible and minimally invasive sample for the study and diagnose of brain-related diseases. In recent years, an increasing number of publications have shown that plasma protein levels of Aβ peptides, tau and neurofilament light (NfL), as well as circulating miRNAs correlated with AD and could be used as disease biomarkers to improve patients diagnosis (as recently reviewed in Zendjabil, 2018; Nagaraj et al., 2019; Zetterberg and Burnham, 2019).

Previous work (summarised in Table 6.1) had mainly investigated plasma or serum TGs activity, either by using plate assays based on putrescine/cadaverine incorporation, hence not TG2 specific (Fujita et al., 1998), or by quantification of EGGL (Harsfalvi et al., 1992; Nemes et al., 2001; Jeitner et al., 2008). In some recent publications, TG2 protein levels were identified by ELISA-based assays (Cusabio Biotech and MAGPIX Merk) in plasma from subjects affected by chronic periodontitis (Becerick et al., 2016-2017) and from endometrial cancer patients (Torres et al., 2019), but never in dementia patients. According to these studies, TG2 plasma levels in CTR subjects ranged from about $2x10^6$ ng/ml to 1575 ng/ml respectively. This huge difference could be due to the different assays used in the two studies, as Cusabio Biotech assay is based on the sandwich enzyme immunoassay technique (Becerick et al., 2016-2017), while MAGPIX is based on the Luminex® xMAP®

technology with capture of antigens on antibody-coated fluorescent-coded magnetic beads (Torres et al., 2019).

To identify TG2 in plasma, an already published and well validated protocol for detection of TG2 in cell lysates (Verderio et al., 2003) was further optimised. This method is based on the capture of TG2 protein on a FN coated plate and detection of TG2 specific antigen by anti-TG2 antibody. TG2 ability to directly bind FN through a specific binding site in its N-terminal domain is not shared by FXIIIa, a transglutaminase also present in plasma, thus eliminating the risk of trapping FXIIIa together with TG2 on the FN coating (Hang et al., 2005). The optimised protocol involved a 1:2 dilution of plasma and supplementation of 2 mM EDTA, for an increased detection of TG2 (**Fig. 6.10-6.12**). The presence of EDTA also ensured that FXIIIa or TG2 present in the plasma samples would not be active and crosslink the FN coating. By this method TG2 was detected in plasma from healthy subjects and patients affected by dementia (AD, FTLD and MCI), however with no statistical difference among the cohorts (**Fig. 6.13**). The average TG2 concentration detected was 73.7±1.8 ng/ml, which was lower than the dynamic range of commercial kit, and also lower compared to the published values in plasma from healthy subjects (Becerick et al., 2016-2017; Torres et al., 2019). The presence of high abundant protein (HAPs) in plasma (e.g. albumin) might have partially masked small variations in less abundant proteins like TG2.

Based on the fact that blood-derived EVs have been proposed as possible biomarkers of disease in neurodegeneration, even if the complexity and diversity of the isolation protocols represent a limitation to clinical application (Fiandaca et al., 2015; Goetzl et al., 2015-2019, Seongju et al., 2019), TG2 was screened in plasma EVs. Notably, Rosas-Hernandez and colleagues just published that Aβ and tau monomers and oligomers are present in brain-derived exosomes isolated from serum in a transgenic mouse model of AD (Rosas-Hernandez et al., 2019). Moreover, we have recently shown that TG2 is present in urinary EVs (Furini et al., 2018). Our data in patients affected by kidney fibrosis suggest that the analysis of uEVs offers a larger fingerprint of disease progression than whole urine, as in comparison EVs carry less plasma HAPs (unpublished data). Consistent with this idea, TG2 was detected in plasma-derived EVs of healthy and AD patients by western blotting and TG2 ELISA. This work opens the door for future investigations aimed at improving consistency of EVs preparations to enable accurate TG2 quantification in biological fluids.

It is important to remember that increased levels of TG2 protein do not necessarily reflect an increase in activity. Indeed, the fact that the extracellular enzyme is finely regulated and

that both high calcium concentrations and reducing conditions are necessary for TG2 activation has been previously discussed. Therefore, the detection of TG2 transamidation by-product, namely the EGGL crosslink, represents an alternative approach to investigate the relevance of TG2 in dementia and the only one to prove TG2 PTM of substrates. Different methods have been used for the quantification of EGGL in biological fluids, especially CSF, mainly based on HPLC-related techniques (Nemes et al., 2001; Jeitner et al., 2008). At the same time, the quantification of EGGL in tissue sections by specific antibody labelling gave rise to the idea to develop an immune-based assay for the detection of EGGL in plasma, using the anti-EGGL antibody. There is only one anti-EGGL antibody (81D4) available to the scientific community and its specificity is still debated (Johnson and LeShoure, 2004). For this reason, the antibody specificity was validated by generating EGGL *in vitro* using FN, a well-known target of TG2 crosslinking (Jeong et al., 1995; Hang et al., 2005). Preliminary results with 81D4 (dot blot) revealed an increase of EGGL in sAD plasma compared to control (**Fig. 6.20**). This is consistent with previously shown crosslinking values in CSF (Nemes et al., 2001; Jeitner et al., 2008), however dot blot did not lead to quantitative data due to high variability of spots (**Fig. 6.21**). A plate-based assay (ELISA) would be a more efficient and suitable quantitative method to measure EGGL in plasma, using conditions validated in the course of this study. Although measuring TG2 and its crosslinking product in plasma has proved to be extremely challenging, several advances have been made that will facilitate reliable and unambiguous evaluations in the future.

CHAPTER 7:

General Discussion

7.1 General discussion

In the course of this project the role of TG2 has been explored in two aspects relevant to the pathophysiology of neurodegeneration. On one hand, the study has focused on the role of extracellular TG2 in the modulation of neuron-astroglia communication and described a novel TG2-mediated pathway of regulation of neuronal calcium homeostasis, which is at the basis of the correct execution of neuronal functions. This work has confirmed that astrocytes are a source of extracellular TG2 in brain and expanded this observation by showing for the first time that TG2 is released as a cargo of astrocytic small EVs. Although at a preliminary stage, this project has shown that EVs-associated TG2 significantly affects calcium homeostasis. A large body of evidence in this study has pointed at the role of extracellular TG2 in increasing calcium cytoplasmic concentration in neurons and elucidated that this might be either an effect of membrane depolarisation, as shown by patch clamp experiments, or caused by the interaction of TG2 with ionic channels, as suggested by the TG2 "transamidome". It cannot be excluded that TG2 could be interacting with an intermediate molecule, like a neurotransmitter, which in turn would mediate the influx of calcium. At this stage a key question is: what are the implications of the finding that extracellular TG2 increases basal $[Ca^{2+}]_i$ in pathology? The dysregulation of calcium homeostasis is a common hallmark of neurodegenerative diseases (Marambaud et al., 2009). This is because calcium signalling regulates basic biological functions such as muscle and cardiac contraction, and also fundamental biological processes at the cellular level, such as cell adhesion, secretion and migration to mention a few. In the brain specifically, variations of calcium levels not only support normal neuronal physiology but also ensure neuronal integrity, synaptic transmission and synaptic plasticity (Brini et al., 2014). Abnormal increase of $[Ca^{2+}]_i$ is deleterious for neurons, as it leads to mitochondrial dysfunction, bioenergetic imbalance and activation of the apoptosis pathway. This has been well documented in many brain conditions, such as AD (Marambaud et al., 2009; Brini et al., 2014) and also shown in a mouse model of AD, where the analysis of cortical neurons by *in vivo* calcium imaging displayed calcium overload at dendritic spines (Kuchibhotla et al., 2008; Lopez et al., 2008). Early work in human cortical neurons also reported that Aβ peptide increased NMDA-mediated excitotoxicity with alteration of neuronal calcium levels (Mattson et al., 1992). Various mechanisms have been proposed to explain Aβ-mediated alteration of calcium homeostasis, such as the formation of calcium-permeable pores by incorporation of Aβ itself into the plasma membrane (Kawahara and Kuroda, 2000), the

activation of calcium channels like ROCCs and VOCCs (Mattson et al., 1992; Price et al., 1998), or the promotion of ER stress and consequent leakage of calcium from the intracellular stores (Tu et al., 2006). Interestingly, calcium-induced hippocampal damage was observed in the hippocampus of mice overexpressing TG2 (Tucholski et al., 2006), a finding that, analysed with the data in this study, leads to the suggestion that extracellular TG2 could impact neuronal survival by altering calcium homeostasis. One possible limitation of this cell model is that considerable TG2 was needed to produce a change in $[Ca^{2+}]_i$, however increased levels and externalisation of TG2 have been long associated to tissue fibrosis in kidney (Johnson et al., 1997-2003; Scarpellini et al., 2014; Burhan et al., 2016; Furini et al., 2008), liver (Grenard et al., 2001; Tastukawa et al., 2017) and heart (Small et al., 1999; Shinde et al., 2017; Wang et al., 2018). Hence, it is not unlikely to hypothesise that the same could happen under neurodegenerative conditions. Indeed, TG2 levels have been shown to increase in astrocytes upon neuroinflammatory stimuli, leading to its externalisation and accumulation in the ECM (Pinzon et al., 2017b). As neurons also express TG2, a similar process could be induced in neuronal cells in stress conditions.

Simulation of AD pathology *ex vivo* in cultured primary rat hippocampal neurons allowed the identification of a number of TG2 substrates ("TG2 transamidome") for the first time. TG2 was shown to post-translationally modify a variety of targets and therefore affect several functions that are still largely unknown in the brain. As expected Aβ, an already known target of TG2 transamidation both *in vitro* and *in vivo* (Benilova et al., 2012), also emerged as a strong substrate of TG2. Furthermore, two ionic channels (AT2B2 and TMC5) emerged as specific targets, which may be part of a novel mechanism mediating TG2-driven increase of intracellular calcium concentration. Additionally, ENOB was a highly specific TG2 target, suggesting a possible effect of TG2 on the cell metabolism, as well as CD81, a tetraspanin expressed in EVs, which suggests that TG2 might also be involved in vesicular trafficking. Finally, also ribosomal proteins were included.

The second part of this work has focused on the detection of TG2 in dementia patients, particularly in plasma, with the ambition to determine if TG2 could be considered a biomarker of dementia, thus unravelling an outstanding debate in the scientific community. Although TG2 could be detected in the plasma of patients by an ELISA-based assay optimised in the course of this study, no statistical difference in TG2 presence was seen among the different cohorts. Therefore, based on this part of the project, TG2 does not emerge as a useful biomarker in AD. Well characterised blood-based biomarkers such as

$A\beta_{1-42}/A\beta_{1-40}$ ratio, p-tau and NfL probably represent the best option to early diagnose AD (Zetterberg and Burnham, 2019). Parallel research however has shown for the first time that TG2 is transported in plasma EVs. These preliminary data suggest that the analysis of vesicular TG2 could be a better way to measure plasma TG2, as EVs represent a purer sample, less contaminated by high abundant plasma proteins, which otherwise might mask the detection of less expressed proteins. Indeed, we have recently demonstrated that TG2 is contained in urinary EVs (Furini et al., 2018) and our unpublished data suggest that EVs offer a larger fingerprint of disease progression compared to whole urine. Future work will be focused on finalising the analysis of EVs isolated from patients' plasma and the development of an assay to detect TG2 crosslinking product (EGGL dipeptide).

TG2 is a multifunctional enzyme able to modify a large array of proteins under sufficient $[Ca^{2+}]_i$ and favourable redox conditions. Moreover, it also acts as a structural protein in a crosslinking independent way (Verderio et al., 2003). An "all round" approach has been used to gain insights on the role of TG2 in neurons pathophysiology. The outcome of this thesis reflects the potentially huge impact that TG2-mediated PTM and TG2 protein could have on the survival of neurons. It also suggests that TG2 outside the cell, mainly deposited by reactive astrocytes in the extracellular environment in which neurons are embedded, drives small but powerful modifications in basal $[Ca^{2+}]_i$ that ultimately may offer an explanation of how TG2 is linked to neurodegeneration. The rise in $[Ca^{2+}]_i$ could in turn reach overload levels and activate intracellular neuronal TG2, thus leading with time to PTM of intracellular substrates, with consequent amplification of the neurotoxic effect (**Fig. 7.1**).

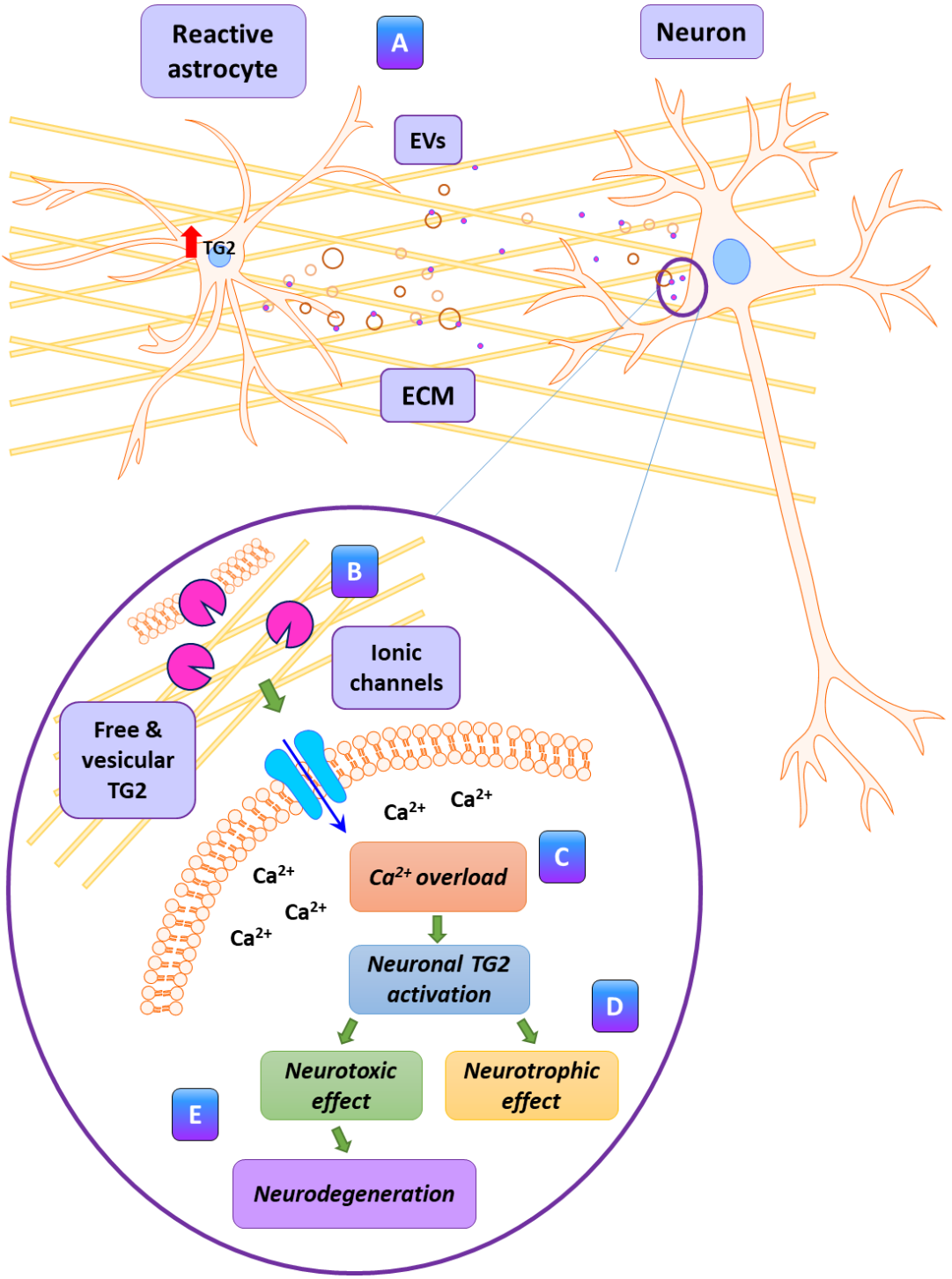

Figure 7.1. The proposed pathway of TG2 role in neurons pathophysiology. A) *Reactive astrocytes activated by neuroinflammatory stimuli release EVs carrying TG2.* ***B)*** *Extracellular TG2 accumulates in the ECM in soluble form or vesicle-bound and interacts with neurons, inducing a calcium influx that increases intracellular calcium levels ($[Ca^{2+}]_i$).* ***C)*** *Increase of $[Ca^{2+}]_i$ activates intracellular neuronal TG2, which in turn could crosslink endogenous substrates. Among these are included both neurotrophic* ***(D)*** *and pro-apoptotic* ***(E)*** *proteins, which might amplify the neurotoxic effect driven by calcium dysregulation. This image was generated with Motifolio (https://www.motifolio.com/).*

CHAPTER 8:

Supplementary data

Table S.1: List of proteins substrates of TG2 upon Aβ exposure compared to untreated controls (CTR), with confidence ≥50%. *Proteins that were more target of TG2 are highlighted in gold (FC>1), while proteins that were less targets of TG2 upon Aβ are highlighted in green (FC<1) (confidence ≥60%).*

Aβ/CTR transamidome					
Protein ID			Log_2(FC)	FC	Confidence
Q5EGY4	YKT6	Synaptobrevin homolog YKT6	-2.417	0.187	0.913
P20760	IGG2A	Ig gamma-2A chain C region	-0.452	0.731	0.830
P62271	RS18	40S ribosomal protein S18	2.105	4.303	0.800
Q5M7W4	TMC5	Transmembrane channel-like protein 5	1.079	2.112	0.761
P00762	TRY1	Anionic trypsin-1	-1.017	0.494	0.741
P15429	ENOB	Beta-enolase	2.006	4.017	0.732
P62853	RS25	40S ribosomal protein S25	1.262	2.398	0.691
Q6AXV4	SAM50	Sorting and assembly machinery component 50 homolog	-2.284	0.205	0.676
Q6IFW2	K1C40	Keratin, type I cytoskeletal 40	3.007	8.041	0.674
P08592	A4	Amyloid beta A4 protein	3.348	10.184	0.614
Q99ML5	PCYOX	Prenylcysteine oxidase	-3.322	0.100	0.611
Q5XI29	CPSF7	Cleavage and polyadenylation specificity factor subunit 7	2.225	4.676	0.599
Q9JJP9	UBQL1	Ubiquilin-1	-2.872	0.137	0.598
P13264	GLSK	Glutaminase kidney isoform, mitochondrial	-3.150	0.113	0.593
P25809	KCRU	Creatine kinase U-type, mitochondrial	-1.010	0.496	0.588
Q64122	MYL9	Myosin regulatory light polypeptide 9	-3.659	0.079	0.588
Q4KMA2	RD23B	UV excision repair protein RAD23 homolog B	-2.645	0.160	0.587
Q5FVN0	MBOA5	Lysophospholipid acyltransferase 5	3.097	8.556	0.576
P55161	NCKP1	Nck-associated protein 1	-2.428	0.186	0.572
Q9QVC8	FKBP4	Peptidyl-prolyl cis-trans isomerase FKBP4	2.873	7.328	0.567
P62850	RS24	40S ribosomal protein S24	1.029	2.041	0.549
Q9JLJ3	AL9A1	4-trimethylaminobutyraldehyde dehydrogenase	3.267	9.626	0.548
P68255	1433T	14-3-3 protein theta	1.605	3.041	0.544
P62902	RL31	60S ribosomal protein L31	-0.608	0.656	0.539
Q9JI92	SDCB1	Syntenin-1	-2.494	0.178	0.537
P54690	BCAT1	Branched-chain-amino-acid aminotransferase, cytosolic	-1.031	0.489	0.537
P41562	IDHC	Isocitrate dehydrogenase NADP cytoplasmic	-1.613	0.327	0.534
Q8CFN2	CDC42	Cell division control protein 42 homolog	-1.025	0.491	0.534
P36876	2ABA	Serine/threonine-protein ph phatase 2A 55 kDa regulatory subunit B alpha isoform	2.559	5.895	0.534
P97612	FAAH1	Fatty-acid amide hydrolase 1	3.661	12.647	0.533
P10536	RAB1B	Ras-related protein Rab-1B	-0.556	0.680	0.531
Q63484	AKT3	RAC-gamma serine/threonine-protein kinase	-2.407	0.189	0.530
Q66HR2	MARE1	Microtubule-associated protein RP/EB family member 1	-2.461	0.182	0.530
Q5I0D1	GLOD4	Glyoxalase domain-containing protein 4	-3.430	0.093	0.526

Aβ/CTR transamidome					
Protein ID			Log_2(FC)	FC	Confidence
Q5U2U2	CRKL	Crk-like protein	3.307	9.897	0.525
P04906	GSTP1	Glutathione S-transferase P	-2.975	0.127	0.525
P63004	LIS1	Platelet-activating factor acetylhydrolase IB subunit alpha	-5.434	0.023	0.524
B2RYG6	OTUB1	Ubiquitin thioesterase OTUB1	1.455	2.742	0.524
P20759	IGHG1	Ig gamma-1 chain C region	0.656	1.576	0.522
Q07984	SSRD	Translocon-associated protein subunit delta	-1.763	0.295	0.521
O35824	DNJA2	DnaJ homolog subfamily A member 2	2.561	5.901	0.519
Q5XFW8	SEC13	Protein SEC13 homolog	3.497	11.288	0.518
B0BN93	PSD13	26S proteasome non-ATPase regulatory subunit 13	1.975	3.931	0.517
Q9QZR6	SEPT9	Septin-9	3.626	12.346	0.517
P30835	PFKAL	ATP-dependent 6-phosphofructokinase, liver type	2.933	7.638	0.516
P47875	CSRP1	Cysteine and glycine-rich protein 1	-0.711	0.611	0.515
Q794E4	HNRPF	Heterogeneous nuclear ribonucleoprotein F	-1.749	0.298	0.512
B0BN56	RT31	28S ribosomal protein S31, mitochondrial	1.527	2.882	0.511
P50137	TKT	Transketolase	2.478	5.573	0.508
Q62625	MLP3B	Microtubule-associated proteins 1A/1B light chain 3B	2.434	5.404	0.508
Q3MIE4	VAT1	Synaptic vesicle membrane protein VAT-1 homolog	1.571	2.972	0.504
Q4KLF8	ARPC5	Actin-related protein 2/3 complex subunit 5	-2.225	0.214	0.501
O35162	HSP13	Heat shock 70 kDa protein 13	-1.889	0.270	0.501

Table S.2: List of proteins substrates of TG2 upon Aβ exposure compared to Aβ+ZDON, with confidence ≥50%. *Proteins that are highly specific targets of TG2 are highlighted in gold (FC>1), while proteins that are not specific substrates of TG2 are highlighted in green (FC<1) (confidence ≥60%).*

Aβ/Aβ+ZDON transamidome					
Protein ID			Log_2(FC)	FC	Confidence
Q07647	GTR3	Solute carrier family 2, facilitated glucose transporter member 3	-4.847	0.035	0.892
Q62745	CD81	CD81 antigen	3.803	13.959	0.881
P62864	RS30	40S ribosomal protein S30	1.351	2.550	0.843
P62271	RS18	40S ribosomal protein S18	1.273	2.416	0.781
P62853	RS25	40S ribosomal protein S25	1.061	2.086	0.752
P20760	IGG2A	Ig gamma-2A chain C region	-0.463	0.726	0.750
P15429	ENOB	Beta-enolase	2.866	7.290	0.720
Q6IFW6	K1C10	Keratin, type I cyt keletal 10	-1.162	0.447	0.711
P97612	FAAH1	Fatty-acid amide hydrolase 1	2.457	5.489	0.706
Q9WU34	SEPT3	Septin-3	-1.593	0.332	0.678
Q9JI92	SDCB1	Syntenin-1	-1.925	0.263	0.657
P41562	IDHC	Isocitrate dehydrogenase NADP cytoplasmic	-4.269	0.052	0.653
Q01728	NAC1	Sodium/calcium exchanger 1	-0.681	0.624	0.642
P11506	AT2B2	Plasma membrane calcium-transporting ATPase 2	2.912	7.528	0.618
P13471	RS14	40S ribosomal protein S14	0.884	1.846	0.612
Q4V8B7	HSDL1	Inactive hydroxysteroid dehydrogenase-like protein 1	-4.527	0.043	0.602
P62850	RS24	40S ribosomal protein S24	0.732	1.661	0.597
P17702	RL28	60S ribosomal protein L28	2.554	5.873	0.588
Q6IG02	K22E	Keratin, type II cyt keletal 2 epidermal	-0.910	0.532	0.582
P47819	GFAP	Glial fibrillary acidic protein	2.590	6.020	0.580
Q5XIF6	TBA4A	Tubulin alpha-4A chain	1.570	2.968	0.575
Q6AXV4	SAM50	Sorting and assembly machinery component 50 homolog	-2.427	0.186	0.573
Q64122	MYL9	Myosin regulatory light polypeptide 9	-2.882	0.136	0.572
P24050	RS5	40S ribosomal protein S5	0.920	1.893	0.571
P62890	RL30	60S ribosomal protein L30	-3.104	0.116	0.564
P69736	EDF1	Endothelial differentiation-related factor 1	-2.427	0.186	0.563
Q5FVH2	PLD3	Ph pholipase D3	-2.303	0.203	0.561
O35964	SH3G1	Endophilin-A2	-1.637	0.322	0.560
Q03555	GEPH	Gephyrin	-2.261	0.209	0.558
Q9Z142	TMM33	Transmembrane protein 33	3.397	10.535	0.549
D3ZE55	PCDH8	Protocadherin-8	-3.020	0.123	0.549
P35284	RAB12	Ras-related protein Rab-12	-1.636	0.322	0.548
B0K020	CISD1	CDGSH iron-sulfur domain-containing protein 1	2.304	4.939	0.548

Aβ/Aβ+ZDON transamidome					
Protein ID			Log_2(FC)	FC	Confidence
Q01177	PLMN	Plasminogen	-2.062	0.240	0.546
Q9EPC6	PROF2	Profilin-2	-2.058	0.240	0.542
P62744	AP2S1	AP-2 complex subunit sigma	-0.924	0.527	0.538
Q64060	DDX4	Probable ATP-dependent RNA helicase DDX4	1.376	2.596	0.538
P30835	PFKAL	ATP-dependent 6-phosphofructokinase, liver type	1.653	3.145	0.538
P04644	RS17	40S ribosomal protein S17	1.469	2.769	0.537
Q9JJW3	USMG5	Up-regulated during skeletal muscle growth protein 5	2.666	6.345	0.535
Q62698	DC1L2	Cytoplasmic dynein 1 light intermediate chain 2	4.342	20.283	0.534
B0BN93	PSD13	26S proteasome non-ATPase regulatory subunit 13	4.017	16.186	0.533
P68255	1433T	14-3-3 protein theta	1.541	2.910	0.532
P61515	RL37P	Putative 60S ribosomal protein L37a	1.230	2.345	0.530
P63029	TCTP	Translationally-controlled tumor protein	2.589	6.015	0.528
P63004	LIS1	Platelet-activating factor acetylhydrolase IB subunit alpha	-5.489	0.022	0.527
O08839	BIN1	Myc box-dependent-interacting protein 1	-2.270	0.207	0.525
P07895	SODM	Superoxide dismutase Mn, mitochondrial	2.042	4.120	0.524
P18437	HMGN2	Non-histone chrom omal protein HMG-17	4.061	16.686	0.523
Q02769	FDFT	Squalene synthase	-1.953	0.258	0.523
P55053	FABP5	Fatty acid-binding protein, epidermal	2.406	5.299	0.522
Q1HAQ0	PCAT1	Lysoph phatidylcholine acyltransferase 1	-2.140	0.227	0.522
P83883	RL36A	60S ribosomal protein L36a	2.362	5.141	0.520
Q6PDU7	ATP5L	ATP synthase subunit g, mitochondrial	-0.607	0.657	0.518
Q6TEK3	VKORL	Vitamin K epoxide reductase complex subunit 1-like protein 1	3.193	9.142	0.518
Q6XVN8	MLP3A	Microtubule-associated proteins 1A/1B light chain 3A	2.900	7.464	0.518
P24470	CP2CN	Cytochrome P450 2C23	-3.576	0.084	0.516
Q07009	CAN2	Calpain-2 catalytic subunit	1.866	3.644	0.515
Q9JMJ4	PRP19	Pre-mRNA-processing factor 19	1.644	3.125	0.510
P0C1X8	AAK1	AP2-associated protein kinase 1	-1.561	0.339	0.509
P27653	C1TC	C-1-tetrahydrofolate synthase, cytoplasmic	-3.358	0.098	0.509
P50137	TKT	Transketolase	3.547	11.689	0.507
Q6IG01	K2C1B	Keratin, type II cyt keletal 1b	-1.477	0.359	0.501

Table S.3: List of proteins significantly changed upon Aβ exposure compared to CTR, with confidence ≥50%. *Proteins that were increased by Aβ compared to CTR are highlighted in gold (FC>1), while proteins that were decreased upon Aβ are highlighted in green (FC<1) (confidence ≥70%).*

Aβ/CTR proteome					
Protein ID			Log_2(FC)	FC	Confidence
Q62745	CD81	CD81 antigen	-1.102	0.466	0.979
Q4KM98	MFF	Mitochondrial fission factor	-3.883	0.068	0.933
P38983	RSSA	40S ribosomal protein SA	0.656	1.576	0.847
O35796	C1QBP	Complement component 1 Q subcomponent-binding protein, mitochondrial	1.250	2.378	0.843
P04636	MDHM	Malate dehydrogenase, mitochondrial	0.843	1.793	0.840
Q6IFW6	K1C10	Keratin, type I cytoskeletal 10	-1.899	0.268	0.831
Q5U2U2	CRKL	Crk-like protein	4.707	26.125	0.827
P31044	PEBP1	Phosphatidylethanolamine-binding protein 1	0.736	1.665	0.790
Q6IMF3	K2C1	Keratin, type II cytoskeletal 1	-2.280	0.206	0.788
P10960	SAP	Sulfated glycoprotein 1	0.597	1.512	0.776
P19234	NDUV2	NADH dehydrogenase ubiquinone flavoprotein 2, mitochondrial	0.653	1.572	0.771
P63331	PP2AA	Serine/threonine-protein phosphatase 2A catalytic subunit alpha isoform	0.752	1.684	0.761
P62076	TIM13	Mitochondrial import inner membrane translocase subunit Tim13	0.488	1.403	0.752
P47868	SCG3	Secretogranin-3	1.670	3.181	0.741
Q6IG01	K2C1B	Keratin, type II cytoskeletal 1b	-3.862	0.069	0.738
P08592	A4	Amyloid beta A4 protein	5.505	45.398	0.733
P35704	PRDX2	Peroxiredoxin-2	0.670	1.591	0.728
Q5XIG4	OCAD1	OCIA domain-containing protein 1	1.707	3.265	0.724
Q1HCL7	NAKD2	NAD kinase 2, mitochondrial	1.145	2.212	0.720
P07335	KCRB	Creatine kinase B-type	0.638	1.557	0.720
Q07936	ANXA2	Annexin A2	-0.825	0.564	0.718
Q9Z0V6	PRDX3	Thioredoxin-dependent peroxide reductase, mitochondrial	1.105	2.151	0.711
Q923W4	HDGR3	Hepatoma-derived growth factor-related protein 3	2.696	6.481	0.705
P31232	TAGL	Transgelin	-0.958	0.515	0.704
Q6PCU8	NDUV3	NADH dehydrogenase ubiquinone flavoprotein 3, mitochondrial	1.588	3.007	0.692
Q78P75	DYL2	Dynein light chain 2, cytoplasmic	1.704	3.258	0.689
P37397	CNN3	Calponin-3	-1.114	0.462	0.684
P97519	HMGCL	Hydroxymethylglutaryl-CoA lyase, mitochondrial	0.973	1.963	0.677
Q5XIF4	SUMO3	Small ubiquitin-related modifier 3	0.653	1.573	0.676
Q812E9	GPM6A	Neuronal membrane glycoprotein M6-a	-0.665	0.631	0.676
B0BN18	PFD2	Prefoldin subunit 2	1.603	3.038	0.675
Q9Z0U4	GABR1	Gamma-aminobutyric acid type B receptor subunit 1	-2.036	0.244	0.671
Q00438	PTBP1	Polypyrimidine tract-binding protein 1	-2.210	0.216	0.671
Q5EB81	NB5R1	NADH-cytochrome b5 reductase 1	-1.807	0.286	0.666
Q03351	NTRK3	NT-3 growth factor receptor	-1.837	0.280	0.664

Aβ/CTR proteome					
Protein ID			**Log_2(FC)**	**FC**	**Confidence**
Q9JJK1	GPM6B	Neuronal membrane glycoprotein M6-b	-0.583	0.668	0.663
P63164	RSMN	Small nuclear ribonucleoprotein-associated protein N	-0.361	0.779	0.660
Q8VIL3	ZWINT	ZW10 interactor	-1.971	0.255	0.660
Q6AYK6	CYBP	Calcyclin-binding protein	2.120	4.348	0.653
D3ZPX4	PLXA3	Plexin-A3	2.497	5.645	0.653
Q03555	GEPH	Gephyrin	-2.115	0.231	0.641
P29457	SERPH	Serpin H1	-0.760	0.590	0.640
Q6UPE1	ETFD	Electron transfer flavoprotein-ubiquinone oxidoreductase, mitochondrial	-2.180	0.221	0.638
Q6MGD0	CUTA	Protein CutA	0.848	1.800	0.633
P62744	AP2S1	AP-2 complex subunit sigma	-0.422	0.746	0.627
Q9WVA1	TIM8A	Mitochondrial import inner membrane translocase subunit Tim8 A	1.091	2.131	0.620
Q62658	FKB1A	Peptidyl-prolyl cis-trans isomerase FKBP1A	0.749	1.681	0.616
P63170	DYL1	Dynein light chain 1, cytoplasmic	-2.017	0.247	0.602
P62329	TYB4	Thymosin beta-4	1.378	2.599	0.599
Q4QQW8	PLBL2	Putative phospholipase B-like 2	1.040	2.056	0.599
Q5U1X1	ORN	Oligoribonuclease, mitochondrial	3.224	9.341	0.597
Q01205	ODO2	Dihydrolipoyllysine-residue succinyltransferase component of 2-oxoglutarate dehydrogenase complex, mitochondrial	0.675	1.597	0.592
P05765	RS21	40S ribosomal protein S21	0.726	1.655	0.591
Q63396	TCP4	Activated RNA polymerase II transcriptional coactivator p15	-0.378	0.769	0.591
P30904	MIF	Macrophage migration inhibitory factor	0.595	1.510	0.589
Q5I0P2	GCSH	Glycine cleavage system H protein, mitochondrial	1.422	2.680	0.587
Q6P7A9	LYAG	Lysosomal alpha-glucosidase	1.994	3.983	0.579
P41498	PPAC	Low molecular weight phosphotyrosine protein phosphatase	3.003	8.014	0.579
P00787	CATB	Cathepsin B	0.838	1.788	0.579
Q4KMA2	RD23B	UV excision repair protein RAD23 homolog B	2.129	4.374	0.578
P62864	RS30	40S ribosomal protein S30	0.682	1.604	0.577
Q5XI31	PIGS	GPI transamidase component PIG-S	-1.419	0.374	0.576
P05508	NU4M	NADH-ubiquinone oxidoreductase chain 4	-0.804	0.573	0.571
P00159	CYB	Cytochrome b	-3.175	0.111	0.570
P25113	PGAM1	Phosphoglycerate mutase 1	1.170	2.250	0.566
O35142	COPB2	Coatomer subunit beta'	-1.951	0.259	0.566
Q9WU49	CHSP1	Calcium-regulated heat stable protein 1	2.956	7.762	0.566
P17702	RL28	60S ribosomal protein L28	2.171	4.504	0.563
P07150	ANXA1	Annexin A1	-0.845	0.557	0.560
Q5PQV5	TPBG	Trophoblast glycoprotein	-0.565	0.676	0.559
P63312	TYB10	Thymosin beta-10	2.346	5.083	0.558
P10959	EST1C	Carboxylesterase 1C	2.898	7.456	0.558
P28073	PSB6	Proteasome subunit beta type-6	0.627	1.545	0.557
P48037	ANXA6	Annexin A6	-0.587	0.666	0.554
B5DFC9	NID2	Nidogen-2	1.882	3.687	0.553

Aβ/CTR proteome					
Protein ID			Log_2(FC)	FC	Confidence
Q9WVE9	ITSN1	Intersectin-1	1.537	2.903	0.552
P07872	ACOX1	Peroxisomal acyl-coenzyme A oxidase 1	1.346	2.543	0.552
P31596	EAA2	Excitatory amino acid transporter 2	-0.539	0.688	0.550
Q1JU68	EIF3A	Eukaryotic translation initiation factor 3 subunit A	-2.458	0.182	0.549
Q6Q7Y5	GNA13	Guanine nucleotide-binding protein subunit alpha-13	-1.074	0.475	0.549
P11232	THIO	Thioredoxin	0.399	1.318	0.549
P84083	ARF5	ADP-ribosylation factor 5	-0.613	0.654	0.548
Q6PEC1	TBCA	Tubulin-specific chaperone A	-3.237	0.106	0.546
Q63610	TPM3	Tropomyosin alpha-3 chain	0.784	1.721	0.546
P46462	TERA	Transitional endoplasmic reticulum ATPase	0.587	1.502	0.545
Q8K3X8	HSBP1	Heat shock factor-binding protein 1	2.480	5.580	0.545
Q63065	PDK1	Pyruvate dehydrogenase (acetyl-transferring) kinase isozyme 1, mitochondrial	2.401	5.282	0.544
Q9HB97	PARVA	Alpha-parvin	-2.883	0.136	0.544
P24942	EAA1	Excitatory amino acid transporter 1	-0.384	0.767	0.542
P12075	COX5B	Cytochrome c oxidase subunit 5B, mitochondrial	0.652	1.572	0.542
P14668	ANXA5	Annexin A5	-0.601	0.659	0.539
Q5M7W4	TMC5	Transmembrane channel-like protein 5	1.468	2.766	0.537
P62083	RS7	40S ribosomal protein S7	0.346	1.271	0.536
Q5FVN0	MBOA5	Lysophospholipid acyltransferase 5	-2.988	0.126	0.536
Q8R491	EHD3	EH domain-containing protein 3	2.022	4.060	0.535
P20069	MPPA	Mitochondrial-processing peptidase subunit alpha	0.708	1.633	0.535
D3ZHA0	FLNC	Filamin-C	-0.694	0.618	0.534
Q7TP54	FA65B	Protein FAM65B	0.746	1.677	0.534
Q6GQP4	RAB31	Ras-related protein Rab-31	1.814	3.515	0.533
O35276	NRP2	Neuropilin-2	-1.556	0.340	0.532
O35263	PA1B3	Platelet-activating factor acetylhydrolase IB subunit gamma	0.417	1.335	0.532
P63102	1433Z	14-3-3 protein zeta/delta	0.319	1.248	0.532
Q63525	NUDC	Nuclear migration protein nudC	0.992	1.989	0.529
O08701	ARGI2	Arginase-2, mitochondrial	2.987	7.927	0.526
P0C5X8	TTYH1	Protein tweety homolog 1	-0.548	0.684	0.525
Q4KLL4	TM9S4	Transmembrane 9 superfamily member 4	2.013	4.037	0.525
P42667	SC11A	Signal peptidase complex catalytic subunit SEC11A	-0.704	0.614	0.525
Q9QVC8	FKBP4	Peptidyl-prolyl cis-trans isomerase FKBP4	3.498	11.297	0.521
Q66H15	RMD3	Regulator of microtubule dynamics protein 3	0.754	1.686	0.521
Q9WVK7	HCDH	Hydroxyacyl-coenzyme A dehydrogenase, mitochondrial	1.608	3.048	0.520
Q6IFV3	K1C15	Keratin, type I cytoskeletal 15	2.675	6.385	0.518
P05065	ALDOA	Fructose-bisphosphate aldolase A	-0.370	0.774	0.516
P62832	RL23	60S ribosomal protein L23	0.466	1.381	0.512
Q5XI73	GDIR1	Rho GDP-dissociation inhibitor 1	0.621	1.538	0.511

Aβ/CTR proteome					
Protein ID			**Log_2(FC)**	**FC**	**Confidence**
Q5XI73	GDIR1	Rho GDP-dissociation inhibitor 1	0.621	1.538	0.511
P60901	PSA6	Proteasome subunit alpha type-6	0.840	1.790	0.510
P24268	CATD	Cathepsin D	0.878	1.838	0.507
P19804	NDKB	Nucleoside diphosphate kinase B	0.546	1.460	0.507
Q4V898	RBMX	RNA-binding motif protein, X chromosome	1.580	2.990	0.504
P15429	ENOB	Beta-enolase	1.510	2.848	0.504
P04905	GSTM1	Glutathione S-transferase Mu 1	-0.507	0.704	0.504
P37996	ARL3	ADP-ribosylation factor-like protein 3	2.965	7.811	0.503

Table S.4: List of proteins significantly changed upon Aβ exposure compared to Aβ+ZDON, with confidence ≥50%. *Proteins that were decreased in the presence of ZDON (they are induced by TG2 activity), are highlighted in gold (FC>1), while proteins that were increased upon ZDON addition (they are reduced by TG2 activity), are highlighted in green (FC<1) (confidence ≥70%).*

Aβ/Aβ+ZDON proteome					
Protein ID			Log_2(FC)	FC	Confidence
Q6MGD0	CUTA	Protein CutA	2.626	6.174	0.868
Q6IG01	K2C1B	Keratin, type II cytoskeletal 1b	-3.779	0.073	0.835
Q63690	BAX	Apoptosis regulator BAX	3.273	9.668	0.811
Q63228	GMFB	Glia maturation factor beta	2.083	4.236	0.803
Q6IMF3	K2C1	Keratin, type II cytoskeletal 1	-1.659	0.317	0.792
Q6IFW6	K1C10	Keratin, type I cytoskeletal 10	-1.415	0.375	0.789
P62083	RS7	40S ribosomal protein S7	0.543	1.457	0.786
P62850	RS24	40S ribosomal protein S24	2.020	4.057	0.781
Q8VIL3	ZWINT	ZW10 interactor	-1.989	0.252	0.748
P68035	ACTC	Actin, alpha cardiac muscle 1	-1.643	0.320	0.743
Q05175	BASP1	Brain acid soluble protein 1	-0.820	0.567	0.718
Q5U2U2	CRKL	Crk-like protein	3.531	11.561	0.717
Q9Z272	GIT1	ARF GTPase-activating protein GIT1	2.093	4.266	0.711
P63245	GBLP	Guanine nucleotide-binding protein subunit beta-2-like 1	0.717	1.644	0.707
Q505J9	ATAD1	ATPase family AAA domain-containing protein 1	2.653	6.292	0.687
Q4AEF8	COPG1	Coatomer subunit gamma-1	1.981	3.946	0.679
P62744	AP2S1	AP-2 complex subunit sigma	-0.618	0.652	0.678
Q4KM98	MFF	Mitochondrial fission factor	-3.507	0.088	0.676
P47860	PFKAP	ATP-dependent 6-phosphofructokinase, platelet type	-1.119	0.460	0.669
Q9JM53	AIFM1	Apoptosis-inducing factor 1, mitochondrial	2.921	7.573	0.669
E9PU28	IMDH2	Inosine-5'-monophosphate dehydrogenase 2	0.674	1.596	0.666
P13437	THIM	3-ketoacyl-CoA thiolase, mitochondrial	3.504	11.346	0.663
P62329	TYB4	Thymosin beta-4	2.528	5.768	0.662
Q63396	TCP4	Activated RNA polymerase II transcriptional coactivator p15	-0.597	0.661	0.657
Q6XVN8	MLP3A	Microtubule-associated proteins 1A/1B light chain 3A	-0.930	0.525	0.651
P05714	RAB4A	Ras-related protein Rab-4A	-3.937	0.065	0.642
P15865	H14	Histone H1.4	-0.480	0.717	0.637
Q6IG02	K22E	Keratin, type II cytoskeletal 2 epidermal	-1.731	0.301	0.636
P68370	TBA1A	Tubulin alpha-1A chain	0.289	1.222	0.632
Q8K3F3	PP14B	REVERSED Protein phosphatase 1 regulatory subunit 14B	3.398	10.543	0.630
Q5PQL5	PTSS1	Phosphatidylserine synthase 1	2.954	7.748	0.629
Q4FZU2	K2C6A	Keratin, type II cytoskeletal 6A	-1.393	0.381	0.629
P62912	RL32	60S ribosomal protein L32	1.750	3.364	0.627
Q1JU68	EIF3A	Eukaryotic translation initiation factor 3 subunit A	-2.402	0.189	0.622
P02770	ALBU	Serum albumin	-0.972	0.510	0.602
Q9ES73	MAGD1	Melanoma-associated antigen D1	1.212	2.317	0.602
P10536	RAB1B	Ras-related protein Rab-1B	3.288	9.768	0.597

Aβ/Aβ+ZDON proteome					
Protein ID			Log_2(FC)	FC	Confidence
P63081	VATL	V-type proton ATPase 16 kDa proteolipid subunit	-1.762	0.295	0.589
P17702	RL28	60S ribosomal protein L28	3.014	8.081	0.589
P62909	RS3	40S ribosomal protein S3	0.520	1.434	0.574
O08662	PI4KA	Phosphatidylinositol 4-kinase alpha	2.096	4.276	0.570
P29314	RS9	40S ribosomal protein S9	0.359	1.282	0.569
P62755	RS6	40S ribosomal protein S6	0.483	1.398	0.566
P62243	RS8	40S ribosomal protein S8	0.590	1.505	0.565
P04550	PTMS	Parathymosin	0.610	1.526	0.556
D4AD37	IMPA3	Inositol monophosphatase 3	-2.266	0.208	0.556
Q5I0D1	GLOD4	Glyoxalase domain-containing protein 4	2.794	6.935	0.551
P85973	PNPH	Purine nucleoside phosphorylase	2.246	4.745	0.549
P62271	RS18	40S ribosomal protein S18	0.427	1.344	0.549
O88377	PI42B	Phosphatidylinositol 5-phosphate 4-kinase type-2 beta	-0.836	0.560	0.547
P13852	PRIO	Major prion protein	-1.332	0.397	0.547
P28075	PSB5	Proteasome subunit beta type-5	1.525	2.878	0.547
Q4KLF8	ARPC5	Actin-related protein 2/3 complex subunit 5	0.350	1.274	0.546
Q6PCU8	NDUV3	NADH dehydrogenase ubiquinone flavoprotein 3, mitochondrial	1.115	2.166	0.546
P0C1X8	AAK1	AP2-associated protein kinase 1	-0.927	0.526	0.543
P24050	RS5	40S ribosomal protein S5	0.429	1.346	0.542
B0BN93	PSD13	26S proteasome non-ATPase regulatory subunit 13	-3.557	0.085	0.541
Q9EPB1	DPP2	Dipeptidyl peptidase 2	1.413	2.662	0.541
Q7TP54	FA65B	Protein FAM65B	0.926	1.900	0.537
P13635	CERU	Ceruloplasmin	-1.982	0.253	0.535
P62914	RL11	60S ribosomal protein L11	0.394	1.314	0.535
Q9R1N3	S4A7	Sodium bicarbonate cotransporter 3	2.369	5.168	0.535
Q1WIM3	CADM3	Cell adhesion molecule 3	-0.585	0.666	0.534
O35276	NRP2	Neuropilin-2	3.701	13.001	0.533
P0CC09	H2A2A	Histone H2A type 2-A	-0.769	0.587	0.531
P47868	SCG3	Secretogranin-3	1.724	3.302	0.528
P23965	ECI1	Enoyl-CoA delta isomerase 1, mitochondrial	3.132	8.765	0.526
P20069	MPPA	Mitochondrial-processing peptidase subunit alpha	0.631	1.549	0.526
Q5XIF4	SUMO3	Small ubiquitin-related modifier 3	0.414	1.332	0.523
P56603	SCAM1	Secretory carrier-associated membrane protein 1	0.395	1.315	0.520
Q6AYQ3	SYFM	REVERSED Phenylalanine--tRNA ligase, mitochondrial	0.388	1.309	0.513
B2RYG6	OTUB1	Ubiquitin thioesterase OTUB1	0.643	1.561	0.513
Q6AYM7	CK085	Uncharacterized protein C11orf85 homolog	-0.809	0.571	0.510
Q5I0H4	TMCO1	Transmembrane and coiled-coil domains protein 1	-0.399	0.758	0.509
Q8VIJ5	OGA	Protein O-GlcNAcase	1.498	2.824	0.509
Q5FVH2	PLD3	Phospholipase D3	0.432	1.349	0.508
P05696	KPCA	Protein kinase C alpha type	-1.736	0.300	0.503
Q10758	K2C8	Keratin, type II cytoskeletal 8	-1.637	0.322	0.502
P42667	SC11A	Signal peptidase complex catalytic subunit SEC11A	-0.662	0.632	0.502
P00173	CYB5	Cytochrome b5	0.909	1.878	0.501

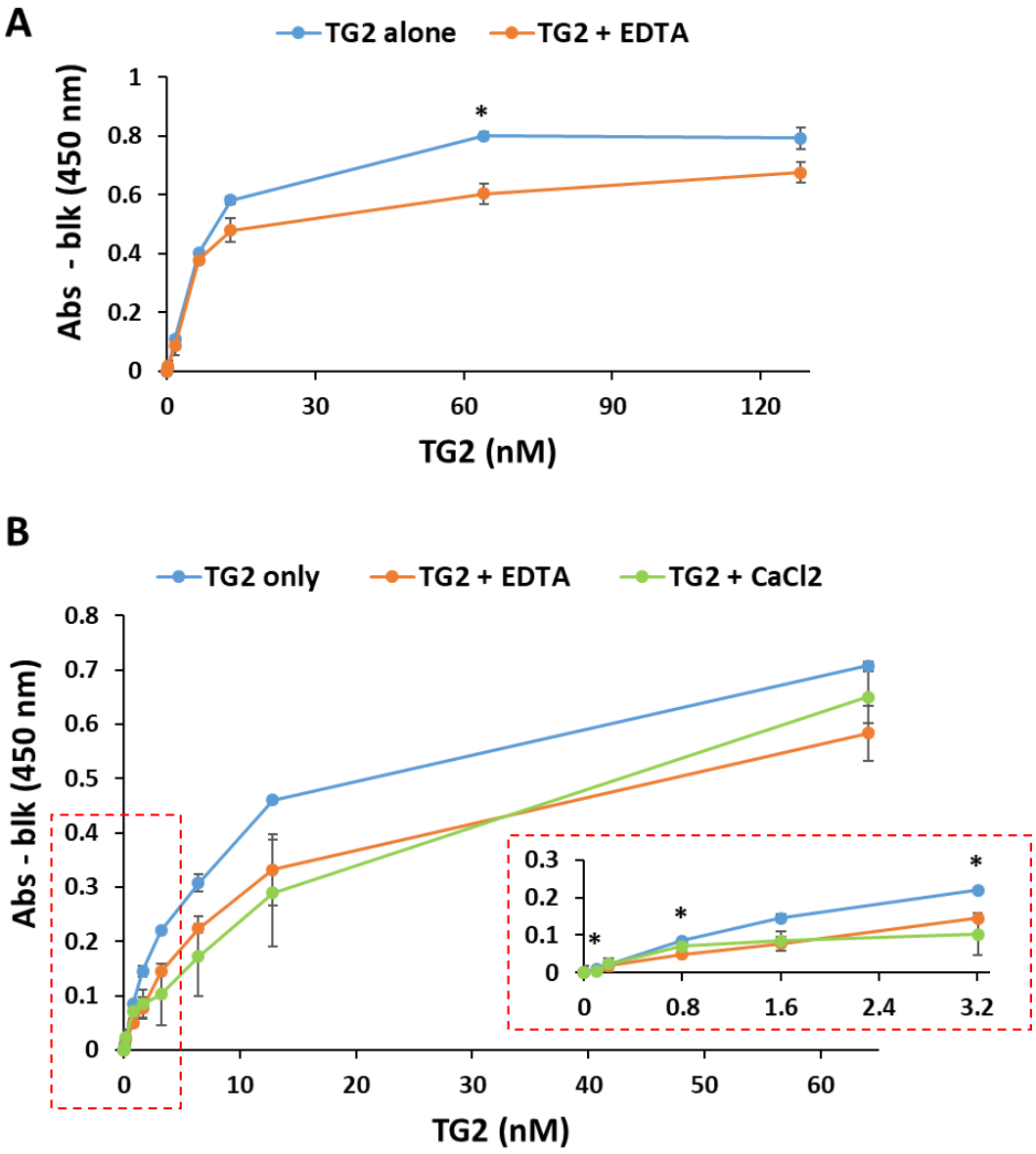

Figure S.1. Optimisation of TG2 standard curve for detection by ELISA. A) *A standard curve of TG2 in blocking buffer (3% BSA w/v in Tris-HCl 50 mM, pH 7.4) was made to assess TG2 binding to the FN-coated plate (range 0.2-128 nM, equal to 0.0156-10 µg/ml of TG2). TG2 was tested with or without addition of 2 mM EDTA, to verify if the presence of a chelating agent inhibiting TG2 crosslinking activity would improve TG2 binding to FN. Data are expressed as average of absorbance readings at 450 nm minus background ± SE (in duplicates). *p≤0.05.* ***B)*** *TG2 standard curve was quantified alone or with addition of either 2 mM EDTA or 1.22 mM CaCl2. A lower dynamic range of TG2 was tested (0.1-64 nM, equal to 0.0078-5 µg/ml of TG2). Data are expressed as average of absorbance readings at 450 nm minus background ± SE (in duplicates). *p≤0.05 (TG2 only and TG2+EDTA comparison). An enlargement of the first 6 points of the TG2 standard curves is included (red dotted square). Incubation time of standard curve on FN was 3 hours.*

List of References

Achyuthan KE, Greenberg CS. Identification of a guanosine triphosphate-binding site on guinea pig liver transglutaminase. Role of GTP and calcium ions in modulating activity. J Biol Chem. 1987;262(4):1901-6.

Aeschlimann D, Paulsson M. Transglutaminases: protein cross-linking enzymes in tissues and body fluids. Thromb Haemost. 1994;71(4):402-15.

Ahn YM, Hong GU, Kim SH, Lee HJ, Baek HS, Kim MN, et al. Transglutaminase 2 expressed in mast cells recruited into skin or bone marrow induces the development of pediatric mastocytosis. Pediatr Allergy Immunol. 2015;26(5):438-45.

Akbar A, McNeil NMR, Albert MR, Ta V, Adhikary G, Bourgeois K, et al. Structure-Activity Relationships of Potent, Targeted Covalent Inhibitors That Abolish Both the Transamidation and GTP Binding Activities of Human Tissue Transglutaminase. J Med Chem. 2017;60(18):7910-27.

Akimov SS, Belkin AM. Cell surface tissue transglutaminase is involved in adhesion and migration of monocytic cells on fibronectin. Blood. 2001;98(5):1567-76.

Akimov SS, Krylov D, Fleischman LF, Belkin AM. Tissue transglutaminase is an integrin-binding adhesion coreceptor for fibronectin. J Cell Biol. 2000;148(4):825-38.

Aksenov M, Aksenova M, Butterfield DA, Markesbery WR. Oxidative modification of creatine kinase BB in Alzheimer's disease brain. J Neurochem. 2000;74(6):2520-7.

Ambron RT, Kremzner LT. Post-translational modification of neuronal proteins: evidence for transglutaminase activity in R2, the giant cholinergic neuron of Aplysia. Proc Natl Acad Sci U S A. 1982;79(11):3442-6.

Ambrosi G, Ghezzi C, Sepe S, Milanese C, Payan-Gomez C, Bombardieri CR, et al. Bioenergetic and proteolytic defects in fibroblasts from patients with sporadic Parkinson's disease. Biochim Biophys Acta. 2014;1842(9):1385-94.

An K, Klyubin I, Kim Y, Jung JH, Mably AJ, T O'Dowd S, et al. Exosomes neutralize synaptic-plasticity-disrupting activity of Aβ assemblies in vivo. Molecular brain. 2013;6(1):47.

Andaloussi SE, Mäger I, Breakefield XO, Wood MJ. Extracellular vesicles: biology and emerging therapeutic opportunities. Nature reviews Drug discovery. 2013;12(5):347.

Andre W, Nondier I, Valensi M, Guillonneau F, Federici C, Hoffner G, et al. Identification of brain substrates of transglutaminase by functional proteomics supports its role in neurodegenerative diseases. Neurobiol Dis. 2017;101:40-58.

Andringa G, Lam KY, Chegary M, Wang X, Chase TN, Bennett MC. Tissue transglutaminase catalyzes the formation of alpha-synuclein crosslinks in Parkinson's disease. FASEB J. 2004;18(7):932-4.

Angeles DC, Ho P, Chua LL, Wang C, Yap YW, Ng C, et al. Thiol peroxidases ameliorate LRRK2 mutant-induced mitochondrial and dopaminergic neuronal degeneration in Drosophila. Hum Mol Genet. 2014;23(12):3157-65.

Annunziato L, Pignataro G, Boscia F, Sirabella R, Formisano L, Saggese M, et al. ncx1, ncx2, and ncx3 gene product expression and function in neuronal anoxia and brain ischemia. Ann N Y Acad Sci. 2007;1099:413-26.

Antonucci F, Turola E, Riganti L, Caleo M, Gabrielli M, Perrotta C, et al. Microvesicles released from microglia stimulate synaptic activity via enhanced sphingolipid metabolism. EMBO J. 2012;31(5):1231-40.

Antonyak MA, Jansen JM, Miller AM, Ly TK, Endo M, Cerione RA. Two isoforms of tissue transglutaminase mediate opposing cellular fates. Proc Natl Acad Sci U S A. 2006;103(49):18609-14.

Antonyak MA, Li B, Boroughs LK, Johnson JL, Druso JE, Bryant KL, et al. Cancer cell-derived microvesicles induce transformation by transferring tissue transglutaminase and fibronectin to recipient cells. Proc Natl Acad Sci U S A. 2011;108(12):4852-7.

Anwar R, Stewart AD, Miloszewski KJ, Losowsky MS, Markham AF. Molecular basis of inherited factor XIII deficiency: identification of multiple mutations provides insights into protein function. Br J Haematol. 1995;91(3):728-35.

Appelt DM, Kopen GC, Boyne LJ, Balin BJ. Localization of transglutaminase in hippocampal neurons: implications for Alzheimer's disease. J Histochem Cytochem. 1996;44(12):1421-7.

Bading H, Ginty DD, Greenberg ME. Regulation of gene expression in hippocampal neurons by distinct calcium signaling pathways. Science. 1993;260(5105):181-6.

Bailey CD, Johnson GV. Developmental regulation of tissue transglutaminase in the mouse forebrain. J Neurochem. 2004;91(6):1369-79.

Ballestar E, Abad C, Franco L. Core histones are glutaminyl substrates for tissue transglutaminase. J Biol Chem. 1996;271(31):18817-24.

Ballestar E, Boix-Chornet M, Franco L. Conformational changes in the nucleosome followed by the selective accessibility of histone glutamines in the transglutaminase reaction: effects of ionic strength. Biochemistry. 2001;40(7):1922-9.

Barile MF, Rottem S. Mycoplasmas in cell culture. Rapid diagnosis of mycoplasmas: Springer; 1993. p. 155-93.

Barna J, Dimen D, Puska G, Kovacs D, Csikos V, Olah S, et al. Complement component 1q subcomponent binding protein in the brain of the rat. Sci Rep. 2019;9(1):4597.

Barres BA. The mystery and magic of glia: a perspective on their roles in health and disease. Neuron. 2008;60(3):430-40.

Basso M, Berlin J, Xia L, Sleiman SF, Ko B, Haskew-Layton R, et al. Transglutaminase inhibition protects against oxidative stress-induced neuronal death downstream of pathological ERK activation. J Neurosci. 2012;32(19):6561-9.

Basso M, Ratan RR. Transglutaminase is a therapeutic target for oxidative stress, excitotoxicity and stroke: a new epigenetic kid on the CNS block. J Cereb Blood Flow Metab. 2013;33(6):809-18.

Beal MF. Mitochondrial dysfunction in neurodegenerative diseases. Biochim Biophys Acta. 1998;1366(1-2):211-23.

Becerik S, Celec P, Gurkan A, Ozturk VO, Kamodyova N, Atilla G, et al. Gingival Crevicular Fluid and Plasma Levels of Transglutaminase-2 and Oxidative Stress Markers in Cyclosporin A-Induced Gingival Overgrowth. J Periodontol. 2016;87(12):1508-16.

Becerik S, Ozturk VO, Celec P, Kamodyova N, Atilla G, Emingil G. Gingival crevicular fluid and plasma oxidative stress markers and TGM-2 levels in chronic periodontitis. Arch Oral Biol. 2017;83:47-54.

Begg GE, Carrington L, Stokes PH, Matthews JM, Wouters MA, Husain A, et al. Mechanism of allosteric regulation of transglutaminase 2 by GTP. Proc Natl Acad Sci U S A. 2006;103(52):19683-8.

Behnisch T, Reymann KG. Thapsigargin blocks long-term potentiation induced by weak, but not strong tetanisation in rat hippocampal CA1 neurons. Neurosci Lett. 1995;192(3):185-8.

Benilova I, Karran E, De Strooper B. The toxic Abeta oligomer and Alzheimer's disease: an emperor in need of clothes. Nat Neurosci. 2012;15(3):349-57.

Bennett V, Stenbuck PJ. Association between ankyrin and the cytoplasmic domain of band 3 isolated from the human erythrocyte membrane. J Biol Chem. 1980;255(13):6424-32.

Benussi L, Ciani M, Tonoli E, Morbin M, Palamara L, Albani D, et al. Loss of exosomes in progranulin-associated frontotemporal dementia. Neurobiol Aging. 2016;40:41-9.

Bergamini CM. GTP modulates calcium binding and cation-induced conformational changes in erythrocyte transglutaminase. FEBS Lett. 1988;239(2):255-8.

Bergamini CM, Signorini M, Poltronieri L. Inhibition of erythrocyte transglutaminase by GTP. Biochim Biophys Acta. 1987;916(1):149-51.

Berridge MJ. Calcium hypothesis of Alzheimer's disease. Pflugers Arch. 2010;459(3):441-9.

Berrocal M, Corbacho I, Vazquez-Hernandez M, Avila J, Sepulveda MR, Mata AM. Inhibition of PMCA activity by tau as a function of aging and Alzheimer's neuropathology. Biochim Biophys Acta. 2015;1852(7):1465-76.

Berrocal M, Marcos D, Sepulveda MR, Perez M, Avila J, Mata AM. Altered Ca2+ dependence of synaptosomal plasma membrane Ca2+-ATPase in human brain affected by Alzheimer's disease. FASEB J. 2009;23(6):1826-34.

Bertram L, Tanzi RE. The genetic epidemiology of neurodegenerative disease. J Clin Invest. 2005;115(6):1449-57.

Bianco F, Pravettoni E, Colombo A, Schenk U, Moller T, Matteoli M, et al. Astrocyte-derived ATP induces vesicle shedding and IL-1 beta release from microglia. J Immunol. 2005;174(11):7268-77.

Biber K, Neumann H, Inoue K, Boddeke HW. Neuronal 'On' and 'Off' signals control microglia. Trends Neurosci. 2007;30(11):596-602.

Blaustein MP, Lederer WJ. Sodium/calcium exchange: its physiological implications. Physiol Rev. 1999;79(3):763-854.

Blennow K, Hampel H, Weiner M, Zetterberg H. Cerebrospinal fluid and plasma biomarkers in Alzheimer disease. Nat Rev Neurol. 2010;6(3):131-44.

Blennow K, Mattsson N, Scholl M, Hansson O, Zetterberg H. Amyloid biomarkers in Alzheimer's disease. Trends Pharmacol Sci. 2015;36(5):297-309.

Bognar P, Nemeth I, Mayer B, Haluszka D, Wikonkal N, Ostorhazi E, et al. Reduced inflammatory threshold indicates skin barrier defect in transglutaminase 3 knockout mice. J Invest Dermatol. 2014;134(1):105-11.

Bonelli RM, Aschoff A, Niederwieser G, Heuberger C, Jirikowski G. Cerebrospinal Fluid Tissue Transglutaminase as a Biochemical Marker for Alzheimer's Disease. Neurobiology of Disease. 2002;11(1):106-10.

Borroni B, Ferrari F, Galimberti D, Nacmias B, Barone C, Bagnoli S, et al. Heterozygous TREM2 mutations in frontotemporal dementia. Neurobiol Aging. 2014;35(4):934 e7-10.

Braggin JE, Bucks SA, Course MM, Smith CL, Sopher B, Osnis L, et al. Alternative splicing in a presenilin 2 variant associated with Alzheimer disease. Ann Clin Transl Neurol. 2019;6(4):762-77.

Brini M, Cali T, Ottolini D, Carafoli E. Neuronal calcium signaling: function and dysfunction. Cell Mol Life Sci. 2014;71(15):2787-814.

Brini M, Carafoli E. The plasma membrane Ca(2)+ ATPase and the plasma membrane sodium calcium exchanger cooperate in the regulation of cell calcium. Cold Spring Harb Perspect Biol. 2011;3(2).

Brorson JR, Bindokas VP, Iwama T, Marcuccilli CJ, Chisholm JC, Miller RJ. The Ca2+ influx induced by β - amyloid peptide 25−35 in cultured hippocampal neurons results from network excitation. Journal of neurobiology. 1995;26(3):325-38.

Budd SL, Nicholls DG. Mitochondria, calcium regulation, and acute glutamate excitotoxicity in cultured cerebellar granule cells. J Neurochem. 1996;67(6):2282-91.

Burhan I, Furini G, Lortat-Jacob H, Atobatele AG, Scarpellini A, Schroeder N, et al. Interplay between transglutaminases and heparan sulphate in progressive renal scarring. Sci Rep. 2016;6:31343.

Burnashev N, Monyer H, Seeburg PH, Sakmann B. Divalent ion permeability of AMPA receptor channels is dominated by the edited form of a single subunit. Neuron. 1992;8(1):189-98.

Butterfield DA, Gnjec A, Poon HF, Castegna A, Pierce WM, Klein JB, et al. Redox proteomics identification of oxidatively modified brain proteins in inherited Alzheimer's disease: an initial assessment. J Alzheimers Dis. 2006;10(4):391-7.

Butterfield DA, Lange ML. Multifunctional roles of enolase in Alzheimer's disease brain: beyond altered glucose metabolism. J Neurochem. 2009;111(4):915-33.

Caccamo D, Campisi A, Curro M, Aguennouz M, Li Volti G, Avola R, et al. Nuclear factor-kappab activation is associated with glutamate-evoked tissue transglutaminase up-regulation in primary astrocyte cultures. J Neurosci Res. 2005;82(6):858-65.

Caccamo D, Curro M, Ferlazzo N, Condello S, Ientile R. Monitoring of transglutaminase 2 under different oxidative stress conditions. Amino Acids. 2012;42(2-3):1037-43.

Calegari F, Coco S, Taverna E, Bassetti M, Verderio C, Corradi N, et al. A regulated secretory pathway in cultured hippocampal astrocytes. J Biol Chem. 1999;274(32):22539-47.

Campioni S, Mannini B, Zampagni M, Pensalfini A, Parrini C, Evangelisti E, et al. A causative link between the structure of aberrant protein oligomers and their toxicity. Nat Chem Biol. 2010;6(2):140-7.

Campisi A, Renis M, Russo A, Sorrenti V, Di Giacomo C, Castorina C, et al. Transglutaminase activity in primary and subcultured rat astroglial cells. Neurochem Res. 1992;17(12):1201-5.

Candi E, Melino G, Lahm A, Ceci R, Rossi A, Kim IG, et al. Transglutaminase 1 mutations in lamellar ichthyosis. Loss of activity due to failure of activation by proteolytic processing. J Biol Chem. 1998;273(22):13693-702.

Candi E, Oddi S, Paradisi A, Terrinoni A, Ranalli M, Teofoli P, et al. Expression of transglutaminase 5 in normal and pathologic human epidermis. J Invest Dermatol. 2002;119(3):670-7.

Candi E, Oddi S, Terrinoni A, Paradisi A, Ranalli M, Finazzi-Agro A, et al. Transglutaminase 5 cross-links loricrin, involucrin, and small proline-rich proteins in vitro. J Biol Chem. 2001;276(37):35014-23.

Carafoli E. INTRACELLULAR CALCIUM HOMEOSTASIS. Annual Review of Biochemistry. 1987;56(1):395-433.

Carecchio M, Fenoglio C, Cortini F, Comi C, Benussi L, Ghidoni R, et al. Cerebrospinal fluid biomarkers in Progranulin mutations carriers. J Alzheimers Dis. 2011;27(4):781-90.

Casadio R, Polverini E, Mariani P, Spinozzi F, Carsughi F, Fontana A, et al. The structural basis for the regulation of tissue transglutaminase by calcium ions. Eur J Biochem. 1999;262(3):672-9.

Cassidy AJ, van Steensel MA, Steijlen PM, van Geel M, van der Velden J, Morley SM, et al. A homozygous missense mutation in TGM5 abolishes epidermal transglutaminase 5 activity and causes acral peeling skin syndrome. Am J Hum Genet. 2005;77(6):909-17.

Cataldi M. The changing landscape of voltage-gated calcium channels in neurovascular disorders and in neurodegenerative diseases. Curr Neuropharmacol. 2013;11(3):276-97.

Catterall WA. Voltage-gated calcium channels. Cold Spring Harb Perspect Biol. 2011;3(8):a003947.

Catterall WA, Few AP. Calcium channel regulation and presynaptic plasticity. Neuron. 2008;59(6):882-901.

Chau DY, Collighan RJ, Verderio EA, Addy VL, Griffin M. The cellular response to transglutaminase-cross-linked collagen. Biomaterials. 2005;26(33):6518-29.

Chaudhuri AD, Dastgheyb RM, Yoo SW, Trout A, Talbot CC, Jr., Hao H, et al. TNFalpha and IL-1beta modify the miRNA cargo of astrocyte shed extracellular vesicles to regulate neurotrophic signaling in neurons. Cell Death Dis. 2018;9(3):363.

Cheek TR. Spatial aspects of calcium signalling. J Cell Sci. 1989;93 (Pt 2):211-6.

Chen J, Fujino R, Zhao R, Semba U, Araki K, Yamamoto T. Role of blood ribosomal protein S19 in coagulum resorption: a study using Gln137Glu-ribosomal protein S19 gene knock-in mouse. Pathol Int. 2014;64(11):543-50.

Chen J, Zhao R, Semba U, Oda M, Suzuki T, Toba K, et al. Involvement of cross-linked ribosomal protein S19 oligomers and C5a receptor in definitive erythropoiesis. Exp Mol Pathol. 2013;95(3):364-75.

Chen JS, Mehta K. Tissue transglutaminase: an enzyme with a split personality. Int J Biochem Cell Biol. 1999;31(8):817-36.

Chen K, Ochalski PG, Tran TS, Sahir N, Schubert M, Pramatarova A, et al. Interaction between Dab1 and CrkII is promoted by Reelin signaling. J Cell Sci. 2004;117(Pt 19):4527-36.

Chin D, Means AR. Calmodulin: a prototypical calcium sensor. Trends Cell Biol. 2000;10(8):322-8.

Chivet M, Hemming F, Pernet-Gallay K, Fraboulet S, Sadoul R. Emerging role of neuronal exosomes in the central nervous system. Front Physiol. 2012;3:145.

Cho SY, Lee JH, Bae HD, Jeong EM, Jang GY, Kim CW, et al. Transglutaminase 2 inhibits apoptosis induced by calcium- overload through down-regulation of Bax. Exp Mol Med. 2010;42(9):639-50.

Chowdhury AR, Ghosh I, Datta K. Excessive reactive oxygen species induces apoptosis in fibroblasts: role of mitochondrially accumulated hyaluronic acid binding protein 1 (HABP1/p32/gC1qR). Exp Cell Res. 2008;314(3):651-67.

Citron BA, SantaCruz KS, Davies PJ, Festoff BW. Intron-exon swapping of transglutaminase mRNA and neuronal Tau aggregation in Alzheimer's disease. J Biol Chem. 2001;276(5):3295-301.

Citron BA, Suo Z, SantaCruz K, Davies PJ, Qin F, Festoff BW. Protein crosslinking, tissue transglutaminase, alternative splicing and neurodegeneration. Neurochem Int. 2002;40(1):69-78.

Clark AR, Ohlmeyer M. Protein phosphatase 2A as a therapeutic target in inflammation and neurodegeneration. Pharmacol Ther. 2019;201:181-201.

Clement S, Velasco PT, Murthy SN, Wilson JH, Lukas TJ, Goldman RD, et al. The intermediate filament protein, vimentin, in the lens is a target for cross-linking by transglutaminase. J Biol Chem. 1998;273(13):7604-9.

Clos AL, Kayed R, Lasagna-Reeves CA. Association of skin with the pathogenesis and treatment of neurodegenerative amyloidosis. Front Neurol. 2012;3:5.

Clouthier CM, Mironov GG, Okhonin V, Berezovski MV, Keillor JW. Real-time monitoring of protein conformational dynamics in solution using kinetic capillary electrophoresis. Angew Chem Int Ed Engl. 2012;51(50):12464-8.

Coco S, Calegari F, Pravettoni E, Pozzi D, Taverna E, Rosa P, et al. Storage and release of ATP from astrocytes in culture. J Biol Chem. 2003;278(2):1354-62.

Cocucci E, Meldolesi J. Ectosomes and exosomes: shedding the confusion between extracellular vesicles. Trends Cell Biol. 2015;25(6):364-72.

Colak G, Johnson GV. Complete transglutaminase 2 ablation results in reduced stroke volumes and astrocytes that exhibit increased survival in response to ischemia. Neurobiol Dis. 2012;45(3):1042-50.

Colak G, Keillor JW, Johnson GV. Cytosolic guanine nucledotide binding deficient form of transglutaminase 2 (R580a) potentiates cell death in oxygen glucose deprivation. PLoS One. 2011;6(1):e16665.

Collingridge GL, Kehl SJ, McLennan H. Excitatory amino acids in synaptic transmission in the Schaffer collateral-commissural pathway of the rat hippocampus. J Physiol. 1983;334:33-46.

Colombo E, Borgiani B, Verderio C, Furlan R. Microvesicles: novel biomarkers for neurological disorders. Front Physiol. 2012;3:63.

Condliffe SB, Corradini I, Pozzi D, Verderio C, Matteoli M. Endogenous SNAP-25 regulates native voltage-gated calcium channels in glutamatergic neurons. J Biol Chem. 2010;285(32):24968-76.

Contractor A, Mulle C, Swanson GT. Kainate receptors coming of age: milestones of two decades of research. Trends Neurosci. 2011;34(3):154-63.

Cserhalmi-Friedman PB, Milstone LM, Christiano AM. Diagnosis of autosomal recessive lamellar ichthyosis with mutations in the TGM1 gene. Br J Dermatol. 2001;144(4):726-30.

Curtis DR, Duggan AW, Felix D, Johnston GA. GABA, bicuculline and central inhibition. Nature. 1970;226(5252):1222-4.

Dale GL, Friese P, Batar P, Hamilton SF, Reed GL, Jackson KW, et al. Stimulated platelets use serotonin to enhance their retention of procoagulant proteins on the cell surface. Nature. 2002;415(6868):175-9.

Dardik R, Inbal A. Complex formation between tissue transglutaminase II (tTG) and vascular endothelial growth factor receptor 2 (VEGFR-2): proposed mechanism for modulation of endothelial cell response to VEGF. Exp Cell Res. 2006;312(16):2973-82.

Das P, Murphy MP, Younkin LH, Younkin SG, Golde TE. Reduced effectiveness of Abeta1-42 immunization in APP transgenic mice with significant amyloid deposition. Neurobiol Aging. 2001;22(5):721-7.

Datta S, Antonyak MA, Cerione RA. GTP-binding-defective forms of tissue transglutaminase trigger cell death. Biochemistry. 2007;46(51):14819-29.

de Jager M, Drukarch B, Hofstee M, Breve J, Jongenelen CA, Bol JG, et al. Tissue transglutaminase-catalysed cross-linking induces Apolipoprotein E multimers inhibiting Apolipoprotein E's protective effects towards amyloid-beta-induced toxicity. J Neurochem. 2015;134(6):1116-28.

De Laurenzi V, Melino G. Gene disruption of tissue transglutaminase. Mol Cell Biol. 2001;21(1):148-55.

DeCarli C. Mild cognitive impairment: prevalence, prognosis, aetiology, and treatment. The Lancet Neurology. 2003;2(1):15-21.

Dedeoglu A, Kubilus JK, Jeitner TM, Matson SA, Bogdanov M, Kowall NW, et al. Therapeutic effects of cystamine in a murine model of Huntington's disease. J Neurosci. 2002;22(20):8942-50.

Demény MA, Korponay-Szabó I, Fesus L. Structure of Transglutaminases: Unique Features Serve Diverse Functions. In: Hitomi K, Kojima S, Fesus L, editors. Transglutaminases, Multiple Functional Modifiers and Targets for New Drug Discovery: Springer Japan; 2015. p. 1-42.

Di Fede G, Catania M, Maderna E, Ghidoni R, Benussi L, Tonoli E, et al. Molecular subtypes of Alzheimer's disease. Sci Rep. 2018;8(1):3269.

Diaz-Hidalgo L, Altuntas S, Rossin F, D'Eletto M, Marsella C, Farrace MG, et al. Transglutaminase type 2-dependent selective recruitment of proteins into exosomes under stressful cellular conditions. Biochim Biophys Acta. 2016;1863(8):2084-92.

Dickens AM, Tovar YRLB, Yoo SW, Trout AL, Bae M, Kanmogne M, et al. Astrocyte-shed extracellular vesicles regulate the peripheral leukocyte response to inflammatory brain lesions. Sci Signal. 2017;10(473).

Dickson DW, Crystal HA, Bevona C, Honer W, Vincent I, Davies P. Correlations of synaptic and pathological markers with cognition of the elderly. Neurobiol Aging. 1995;16(3):285-98; discussion 98-304.

Dieterich W, Ehnis T, Bauer M, Donner P, Volta U, Riecken EO, et al. Identification of tissue transglutaminase as the autoantigen of celiac disease. Nat Med. 1997;3(7):797-801.

Ding Y, Zhang J, Wang R. Inhibition of tissue transglutaminase attenuates lipopolysaccharide-induced inflammation in glial cells through AKT/mTOR signal pathway. Biomed Pharmacother. 2017;89:1310-9.

Doeuvre L, Plawinski L, Toti F, Angles-Cano E. Cell-derived microparticles: a new challenge in neuroscience. J Neurochem. 2009;110(2):457-68.

D'Souza-Schorey C, Clancy JW. Tumor-derived microvesicles: shedding light on novel microenvironment modulators and prospective cancer biomarkers. Genes Dev. 2012;26(12):1287-99.

Dubois B, Feldman HH, Jacova C, DeKosky ST, Barberger-Gateau P, Cummings J, et al. Research criteria for the diagnosis of Alzheimer's disease: revising the NINCDS–ADRDA criteria. The Lancet Neurology. 2007;6(8):734-46.

Eckert RL, Kaartinen MT, Nurminskaya M, Belkin AM, Colak G, Johnson GVW, et al. Transglutaminase regulation of cell function. Physiological reviews. 2014;94(2):383-417.

Faure J, Lachenal G, Court M, Hirrlinger J, Chatellard-Causse C, Blot B, et al. Exosomes are released by cultured cortical neurones. Mol Cell Neurosci. 2006;31(4):642-8.

Fellin T, Pascual O, Gobbo S, Pozzan T, Haydon PG, Carmignoto G. Neuronal synchrony mediated by astrocytic glutamate through activation of extrasynaptic NMDA receptors. Neuron. 2004;43(5):729-43.

Feola J, Barton A, Akbar A, Keillor J, Johnson GVW. Transglutaminase 2 modulation of NF-kappaB signaling in astrocytes is independent of its ability to mediate astrocytic viability in ischemic injury. Brain Res. 2017;1668:1-11.

Fernandes HB, Baimbridge KG, Church J, Hayden MR, Raymond LA. Mitochondrial sensitivity and altered calcium handling underlie enhanced NMDA-induced apoptosis in YAC128 model of Huntington's disease. J Neurosci. 2007;27(50):13614-23.

Fesus L. Biochemical events in naturally occurring forms of cell death. FEBS Lett. 1993;328(1-2):1-5.

Fiacco TA, McCarthy KD. Astrocyte calcium elevations: properties, propagation, and effects on brain signaling. Glia. 2006;54(7):676-90.

Fiandaca MS, Kapogiannis D, Mapstone M, Boxer A, Eitan E, Schwartz JB, et al. Identification of preclinical Alzheimer's disease by a profile of pathogenic proteins in neurally derived blood exosomes: A case-control study. Alzheimers Dement. 2015;11(6):600-7 e1.

Filiano AJ, Bailey CD, Tucholski J, Gundemir S, Johnson GV. Transglutaminase 2 protects against ischemic insult, interacts with HIF1beta, and attenuates HIF1 signaling. FASEB J. 2008;22(8):2662-75.

Filiano AJ, Tucholski J, Dolan PJ, Colak G, Johnson GV. Transglutaminase 2 protects against ischemic stroke. Neurobiol Dis. 2010;39(3):334-43.

Fisher ML, Kerr C, Adhikary G, Grun D, Xu W, Keillor JW, et al. Transglutaminase Interaction with alpha6/beta4-Integrin Stimulates YAP1-Dependent DeltaNp63alpha Stabilization and Leads to Enhanced Cancer Stem Cell Survival and Tumor Formation. Cancer Res. 2016;76(24):7265-76.

Folk JE. Mechanism of action of guinea pig liver transglutaminase. VI. Order of substrate addition. J Biol Chem. 1969;244(13):3707-13.

Folk JE, Finlayson JS. The ε-(γ-Glutamyl)Lysine Crosslink and the Catalytic Role of Transglutaminases. Advances in Protein Chemistry Volume 31. Advances in Protein Chemistry1977. p. 1-133.

Folstein M. A practical method for grading the cognitive state of patients for the children. J Psychiatr res. 1975;12:189-98.

Fonseca AC, Ferreiro E, Oliveira CR, Cardoso SM, Pereira CF. Activation of the endoplasmic reticulum stress response by the amyloid-beta 1-40 peptide in brain endothelial cells. Biochim Biophys Acta. 2013;1832(12):2191-203.

Fraij BM, Birckbichler PJ, Patterson MK, Jr., Lee KN, Gonzales RA. A retinoic acid-inducible mRNA from human erythroleukemia cells encodes a novel tissue transglutaminase homologue. J Biol Chem. 1992;267(31):22616-23.

Fraij BM, Gonzales RA. A third human tissue transglutaminase homologue as a result of alternative gene transcripts. Biochim Biophys Acta. 1996;1306(1):63-74.

Frisoni GB, Fox NC, Jack CR, Jr., Scheltens P, Thompson PM. The clinical use of structural MRI in Alzheimer disease. Nat Rev Neurol. 2010;6(2):67-77.

Fujita K, Honda M, Hayashi R, Ogawa K, Ando M, Yamauchi M, et al. Transglutaminase activity in serum and cerebrospinal fluid in sporadic amyotrophic lateral sclerosis: a possible use as an indicator of extent of the motor neuron loss. J Neurol Sci. 1998;158(1):53-7.

Fujita K, Kato T, Shibayama K, Imada H, Yamauchi M, Yoshimoto N, et al. Protective effect against 17beta-estradiol on neuronal apoptosis in hippocampus tissue following transient ischemia/recirculation in mongolian gerbils via down-regulation of tissue transglutaminase activity. Neurochem Res. 2006;31(8):1059-68.

Furini G, Schroeder N, Huang L, Boocock D, Scarpellini A, Coveney C, et al. Proteomic Profiling Reveals the Transglutaminase-2 Externalization Pathway in Kidneys after Unilateral Ureteric Obstruction. J Am Soc Nephrol. 2018;29(3):880-905.

Furutani Y and Kojima S. Control of TG Functions Depending on Their Localization. In: Hitomi K, Kojima S, Fesus L, editors. Transglutaminases, Multiple Functional Modifiers and Targets for New Drug Discovery: Springer Japan; 2015. p. 43-62.

Gadoth A, Nefussy B, Bleiberg M, Klein T, Artman I, Drory VE. Transglutaminase 6 Antibodies in the Serum of Patients With Amyotrophic Lateral Sclerosis. JAMA Neurol. 2015;72(6):676-81.

Gagni P, Cretich M, Benussi L, Tonoli E, Ciani M, Ghidoni R, et al. Combined mass quantitation and phenotyping of intact extracellular vesicles by a microarray platform. Anal Chim Acta. 2016;902:160-7.

Garcia-Alloza M, Subramanian M, Thyssen D, Borrelli LA, Fauq A, Das P, et al. Existing plaques and neuritic abnormalities in APP:PS1 mice are not affected by administration of the gamma-secretase inhibitor LY-411575. Mol Neurodegener. 2009;4:19.

Gaudry CA, Verderio E, Aeschlimann D, Cox A, Smith C, Griffin M. Cell surface localization of tissue transglutaminase is dependent on a fibronectin-binding site in its N-terminal beta-sandwich domain. J Biol Chem. 1999;274(43):30707-14.

Gehrmann J, Matsumoto Y, Kreutzberg GW. Microglia: intrinsic immuneffector cell of the brain. Brain Res Brain Res Rev. 1995;20(3):269-87.

Gerace E, Resta F, Landucci E, Renzi D, Masi A, Pellegrini-Giampietro DE, et al. The gliadin peptide 31-43 exacerbates kainate neurotoxicity in epilepsy models. Sci Rep. 2017;7(1):15146.

Ghidoni R, Benussi L, Glionna M, Franzoni M, Binetti G. Low plasma progranulin levels predict progranulin mutations in frontotemporal lobar degeneration. Neurology. 2008;71(16):1235-9.

Ghidoni R, Flocco R, Paterlini A, Glionna M, Caruana L, Tonoli E, et al. Secretory leukocyte protease inhibitor protein regulates the penetrance of frontotemporal lobar degeneration in progranulin mutation carriers. J Alzheimers Dis. 2014;38(3):533-9.

Ghidoni R, Paterlini A, Albertini V, Glionna M, Monti E, Schiaffonati L, et al. Cystatin C is released in association with exosomes: a new tool of neuronal communication which is unbalanced in Alzheimer's disease. Neurobiol Aging. 2011;32(8):1435-42.

Gibson G, Martins R, Blass J, Gandy S. Altered oxidation and signal transduction systems in fibroblasts from Alzheimer patients. Life Sci. 1996;59(5-6):477-89.

Gilad GM, Varon LE. Transglutaminase activity in rat brain: characterization, distribution, and changes with age. J Neurochem. 1985;45(5):1522-6.

Gillet LC, Navarro P, Tate S, Rost H, Selevsek N, Reiter L, et al. Targeted data extraction of the MS/MS spectra generated by data-independent acquisition: a new concept for consistent and accurate proteome analysis. Mol Cell Proteomics. 2012;11(6):O111 016717.

Glenner GG, Wong CW. Alzheimer's disease and Down's syndrome: sharing of a unique cerebrovascular amyloid fibril protein. Biochem Biophys Res Commun. 1984;122(3):1131-5.

Goetzl EJ, Boxer A, Schwartz JB, Abner EL, Petersen RC, Miller BL, et al. Altered lysosomal proteins in neural-derived plasma exosomes in preclinical Alzheimer disease. Neurology. 2015;85(1):40-7.

Goetzl EJ, Ledreux A, Granholm AC, Elahi FM, Goetzl L, Hiramoto J, et al. Neuron-Derived Exosome Proteins May Contribute to Progression From Repetitive Mild Traumatic Brain Injuries to Chronic Traumatic Encephalopathy. Front Neurosci. 2019;13:452.

Goetzl EJ, Schwartz JB, Abner EL, Jicha GA, Kapogiannis D. High complement levels in astrocyte-derived exosomes of Alzheimer disease. Ann Neurol. 2018;83(3):544-52.

Goldman JS, Adamson J, Karydas A, Miller BL, Hutton M. New genes, new dilemmas: FTLD genetics and its implications for families. Am J Alzheimers Dis Other Demen. 2007;22(6):507-15.

Gonzalez D, Arribas RL, Viejo L, Lajarin-Cuesta R, de Los Rios C. Substituent effect of N-benzylated gramine derivatives that prevent the PP2A inhibition and dissipate the neuronal Ca(2+) overload, as a multitarget strategy for the treatment of Alzheimer's disease. Bioorg Med Chem. 2018;26(9):2551-60.

Gonzalez-Casacuberta I, Juarez-Flores DL, Ezquerra M, Fucho R, Catalan-Garcia M, Guitart-Mampel M, et al. Mitochondrial and autophagic alterations in skin fibroblasts from Parkinson disease patients with Parkin mutations. Aging (Albany NY). 2019;11(11):3750-67.

Gorno-Tempini ML, Hillis AE, Weintraub S, Kertesz A, Mendez M, Cappa SF, et al. Classification of primary progressive aphasia and its variants. Neurology. 2011;76(11):1006-14.

Govoni S, Bergamaschi S, Racchi M, Battaini F, Binetti G, Bianchetti A, et al. Cytosol protein kinase C downregulation in fibroblasts from Alzheimer's disease patients. Neurology. 1993;43(12):2581-6.

Gray NE, Quinn JF. Alterations in mitochondrial number and function in Alzheimer's disease fibroblasts. Metab Brain Dis. 2015;30(5):1275-8.

Green KN, LaFerla FM. Linking calcium to Abeta and Alzheimer's disease. Neuron. 2008;59(2):190-4.

Greenberg CS, Birckbichler PJ, Rice RH. Transglutaminases: multifunctional cross-linking enzymes that stabilize tissues. FASEB J. 1991;5(15):3071-7.

Grenard P, Bresson-Hadni S, El Alaoui S, Chevallier M, Vuitton DA, Ricard-Blum S. Transglutaminase-mediated cross-linking is involved in the stabilization of extracellular matrix in human liver fibrosis. J Hepatol. 2001;35(3):367-75.

Griffin M, Smith LL, Wynne J. Changes in transglutaminase activity in an experimental model of pulmonary fibrosis induced by paraquat. Br J Exp Pathol. 1979;60(6):653-61.

Gross JC, Chaudhary V, Bartscherer K, Boutros M. Active Wnt proteins are secreted on exosomes. Nat Cell Biol. 2012;14(10):1036-45.

Grosso H, Woo JM, Lee KW, Im JY, Masliah E, Junn E, et al. Transglutaminase 2 exacerbates alpha-synuclein toxicity in mice and yeast. FASEB J. 2014;28(10):4280-91.

Grover LM, Teyler TJ. Two components of long-term potentiation induced by different patterns of afferent activation. Nature. 1990;347(6292):477-9.

Gundemir S, Colak G, Feola J, Blouin R, Johnson GV. Transglutaminase 2 facilitates or ameliorates HIF signaling and ischemic cell death depending on its conformation and localization. Biochim Biophys Acta. 2013;1833(1):1-10.

Gyorgy B, Szabo TG, Pasztoi M, Pal Z, Misjak P, Aradi B, et al. Membrane vesicles, current state-of-the-art: emerging role of extracellular vesicles. Cell Mol Life Sci. 2011;68(16):2667-88.

Hadjivassiliou M, Aeschlimann P, Sanders DS, Maki M, Kaukinen K, Grunewald RA, et al. Transglutaminase 6 antibodies in the diagnosis of gluten ataxia. Neurology. 2013;80(19):1740-5.

Hadjivassiliou M, Aeschlimann P, Strigun A, Sanders DS, Woodroofe N, Aeschlimann D. Autoantibodies in gluten ataxia recognize a novel neuronal transglutaminase. Ann Neurol. 2008;64(3):332-43.

Hallermayer K, Harmening C, Hamprecht B. Cellular localization and regulation of glutamine synthetase in primary cultures of brain cells from newborn mice. J Neurochem. 1981;37(1):43-52.

Hallock PT, Xu CF, Park TJ, Neubert TA, Curran T, Burden SJ. Dok-7 regulates neuromuscular synapse formation by recruiting Crk and Crk-L. Genes Dev. 2010;24(21):2451-61.

Hamby ME, Sofroniew MV. Reactive astrocytes as therapeutic targets for CNS disorders. Neurotherapeutics. 2010;7(4):494-506.

Hand D, Campoy FJ, Clark S, Fisher A, Haynes LW. Activity and distribution of tissue transglutaminase in association with nerve-muscle synapses. J Neurochem. 1993;61(3):1064-72.

Hang J, Zemskov EA, Lorand L, Belkin AM. Identification of a novel recognition sequence for fibronectin within the NH2-terminal beta-sandwich domain of tissue transglutaminase. J Biol Chem. 2005;280(25):23675-83.

Hardy J, Selkoe DJ. The amyloid hypothesis of Alzheimer's disease: progress and problems on the road to therapeutics. Science. 2002;297(5580):353-6.

Harris LK, Pabst MJ, Johnston RB, Jr. Increased transglutaminase activity in elicited and activated macrophages: relationship to production of superoxide anion. J Leukoc Biol. 1984;36(6):719-27.

Harsfalvi J, Tarcsa E, Udvardy M, Zajka G, Szarvas T, Fesus L. Presence and Possible Origin of ε (γ-Glutamyl) Lysine Isodipeptide in Human Plasma. Thrombosis and haemostasis. 1992;67(01):060-2.

Hartley DM, Zhao C, Speier AC, Woodard GA, Li S, Li Z, et al. Transglutaminase induces protofibril-like amyloid beta-protein assemblies that are protease-resistant and inhibit long-term potentiation. J Biol Chem. 2008;283(24):16790-800.

Harvey J, Collingridge GL. Thapsigargin blocks the induction of long-term potentiation in rat hippocampal slices. Neuroscience letters. 1992;139(2):197-200.

He M, Gu J, Zhu J, Wang X, Wang C, Duan C, et al. Up-regulation of Dyrk1b promote astrocyte activation following lipopolysaccharide-induced neuroinflammation. Neuropeptides. 2018;69:76-83.

Hernandez F, Cuadros R, Olla I, Garcia C, Ferrer I, Perry G, et al. Differences in structure and function between human and murine tau. Biochim Biophys Acta Mol Basis Dis. 2019;1865(8):2024-30.

Hethershaw EL, Adamson PJ, Smith KA, Goldsberry WN, Pease RJ, Radford SE, et al. The role of beta-barrels 1 and 2 in the enzymatic activity of factor XIII A-subunit. J Thromb Haemost. 2018;16(7):1391-401.

Hitomi K, Horio Y, Ikura K, Yamanishi K, Maki M. Analysis of epidermal-type transglutaminase (TGase 3) expression in mouse tissues and cell lines. Int J Biochem Cell Biol. 2001;33(5):491-8.

Hitomi K, Kanehiro S, Ikura K, Maki M. Characterization of recombinant mouse epidermal-type transglutaminase (TGase 3): regulation of its activity by proteolysis and guanine nucleotides. J Biochem. 1999;125(6):1048-54.

Hitomi K, Presland RB, Nakayama T, Fleckman P, Dale BA, Maki M. Analysis of epidermal-type transglutaminase (transglutaminase 3) in human stratified epithelia and cultured keratinocytes using monoclonal antibodies. J Dermatol Sci. 2003;32(2):95-103.

Hitomi K, Tatsukawa H. Preferred Substrate Structure of Transglutaminases. In: Hitomi K, Kojima S, Fesus L, editors. Transglutaminases, Multiple Functional Modifiers and Targets for New Drug Discovery: Springer Japan; 2015. p. 63-82.

Hosaka M, Watanabe T, Sakai Y, Uchiyama Y, Takeuchi T. Identification of a chromogranin A domain that mediates binding to secretogranin III and targeting to secretory granules in pituitary cells and pancreatic beta-cells. Mol Biol Cell. 2002;13(10):3388-99.

Hou P, Liu G, Zhao Y, Shi Z, Zheng Q, Bu G, et al. Role of copper and the copper-related protein CUTA in mediating APP processing and Abeta generation. Neurobiol Aging. 2015;36(3):1310-5.

Hu W, Dang XB, Wang G, Li S, Zhang YL. Peroxiredoxin-3 attenuates traumatic neuronal injury through preservation of mitochondrial function. Neurochem Int. 2018;114:120-6.

Huber M, Rettler I, Bernasconi K, Frenk E, Lavrijsen SP, Ponec M, et al. Mutations of keratinocyte transglutaminase in lamellar ichthyosis. Science. 1995;267(5197):525-8.

Hummerich R, Schloss P. Serotonin--more than a neurotransmitter: transglutaminase-mediated serotonylation of C6 glioma cells and fibronectin. Neurochem Int. 2010;57(1):67-75.

Hummerich R, Thumfart JO, Findeisen P, Bartsch D, Schloss P. Transglutaminase-mediated transamidation of serotonin, dopamine and noradrenaline to fibronectin: evidence for a general mechanism of monoaminylation. FEBS Lett. 2012;586(19):3421-8.

Hwang IK, Yoo KY, Yi SS, Kim IY, Hwang HS, Lee KY, et al. Expression of tissue-type transglutaminase (tTG) and the effect of tTG inhibitor on the hippocampal CA1 region after transient ischemia in gerbils. Brain Res. 2009;1263:134-42.

Iannaccone M, Stefanile A, Vivo GD, Martin A, Serretiello E, Gentile V. Transglutaminase inhibition: A therapy to protect cells from death in neurodegeneration? World J Biol Chem. 2012;3(11):184-6.

Ientile R, Caccamo D, Marciano MC, Curro M, Mannucci C, Campisi A, et al. Transglutaminase activity and transglutaminase mRNA transcripts in gerbil brain ischemia. Neurosci Lett. 2004;363(2):173-7.

Ientile R, Curro M, Caccamo D. Transglutaminase 2 and neuroinflammation. Amino Acids. 2015;47(1):19-26.

Ikeda M, Ishikawa T, Tanabe H. Epidemiology of frontotemporal lobar degeneration. Dement Geriatr Cogn Disord. 2004;17(4):265-8.

Ikura K, Shinagawa R, Suto N, Sasaki R. Increase caused by interleukin-6 in promoter activity of guinea pig liver transglutaminase gene. Biosci Biotechnol Biochem. 1994;58(8):1540-1.

Ito Y, Tatsukawa H, Yamaguchi H, Takahashi K, Hitomi K, Yuzawa Y. Detection and identification of potential transglutaminase 2 substrates in the mouse renal glomeruli. Arch Biochem Biophys. 2018;660:11-9.

James P, Maeda M, Fischer R, Verma AK, Krebs J, Penniston JT, et al. Identification and primary structure of a calmodulin binding domain of the Ca2+ pump of human erythrocytes. J Biol Chem. 1988;263(6):2905-10.

Jeitner TM, Bogdanov MB, Matson WR, Daikhin Y, Yudkoff M, Folk JE, et al. N(epsilon)-(gamma-L-glutamyl)-L-lysine (GGEL) is increased in cerebrospinal fluid of patients with Huntington's disease. J Neurochem. 2001;79(5):1109-12.

Jeitner TM, Matson WR, Folk JE, Blass JP, Cooper AJ. Increased levels of gamma-glutamylamines in Huntington disease CSF. J Neurochem. 2008;106(1):37-44.

Jeong JM, Murthy SN, Radek JT, Lorand L. The fibronectin-binding domain of transglutaminase. J Biol Chem. 1995;270(10):5654-8.

Jiang WG, Ablin R, Douglas-Jones A, Mansel RE. Expression of transglutaminases in human breast cancer and their possible clinical significance. Oncology reports. 2003;10(6):2039-44.

Jiang WG, Ablin RJ. Prostate transglutaminase: a unique transglutaminase and its role in prostate cancer. Biomark Med. 2011;5(3):285-91.

Jin X, Stamnaes J, Klock C, DiRaimondo TR, Sollid LM, Khosla C. Activation of extracellular transglutaminase 2 by thioredoxin. J Biol Chem. 2011;286(43):37866-73.

John S, Thiebach L, Frie C, Mokkapati S, Bechtel M, Nischt R, et al. Epidermal transglutaminase (TGase 3) is required for proper hair development, but not the formation of the epidermal barrier. PLoS One. 2012;7(4):e34252.

Johnson GV, Cox TM, Lockhart JP, Zinnerman MD, Miller ML, Powers RE. Transglutaminase activity is increased in Alzheimer's disease brain. Brain Res. 1997;751(2):323-9.

Johnson GV, LeShoure R, Jr. Immunoblot analysis reveals that isopeptide antibodies do not specifically recognize the epsilon-(gamma-glutamyl)lysine bonds formed by transglutaminase activity. J Neurosci Methods. 2004;134(2):151-8.

Johnson TS, El-Koraie AF, Skill NJ, Baddour NM, El Nahas AM, Njloma M, et al. Tissue transglutaminase and the progression of human renal scarring. J Am Soc Nephrol. 2003;14(8):2052-62.

Johnson TS, Griffin M, Thomas GL, Skill J, Cox A, Yang B, et al. The role of transglutaminase in the rat subtotal nephrectomy model of renal fibrosis. J Clin Invest. 1997;99(12):2950-60.

Johnson TS, Skill NJ, El Nahas AM, Oldroyd SD, Thomas GL, Douthwaite JA, et al. Transglutaminase transcription and antigen translocation in experimental renal scarring. J Am Soc Nephrol. 1999;10(10):2146-57.

Jones HC, Keep RF. Brain fluid calcium concentration and response to acute hypercalcaemia during development in the rat. J Physiol. 1988;402:579-93.

Jones RA, Kotsakis P, Johnson TS, Chau DY, Ali S, Melino G, et al. Matrix changes induced by transglutaminase 2 lead to inhibition of angiogenesis and tumor growth. Cell Death Differ. 2006;13(9):1442-53.

Jones RA, Nicholas B, Mian S, Davies PJ, Griffin M. Reduced expression of tissue transglutaminase in a human endothelial cell line leads to changes in cell spreading, cell adhesion and reduced polymerisation of fibronectin. J Cell Sci. 1997;110 (Pt 19):2461-72.

Joshi P, Turola E, Ruiz A, Bergami A, Libera DD, Benussi L, et al. Microglia convert aggregated amyloid-beta into neurotoxic forms through the shedding of microvesicles. Cell Death Differ. 2014;21(4):582-93.

Junn E, Ronchetti RD, Quezado MM, Kim SY, Mouradian MM. Tissue transglutaminase-induced aggregation of alpha-synuclein: Implications for Lewy body formation in Parkinson's disease and dementia with Lewy bodies. Proc Natl Acad Sci U S A. 2003;100(4):2047-52.

Kandel E, Schwartz J, Jessell DoB, Molecular Biophysics T, Siegelbaum S, Hudspeth AJ. Principles of Neural Science, Fifth Edition. Blacklick, UNITED STATES: McGraw-Hill Publishing; 2012.

Karpuj MV, Becher MW, Steinman L. Evidence for a role for transglutaminase in Huntington's disease and the potential therapeutic implications. Neurochem Int. 2002;40(1):31-6.

Katt WP, Antonyak MA, Cerione RA. Opening up about Tissue Transglutaminase: When Conformation Matters More than Enzymatic Activity. Med One. 2018;3(6).

Kawabe K, Takano K, Moriyama M, Nakamura Y. Lipopolysaccharide-Stimulated Transglutaminase 2 Expression Enhances Endocytosis Activity in the Mouse Microglial Cell Line BV-2. Neuroimmunomodulation. 2015;22(4):243-9.

Kawabe K, Takano K, Moriyama M, Nakamura Y. Transglutaminases Derived from Astrocytes Accelerate Amyloid beta Aggregation. Neurochem Res. 2017;42(8):2384-91.

Kawahara M, Kuroda Y. Molecular mechanism of neurodegeneration induced by Alzheimer's beta-amyloid protein: channel formation and disruption of calcium homeostasis. Brain Res Bull. 2000;53(4):389-97.

Keerthikumar S, Gangoda L, Liem M, Fonseka P, Atukorala I, Ozcitti C, et al. Proteogenomic analysis reveals exosomes are more oncogenic than ectosomes. Oncotarget. 2015;6(17):15375-96.

Keillor JW, Chica RA, Chabot N, Vinci V, Pardin C, Fortin E, et al. The bioorganic chemistry of transglutaminase — from mechanism to inhibition and engineering. Canadian Journal of Chemistry. 2008;86(4):271-6.

Keresztes G, Mutai H, Heller S. TMC and EVER genes belong to a larger novel family, the TMC gene family encoding transmembrane proteins. BMC Genomics. 2003;4(1):24.

Kershner L, Welshhans K. RACK1 is necessary for the formation of point contacts and regulates axon growth. Dev Neurobiol. 2017;77(9):1038-56.

Kettenmann H, Hanisch UK, Noda M, Verkhratsky A. Physiology of microglia. Physiol Rev. 2011;91(2):461-553.

Kettenmann H, Kirchhoff F, Verkhratsky A. Microglia: new roles for the synaptic stripper. Neuron. 2013;77(1):10-8.

Kim S, Rhim H. Effects of amyloid-beta peptides on voltage-gated L-type Ca(V)1.2 and Ca(V)1.3 Ca(2+) channels. Mol Cells. 2011;32(3):289-94.

Kim SH, Fountoulakis M, Cairns N, Lubec G. Protein levels of human peroxiredoxin subtypes in brains of patients with Alzheimer's disease and Down syndrome. J Neural Transm Suppl. 2001(61):223-35.

Kim SY, Chung SI, Steinert PM. Highly active soluble processed forms of the transglutaminase 1 enzyme in epidermal keratinocytes. J Biol Chem. 1995;270(30):18026-35.

Kim SY, Grant P, Lee JH, Pant HC, Steinert PM. Differential expression of multiple transglutaminases in human brain. Increased expression and cross-linking by transglutaminases 1 and 2 in Alzheimer's disease. J Biol Chem. 1999;274(43):30715-21.

Kim Y, Eom S, Kim K, Lee YS, Choe J, Hahn JH, et al. Transglutaminase II interacts with rac1, regulates production of reactive oxygen species, expression of snail, secretion of Th2 cytokines and mediates in vitro and in vivo allergic inflammation. Mol Immunol. 2010;47(5):1010-22.

Kindy MS, Bhat AN, Bhat NR. Transient ischemia stimulates glial fibrillary acid protein and vimentin gene expression in the gerbil neocortex, striatum and hippocampus. Brain Res Mol Brain Res. 1992;13(3):199-206.

Kiraly R, Csosz E, Kurtan T, Antus S, Szigeti K, Simon-Vecsei Z, et al. Functional significance of five noncanonical Ca2+-binding sites of human transglutaminase 2 characterized by site-directed mutagenesis. FEBS J. 2009;276(23):7083-96.

Korsgren C, Cohen CM. Purification and properties of human erythrocyte band 4.2. Association with the cytoplasmic domain of band 3. J Biol Chem. 1986;261(12):5536-43.

Kosik KS, Joachim CL, Selkoe DJ. Microtubule-associated protein tau (tau) is a major antigenic component of paired helical filaments in Alzheimer disease. Proc Natl Acad Sci U S A. 1986;83(11):4044-8.

Kovacs GG. Molecular Pathological Classification of Neurodegenerative Diseases: Turning towards Precision Medicine. Int J Mol Sci. 2016;17(2).

Krapfenbauer K, Engidawork E, Cairns N, Fountoulakis M, Lubec G. Aberrant expression of peroxiredoxin subtypes in neurodegenerative disorders. Brain Research. 2003;967(1-2):152-60.

Kuchibhotla KV, Goldman ST, Lattarulo CR, Wu HY, Hyman BT, Bacskai BJ. Abeta plaques lead to aberrant regulation of calcium homeostasis in vivo resulting in structural and functional disruption of neuronal networks. Neuron. 2008;59(2):214-25.

Kurima K, Peters LM, Yang Y, Riazuddin S, Ahmed ZM, Naz S, et al. Dominant and recessive deafness caused by mutations of a novel gene, TMC1, required for cochlear hair-cell function. Nat Genet. 2002;30(3):277-84.

Lacor PN, Buniel MC, Furlow PW, Clemente AS, Velasco PT, Wood M, et al. Abeta oligomer-induced aberrations in synapse composition, shape, and density provide a molecular basis for loss of connectivity in Alzheimer's disease. J Neurosci. 2007;27(4):796-807.

LaFerla FM. Calcium dyshomeostasis and intracellular signalling in Alzheimer's disease. Nat Rev Neurosci. 2002;3(11):862-72.

Lai TS, Liu Y, Li W, Greenberg CS. Identification of two GTP-independent alternatively spliced forms of tissue transglutaminase in human leukocytes, vascular smooth muscle, and endothelial cells. FASEB J. 2007;21(14):4131-43.

Lajarin-Cuesta R, Nanclares C, Arranz-Tagarro JA, Gonzalez-Lafuente L, Arribas RL, Araujo de Brito M, et al. Gramine Derivatives Targeting Ca(2+) Channels and Ser/Thr Phosphatases: A New Dual Strategy for the Treatment of Neurodegenerative Diseases. J Med Chem. 2016;59(13):6265-80.

Lawson LJ, Perry VH, Dri P, Gordon S. Heterogeneity in the distribution and morphology of microglia in the normal adult mouse brain. Neuroscience. 1990;39(1):151-70.

Lee A, Wong ST, Gallagher D, Li B, Storm DR, Scheuer T, et al. Ca2+/calmodulin binds to and modulates P/Q-type calcium channels. Nature. 1999;399(6732):155-9.

Lee J, Kim D, Shin HS. Lack of delta waves and sleep disturbances during non-rapid eye movement sleep in mice lacking alpha1G-subunit of T-type calcium channels. Proc Natl Acad Sci U S A. 2004;101(52):18195-9.

Lee S, Mankhong S, Kang JH. Extracellular Vesicle as a Source of Alzheimer's Biomarkers: Opportunities and Challenges. Int J Mol Sci. 2019;20(7).

Leitch B, Szostek A, Lin R, Shevtsova O. Subcellular distribution of L-type calcium channel subtypes in rat hippocampal neurons. Neuroscience. 2009;164(2):641-57.

Lesort M, Attanavanich K, Zhang J, Johnson GV. Distinct nuclear localization and activity of tissue transglutaminase. J Biol Chem. 1998;273(20):11991-4.

Lesort M, Chun W, Johnson GV, Ferrante RJ. Tissue transglutaminase is increased in Huntington's disease brain. J Neurochem. 1999;73(5):2018-27.

Lewis TL, Jr., Kwon SK, Lee A, Shaw R, Polleux F. MFF-dependent mitochondrial fission regulates presynaptic release and axon branching by limiting axonal mitochondria size. Nat Commun. 2018;9(1):5008.

Li YS, Qin LX, Liu J, Xia WL, Li JP, Shen HL, et al. GIT1 enhances neurite outgrowth by stimulating microtubule assembly. Neural Regen Res. 2016;11(3):427-34.

Lim R, Miller JF, Zaheer A. Purification and characterization of glia maturation factor beta: a growth regulator for neurons and glia. Proc Natl Acad Sci U S A. 1989;86(10):3901-5.

Lindemann I. Structure-based drug design using the example of three target proteins: HIV-1 Protease, Transglutaminase 2 and Factor XIII: Universität Marburg; 2011.

Liu S, Cerione RA, Clardy J. Structural basis for the guanine nucleotide-binding activity of tissue transglutaminase and its regulation of transamidation activity. Proc Natl Acad Sci U S A. 2002;99(5):2743-7.

Lopez JR, Lyckman A, Oddo S, Laferla FM, Querfurth HW, Shtifman A. Increased intraneuronal resting [Ca2+] in adult Alzheimer's disease mice. J Neurochem. 2008;105(1):262-71.

Lopez-Fabuel I, Martin-Martin L, Resch-Beusher M, Azkona G, Sanchez-Pernaute R, Bolanos JP. Mitochondrial respiratory chain disorganization in Parkinson's disease-relevant PINK1 and DJ1 mutants. Neurochem Int. 2017;109:101-5.

Lorand L. Neurodegenerative diseases and transglutaminase. Proc Natl Acad Sci U S A. 1996;93(25):14310-3.

Lorand L. Factor XIII: structure, activation, and interactions with fibrinogen and fibrin. Annals of the New York Academy of Sciences. 2001;936(1):291-311.

Lorand L, Graham RM. Transglutaminases: crosslinking enzymes with pleiotropic functions. Nat Rev Mol Cell Biol. 2003;4(2):140-56.

Lorand L, Jeong JM, Radek JT, Wilson J. Human plasma factor XIII: subunit interactions and activation of zymogen. Methods Enzymol. 1993;222:22-35.

Lorand L, Iismaa SE. Transglutaminase diseases: from biochemistry to the bedside. FASEB J. 2019 Jan;33(1):3-12. doi: 10.1096/fj.201801544R. Erratum in: FASEB J. 2019 Mar;33(3):4653.

Lortat-Jacob H, Burhan I, Scarpellini A, Thomas A, Imberty A, Vives RR, et al. Transglutaminase-2 interaction with heparin: identification of a heparin binding site that regulates cell adhesion to fibronectin-transglutaminase-2 matrix. J Biol Chem. 2012;287(22):18005-17.

Lovell MA, Xiong S, Markesbery WR, Lynn BC. Quantitative proteomic analysis of mitochondria from primary neuron cultures treated with amyloid beta peptide. Neurochem Res. 2005;30(1):113-22.

Luarte A, Cisternas P, Caviedes A, Batiz LF, Lafourcade C, Wyneken U, et al. Astrocytes at the Hub of the Stress Response: Potential Modulation of Neurogenesis by miRNAs in Astrocyte-Derived Exosomes. Stem Cells Int. 2017;2017:1719050.

Luo R, Liu C, Elliott SE, Wang W, Parchim N, Iriyama T, et al. Transglutaminase is a Critical Link Between Inflammation and Hypertension. J Am Heart Assoc. 2016;5(7).

Maccioni RB, Seeds NW. Transglutaminase and neuronal differentiation. Mol Cell Biochem. 1986;69(2):161-8.

Mackenzie IR, Neumann M. Molecular neuropathology of frontotemporal dementia: insights into disease mechanisms from postmortem studies. J Neurochem. 2016;138 Suppl 1:54-70.

Mackenzie IR, Neumann M, Bigio EH, Cairns NJ, Alafuzoff I, Kril J, et al. Nomenclature and nosology for neuropathologic subtypes of frontotemporal lobar degeneration: an update. Acta Neuropathol. 2010;119(1):1-4.

MacManus A, Ramsden M, Murray M, Henderson Z, Pearson HA, Campbell VA. Enhancement of (45)Ca(2+) influx and voltage-dependent Ca(2+) channel activity by beta-amyloid-(1-40) in rat cortical synaptosomes and cultured cortical neurons. Modulation by the proinflammatory cytokine interleukin-1beta. J Biol Chem. 2000;275(7):4713-8.

Madi A, Kele Z, Janaky T, Punyiczki M, Fesus L. Identification of protein substrates for transglutaminase in Caenorhabditis elegans. Biochem Biophys Res Commun. 2001;283(4):964-8.

Maekawa S, Maekawa M, Hattori S, Nakamura S. Purification and molecular cloning of a novel acidic calmodulin binding protein from rat brain. J Biol Chem. 1993;268(18):13703-9.

Maggio N, Sellitti S, Capano CP, Papa M. Tissue-transglutaminase in rat and human brain: light and electron immunocytochemical analysis and in situ hybridization study. Brain Res Bull. 2001;56(3-4):173-82.

Mahoney SA, Wilkinson M, Smith S, Haynes LW. Stabilization of neurites in cerebellar granule cells by transglutaminase activity: identification of midkine and galectin-3 as substrates. Neuroscience. 2000;101(1):141-55.

Malenka RC, Bear MF. LTP and LTD: an embarrassment of riches. Neuron. 2004;44(1):5-21.

Malorni W, Farrace MG, Matarrese P, Tinari A, Ciarlo L, Mousavi-Shafaei P, et al. The adenine nucleotide translocator 1 acts as a type 2 transglutaminase substrate: implications for mitochondrial-dependent apoptosis. Cell Death Differ. 2009;16(11):1480-92.

Marambaud P, Dreses-Werringloer U, Vingtdeux V. Calcium signaling in neurodegeneration. Mol Neurodegener. 2009;4:20.

Markesbery WR. The role of oxidative stress in Alzheimer disease. Arch Neurol. 1999;56(12):1449-52.

Martin A, Giuliano A, Collaro D, De Vivo G, Sedia C, Serretiello E, et al. Possible involvement of transglutaminase-catalyzed reactions in the physiopathology of neurodegenerative diseases. Amino Acids. 2013;44(1):111-8.

Martin KJ, Bell G, Pickthorn K, Huang S, Vick A, Hodsman P, et al. Velcalcetide (AMG 416), a novel peptide agonist of the calcium-sensing receptor, reduces serum parathyroid hormone and FGF23 levels in healthy male subjects. Nephrol Dial Transplant. 2014;29(2):385-92.

Martin L, Latypova X, Terro F. Post-translational modifications of tau protein: implications for Alzheimer's disease. Neurochem Int. 2011;58(4):458-71.

Martire S, Fuso A, Mosca L, Forte E, Correani V, Fontana M, et al. Bioenergetic Impairment in Animal and Cellular Models of Alzheimer's Disease: PARP-1 Inhibition Rescues Metabolic Dysfunctions. J Alzheimers Dis. 2016;54(1):307-24.

Marubuchi S, Okuda T, Tagawa K, Enokido Y, Horiuchi D, Shimokawa R, et al. Hepatoma-derived growth factor, a new trophic factor for motor neurons, is up-regulated in the spinal cord of PQBP-1 transgenic mice before onset of degeneration. J Neurochem. 2006;99(1):70-83.

Mastroberardino PG, Farrace MG, Viti I, Pavone F, Fimia GM, Melino G, et al. "Tissue" transglutaminase contributes to the formation of disulphide bridges in proteins of mitochondrial respiratory complexes. Biochim Biophys Acta. 2006;1757(9-10):1357-65.

Mastroberardino PG, Iannicola C, Nardacci R, Bernassola F, De Laurenzi V, Melino G, et al. 'Tissue' transglutaminase ablation reduces neuronal death and prolongs survival in a mouse model of Huntington's disease. Cell Death Differ. 2002;9(9):873-80.

Mata AM, Berrocal M, Sepulveda MR. Impairment of the activity of the plasma membrane Ca(2)(+)-ATPase in Alzheimer's disease. Biochem Soc Trans. 2011;39(3):819-22.

Matsuda T, Arakawa N, Takuma K, Kishida Y, Kawasaki Y, Sakaue M, et al. SEA0400, a novel and selective inhibitor of the Na+-Ca2+ exchanger, attenuates reperfusion injury in the in vitro and in vivo cerebral ischemic models. J Pharmacol Exp Ther. 2001;298(1):249-56.

Mattson MP, Cheng B, Davis D, Bryant K, Lieberburg I, Rydel RE. beta-Amyloid peptides destabilize calcium homeostasis and render human cortical neurons vulnerable to excitotoxicity. J Neurosci. 1992;12(2):376-89.

Mattsson N, Andreasson U, Zetterberg H, Blennow K, Alzheimer's Disease Neuroimaging I. Association of Plasma Neurofilament Light With Neurodegeneration in Patients With Alzheimer Disease. JAMA Neurol. 2017;74(5):557-66.

Mattsson N, Carrillo MC, Dean RA, Devous MD, Sr., Nikolcheva T, Pesini P, et al. Revolutionizing Alzheimer's disease and clinical trials through biomarkers. Alzheimers Dement (Amst). 2015;1(4):412-9.

Mause SF, Weber C. Microparticles: protagonists of a novel communication network for intercellular information exchange. Circ Res. 2010;107(9):1047-57.

McConoughey SJ, Basso M, Niatsetskaya ZV, Sleiman SF, Smirnova NA, Langley BC, et al. Inhibition of transglutaminase 2 mitigates transcriptional dysregulation in models of Huntington disease. EMBO Mol Med. 2010;2(9):349-70.

McFerran BW, Graham ME, Burgoyne RD. Neuronal Ca2+ sensor 1, the mammalian homologue of frequenin, is expressed in chromaffin and PC12 cells and regulates neurosecretion from dense-core granules. J Biol Chem. 1998;273(35):22768-72.

McFerran BW, Weiss JL, Burgoyne RD. Neuronal Ca(2+) sensor 1. Characterization of the myristoylated protein, its cellular effects in permeabilized adrenal chromaffin cells, Ca(2+)-independent membrane association, and interaction with binding proteins, suggesting a role in rapid Ca(2+) signal transduction. J Biol Chem. 1999;274(42):30258-65.

McGeer PL, McGeer EG. Mechanisms of cell death in Alzheimer disease--immunopathology. J Neural Transm Suppl. 1998;54:159-66.

McKhann G, Drachman D, Folstein M, Katzman R, Price D, Stadlan EM. Clinical diagnosis of Alzheimer's disease: report of the NINCDS-ADRDA Work Group under the auspices of Department of Health and Human Services Task Force on Alzheimer's Disease. Neurology. 1984;34(7):939-44.

Meenakshi J, Anupama, Goswami SK, Datta K. Constitutive expression of hyaluronan binding protein 1 (HABP1/p32/gC1qR) in normal fibroblast cells perturbs its growth characteristics and induces apoptosis. Biochemical and Biophysical Research Communications. 2003;300(3):686-93.

Megias M, Emri Z, Freund TF, Gulyas AI. Total number and distribution of inhibitory and excitatory synapses on hippocampal CA1 pyramidal cells. Neuroscience. 2001;102(3):527-40.

Mehta K, Eckert RL. Transglutaminases: family of enzymes with diverse functions: Karger Medical and Scientific Publishers; 2005.

Mehta K, Kumar A, Kim HI. Transglutaminase 2: a multi-tasking protein in the complex circuitry of inflammation and cancer. Biochem Pharmacol. 2010;80(12):1921-9.

Melino G, Piacentini M. 'Tissue' transglutaminase in cell death: a downstream or a multifunctional upstream effector? FEBS Lett. 1998;430(1-2):59-63.

Merchant ML, Rood IM, Deegens JKJ, Klein JB. Isolation and characterization of urinary extracellular vesicles: implications for biomarker discovery. Nat Rev Nephrol. 2017;13(12):731-49.

Mi H, Muruganujan A, Casagrande JT, Thomas PD. Large-scale gene function analysis with the PANTHER classification system. Nat Protoc. 2013;8(8):1551-66.

Mi Z, Si T, Kapadia K, Li Q, Muma NA. Receptor-stimulated transamidation induces activation of Rac1 and Cdc42 and the regulation of dendritic spines. Neuropharmacology. 2017;117:93-105.

Mirza A, Liu SL, Frizell E, Zhu J, Maddukuri S, Martinez J, et al. A role for tissue transglutaminase in hepatic injury and fibrogenesis, and its regulation by NF-kappaB. Am J Physiol. 1997;272(2 Pt 1):G281-8.

Molberg O, McAdam SN, Korner R, Quarsten H, Kristiansen C, Madsen L, et al. Tissue transglutaminase selectively modifies gliadin peptides that are recognized by gut-derived T cells in celiac disease. Nat Med. 1998;4(6):713-7.

Moller UK, Jensen LT, Mosekilde L, Rejnmark L. Effects of adding chymosin to milk on calcium homeostasis: a randomized, double-blind, cross-over study. Calcif Tissue Int. 2015;96(2):105-12.

Monsonego A, Shani Y, Friedmann I, Paas Y, Eizenberg O, Schwartz M. Expression of GTP-dependent and GTP-independent tissue-type transglutaminase in cytokine-treated rat brain astrocytes. J Biol Chem. 1997;272(6):3724-32.

Monteagudo A, Feola J, Natola H, Ji C, Proschel C, Johnson GVW. Depletion of astrocytic transglutaminase 2 improves injury outcomes. Mol Cell Neurosci. 2018;92:128-36.

Monteagudo A, Ji C, Akbar A, Keillor JW, Johnson GVW. Inhibition or ablation of transglutaminase 2 impairs astrocyte migration. Biochem Biophys Res Commun. 2017;482(4):942-7.

Montecalvo A, Larregina AT, Shufesky WJ, Stolz DB, Sullivan ML, Karlsson JM, et al. Mechanism of transfer of functional microRNAs between mouse dendritic cells via exosomes. Blood. 2012;119(3):756-66.

Moreira PI, Harris PL, Zhu X, Santos MS, Oliveira CR, Smith MA, et al. Lipoic acid and N-acetyl cysteine decrease mitochondrial-related oxidative stress in Alzheimer disease patient fibroblasts. J Alzheimers Dis. 2007;12(2):195-206.

Muma NA. Transglutaminase in Receptor and Neurotransmitter-Regulated Functions. Med One. 2018;3(6).

Muralidharan-Chari V, Clancy J, Plou C, Romao M, Chavrier P, Raposo G, et al. ARF6-regulated shedding of tumor cell-derived plasma membrane microvesicles. Curr Biol. 2009;19(22):1875-85.

Muszbek L, Bereczky Z, Bagoly Z, Komaromi I, Katona E. Factor XIII: a coagulation factor with multiple plasmatic and cellular functions. Physiol Rev. 2011;91(3):931-72.

Mycek MJ, Clarke DD, Neidle A, Waelsch H. Amine incorporation into insulin as catalyzed by transglutaminase. Arch Biochem Biophys. 1959;84:528-40.

Mycek MJ, Waelsch H. The enzymatic deamidation of proteins. J Biol Chem. 1960;235:3513-7.

Nagaraj S, Zoltowska KM, Laskowska-Kaszub K, Wojda U. microRNA diagnostic panel for Alzheimer's disease and epigenetic trade-off between neurodegeneration and cancer. Ageing Res Rev. 2019;49:125-43.

Nagy Z, Jobst KA, Esiri MM, Morris JH, King EM, MacDonald B, et al. Hippocampal pathology reflects memory deficit and brain imaging measurements in Alzheimer's disease: clinicopathologic correlations using three sets of pathologic diagnostic criteria. Dementia. 1996;7(2):76-81.

Nakajima K, Tohyama Y, Maeda S, Kohsaka S, Kurihara T. Neuronal regulation by which microglia enhance the production of neurotrophic factors for GABAergic, catecholaminergic, and cholinergic neurons. Neurochem Int. 2007;50(6):807-20.

Nakamura A, Kaneko N, Villemagne VL, Kato T, Doecke J, Dore V, et al. High performance plasma amyloid-beta biomarkers for Alzheimer's disease. Nature. 2018;554(7691):249-54.

Nakano I, Garnier D, Minata M, Rak J. Extracellular vesicles in the biology of brain tumour stem cells--Implications for inter-cellular communication, therapy and biomarker development. Semin Cell Dev Biol. 2015;40:17-26.

Nash B, Thomson CE, Linington C, Arthur AT, McClure JD, McBride MW, et al. Functional duality of astrocytes in myelination. J Neurosci. 2011;31(37):13028-38.

Navakkode S, Liu C, Soong TW. Altered function of neuronal L-type calcium channels in ageing and neuroinflammation: Implications in age-related synaptic dysfunction and cognitive decline. Ageing Res Rev. 2018;42:86-99.

Neary D, Snowden JS, Gustafson L, Passant U, Stuss D, Black S, et al. Frontotemporal lobar degeneration: a consensus on clinical diagnostic criteria. Neurology. 1998;51(6):1546-54.

Nedergaard M, Ransom B, Goldman SA. New roles for astrocytes: redefining the functional architecture of the brain. Trends Neurosci. 2003;26(10):523-30.

Nemes Z, Jr., Adany R, Balazs M, Boross P, Fesus L. Identification of cytoplasmic actin as an abundant glutaminyl substrate for tissue transglutaminase in HL-60 and U937 cells undergoing apoptosis. J Biol Chem. 1997;272(33):20577-83.

Nemes Z, Devreese B, Steinert PM, Van Beeumen J, Fesus L. Cross-linking of ubiquitin, HSP27, parkin, and alpha-synuclein by gamma-glutamyl-epsilon-lysine bonds in Alzheimer's neurofibrillary tangles. FASEB J. 2004;18(10):1135-7.

Nemes Z, Fesus L, Egerhazi A, Keszthelyi A, Degrell IM. N(epsilon)(gamma-glutamyl)lysine in cerebrospinal fluid marks Alzheimer type and vascular dementia. Neurobiol Aging. 2001;22(3):403-6.

Nemes Z, Steinert PM. Bricks and mortar of the epidermal barrier. Exp Mol Med. 1999;31(1):5-19.

Nett WJ, Oloff SH, McCarthy KD. Hippocampal astrocytes in situ exhibit calcium oscillations that occur independent of neuronal activity. J Neurophysiol. 2002;87(1):528-37.

Nikolajsen CL, Dyrlund TF, Poulsen ET, Enghild JJ, Scavenius C. Coagulation factor XIIIa substrates in human plasma: identification and incorporation into the clot. J Biol Chem. 2014;289(10):6526-34.

Nimmerjahn A, Kirchhoff F, Helmchen F. Resting microglial cells are highly dynamic surveillants of brain parenchyma in vivo. Science. 2005;308(5726):1314-8.

Nimmrich V, Eckert A. Calcium channel blockers and dementia. Br J Pharmacol. 2013;169(6):1203-10.

Nishiura H, Shibuya Y, Matsubara S, Tanase S, Kambara T, Yamamoto T. Monocyte chemotactic factor in rheumatoid arthritis synovial tissue. Probably a cross-linked derivative of S19 ribosomal protein. J Biol Chem. 1996;271(2):878-82.

Nurminskaya MV, Belkin AM. Cellular functions of tissue transglutaminase. Int Rev Cell Mol Biol. 2012;294:1-97.

Oberheim NA, Wang X, Goldman S, Nedergaard M. Astrocytic complexity distinguishes the human brain. Trends Neurosci. 2006;29(10):547-53.

Oeckl P, Steinacker P, Feneberg E, Otto M. Neurochemical biomarkers in the diagnosis of frontotemporal lobar degeneration: an update. J Neurochem. 2016;138 Suppl 1:184-92.

Oh K, Park HB, Byoun OJ, Shin DM, Jeong EM, Kim YW, et al. Epithelial transglutaminase 2 is needed for T cell interleukin-17 production and subsequent pulmonary inflammation and fibrosis in bleomycin-treated mice. J Exp Med. 2011;208(8):1707-19.

Okada S, Nakamura M, Katoh H, Miyao T, Shimazaki T, Ishii K, et al. Conditional ablation of Stat3 or Socs3 discloses a dual role for reactive astrocytes after spinal cord injury. Nat Med. 2006;12(7):829-34.

Oliet SH, Piet R, Poulain DA. Control of glutamate clearance and synaptic efficacy by glial coverage of neurons. Science. 2001;292(5518):923-6.

Olsen KC, Sapinoro RE, Kottmann RM, Kulkarni AA, Iismaa SE, Johnson GV, et al. Transglutaminase 2 and its role in pulmonary fibrosis. Am J Respir Crit Care Med. 2011;184(6):699-707.

Oono M, Okado-Matsumoto A, Shodai A, Ido A, Ohta Y, Abe K, et al. Transglutaminase 2 accelerates neuroinflammation in amyotrophic lateral sclerosis through interaction with misfolded superoxide dismutase 1. J Neurochem. 2014;128(3):403-18.

Orru S, Caputo I, D'Amato A, Ruoppolo M, Esposito C. Proteomics identification of acyl-acceptor and acyl-donor substrates for transglutaminase in a human intestinal epithelial cell line. Implications for celiac disease. J Biol Chem. 2003;278(34):31766-73.

Ostrowski M, Carmo NB, Krumeich S, Fanget I, Raposo G, Savina A, et al. Rab27a and Rab27b control different steps of the exosome secretion pathway. Nat Cell Biol. 2010;12(1):19-30; sup pp 1-13.

Ottiger HP, Battenberg EF, Tsou AP, Bloom FE, Sutcliffe JG. 1B1075: a brain- and pituitary-specific mRNA that encodes a novel chromogranin/secretogranin-like component of intracellular vesicles. J Neurosci. 1990;10(9):3135-47.

Pankratov Y, Lalo U, Krishtal OA, Verkhratsky A. P2X receptors and synaptic plasticity. Neuroscience. 2009;158(1):137-48.

Paolicelli RC, Bolasco G, Pagani F, Maggi L, Scianni M, Panzanelli P, et al. Synaptic pruning by microglia is necessary for normal brain development. Science. 2011;333(6048):1456-8.

Park D, Choi SS, Ha KS. Transglutaminase 2: a multi-functional protein in multiple subcellular compartments. Amino Acids. 2010;39(3):619-31.

Park KC, Chung KC, Kim YS, Lee J, Joh TH, Kim SY. Transglutaminase 2 induces nitric oxide synthesis in BV-2 microglia. Biochem Biophys Res Commun. 2004;323(3):1055-62.

Pastuzyn ED, Day CE, Kearns RB, Kyrke-Smith M, Taibi AV, McCormick J, et al. The Neuronal Gene Arc Encodes a Repurposed Retrotransposon Gag Protein that Mediates Intercellular RNA Transfer. Cell. 2018;172(1-2):275-88 e18.

Pena-Altamira LE, Polazzi E, Giuliani P, Beraudi A, Massenzio F, Mengoni I, et al. Release of soluble and vesicular purine nucleoside phosphorylase from rat astrocytes and microglia induced by pro-inflammatory stimulation with extracellular ATP via P2X7 receptors. Neurochem Int. 2018;115:37-49.

Peng X, Zhang Y, Zhang H, Graner S, Williams JF, Levitt ML, et al. Interaction of tissue transglutaminase with nuclear transport protein importin-alpha3. FEBS Lett. 1999;446(1):35-9.

Perea G, Navarrete M, Araque A. Tripartite synapses: astrocytes process and control synaptic information. Trends Neurosci. 2009;32(8):421-31.

Perez MJ, Ponce DP, Aranguiz A, Behrens MI, Quintanilla RA. Mitochondrial permeability transition pore contributes to mitochondrial dysfunction in fibroblasts of patients with sporadic Alzheimer's disease. Redox Biol. 2018;19:290-300.

Perez MJ, Ponce DP, Osorio-Fuentealba C, Behrens MI, Quintanilla RA. Mitochondrial Bioenergetics Is Altered in Fibroblasts from Patients with Sporadic Alzheimer's Disease. Front Neurosci. 2017;11:553.

Perrin RJ, Fagan AM, Holtzman DM. Multimodal techniques for diagnosis and prognosis of Alzheimer's disease. Nature. 2009;461(7266):916-22.

Perry MJ, Haynes LW. Localization and activity of transglutaminase, a retinoid-inducible protein, in developing rat spinal cord. Int J Dev Neurosci. 1993;11(3):325-37.

Perry MJ, Mahoney SA, Haynes LW. Transglutaminase C in cerebellar granule neurons: regulation and localization of substrate cross-linking. Neuroscience. 1995;65(4):1063-76.

Perry VH, Nicoll JA, Holmes C. Microglia in neurodegenerative disease. Nat Rev Neurol. 2010;6(4):193-201.

Petersen RC, Smith GE, Waring SC, Ivnik RJ, Tangalos EG, Kokmen E. Mild cognitive impairment: clinical characterization and outcome. Arch Neurol. 1999;56(3):303-8.

Phatak VM, Croft SM, Rameshaiah Setty SG, Scarpellini A, Hughes DC, Rees R, et al. Expression of transglutaminase-2 isoforms in normal human tissues and cancer cell lines: dysregulation of alternative splicing in cancer. Amino Acids. 2013;44(1):33-44.

Piacentini M, Amendola A, Ciccosanti F, Falasca L, Farrace MG, Mastroberardino PG, et al. Type 2 transglutaminase and cell death. Prog Exp Tumor Res. 2005;38:58-74.

Piacentini M, Farrace MG, Piredda L, Matarrese P, Ciccosanti F, Falasca L, et al. Transglutaminase overexpression sensitizes neuronal cell lines to apoptosis by increasing mitochondrial membrane potential and cellular oxidative stress. J Neurochem. 2002;81(5):1061-72.

Pinkas DM, Strop P, Brunger AT, Khosla C. Transglutaminase 2 undergoes a large conformational change upon activation. PLoS Biol. 2007;5(12):e327.

Pinzon NE, Breve JJP, Bol J, Drukarch B, Baron W, van Dam AM. Tissue transglutaminase in astrocytes is enhanced by inflammatory mediators and is involved in the formation of fibronectin fibril-like structures. J Neuroinflammation. 2017b;14(1):260.

Pinzon NE, Sanz-Morello B, Breve JJ, Bol JG, Drukarch B, Bauer J, et al. Astrocyte-derived tissue Transglutaminase affects fibronectin deposition, but not aggregation, during cuprizone-induced demyelination. Sci Rep. 2017a;7:40995.

Piredda L, Farrace MG, Lo Bello M, Malorni W, Melino G, Petruzzelli R, et al. Identification of 'tissue' transglutaminase binding proteins in neural cells committed to apoptosis. FASEB J. 1999;13(2):355-64.

Pomerantz DJ, Ferdinandusse S, Cogan J, Cooper DN, Reimschisel T, Robertson A, et al. Clinical heterogeneity of mitochondrial NAD kinase deficiency caused by a NADK2 start loss variant. Am J Med Genet A. 2018;176(3):692-8.

Prada I, Gabrielli M, Turola E, Iorio A, D'Arrigo G, Parolisi R, et al. Glia-to-neuron transfer of miRNAs via extracellular vesicles: a new mechanism underlying inflammation-induced synaptic alterations. Acta Neuropathol. 2018;135(4):529-50.

Pravettoni E, Bacci A, Coco S, Forbicini P, Matteoli M, Verderio C. Different localizations and functions of L-type and N-type calcium channels during development of hippocampal neurons. Dev Biol. 2000;227(2):581-94.

Price S, Held B, Pearson H. Amyloid beta protein increases Ca2+ currents in rat cerebellar granule neurones. Neuroreport. 1998;9(3):539-45.

Prince M, Knapp M, Guerchet M, McCrone P, Prina M, Comas-Herrera A, et al. Dementia UK: Update. 2014.

Proia P, Schiera G, Mineo M, Ingrassia AM, Santoro G, Savettieri G, et al. Astrocytes shed extracellular vesicles that contain fibroblast growth factor-2 and vascular endothelial growth factor. Int J Mol Med. 2008;21(1):63-7.

Quinn BR, Yunes-Medina L, Johnson GVW. Transglutaminase 2: Friend or foe? The discordant role in neurons and astrocytes. J Neurosci Res. 2018;96(7):1150-8.

Rademakers R, Neumann M, Mackenzie IR. Advances in understanding the molecular basis of frontotemporal dementia. Nat Rev Neurol. 2012;8(8):423-34.

Rademakers R, Rovelet-Lecrux A. Recent insights into the molecular genetics of dementia. Trends Neurosci. 2009;32(8):451-61.

Rajendran L, Bali J, Barr MM, Court FA, Kramer-Albers EM, Picou F, et al. Emerging roles of extracellular vesicles in the nervous system. J Neurosci. 2014;34(46):15482-9.

Raposo G, Tenza D, Mecheri S, Peronet R, Bonnerot C, Desaymard C. Accumulation of major histocompatibility complex class II molecules in mast cell secretory granules and their release upon degranulation. Mol Biol Cell. 1997 Dec;8(12):2631-45.

Raposo G, Stoorvogel W. Extracellular vesicles: exosomes, microvesicles, and friends. J Cell Biol. 2013;200(4):373-83.

Rascovsky K, Hodges JR, Knopman D, Mendez MF, Kramer JH, Neuhaus J, et al. Sensitivity of revised diagnostic criteria for the behavioural variant of frontotemporal dementia. Brain. 2011;134(Pt 9):2456-77.

Ratajczak J, Miekus K, Kucia M, Zhang J, Reca R, Dvorak P, et al. Embryonic stem cell-derived microvesicles reprogram hematopoietic progenitors: evidence for horizontal transfer of mRNA and protein delivery. Leukemia. 2006;20(5):847-56.

Ratnavalli E, Brayne C, Dawson K, Hodges J. The prevalence of frontotemporal dementia. Neurology. 2002;58(11):1615-21.

Raymond CR, Redman SJ. Different calcium sources are narrowly tuned to the induction of different forms of LTP. J Neurophysiol. 2002;88(1):249-55.

Renault-Mihara F, Okada S, Shibata S, Nakamura M, Toyama Y, Okano H. Spinal cord injury: emerging beneficial role of reactive astrocytes' migration. Int J Biochem Cell Biol. 2008;40(9):1649-53.

Richards RJ, Masek LC, Brown RF. Biochemical and cellular mechanisms of pulmonary fibrosis. Toxicol Pathol. 1991;19(4 Pt 1):526-39.

Rodolfo C, Mormone E, Matarrese P, Ciccosanti F, Farrace MG, Garofano E, et al. Tissue transglutaminase is a multifunctional BH3-only protein. J Biol Chem. 2004;279(52):54783-92.

Rosaria Carratù M, Signorile A, De Rasmo D, Reale A, Vacca A. Pharmacological activation of protein phosphatase 2 a (pp2a): a novel strategy to fight against human malignancies? Current medicinal chemistry. 2016;23(38):4286-96.

Rosaria Carratù M, Signorile A, De Rasmo D, Reale A, Vacca A. Pharmacological activation of protein phosphatase 2 a (pp2a): a novel strategy to fight against human malignancies? Current medicinal chemistry. 2016;23(38):4286-96.

Rosas-Hernandez H, Cuevas E, Raymick JB, Robinson BL, Ali SF, Hanig J, et al. Characterization of Serum Exosomes from a Transgenic Mouse Model of Alzheimer's Disease. Current Alzheimer Research. 2019;16(5):388-95.

Rothstein JD, Dykes-Hoberg M, Pardo CA, Bristol LA, Jin L, Kuncl RW, et al. Knockout of glutamate transporters reveals a major role for astroglial transport in excitotoxicity and clearance of glutamate. Neuron. 1996;16(3):675-86.

Rubino E, Rainero I, Chio A, Rogaeva E, Galimberti D, Fenoglio P, et al. SQSTM1 mutations in frontotemporal lobar degeneration and amyotrophic lateral sclerosis. Neurology. 2012;79(15):1556-62.

Ruiz A, Joshi P, Mastrangelo R, Francolini M, Verderio C, Matteoli M. Testing Abeta toxicity on primary CNS cultures using drug-screening microfluidic chips. Lab Chip. 2014;14(15):2860-6.

Saman S, Kim W, Raya M, Visnick Y, Miro S, Saman S, et al. Exosome-associated tau is secreted in tauopathy models and is selectively phosphorylated in cerebrospinal fluid in early Alzheimer disease. J Biol Chem. 2012;287(6):3842-9.

Sarang Z, Toth B, Balajthy Z, Koroskenyi K, Garabuczi E, Fesus L, et al. Some lessons from the tissue transglutaminase knockout mouse. Amino Acids. 2009;36(4):625-31.

Sárvári M, Fésüs L, Nemes Z. Transglutaminase-mediated crosslinking of neural proteins in Alzheimer's disease and other primary dementias. Drug Development Research. 2002;56(3):458-72.

Savina A, Fader CM, Damiani MT, Colombo MI. Rab11 promotes docking and fusion of multivesicular bodies in a calcium-dependent manner. Traffic. 2005 Feb;6(2):131-43.

Savoca MP, Tonoli E, Atobatele AG, Verderio EAM. Biocatalysis by Transglutaminases: A Review of Biotechnological Applications. Micromachines-Basel. 2018;9(11).

Scarpellini A, Germack R, Lortat-Jacob H, Muramatsu T, Billett E, Johnson T, et al. Heparan sulfate proteoglycans are receptors for the cell-surface trafficking and biological activity of transglutaminase-2. J Biol Chem. 2009;284(27):18411-23.

Scarpellini A, Huang L, Burhan I, Schroeder N, Funck M, Johnson TS, et al. Syndecan-4 knockout leads to reduced extracellular transglutaminase-2 and protects against tubulointerstitial fibrosis. J Am Soc Nephrol. 2014;25(5):1013-27.

Schaerer MT, Kannenberg K, Hunziker P, Baumann SW, Sigel E. Interaction between GABA(A) receptor beta subunits and the multifunctional protein gC1q-R. J Biol Chem. 2001;276(28):26597-604.

Schulze-Krebs A, Canneva F, Schnepf R, Dobner J, Dieterich W, von Horsten S. In situ enzymatic activity of transglutaminase isoforms on brain tissue sections of rodents: A new approach to monitor differences in post-translational protein modifications during neurodegeneration. Brain Res. 2016;1631:22-33.

Schwaller B, Tetko IV, Tandon P, Silveira DC, Vreugdenhil M, Henzi T, et al. Parvalbumin deficiency affects network properties resulting in increased susceptibility to epileptic seizures. Mol Cell Neurosci. 2004;25(4):650-63.

Secondo A, Pignataro G, Ambrosino P, Pannaccione A, Molinaro P, Boscia F, et al. Pharmacological characterization of the newly synthesized 5-amino-N-butyl-2-(4-ethoxyphenoxy)-benzamide hydrochloride (BED) as a potent NCX3 inhibitor that worsens anoxic injury in cortical neurons, organotypic hippocampal cultures, and ischemic brain. ACS Chem Neurosci. 2015;6(8):1361-70.

Seelaar H, Rohrer JD, Pijnenburg YA, Fox NC, van Swieten JC. Clinical, genetic and pathological heterogeneity of frontotemporal dementia: a review. J Neurol Neurosurg Psychiatry. 2011;82(5):476-86.

Seipold L, Saftig P. The Emerging Role of Tetraspanins in the Proteolytic Processing of the Amyloid Precursor Protein. Front Mol Neurosci. 2016;9:149.

Selkoe DJ, Abraham C, Ihara Y. Brain transglutaminase: in vitro crosslinking of human neurofilament proteins into insoluble polymers. Proc Natl Acad Sci U S A. 1982;79(19):6070-4.

Sestito C, Breve JJP, van Eggermond M, Killestein J, Teunissen CE, van Rossum J, et al. Monocyte-derived tissue transglutaminase in multiple sclerosis patients: reflecting an anti-inflammatory status and function of the cells? J Neuroinflammation. 2017;14(1):257.

Shinde AV, Dobaczewski M, de Haan JJ, Saxena A, Lee KK, Xia Y, et al. Tissue transglutaminase induction in the pressure-overloaded myocardium regulates matrix remodelling. Cardiovasc Res. 2017;113(8):892-905.

Siddiqui A, Rivera-Sanchez S, Castro Mdel R, Acevedo-Torres K, Rane A, Torres-Ramos CA, et al. Mitochondrial DNA damage is associated with reduced mitochondrial bioenergetics in Huntington's disease. Free Radic Biol Med. 2012;53(7):1478-88.

Singh G, Zhang J, Ma Y, Cerione RA, Antonyak MA. The Different Conformational States of Tissue Transglutaminase Have Opposing Affects on Cell Viability. J Biol Chem. 2016;291(17):9119-32.

Singh US, Kunar MT, Kao YL, Baker KM. Role of transglutaminase II in retinoic acid-induced activation of RhoA-associated kinase-2. EMBO J. 2001;20(10):2413-23.

Singh US, Pan J, Kao YL, Joshi S, Young KL, Baker KM. Tissue transglutaminase mediates activation of RhoA and MAP kinase pathways during retinoic acid-induced neuronal differentiation of SH-SY5Y cells. J Biol Chem. 2003;278(1):391-9.

Sippy T, Cruz-Martin A, Jeromin A, Schweizer FE. Acute changes in short-term plasticity at synapses with elevated levels of neuronal calcium sensor-1. Nat Neurosci. 2003;6(10):1031-8.

Small K, Feng JF, Lorenz J, Donnelly ET, Yu A, Im MJ, et al. Cardiac specific overexpression of transglutaminase II (G(h)) results in a unique hypertrophy phenotype independent of phospholipase C activation. J Biol Chem. 1999;274(30):21291-6.

Smethurst PA, Griffin M. Measurement of tissue transglutaminase activity in a permeabilized cell system: its regulation by Ca2+ and nucleotides. Biochem J. 1996;313 (Pt 3):803-8.

Smith JA, Leonardi T, Huang B, Iraci N, Vega B, Pluchino S. Extracellular vesicles and their synthetic analogues in aging and age-associated brain diseases. Biogerontology. 2015;16(2):147-85.

Sontag E, Nunbhakdi-Craig V, Lee G, Brandt R, Kamibayashi C, Kuret J, et al. Molecular interactions among protein phosphatase 2A, tau, and microtubules. Implications for the regulation of tau phosphorylation and the development of tauopathies. J Biol Chem. 1999;274(36):25490-8.

Sontag JM, Sontag E. Protein phosphatase 2A dysfunction in Alzheimer's disease. Front Mol Neurosci. 2014;7:16.

Sorolla MA, Reverter-Branchat G, Tamarit J, Ferrer I, Ros J, Cabiscol E. Proteomic and oxidative stress analysis in human brain samples of Huntington disease. Free Radic Biol Med. 2008;45(5):667-78.

Squitieri F, Falleni A, Cannella M, Orobello S, Fulceri F, Lenzi P, et al. Abnormal morphology of peripheral cell tissues from patients with Huntington disease. J Neural Transm (Vienna). 2010;117(1):77-83.

Stamnaes J, Pinkas DM, Fleckenstein B, Khosla C, Sollid LM. Redox regulation of transglutaminase 2 activity. J Biol Chem. 2010;285(33):25402-9.

Steinert PM, Marekov LN. The proteins elafin, filaggrin, keratin intermediate filaments, loricrin, and small proline-rich proteins 1 and 2 are isodipeptide cross-linked components of the human epidermal cornified cell envelope. J Biol Chem. 1995;270(30):17702-11.

Stellwagen D, Malenka RC. Synaptic scaling mediated by glial TNF-α. Nature. 2006;440(7087):1054.

Stevens B, Allen NJ, Vazquez LE, Howell GR, Christopherson KS, Nouri N, et al. The classical complement cascade mediates CNS synapse elimination. Cell. 2007;131(6):1164-78.

Sudhof TC. The synaptic vesicle cycle. Annu Rev Neurosci. 2004;27:509-47.

Sung LA, Chien S, Chang LS, Lambert K, Bliss SA, Bouhassira EE, et al. Molecular cloning of human protein 4.2: a major component of the erythrocyte membrane. Proc Natl Acad Sci U S A. 1990;87(3):955-9.

Sunico CR, Sultan A, Nakamura T, Dolatabadi N, Parker J, Shan B, et al. Role of sulfiredoxin as a peroxiredoxin-2 denitrosylase in human iPSC-derived dopaminergic neurons. Proc Natl Acad Sci U S A. 2016;113(47):E7564-E71.

Tarazi FI, Sahli ZT, Wolny M, Mousa SA. Emerging therapies for Parkinson's disease: from bench to bedside. Pharmacol Ther. 2014;144(2):123-33.

Tatsukawa H, Fukaya Y, Frampton G, Martinez-Fuentes A, Suzuki K, Kuo TF, et al. Role of transglutaminase 2 in liver injury via cross-linking and silencing of transcription factor Sp1. Gastroenterology. 2009;136(5):1783-95 e10.

Tatsukawa H, Kojima S. Recent advances in understanding the roles of transglutaminase 2 in alcoholic steatohepatitis. Cell Biol Int. 2010;34(3):325-34.

Tatsukawa H, Otsu R, Tani Y, Wakita R, Hitomi K. Isozyme-specific comprehensive characterization of transglutaminase-crosslinked substrates in kidney fibrosis. Sci Rep. 2018;8(1):7306.

Tatsukawa H, Tani Y, Otsu R, Nakagawa H, Hitomi K. Global identification and analysis of isozyme-specific possible substrates crosslinked by transglutaminases using substrate peptides in mouse liver fibrosis. Sci Rep. 2017;7:45049.

Teesalu K, Uibo O, Uibo R, Utt M. Kinetic and functional characterisation of the heparin-binding peptides from human transglutaminase 2. J Pept Sci. 2012;18(5):350-6.

Telci D, Wang Z, Li X, Verderio EA, Humphries MJ, Baccarini M, et al. Fibronectin-tissue transglutaminase matrix rescues RGD-impaired cell adhesion through syndecan-4 and beta1 integrin co-signaling. J Biol Chem. 2008;283(30):20937-47.

Terry RD, Masliah E, Salmon DP, Butters N, DeTeresa R, Hill R, et al. Physical basis of cognitive alterations in Alzheimer's disease: synapse loss is the major correlate of cognitive impairment. Ann Neurol. 1991;30(4):572-80.

Thery C, Witwer KW, Aikawa E, Alcaraz MJ, Anderson JD, Andriantsitohaina R, et al. Minimal information for studies of extracellular vesicles 2018 (MISEV2018): a position statement of the

International Society for Extracellular Vesicles and update of the MISEV2014 guidelines. J Extracell Vesicles. 2018;7(1):1535750.

Thomas H, Beck K, Adamczyk M, Aeschlimann P, Langley M, Oita RC, et al. Transglutaminase 6: a protein associated with central nervous system development and motor function. Amino Acids. 2013;44(1):161-77.

Tolentino PJ, Waghray A, Wang KK, Hayes RL. Increased expression of tissue-type transglutaminase following middle cerebral artery occlusion in rats. J Neurochem. 2004;89(5):1301-7.

Torres A, Pac-Sosinska M, Wiktor K, Paszkowski T, Maciejewski R, Torres K. CD44, TGM2 and EpCAM as novel plasma markers in endometrial cancer diagnosis. BMC Cancer. 2019;19(1):401.

Trajkovic K, Hsu C, Chiantia S, Rajendran L, Wenzel D, Wieland F, et al. Ceramide triggers budding of exosome vesicles into multivesicular endosomes. Science. 2008;319(5867):1244-7.

Tripathy D, Vignoli B, Ramesh N, Polanco MJ, Coutelier M, Stephen CD, et al. Mutations in TGM6 induce the unfolded protein response in SCA35. Hum Mol Genet. 2017;26(19):3749-62.

Tsien JZ, Huerta PT, Tonegawa S. The Essential Role of Hippocampal CA1 NMDA Receptor–Dependent Synaptic Plasticity in Spatial Memory. Cell. 1996;87(7):1327-38.

Tsujimoto T, Jeromin A, Saitoh N, Roder JC, Takahashi T. Neuronal calcium sensor 1 and activity-dependent facilitation of P/Q-type calcium currents at presynaptic nerve terminals. Science. 2002;295(5563):2276-9.

Tu H, Nelson O, Bezprozvanny A, Wang Z, Lee SF, Hao YH, et al. Presenilins form ER Ca2+ leak channels, a function disrupted by familial Alzheimer's disease-linked mutations. Cell. 2006;126(5):981-93.

Tucholski J, Lesort M, Johnson GV. Tissue transglutaminase is essential for neurite outgrowth in human neuroblastoma SH-SY5Y cells. Neuroscience. 2001;102(2):481-91.

Tucholski J, Roth KA, Johnson GV. Tissue transglutaminase overexpression in the brain potentiates calcium-induced hippocampal damage. J Neurochem. 2006;97(2):582-94.

Turner CE, West KA, Brown MC. Paxillin-ARF GAP signaling and the cytoskeleton. Curr Opin Cell Biol. 2001;13(5):593-9.

Ueno S, Miyoshi H, Maruyama Y, Morita M, Maekawa S. Interaction of dynamin I with NAP-22, a neuronal protein enriched in the presynaptic region. Neurosci Lett. 2018;675:59-63.

van Strien ME, Breve JJ, Fratantoni S, Schreurs MW, Bol JG, Jongenelen CA, et al. Astrocyte-derived tissue transglutaminase interacts with fibronectin: a role in astrocyte adhesion and migration? PLoS One. 2011;6(9):e25037.

van Strien ME, de Vries HE, Chrobok NL, Bol J, Breve JJP, van der Pol SMP, et al. Tissue Transglutaminase contributes to experimental multiple sclerosis pathogenesis and clinical outcome by promoting macrophage migration. Brain Behav Immun. 2015;50:141-54.

Venkiteswaran G, Hasan G. Intracellular Ca2+ signaling and store-operated Ca2+ entry are required in Drosophila neurons for flight. Proc Natl Acad Sci U S A. 2009;106(25):10326-31.

Ventura R, Harris KM. Three-dimensional relationships between hippocampal synapses and astrocytes. J Neurosci. 1999;19(16):6897-906.

Verderio C, Matteoli M. ATP mediates calcium signaling between astrocytes and microglial cells: modulation by IFN-gamma. J Immunol. 2001;166(10):6383-91.

Verderio C, Muzio L, Turola E, Bergami A, Novellino L, Ruffini F, et al. Myeloid microvesicles are a marker and therapeutic target for neuroinflammation. Ann Neurol. 2012;72(4):610-24.

Verderio E, Gaudry C, Gross S, Smith C, Downes S, Griffin M. Regulation of cell surface tissue transglutaminase: effects on matrix storage of latent transforming growth factor-beta binding protein-1. J Histochem Cytochem. 1999;47(11):1417-32.

Verderio E, Nicholas B, Gross S, Griffin M. Regulated expression of tissue transglutaminase in Swiss 3T3 fibroblasts: effects on the processing of fibronectin, cell attachment, and cell death. Exp Cell Res. 1998;239(1):119-38.

Verderio EA, Telci D, Okoye A, Melino G, Griffin M. A novel RGD-independent cel adhesion pathway mediated by fibronectin-bound tissue transglutaminase rescues cells from anoikis. J Biol Chem. 2003;278(43):42604-14.

Verkhratsky A, Nedergaard M. Physiology of Astroglia. Physiol Rev. 2018;98(1):239-389.

Vermes I, Steur EN, Jirikowski GF, Haanen C. Elevated concentration of cerebrospinal fluid tissue transglutaminase in Parkinson's disease indicating apoptosis. Mov Disord. 2004;19(10):1252-4.

Volgyi K, Gulyassy P, Haden K, Kis V, Badics K, Kekesi KA, et al. Synaptic mitochondria: a brain mitochondria cluster with a specific proteome. J Proteomics. 2015;120:142-57.

Vowinckel J, Stahlberg S, Paulmann N, Bluemlein K, Grohmann M, Ralser M, et al. Histaminylation of glutamine residues is a novel posttranslational modification implicated in G-protein signaling. FEBS Lett. 2012;586(21):3819-24.

Vyas FS, Hargreaves AJ, Bonner PL, Boocock DJ, Coveney C, Dickenson JM. A1 adenosine receptor-induced phosphorylation and modulation of transglutaminase 2 activity in H9c2 cells: A role in cell survival. Biochem Pharmacol. 2016;107:41-58.

Vyas FS, Nelson CP, Dickenson JM. Role of transglutaminase 2 in A1 adenosine receptor- and beta2-adrenoceptor-mediated pharmacological pre- and post-conditioning against hypoxia-reoxygenation-induced cell death in H9c2 cells. Eur J Pharmacol. 2018;819:144-60.

Vyas FS, Nelson CP, Freeman F, Boocock DJ, Hargreaves AJ, Dickenson JM. beta2-adrenoceptor-induced modulation of transglutaminase 2 transamidase activity in cardiomyoblasts. Eur J Pharmacol. 2017;813:105-21.

Walsh DM, Klyubin I, Fadeeva JV, Cullen WK, Anwyl R, Wolfe MS, et al. Naturally secreted oligomers of amyloid beta protein potently inhibit hippocampal long-term potentiation in vivo. Nature. 2002;416(6880):535-9.

Walther DJ, Peter J-U, Winter S, Höltje M, Paulmann N, Grohmann M, et al. Serotonylation of small GTPases is a signal transduction pathway that triggers platelet α-granule release. Cell. 2003;115(7):851-62.

Walther DJ, Stahlberg S, Vowinckel J. Novel roles for biogenic monoamines: from monoamines in transglutaminase-mediated post-translational protein modification to monoaminylation deregulation diseases. FEBS J. 2011;278(24):4740-55.

Wang R, Sweeney D, Gandy SE, Sisodia SS. The profile of soluble amyloid beta protein in cultured cell media. Detection and quantification of amyloid beta protein and variants by immunoprecipitation-mass spectrometry. J Biol Chem. 1996;271(50):31894-902.

Wang Y, Balaji V, Kaniyappan S, Kruger L, Irsen S, Tepper K, et al. The release and trans-synaptic transmission of Tau via exosomes. Mol Neurodegener. 2017;12(1):5.

Wang Y, Mattson MP. L-type Ca2+ currents at CA1 synapses, but not CA3 or dentate granule neuron synapses, are increased in 3xTgAD mice in an age-dependent manner. Neurobiol Aging. 2014;35(1):88-95.

Wang Z, Collighan RJ, Pytel K, Rathbone DL, Li X, Griffin M. Characterization of heparin-binding site of tissue transglutaminase: its importance in cell surface targeting, matrix deposition, and cell signaling. J Biol Chem. 2012;287(16):13063-83.

Wang Z, Stuckey DJ, Murdoch CE, Camelliti P, Lip GYH, Griffin M. Cardiac fibrosis can be attenuated by blocking the activity of transglutaminase 2 using a selective small-molecule inhibitor. Cell Death Dis. 2018;9(6):613.

Watanabe K, Tsunoda K, Itoh M, Fukui M, Mori H, Hitomi K. Transglutaminase 2 and Factor XIII catalyze distinct substrates in differentiating osteoblastic cell line: utility of highly reactive substrate peptides. Amino Acids. 2013;44(1):209-14.

Watson C, Kirkcaldie M, Paxinos G. The Brain : An Introduction to Functional Neuroanatomy. Saint Louis, UNITED STATES: Elsevier Science & Technology; 2010.

Weston PSJ, Poole T, Ryan NS, Nair A, Liang Y, Macpherson K, et al. Serum neurofilament light in familial Alzheimer disease: A marker of early neurodegeneration. Neurology. 2017;89(21):2167-75.

Wilhelmus MM, de Jager M, Bakker EN, Drukarch B. Tissue transglutaminase in Alzheimer's disease: involvement in pathogenesis and its potential as a therapeutic target. J Alzheimers Dis. 2014;42 Suppl 3:S289-303.

Wilhelmus MM, de Jager M, Smit AB, van der Loo RJ, Drukarch B. Catalytically active tissue transglutaminase colocalises with Abeta pathology in Alzheimer's disease mouse models. Sci Rep. 2016;6:20569.

Wilhelmus MM, Grunberg SC, Bol JG, van Dam AM, Hoozemans JJ, Rozemuller AJ, et al. Transglutaminases and transglutaminase-catalyzed cross-links colocalize with the pathological lesions in Alzheimer's disease brain. Brain Pathol. 2009;19(4):612-22.

Wilhelmus MM, van Dam AM, Drukarch B. Tissue transglutaminase: a novel pharmacological target in preventing toxic protein aggregation in neurodegenerative diseases. Eur J Pharmacol. 2008;585(2-3):464-72.

Wilhelmus MMM, Drukarch B. Tissue transglutaminase is a biochemical marker for Alzheimer's disease. Neurobiology of Aging. 2014;35(4):E3-E4.

Williams-Ashman HG, Wilson J, Beil RE, Lorand L. Transglutaminase reactions associated with the rat semen clotting system: modulation by macromolecular polyanions. Biochem Biophys Res Commun. 1977;79(4):1192-8.

Witter MP, Amaral DG. CHAPTER 21 - Hippocampal Formation. In: Paxinos G, editor. The Rat Nervous System (Third Edition). Burlington: Academic Press; 2004. p. 635-704.

Wolf J, Jager C, Lachmann I, Schonknecht P, Morawski M, Arendt T, et al. Tissue transglutaminase is not a biochemical marker for Alzheimer's disease. Neurobiol Aging. 2013;34(11):2495-8.

Yagami T, Kohma H, Yamamoto Y. L-type voltage-dependent calcium channels as therapeutic targets for neurodegenerative diseases. Current medicinal chemistry. 2012;19(28):4816-27.

Yagami T, Ueda K, Sakaeda T, Itoh N, Sakaguchi G, Okamura N, et al. Protective effects of a selective L-type voltage-sensitive calcium channel blocker, S-312-d, on neuronal cell death. Biochem Pharmacol. 2004;67(6):1153-65.

Yagi M, Uchiumi T, Sagata N, Setoyama D, Amamoto R, Matsushima Y, et al. Neural-specific deletion of mitochondrial p32/C1qbp leads to leukoencephalopathy due to undifferentiated oligodendrocyte and axon degeneration. Sci Rep. 2017;7(1):15131.

Yamane M, Sugimura K, Kawasaki H, Tatsukawa H, Hitomi K. Analysis on transglutaminase 1 and its substrates using specific substrate peptide in cultured keratinocytes. Biochem Biophys Res Commun. 2016;478(1):343-8.

Yanez-Mo M, Siljander PR, Andreu Z, Zavec AB, Borras FE, Buzas EI, et al. Biological properties of extracellular vesicles and their physiological functions. J Extracell Vesicles. 2015;4:27066.

Yoo JO, Lim YC, Kim YM, Ha KS. Transglutaminase 2 promotes both caspase-dependent and caspase-independent apoptotic cell death via the calpain/Bax protein signaling pathway. J Biol Chem. 2012;287(18):14377-88.

Yunes-Medina L, Feola J, Johnson GVW. Subcellular localization patterns of transglutaminase 2 in astrocytes and neurons are differentially altered by hypoxia. Neuroreport. 2017;28(18):1208-14.

Zainelli GM, Dudek NL, Ross CA, Kim SY, Muma NA. Mutant huntingtin protein: a substrate for transglutaminase 1, 2, and 3. J Neuropathol Exp Neurol. 2005;64(1):58-65.

Zainelli GM, Ross CA, Troncoso JC, Muma NA. Transglutaminase cross-links in intranuclear inclusions in Huntington disease. J Neuropathol Exp Neurol. 2003;62(1):14-24.

Zamanian JL, Xu L, Foo LC, Nouri N, Zhou L, Giffard RG, et al. Genomic analysis of reactive astrogliosis. J Neurosci. 2012;32(18):6391-410.

Zanellati MC, Monti V, Barzaghi C, Reale C, Nardocci N, Albanese A, et al. Mitochondrial dysfunction in Parkinson disease: evidence in mutant PARK2 fibroblasts. Front Genet. 2015;6:78.

Zemaitaitis MO, Kim SY, Halverson RA, Troncoso JC, Lee JM, Muma NA. Transglutaminase activity, protein, and mRNA expression are increased in progressive supranuclear palsy. J Neuropathol Exp Neurol. 2003;62(2):173-84.

Zemaitaitis MO, Lee JM, Troncoso JC, Muma NA. Transglutaminase-induced cross-linking of tau proteins in progressive supranuclear palsy. J Neuropathol Exp Neurol. 2000;59(11):983-9.

Zendjabil M. Circulating microRNAs as novel biomarkers of Alzheimer's disease. Clin Chim Acta. 2018;484:99-104.

Zetterberg H, Burnham SC. Blood-based molecular biomarkers for Alzheimer's disease. Mol Brain. 2019;12(1):26.

Zhang J, Lesort M, Guttmann RP, Johnson GV. Modulation of the in situ activity of tissue transglutaminase by calcium and GTP. J Biol Chem. 1998a;273(4):2288-95.

Zhang R, Yang D, Zhou C, Cheng K, Liu Z, Chen L, et al. beta-actin as a loading control for plasma-based Western blot analysis of major depressive disorder patients. Anal Biochem. 2012;427(2):116-20.

Zhang W, Johnson BR, Suri DE, Martinez J, Bjornsson TD. Immunohistochemical demonstration of tissue transglutaminase in amyloid plaques. Acta Neuropathol. 1998b;96(4):395-400.

Zhang W, Wang S, Zhang X, Liu K, Song J, Leng X, et al. Transmembrane Channel-Like 5 (TMC5) promotes prostate cancer cell proliferation through cell cycle regulation. Biochimie. 2019;165:115-22.